Polymer 2D crystals via crystallization self-assembly: preparation, properties and features

Dissertation

zur Erlangung des akademischen Grades eines

„Doctor rerum naturalium (Dr. rer. nat.)“

des Fachbereiches Chemie, Pharmazie und Geowissenschaften (FB09)

der Johannes Gutenberg-Universität Mainz

vorgelegt von

Oksana Suraeva

geboren in Moskau

Mainz, November 2020

JOHANNES GUTENBERG UNIVERSITÄT MAINZ

JG|U

MAX PLANCK INSTITUTE FOR POLYMER RESEARCH

Erklärung

Hiermit versichere ich, die vorliegende Arbeit selbstständig und ohne Benutzung anderer als der angegebenen Hilfsmittel angefertigt zu haben. Alle Stellen, die wörtlich oder sinngemäß aus Veröffentlichungen oder anderen Quellen entnommen sind, wurden als solche eindeutig kenntlich gemacht. Diese Arbeit ist in gleicher oder ähnlicher Form noch nicht veröffentlicht und auch keiner anderen Prüfungsbehörde vorgelegt worden.

Oksana Suraeva

Mainz, November 2020

“Research is to see what everybody else has seen, and to think what nobody else has thought.”

Albert Szent-Györgyi

Table of Contents

Abstract

Polymer 2D structures are a wide class of materials with unique properties, coming from their highly anisotropic nature. Functional 2D polymers may prove useful as membranes, chemical platforms for catalysis, optoelectronic devices, ultrasensitive pressure sensors and in environmental science. This thesis focuses on the formation of polymer 2D crystals, comprising the synthesis of polymers with incorporated functional groups, crystallization driven formation of 2D crystals and subsequent functionalization of the functional groups on the crystal surface. Several parameters determine this process. From the synthesis part, the introduced functional groups should be equidistantly distributed along the polymer backbone to facilitate controlled crystallization and to yield a perfect arrangement of the functional groups on the crystal surface. This was achieved by using acyclic diene metathesis (ADMET) polymerization. During crystallization, introduced functional groups will be expelled from the crystal lattice forming a functional surface. By varying the length of aliphatic part between the groups, we can change thermomechanical properties of the obtained crystals. From the crystallization part, parameters such as choice of solvent, concentration of polymer, temperature and speed of crystallization define the size and shape of the final crystals. By varying these parameters, we adjust the optimal condition to form polymer 2D nanocrystals with the desired thermomechanical properties. Moreover, a sequential polymer solution crystallization (SPSC) approach allows to achieve a laterally structured chemical functionalization on the surface of polymer nanoplatelets - where the core and the rim of the crystal surface have a different functionality. Variable functional groups thus can be placed on the surface, whereby the obtained nanocrystals have a broad potential application.

Chapter 1 describes crystallizable polymers as part of colloidal chemistry and the importance of 2D polymer crystals for the various applications. It is demonstrated which mechanisms are responsible for the crystallization process in solution and in bulk and how seeded growth approach helps to form uniform polymer crystals. In this chapter, we show that shape and properties of obtained 2D platelets depends on many parameters, such as size and functionality of incorporated groups, frequency and regularity of their distribution, speed and temperature control of the crystallization process. As a result, we can use crystallizable polymers as a uniform platform to obtain 2D nanoplatelets with programmable physical and chemical properties. Depending on the requirements for the final composition, one can choose among three distinct groups of initial materials: synthetic homogeneous homopolymers, block copolymers and bio-based polymers. Taken together, this chapter is intended as a contribution towards evaluating the potential of crystallizable polymers as a promising way to obtain 2D nanomaterials.

Chapter 2 presents an impact of the frequency of incorporated defects on the structure and properties of obtained polymer 2D nanoplatelets. The solution-crystallized anisotropic polymer platelets are based on PE-like polyphosphates with a variable length of methylene spacers (20, 30, and 40 CH_2 groups between each phosphate group). Linear polyphosphates with molecular weights up 23,100 g mol^{-1} were prepared by acyclic diene metathesis (ADMET) polymerization. Post-polymerization hydrogenation yielded solid, PE-like materials. Crystallization of these polymers into 2D polymer platelets was achieved by crystallization from dilute solution.

The morphology of the polymer crystals was investigated using differential scanning calorimetry (DSC), small-angle X-ray diffraction (SAXS), wide-angle X-ray diffraction (WAXD), transmission electron microscopy (TEM) and atomic force microscopy (AFM). With extending the length of aliphatic segment, melting points increases from 56 to 62 and 91 °C. The thickness of crystalline part, as well as the total thickness of crystals lamellar, increased from the sample with 20 CH_2 to 40 CH_2. At the same time, by changing the length of aliphatic spacer from C20 to C40 a change in crystal structure from pseudo-hexagonal to orthorhombic was observed. These findings demonstrate that the functional groups in the PE chain act as defects for the crystallization process. With increasing defect concentration, the crystal lattice becomes distorted. Moreover, the direct correlation of the crystal thickness with the length of the aliphatic segment clearly demonstrates that the in-chain functional groups are expelled to the lateral surface of the 2D nanoplatelets.

Chapter 3 presents the formation PE-derivatives with equidistant in-chain thiophene groups, capable of further postfunctionalization. Two polymers with 20 and 38 CH_2 groups between thiophenes were synthesized to show the effect of the variation of the length of aliphatic part on the properties of the resulting polymer crystals. Thiophene was integrate in the polymer chain to introduce conductive properties to the obtained polymer crystals. Polymers were prepared by acyclic diene metathesis (ADMET) polymerization. Thermomechanical properties of the synthesized polymers were characterized using thermogravimetric analysis (TGA), differential scanning calorimetry (DSC) and wide-angle X-ray diffraction (WAXD). Because the polymer with the 20 CH_2 spacer does not reveals crystalline structure at the room temperature, all postfunctionalization experiments were conducted with 38 CH_2 polymer. During crystallization, the thiophene groups are expelled to the crystal surface. Subsequently, they were copolymerized with 3,4-Ethylenedioxythiophene (EDOT) molecules, forming conductive 2D platelets.

Chapter 4 focuses on the influence of the incorporated chemical groups on the properties of obtained material. Here, we perform the synthesis and characterization of polyethylene-based polymers containing vitamin C groups in the polymer chain. Polymers with molecular weights up to 35,800 g mol^{-1} were prepared by acyclic diene metathesis (ADMET) polymerization. Post-polymerization hydrogenation leads to formation of a fully saturated, semicrystalline polymer with a precise spacing of 20 CH_2 groups between vitamin C groups. During crystallization, the vitamin C groups are expelled from the crystal and are located on the basal surface of the crystals. Thermomechanical properties and morphology of the polymer crystals were investigated using thermogravimetric analysis (TGA), differential scanning calorimetry (DSC), wide-angle X-ray diffraction (WAXD), small-angle X-ray diffraction (SAXD), transmission electron microscopy (TEM) and atomic force microscopy (AFM). Furthermore, incorporation of vitamin C groups in the polymer backbone introduces bioactive properties, such as radical scavenging. Moreover, the polymer is not cytotoxic and is taken up by cells, which makes it a suitable candidate for biomedical applications.

Chapter 5 is dedicated to the problem that two-dimensional nanoplatelets commonly have a homogeneous surface. Therefore, structuring the surface of a nanoplatelet is a major challenge. By consecutively crystallizing

polymers with a precise molecular architecture and different functional groups in the polymer backbone, we can form 2D organic nanoplatelets with a heterogeneously functionalized surface. We achieve this by using polymers with the same length of aliphatic part in a two-step approach: crystallization of first polymer to form a core followed by cocrystallization of second polymer around it. As a result, the central area of the platelets has a different surface functionality than the periphery. Obtained platelets are stable in dispersion, which considerably simplifies their further chemical modification and processing. Furthermore, various functional groups can be incorporated into the backbone of the initial polymers, what makes this simple concept a promising platform to create a new class of nanostructured 2D materials with desirable and controllable surface functionality.

In Chapter 6 we considered functionalized polymer 2D platelets, obtained from solution crystallization, as synthetic secondary structures and investigated their supramolecular interactions and ability to fold. It is known, that in nature complex biomolecules fold into defined structures by various intra- and intermolecular interactions. Primary structures, consisting of a linear sequence of nucleotides or amino acids, self-assemble to secondary alpha helices and beta sheets structure or protein tertiary structures. In synthetic polymers, single chain nanoparticles have been used as simple mimics of macromolecular chain folding. However, folding of polymer platelets had not been achieved so far. To achieve this, we functionalized a PE-like polyphosphate with pendant terpyridine groups. This polymer was crystallized from solution to form a functional polymer platelet dispersions, i.e. the synthetic secondary structure. By the addition of nickel salts to the dispersion, the strong metal-terpyridine complexation lead to a folding of the polymer platelets into a “synthetic tertiary structure”, which was investigated by TEM. Hereby, the size of the obtained assemblies could be altered by varying the concentration of metal ions present. Such assemblies might be used in catalysis or for the generation of hierarchical assemblies.

Zusammenfassung

Teilkristalline Polymere sind die am häufigsten verwendeten synthetischen Polymere in unserem Leben. Indem wir die Dimensionalität dieser Materialien von 3D auf 2D reduzieren, können wir neue Eigenschaften erzielen. Aufgrund der extrem großen Oberfläche von 2D Nanomaterialien eröffnen sich eine Vielzahl von möglichen Anwendungen.

Um ein Polymer-2D-Material mit bestimmten Eigenschaften zu erstellen und die gewünschte Struktur zu generieren, muss man die zur Selbstorganisation nötigen Parameter genau kontrollieren und einstellen. Synthetische Polymer-2D-Materialien folgen denselben Regeln wie die Proteinstrukturen in der Natur, die sich mit unterschiedlich geordneten Strukturen über die Bindung und Anordnung von Molekülen mittels Selbstfaltung zur endgültigen Konformation anordnen,

Der wichtigste Parameter ist hierbei die chemische Struktur. Im Gegensatz zu reinem Polyethylen mit homogener Struktur verändern bereits geringe funktionelle Defekte die Polymereigenschaften drastisch. Die äquidistante Verteilung der funktionellen Gruppen führt zur Bildung einer präzisen chemischen Struktur und beeinflußt so die Kristallisation. Die Polymerisation der acyclischen Dienmetathese (ADMET) erwies sich als bequemes Verfahren zur Herstellung von Polymeren mit präziser Struktur.

Die Größe der funktionellen Gruppen und der Abstand dazwischen definiert in einfacher Weise bereits die Form der erhaltenen Kristalle. Während der Kristallisation können kleine Defekte in das Kristallgitter aufgenommen werden, während sperrige Defekte an die Oberfläche ausgestoßen werden. Da sperrige Defekte die Position der Kettenfaltung definieren, ist es durch Variieren der Länge des aliphatischen Teils möglich, die Dicke der erhaltenen Kristalle, den Kristallinitätsgrad und die Schmelztemperatur zu ändern. Wir haben die sequentielle Lösungskristallisation von Polymeren mit verschiedenen funktionellen Gruppen entwickelt. Sie ist eine einfache, universelle Methode zur Herstellung von Materialien mit programmierbarer Oberflächenchemie.

2D-Polymerkristalle sind synthetische, sekundärgeordnete Strukturen und es ist möglich, sie durch schichtweises Stapeln oder Falten zu komplexeren Systemen anzuordnen. Die Verwendung biobasierter Inhaltsstoffe und die Einführung der biologischen Abbaubarkeit in die endgültige Zusammensetzung kann dazu beitragen, den ökologischen Fußabdruck synthetisierter Materialien im Vergleich zu klassischen Polymeren zu verringern und sie nachhaltiger zu machen.

Durch Variieren all dieser Parameter können Polymer-2D-Materialien mit gewünschten Eigenschaften erzeugt werden. Infolgedessen erweitert es die Anwendungsmöglichkeiten von 2D-Polymerstrukturen und macht sie in so unterschiedlichen Bereichen wie Membranen, chemischen Plattformen für die Katalyse, optoelektronischen Geräten, ultrasensitiven Drucksensoren und in den Umweltwissenschaften wertvoll.

Graphical abstract

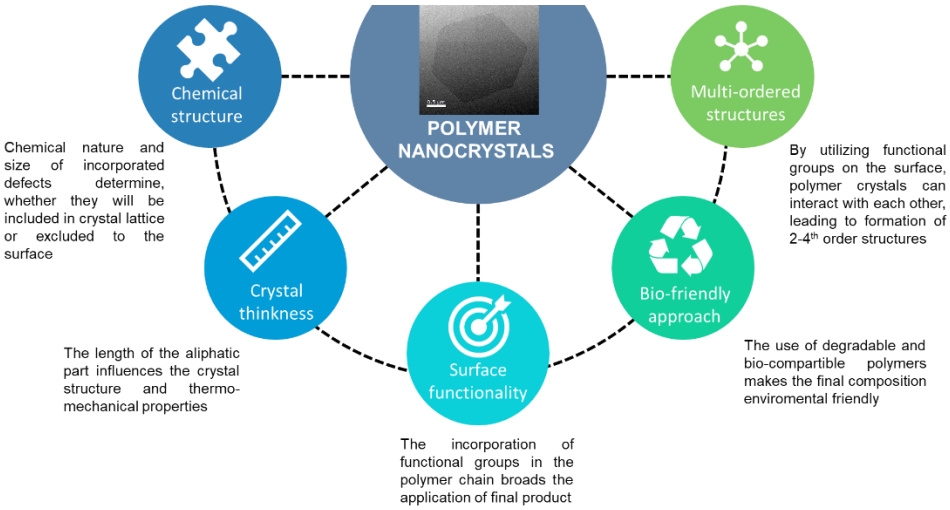

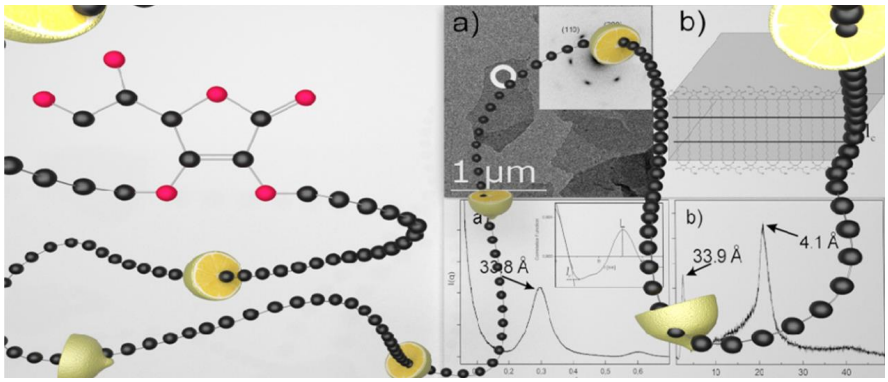

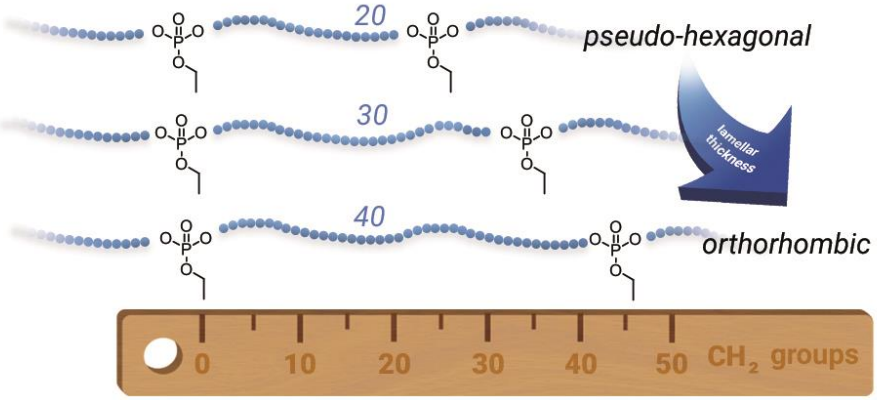

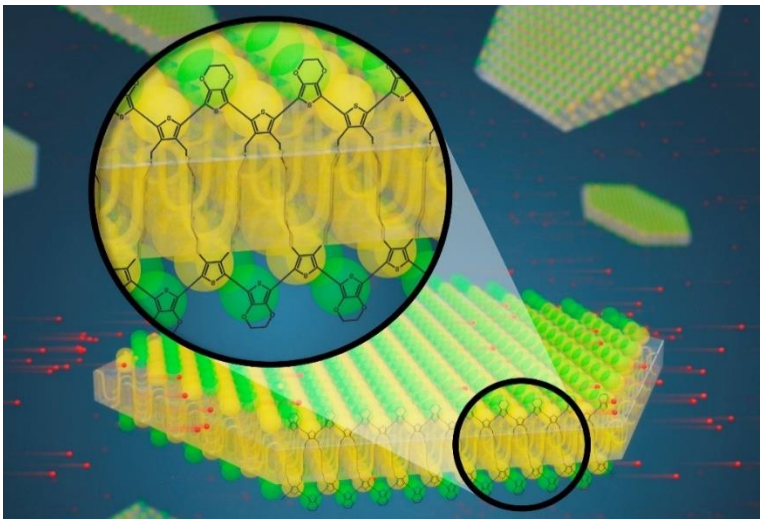

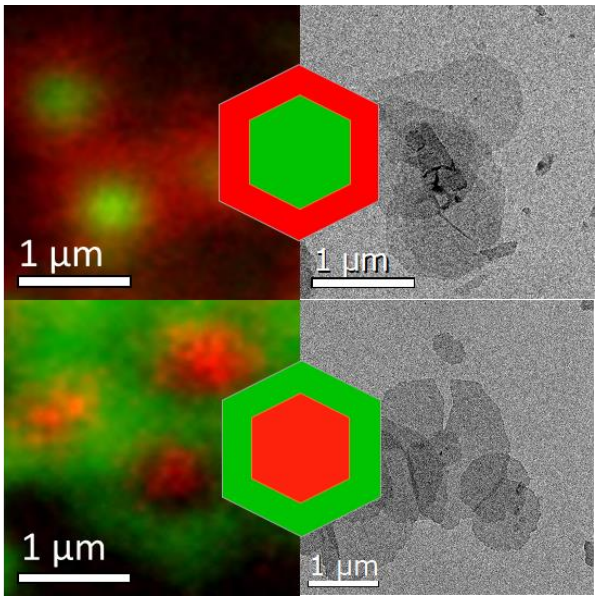

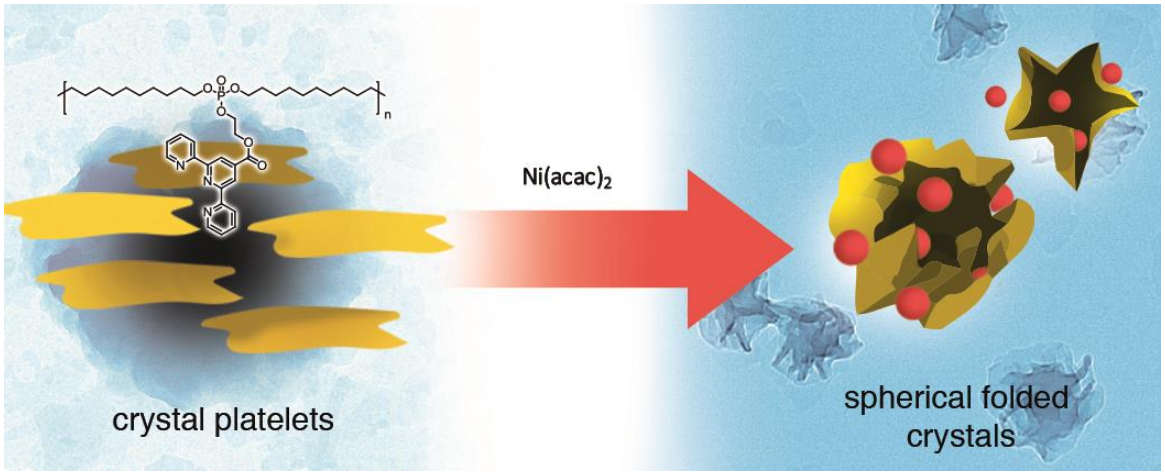

1. Polymer 2D materials: crystallization features and properties

1.1. Colloidal nature of polymer crystallization process

The reduction of the dimensionality of a material can produce novel topographic properties, which has been impressively demonstrated for graphene[1,2] and has triggered a boom of interest in 2D materials. Beside inorganic materials - such as hexagonal boron nitride, metal chalcogenides and layered perovskites - organic 2D materials are also experiencing increasing interest due to their special properties. These organic nanosheets are of interest for membrane applications, in biomedical settings,[3] as high surface area adsorbents, catalyst supports and sensors.[4–6]

Already since the works of Keller[7] and Fischer[8] in 1957 it is known that semi-crystalline polymers crystallize in the form of nanoplatelets, whereby the polymer chain is back-folded at the basal surfaces of these platelets (Figure 1.1).[9] Crystallization from solution thus produces individual lamellar platelets with a thickness in the range of several nanometers. The lateral extension of these platelets can extend over several micrometers. In general, polymer crystals exhibit a high regularity and periodicity over reasonable domain sizes, a critical feature of 2D layers. Thus, the solution-crystallized polymer crystals can be regarded as 2D organic layers or nanoplatelets.

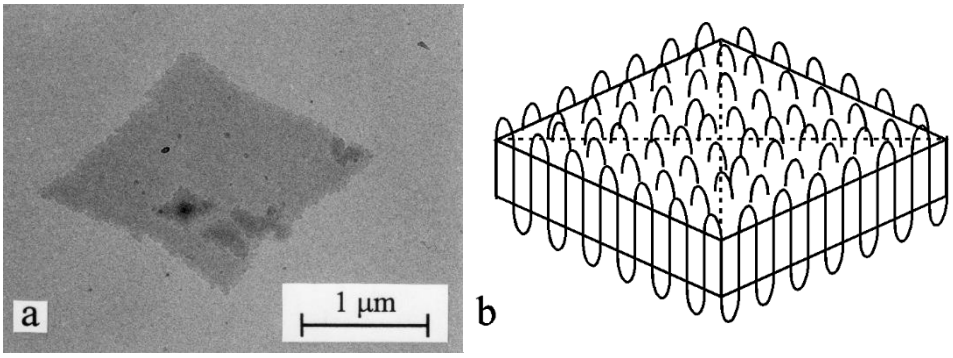

Figure 1.1. a) TEM bright-field image of diamond-shaped single crystal of polyethylene, grown from solution. b) Simplified scheme of back-folded arrangements of polymer chains to form polymer crystals. Reprinted with permission from ref [9]

To understand how crystallization of polymers occurs, we will explain the general process of nanoparticle formation from a colloidal chemistry point of view. Synthesis of a colloidal system of polymer nanoparticles (NP) involves two steps: nucleation and growth[10]. The nucleation process results from an unstable density fluctuation in which several molecules agglomerate and transition to a denser phase. If the size of these nuclei exceeds a critical size, these nuclei are stable. Subsequently, they can further grow to form bigger clusters either by continuous deposition of unimers on their surface or by coagulation. The nucleation−growth theory was introduced by LaMer in the 1950s, who adapted a classical nucleation theory developed by Becker and Döring in the 1920s.[11,12]

There are two distinct kinds of nucleation – homogeneous and heterogeneous. Homogeneous nucleation occurs spontaneously and randomly, without the necessity for a nucleation site. However, it requires a supersaturated precursor solution. In contrast, heterogeneous nucleation occurs at preferential sites of surfaces, inhomogeneities or intentionally added nucleation agents. In LaMer's theory, the so-called nucleation, which is the spontaneous formation of nuclei in the solution, is a homogeneous process, while the growth can be considered as a heterogeneous process, because the precursor molecules will deposit on the already formed nuclei.

The basic idea behind the theory is that a thermodynamic system tends to minimize its Gibbs free energy and to increase its enthropy.[13] Figure 1.2a shows the evolution of the Gibbs free energy depending on the nuclei radius. The system gains free energy by the phase transition, forming a volume with a higher density (the bulk energy). In contrast, the formation of the surface consumes free energy. The superposition of these two terms yields a maximum at the critical radius r_c. The energy barrier ΔG_c corresponds to ΔG at r_c. Once this energy barrier is overcome and the critical radius reached, the nuclei are stable. These nuclei can further grow through heterogeneous nucleation processes. This so-called secondary nucleation profits from the presence of the existing surface area of the nuclei, which reduces the energy penalty for the formation of a new surface. Consequently, the surface energy necessary for secondary nucleation is lower and the surface of the existing nuclei become new nucleation sites. Therefore, once the nuclei are formed, they will grow radially by attaching molecular precursors to the stable nuclei.

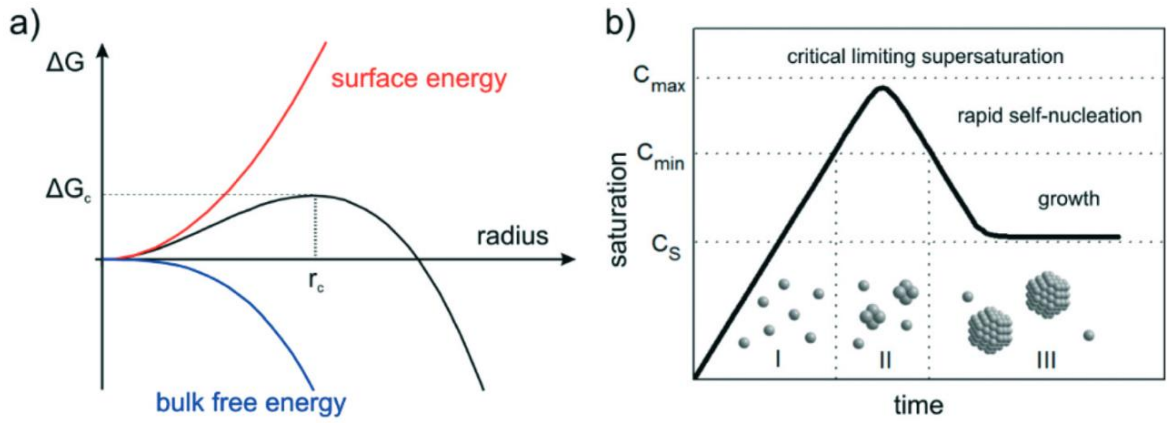

Figure 1.2. a) The dependence of cluster free energy ΔG on the cluster radius r. The total Gibbs free energy (black curve) is a superposition of the energy penalty for the formation of a surface (red curve) and the energy gain from the bulk (blue curve). The maximum in Gibbs free energy at r_c defines the critical nucleus radius. Clusters smaller than r_c are instable and will dissolve again. When the cluster size exceeds the critical radius r_c, the nuclei are stable and further growth will gain Gibbs free energy. (b) Kinetic model describing the nucleation process according to LaMer. Starting from a stable solution (phase I) the supersaturation is increased until a spontaneous, burst nucleation sets in (phase II). Due to the consumption of monomer the concentration falls below the minimum necessary saturation C_{min} and the nucleation breaks down. In phase III, the nuclei grow by attaching monomers from the saturated solution. Reprinted with permission from ref [13]. Copyright 2015 The Royal Society of Chemistry.

Figure 1.2b describes the evolution of the concentration of monomers versus time, showing the mechanism of burst nucleation according to LaMer.[11] Starting point is a stable solution of a molecule or a polymer (phase I). We now increase the saturation of the solution either by adding more substance, by adding a non-solvent or by cooling the solution. At a certain point, the critical limiting supersaturation is reached (phase II). The absence of nucleation sites leads to a spontaneous, homogeneous nucleation. The nucleation rate at this point is so high, that nuclei will form throughout the solution. This rapid self-nucleation induces a fast reduction of the supersaturation below the minimal necessary concentration C_{min} and the nucleation process breaks down. Finally, in phase III, nucleation has stopped and the remaining monomers will only attach to the existing nuclei to grow the NPs. Due to the fast nucleation process (burst nucleation) the nanoparticle dispersion has a narrow size distribution.

We can now consider the solution crystallization of a polymer under the thermodynamic and kinetic aspects of nucleation. However, polymers have unique features which are directly related to their molecular architecture. Upon crystallization, the polymer chain is folded at the crystal surface and reenters into the crystal. It forms a lamellar crystal with a crystal thickness l_C. The lateral dimension of the crystal can reach up to several µm (Figure 1.1 a). According to Figure 1.2 (a), the lamellar thickness l_C results from the critical nucleus size r_C. Hence, for common polymer systems, the nucleation conditions determine the lamellar thickness of the solution grown polymer nanocrystals (PNC).

The solution crystallization of a polymer is usually done by forming a supersaturated solution. Most olefin polymers show a low solubility in organic solvents. This solubility can be increased by increasing the solvent temperature. Accordingly, we can induce the rapid self-nucleation (Figure 1 (b)) by cooling the solution and thus reaching the critical supersaturation concentration C_S. The monomer, remaining in solution, will attach to the nuclei, forming the energetically favorable shape of polymer nanocrystals.

The PNC will grow in such a way to reduce its surface energy, which is the limiting parameter, already present in the nucleation step. Historically, in 1874, Gibbs suggested that the shape of a crystal is dictated by the minimization of the total surface energy.[14] Therefore, the shape of crystals is therefore not dictated by the minimum total surface (which is a sphere) but strongly depends on crystalline facets. The facets with the lowest surface energies will dominate the final equilibrium shape. In 1901, Wulff assumed[15] that the surface free energy of a crystal depends on the facet's crystallographic orientation: by the crystallographic nature of the expressed facets with low surface energy determines the shape of the obtained polymer nanocrystals.

1.2. General behavior of crystalline polymers

The size and structure of the crystals and the degree of crystallinity depend on the structure of the polymer and on the growth conditions. During crystallization, polymer chains fold back and forth (***Figure 1.1.*** *a) TEM bright-field image of diamond-shaped single crystal of polyethylene, grown from solution. b) Simplified scheme of back-folded arrangements of polymer chains to form polymer crystals. Reprinted with permission from ref* [9]Figure 1.1), leading to the formation of ultrathin 2D structures. The lamellar thickness of the crystals is set during the nucleation process and corresponds closely to the critical nucleation radius r_c.

Primarily, the chemical structure determines whether a linear polymer is able to crystallize. Accordingly, polymers can be divided into amorphous and crystalline materials. Examples of amorphous polymers include polycarbonate, polyvinyl chloride or polymetharcrylates. In contrast, polyolefins, such as polyethylene and polypropylene, belong to the crystalline polymers.

Another essential factor that determines the crystallization of a polymer is the perfection of the linear chain. Polymer chains usually contain defects, some of them are “natural” as chain ends and branching, some can be artificially introduced into the structure. Depending on the frequency[16] and size[17] of these defects they can be either incorporated into crystal bulk or will be expelled to the surface of the crystal. Random incorporation of defects inhibits the crystallization due the difficulties for the segments to pack into crystallites. This issue can be solved by precise location of defects, and one of the most convenient methods to achieve it is acyclic diene metathesis (ADMET) polymerization, established by the Wagener group.[18] Moreover, an equidistant distribution of bulky defects along the polymer chain promotes formation of crystals, where the lamellar thickness is predetermined by the length of the aliphatic segment between these defects. The reason for this is that chain folding occurs preferentially on the position of the incorporated defects, thus the distance between defects in the chain defines the final structure. Because the lamellar thickness is limited by the length of the aliphatic segment between two defects, the melting point of these lamellar crystals can be adjusted by the molecular architecture of the polymer chain, i.e. by the equidistant distribution of the bulky defects. Thus, by varying the length of the aliphatic segment between defects, it is possible to tune the melting point of the obtained polymer crystals.[16,19] When the inserted defect has variable options to be incorporated into polymer chain (ortho-, meta- or para-substitution of aryl side groups), position of this substitution defines if defect will be included in the crystal lattice or excluded to the surface and also influence the type of the crystalline structure.[20]

Crystallization is also affected by extrinsic factors, like temperature and cooling rate. Nucleating agents such as organic salts, small filler particles and ionomers act as seeds and can increase the crystallization rate.[21] Rigid chain backbone and intermolecular forces favor the crystallization process because molecules prefer an ordered and densely packed arrangement with a maximal number of secondary bonds.[22] Thus, the molecules tend to cooperatively organize and develop a crystalline structure. The high crystallinity and strong intermolecular interactions also increase the mechanical strength of the polymer.[23]

Introduction of functional groups as chain defects can bring certain properties to the final composition and offer a broad range of applications. There are two distinct approaches to insert functional group in the polymer: as a part of polymer backbone or as a side-chain. Thanks to the first approach, it is possible to fabricate degradable and flame-retardant polyethylene-like polymers.[24,25] The second method allows to introduce various groups into the 2D polymer system and bring conductive,[26] free-radical scavenging[27] or anti-inflammatory[28] properties. Crystallization of polymers with precisely distributed groups leads to the formation of a homogeneous functional surface.

Synthesis of bio-degradable and bio-based polymers makes this field more bio-friendly. Different natural sources, such as lignin derivatives,[29] sugars,[30,31] plant and vegetable oils[32–35] serve as a building blocks for

polymer chains, and molecules as vanillin[36] or ascorbic acid[27] can work as a functional defects. Together with environment-friendly synthesis process it is possible to create more sustainable materials.

By varying all these parameters, creation of polymer nanocrystals with desirable properties can be achieved. A summarized scheme of parameters, which were investigated in this thesis, is presented in

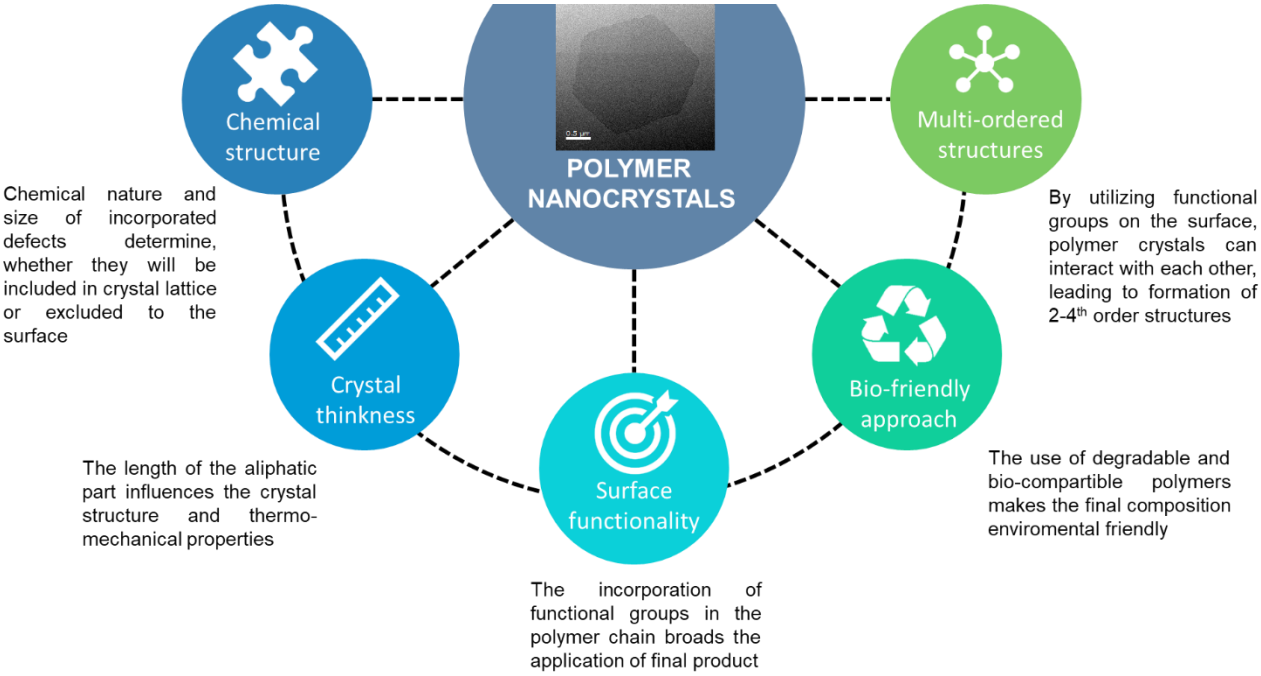

Scheme 1.1. Parameters, influencing crystallization process and properties of the obtained polymer 2D nanocrystals.

1.3. Polymer crystallization: the chain arrangement

In 1930, Herrmann at al. proposed the fringed-micelle model (Figure 1.3) showing that the crystalline regions serve as physical crosslinking, in order to explain the good elasticity of LDPE (showing X-ray diffraction peaks).[37] It was already known at this time that polymers have an extremely high molecular weight, although the monomer units are quite small. At that time, the problem was to accommodate the entire molecule - in its entire length - in a crystal, as is the case with all other low-molecular crystal systems.

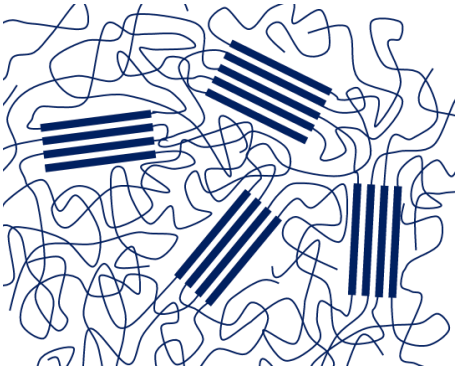

Figure 1.3. Schematic illustration of the fringed micelle model, assuming that in regions of sufficient chain alignment long linear macromolecules form a crystal lattice, which function as cross-linkers.

In 1938 Storks proposed the chain-folding model for polymer crystallization.[38] He observed very thin rhomboid-shaped polymer lamellar crystals and as a polymer chain was much longer than the lamellar thickness, Storks assumed that the polymer chain is folded back and forth in the crystals. Nevertheless, due to the prevailing influence of the Herrmann theory, this concept stayed unattended for another 20 year. In 1957 Keller prepared lamellar single crystals of polyethylene from dilute solutions, and observed – as Storks did before - that the lamellar thickness appears to be much smaller than the chain length.[39,40] The electron diffraction pattern of polymer crystals clearly indicated, that the molecular backbone oriented along the thinnest dimension of the crystal and is extended in a continuous manner no more than 40 to 50 nm. Based on these experimental facts, Keller[7] and Fischer[8] proposed the “folded chain model.” In this model, they assumed that the polymer chain folds back and forth on itself in an adjacently re-entered manner, which is also frequently referred to as the tightly folded chain model or the adjacently folded chain model (Figure 1.1). In addition, Flory[41] and Zachman[42,43] did theoretical calculations and demonstrated that the fringed micelle model was inappropriate, so the folded chain model was proved and widely accepted.[44]

1.3.1. Solution-grown single crystals

In a dilute solution, since polymer chains are separated from each other, we can focus on one single chain and regard it as an isolated system. At high enough supersaturation of the solution, a stable nucleus with a critical size will emerge. As the extended single polymer chain gains the largest surface area, folding process is thermodynamically preferable. It is not yet clear, if this nucleus already shows a fold surface or if it arranges like a fringed micelle. However, upon further growth of the crystal, more polymer chains from the diluted solution will attach to this existing nucleus and align the molecular chain direction to the predetermined chain

direction of the nucleus. This secondary nucleation process on the lateral surface of the nucleus induces the refolding of the polymer chain, which finally leads to the folded basal surfaces of the lamellar crystal. Due to the low concentration of polymer chains in the vicinity of the growth front of the crystal, this process is kinetically dominated. When a segment is attached to the growth front, it is much more likely that the free dangling part of this polymer chain will fold back at an adjacent position on the growth front than an attachment of a new polymer chain at the same position. For this reason, crystallization from dilute solution mainly produces polymer crystals with fold surfaces having adjacent reentry.

Experimental proof of this assumed structure was performed by Bu *et al*.[45], who sprayed an extremely dilute poly(ethylene oxide) (PEO) polymer solution onto the surface of hot water dropwise. Diffraction pattern of the single crystals under a transmission electron microscope confirmed the formation of a folded chain structure.

1.3.2. Melt-grown polymer crystals

In comparison to the crystallization in dilute solutions, the melt crystallization process is more complicated. In 1961 Fischer and Schmidt proposed the long period of alternating amorphous and lamellar crystal as observed by X-ray scattering of stretched polyethylene.[46] Almost at the same time, Flory suggested that polymer chains may not be able to fold up quickly into the regularly adjacent chain-folding state in lamellar crystals and many chains will form loops and cilia.[41]

Even though there were no doubt concerning the folded chain model, various mechanisms of chain folding were under discussion. For instance, Hoffman[47] and his colleagues believed that crystals should be organized in an adjacent reentry fashion (also termed as “tightly folded fashion”), while Flory[41] argued, that “switchboard model” explains polymer crystallization better due to the slow dynamics of polymer motion. According to the switchboard model, one polymer chain can either penetrate different lamellae forming tie molecules or enter into different positions of one lamella yielding loops. This concept was later generalized by Mandelkern[48] and recently revisited by Hu *et al*.[49], who proposed the so-called “intramolecular nucleation model” (Figure 1.4)

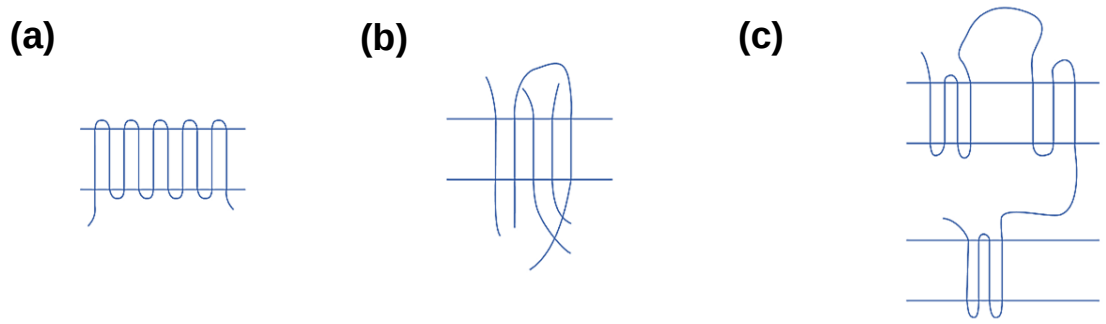

Figure 1.4. Schematic diagram of molecular trajectory in various models: (a) adjacent re-entry model, where polymer chains a regularly folded, making hairpins turns at the surface, (b) switchboard model, where the polymer chain give rise to an amorphous overlayer and (c) intramolecular nucleation model, where one polymer chain can take part in the formation of two different lamellae.

Thermoplastic polymers, crystallized from the melt usually exhibit high toughness and mechanical strength. Accordingly, the lamellar crystals must be connected by tie molecules. Otherwise, they would show poor mechanical performance, typical for low molecular weight alkanes such as paraffin. Generation of a certain amount of tie molecules between different lamellas during crystallization from melt represents the intramolecular nucleation model. The various models of chain folding are presented in Figure 1.4.

Regarding the nucleus formation of polymer crystals, there are two basic types. First the so-called inter-chain nucleation, where a bundle of chains stacked parallel in molecular direction, very similar to the fringed-micelle model (Figure 1.3). In this case a large fraction of amorphous segments, crosslinked by the fringed micellar nuclei, lose conformational entropy due to the overcrowding at the exit surface. This raises the surface free energy and the nucleation barrier will be very high. Another type of nucleation process, called the intra-chain nucleation, involves the adjacent chain folding with the chains packed parallel and folded back at the surface of the nucleus and overcrowding at the lamellar surfaces is avoided. Accordingly, the amorphous chains are relatively free. In this case the surface free energy and the nucleation barrier is relatively low. As a result, the intra-chain nucleation dominates not only the primary crystal nucleation but also the secondary crystal nucleation at the lateral growth front of lamellar polymer crystals.[37] Both these processes are dominated by the crystallization kinetics. A slow crystallization process will allow the system enough time, to develop via the intra-chain nucleation, whereas fast crystallization processes will go via the inter-chain nucleation. By annealing of the polymer crystals, formed via fast nucleation, thicker crystals with better-ordered chain-folding structure can be obtained. These chain-folding principles of polymer crystallization are shown in Figure 1.5.

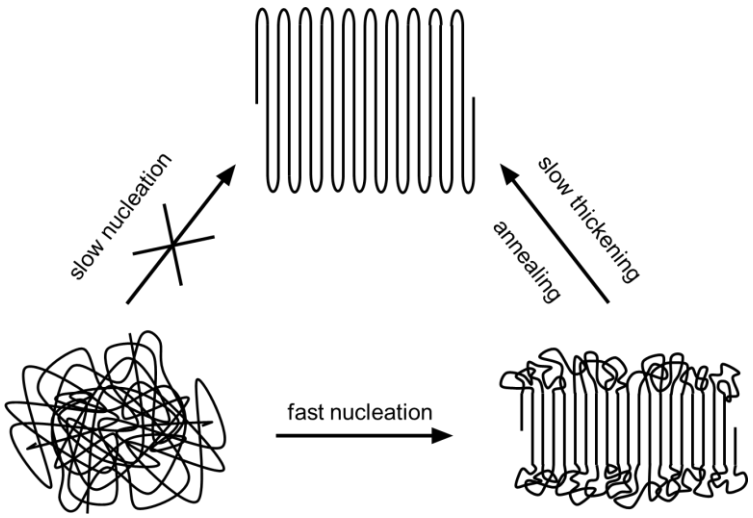

Figure 1.5. Schematic representation of the chain-folding principle of polymer nonisothermal crystallization. Fast cooling leads to the formation of thin crystals with large amorphous region. By annealing it is possible to arrange part of polymer chains on the surface, resulting in thicker crystals with higher degree of crystallinity.

1.3.3. Self-seeding process

The growth of polymer crystals is a complex process, as it requires the organization of polymer chains, which involves chain diffusion and chain folding.[50] Self-seeding has established itself as one of the most promising methods to produce uniform 2D polymer crystals.[51] As for polymers, in comparison to small molecules, it is more difficult and takes more time to form uniformly crystallized confinements. During polymer crystallization domains with different levels of crystallinity are formed which results in a crystal ensemble with a broad melting point distribution. The higher the speed of crystallization for the polymer molecule, the higher the probability to form a crystalline structure with a high level of imperfect chain folding and low crystallinity. Variations in crystal perfection and lamellar thickness throughout the polymer crystal result in different regions of the same crystal effectively possessing different melting points.[52]

Self-seeding helps to solve this issue and to create uniform 2D crystals with evenly distributed properties.[53] This process consists of two steps. First step involves heating a solution of the crystalline polymer to just below its melting point. At this temperature, molten and crystalline regions co-exist and the regions with the highest level of perfection survive the melting process. During the subsequent cooling step, the remaining crystallites act as initiation sites for the growth of the dissolved polymer chains, and single crystals of uniform size and shape are obtained.

Xu and co-workers demonstrated one of the features of this process in 2009. They were able to regenerate crystals with the same orientation as the starting single crystals.[54] For this study, they used the crystalline-coil block copolymer poly(2-vinyl pyridine)-*b*-poly(ethylene oxide) (P2VP-*b*-PEO), where PEO is the crystalline block that undergoes self-seeding, P2VP is the amorphous part. The researchers showed that even after the annealing process the preservation of the orientation of the crystals is a consequence of the regions of highest crystal perfection surviving and then acting as seeds for the dissolved polymer chains (unimers). This result disproved the melt memory phenomenon, an alternative hypothesis, where all polymer chains are dissolved, but those that dissolved last “remember” their orientation prior to melting.[55] The self-seeding approach provides a facile route to generate a large number of uniform polymer crystals with programmable shape that can be applied to both homopolymers and crystallizable block copolymers.

1.4. Organic 2D platelets.

Two-dimensional crystalline materials are a fundamentally important geometry to control surface properties, which is crucial for e.g. device fabrication. Depending on the nature of the used polymer, the following groups can be distinguished:

1. Synthetic homopolymers, including polyethylene and analogues with possible incorporation of functional groups in the polymer chain.
2. Synthetic block copolymers, composed of chemically distinct blocks covalently bonded together
3. Bio-based polymers, including various biomolecules, such as DNA, RNA, proteins, peptides, peptoids (poly-N-substituted glycines), and other biopolymers produced by nature.

Each group has special features and benefits, which allows to create 2D platelets with certain properties.

1.4.1. 2D crystalline homopolymers

Synthetic homopolymers are the most studied class of polymers. In 1957, polyethylene was crystallized into thin platelets from solution.[7] Since then, nearly all crystallizable homopolymers have been shown to form 2D crystals in which the chains are folded back and forth perpendicular to the planar surface[56–58] However, polyethylene chains have no sequence information and the crystallization process depends mostly on crystallization kinetics[59,60] and the molecular weight of the polymer chain.[61] In addition, by crystallizing homopolymers without incorporated functional groups, there is no chemical distinction between the surface and the interior, severely limiting the ability to functionalize or engineer these materials. Utilization of functional 2D polymers with in-chain functional groups will help to significantly expand the application scope of 2D materials. These novel macromolecules may prove useful as membranes, chemical platforms for catalysis, optoelectronic devices, and ultrasensitive pressure sensors.

There are several common methods to obtain periodic two-dimensional (2D) layered nanomaterials: exfoliation of the layered bulk materials[2,62] or by thermolytic synthesis, e.g. chemical vapor deposition.[63] Both approaches do not allow to incorporate defined chemical functionalities at predetermined positions or engineer structures of the materials at the atomic level. Recently developed methods such as synthesis by photopolymerization in single crystals, formation of 2D crystals at air-water interface[64–67] and in solution[63,68,69] allow to meet these requirements and broaden the choice of used functional groups[70].

Regularity of incorporated functional groups plays a crucial role in the formation of polymer crystals. Kryuchkov *et al*. showed that anisotropic surfactant-free particles can be formed by dispersion of a random ethylene−acrylic acid copolymer. But due to the large degree of incorporated acrylic acid repeat units required for colloidal stability (12 mol%) and the random nature of the copolymer, crystalline domains may contain both pure polyethylene segments and domains with carboxylic acid. This results in a clearly anisotropic, but irregular structure.[71] Works by the Wagener group[72,73] show that frequency of incorporated defects also alter the crystallization behavior. In most cases, the longer the aliphatic segment between incorporated defects the

more efficient molecular packing of elongated alkyl chains. Increasing the length of alkyl chain leads to the optimization of intermolecular interactions between methylene segments in adjacent chains and to the reorganization of the lamellae structure. Therefore, the melting temperature is increasing.

Another situation is observed, when polymers contain bulky in-chain or side-groups, regularly distributed along the polymer chain. These defects cannot be included in the crystal lattice and will be expelled from the crystalline lamellae to the surface during crystallization. Thus the lamellar thickness is basically predetermined by the distance between two neighboring side-groups.[74–76] Chain folding is expected to take place at the position of the side-groups. Consequently, the surface of such lamellar crystals will be covered by side-groups and an appropriate choice of these groups opens up the opportunity to perform chemical reactions at the surface.[77]

Hasan *et al.* performed crystallization of a polyphosphoester at the air-water interface using Langmuir-Blodgett Trough (LBT).[78] Polymer chain consist of phosphoester groups separated from each other by 20 CH_2 units. This precise structure is key to form 2D crystals with aliphatic crystalline core and phosphoester groups on each surface. In this work the polymer was dissolved in chloroform and spread on a water surface. The extended plateau region of the surface pressure vs area per monomer unit (π-A) in the Langmuir isotherm together with epifluorescence and Brewster angle microscopy proved formation of 2D polymer crystals. Epifluorescence microscopy shows formation of single crystal-like hexagonal entities with lateral dimensions of up to 20 µm in the Langmuir film during the crystallization of PPE. The thickness of the crystals is about 2.5 nm at the end of the plateau range and reaches 3.0 nm upon further compression (Figure 1.6).

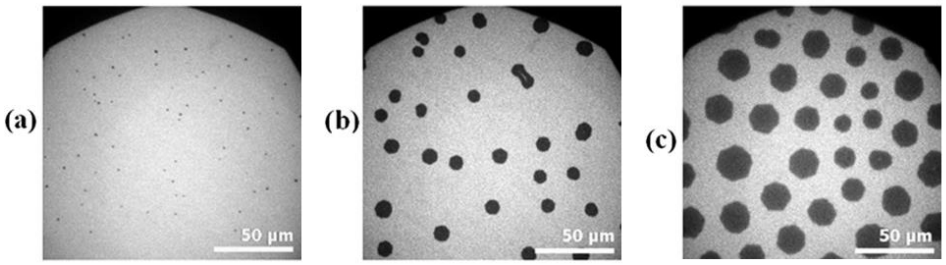

Figure 1.6. Epifluorescence microscopy images of PPE captured during film compression on the Langmuir trough at selected π and A values. (a) 0 mN m^{-1}, 1.3 nm^2, (b) 4.6 mN m^{-1}, 0.85 nm^2, (c) 8.0 mN m^{-1}, 0.27 nm^2. Reprinted with permission from [78]. Copyright 2018 European Polymer Journal.

Machatschek *et al*. showed an opportunity to functionalize 2D lamellar crystalline polymer by covalent attachment of semiconducting molecules.[77]. During crystallization, the side-branches of polymer chain were excluded from the crystalline lattice and thus covered the surfaces of these crystals. By using carboxyl groups as side-branches, capable for chemical reactions, they functionalized the crystal surface with semiconducting molecules. To form single crystals of the precisely side-branched polymer they were using two approaches: supersaturation from solution or by assembling nanocrystals on a Langmuir trough to form large areas, consisting of randomly arranged monolayers nanocrystals. However, they did not provide any experimental evidence of the conductive properties of the crystals with functionalized surface.

In work of Ortmann *et al*. an anisotropic shape of polymer nanoparticles was achieved during crystallization by packing chain segments and forming bonds between adjacent stretched chain segments via van der Waals interactions (Figure 1.7).[79] Precisely engineered polymer molecular structure allows to encode nanocrystal thickness and thus provide particles with a defined shape and surface chemistry. It was achieved by spacing of carboxylic groups precisely on every 21st or 45th carbon atom of linear polyethylene chains using acyclic diene metathesis polymerization (ADMET). These hydrophilic functional groups form a layer on the nanocrystal surface, which interacts with the aqueous dispersing medium and, thus, self-stabilizes the nanocrystals.[80] The nanocrystal thickness is directly predeterminded by the length of the long-chain aliphatic spacer between the functional groups.

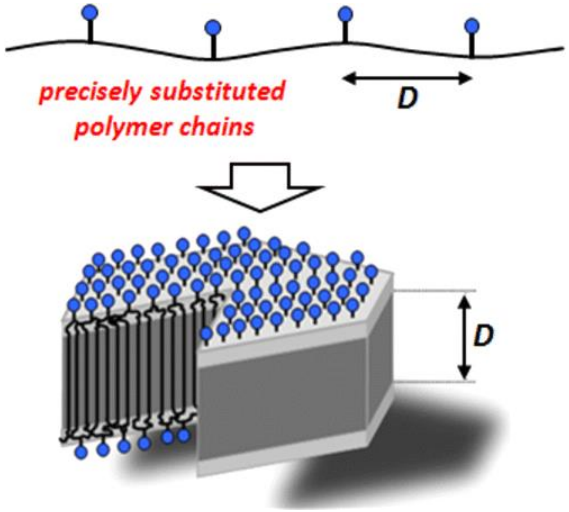

Figure 1.7. Schematic Representation of a Self-Stabilized Nanocrystal from Precisely, Long-Spaced Carboxy-Substituted Polymer Chains. Reprinted with permission from[79]. Copyright 2013 ACS Macro Letters.

The work of Rank *et al* shows how to impart an anisotropic shape in polymer nanoparticles.[81] Due to the high molecular weight of polymers, the postpolymerization chain folding[39,82] is much slower, compared to that of the low molecular weight analogues. This impacts the crystallization process and can hinder the formation of regular-shaped crystals. Also, the synthesis of polymers with precise distribution of ionic groups at sufficiently long intervals along the chain is a time consuming process. To overcome these limitations, they formed crystalline nanoparticles from telechelics polyethylene $HOOC(CH_2)_{46}COOH$ chains of uniform length that correspond to a single full run length through the anticipated nanocrystal and with two end groups that will form the crystal surface. Injection of the polymer into aqueous CsOH solution leads to formation of crystalline nanoparticles, with a thickness corresponding to an extended chain (Figure 1.8).

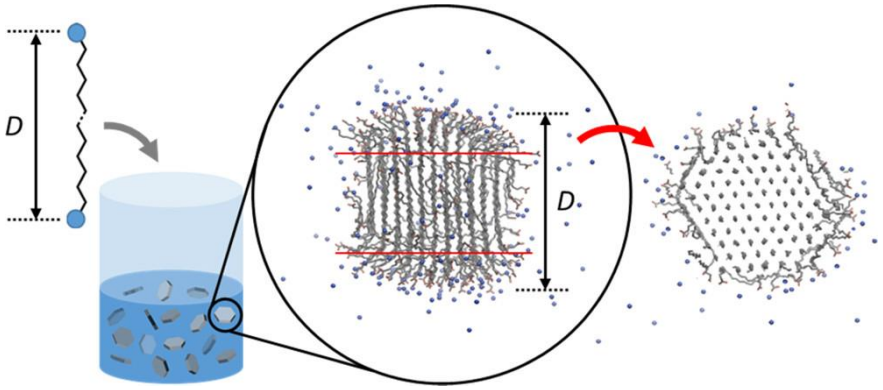

Figure 1.8. Schematic representation of C48-COOCs nanoparticle formation in water. Reprinted with permission from[81]. Copyright 2019 Macromolecules.

An alternative way to create two-dimensional polymers with versatile functionalities via gemini monomers was proposed by Li *et al*.[83] They chose a non-crystallization method to obtain two-dimensional synthetic polymers (2DSPs) via free radical co-polymerization of amphiphilic gemini monomers and their monomeric derivatives arranged in a bilayer at solid- liquid interfaces (Figure 1.9). Due to the mechanical strength of the resulting 2DSPs, multiple applications, such as nanolithographic resist and antibacterial agent, are possible. The simplicity of this strategy allows the preparation of 2DSPs with diverse functionality, well-controlled shape and size. Moreover, various materials with wide-ranging surface curvatures and dimensions can be used as a solid templates.

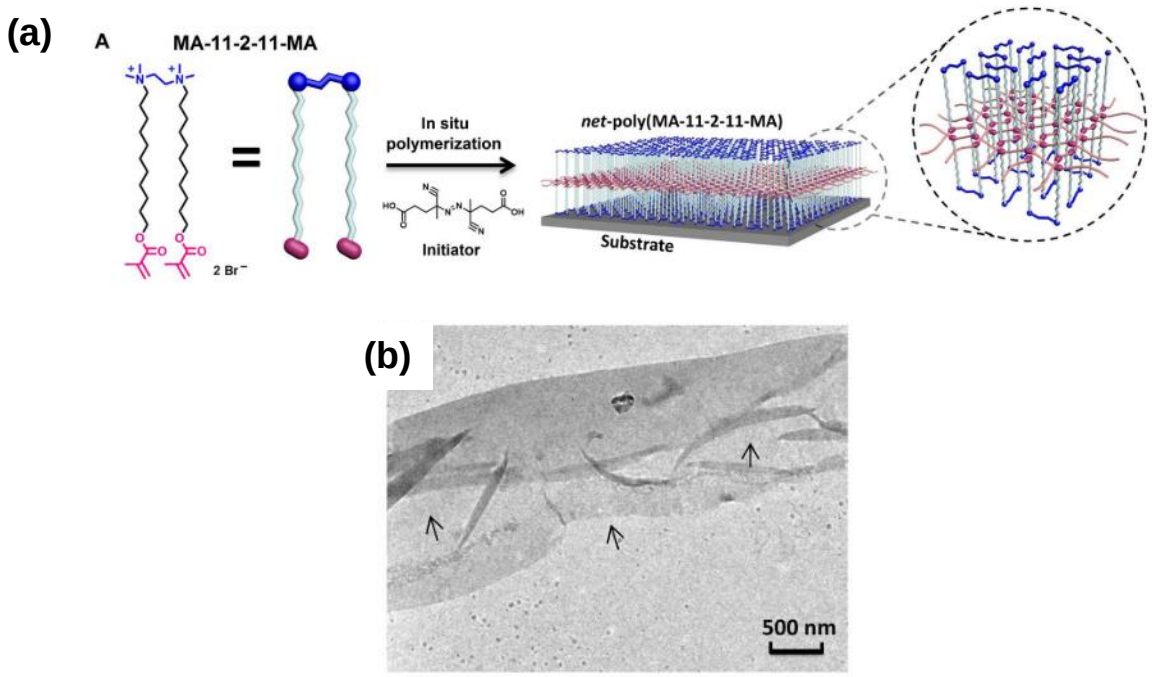

Figure 1.9. Preparation and characterization of 2Dnet-poly(MA-11-2-11-MA).(a) Schematic illustration of the molecular structure of gemini monomer MA-11-2-11-MAand 2Dnet-poly(MA-11-2-11-MA (b) TEM image of the freestanding film of 2Dnet-poly(MA-11-2-11-MA). Reprinted with permission from [83]. Copyright 2019 Science Advance.

1.4.2. Self-assembly of block-copolymers

Self-assembly is a spontaneous process, where structures assemble without guidance or influence of external forces.[84] Formed coordinate bonds are noncovalent interactions, such as van der Waals attractions, ion-paring interactions, hydrophobic/hydrophilic interactions, hydrogen bonding and p–p donor–acceptor interactions,[85] which are strong enough to hold amphiphilic molecules together and to provide their stability in solution. The strength of bonding and autonomy make this approach a promising way to form nanostructures[86] with a high degree of precision, due to the minimization of energy leading to the final state of assembly. Potentially, this could lead to fewer defects and more stable structures.[87,88]

One of the most studied synthetic system, which can undergo a self-assembly process, are the amorphous amphiphilic block copolymers (BCPs). They consist of chemically distinct blocks that are in most cases covalently bonded together and tend to phase separate instantaneously to form aggregates when exposed to a selective solvent that is good for one block but poor for the other.[89] The solvophilic corona-forming blocks are swollen by the selective solvent and stretched beyond their random coil conformation, whereas the solvophobic core-forming block is packed tightly within the core. Most commonly, the structures generated include spherical micelles, cylindrical micelles, vesicles and lamellae.[90]

When the core-forming block is crystalline, the self-assembly is driven by both solvophobic interaction and core-crystallization. The resulting morphologies are therefore a result of the balance between microphase separation and core-crystallization (Scheme 1.2). According to the theory of Vilgis and Halperin,[91] the insoluble, crystalline block undergoes phase separation to minimize contact with the poor solvent and crystallizes by adjacent chain folding within the core. Through this process, a sharp interface is formed, dividing the crystalline core from the solvent-swollen corona. The corona chains are grafted to the core and occupy the space permitted by the number of chain folds per crystalline block. The crystalline nature of the core-forming block favors the formation of 2D lamellas where the crystalline core is sandwiched between the solvated corona chains tethered on the flat interface of the lamellae.

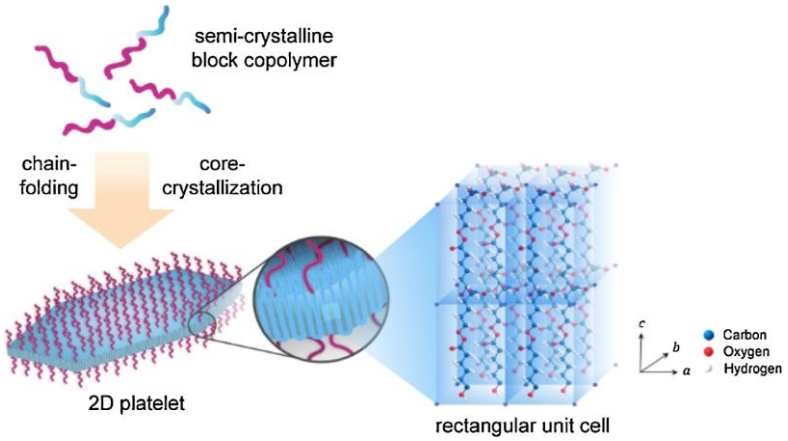

Scheme 1.2. General mechanism of the core-crystallization of a semi-crystalline block copolymer when a non-solvent is introduced. The colors blue and purple are used to depict the crystalline core and solvophilic corona respectively. In this process, chain-folding of the crystalline block takes place and forms a sharp interface that

divides the core and solvent-swollen corona to form 2D platelet structure. Reprinted with permission from[89]. Copyright 2020 Progress in Polymer Science.

The ability to form 2D nanoobjects of controlled size in solution was reported by Manners and Winnik and by Jiang and their respective co-workers by applying seeded growth (Figure 1.10) to form platelets[92] and nanosheets[93] by living crystallization driven self-assembly (CDSA). The main feature of living CDSA is, that in this process the ends of the growing micelles or crystals remain active to further epitaxial growth (analog to living covalent polymerization) by the sequential addition of BCPs with a common crystallizable core block[94,95] or different core blocks with a small lattice mismatch.[96] This approach to fabricate 2D systems can yield materials with potential applications in thermosets,[97] composites,[98,99] and as platforms for nanoparticles.[100–102]

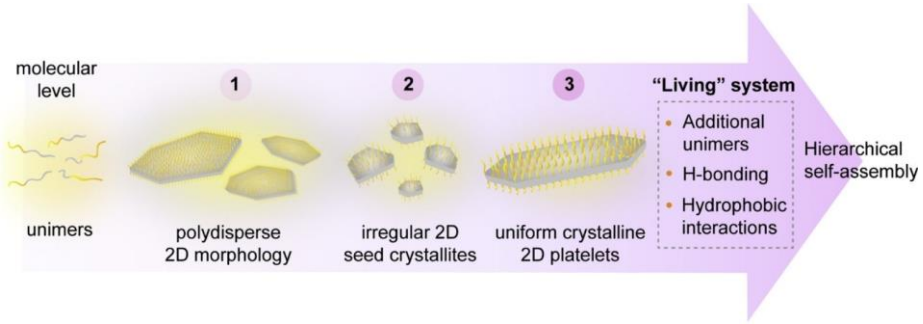

Figure 1.10. General synthetic pathway for the fabrication of uniform 2D platelet particles by seeded-growth method from semi-crystalline block copolymers in solution. A typical process involves (1) solvent-induced self (homogenous) nucleation, (2) sonication to form seeds, and (3) unimer addition. Reprinted with permission from[89]. Copyright 2020 Progress in Polymer Science.

In seeded growth approach short seed micelles with a crystalline core work as the initiation site for further epitaxial elongation. Jiang *et al*. fabricated polymer nanosheets using hyperbranched poly(ether amine) (hPEA) capped with heptaisobutyl polyhedral oligomeric silsesquioxane (POSS) groups by adding water as a selective solvent to a unimer solution of the material in 1,4-dioxane.[93] Using fragments of the nanosheets as seeds for further growth, 2D platelets with a low polydispersity and tunable size can be formed.

Self-assembly of BCP depends not only on parameters that define the crystallization of homopolymers, such as the molecular structure of the polymers, solvent condition,[103,104] concentration and temperature,[105] but also variations of block length and ratios between the soluble and insoluble blocks[105,106] lead to different shape of obtained 2D crystals.

In some cases, addition of a crystalline homopolymer has also been shown to drive morphological transition to yield crystalline platelets. Eisenberg and co-workers showed that by adding polycaprolactone (PCL) homopolymer during the self-assembly of PEO-*b*-PCL or PAA-*b*-PCL BCPs in water.[107,108] Incorporation of homopolymer into the core of initially formed spherical micelles resulted in morphological transformation to rods and micron-sized lamellae.[89]

Su *et al*. prepared well-defined anisotropic elongated lozenge-shaped platelets using CDSA BCP self-assembly approach from poly(2-vinylpyridine)$_{199}$-*b* -poly(ε-caprolactone)$_{310}$ BCP by the addition of water to a unimer solution in DMF.[109] Due to the differential growth rates of the crystal faces of the PCL homopolymer,

formation of crystals with a high aspect ratio occurs. The PCL-containing BCP keeps this shape and therefore the produced platelets also have a high aspect ratio. This ratio can be reduced by lowering the temperature to 10 °C, which is consistent with changes observed in PCL crystal formation at lower temperatures.

The role of the solvent as a shape-defining factor was demonstrated in the work of Pearce *et al.*, who formed 2D seeded crystals of poly(ferrocenyldimethylsilane) (PFS) homopolymers with hydrophilic ammonium moieties as stabilizing terminal group using the living crystallization-driven self-assembly method (Figure 1.11).[110] By changing either the solvent polarity of the seeded growth medium, the substituents on the charged terminal group or the characteristics of the seed micelle it is possible to control the aspect ratio of the resultant 2D platelets. The counter anion associated with the charge-terminated PFS[NMe_3]+homopolymers has a significant effect on the resulting morphology and colloidal stability of the resulting 2D platelets.

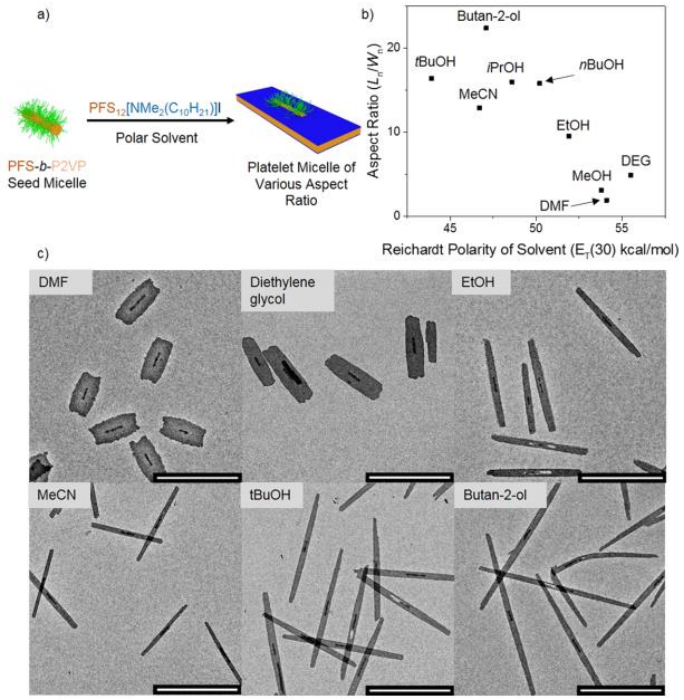

Figure 1.11. (a) Schematic depicting the seeded growth of $PFS_{12}[NMe_2(C_{10}H_{21})]I$ from PFS_{20}-*b*-$P2VP_{180}$ seed micelles (L_n= 260 nm and L_w/L_n= 1.04) in solvents of varying polarity. (b) Dependence of observed platelet aspect ratio (L_n/W_n) from the defined Reichardt polarity of solvent (ET(30) kcal/mol). (c) Bright-field TEM images, representing the influence of solvent on the shape of obtained 2D platelet micelles. m_{unimer}/m_{seed} = 10 for every experiment. Scale bars = 2000 nm. Reprinted with permission from[110]. Copyright 2019 Macromolecules.

The influence of different corona and core block lengths on the micelle morphologies was explored by Chen and co-workers.[101] They obtained ellipsoidal platelets using a range of poly(ε-caprolactone)-*b*-poly[2-(dimethylamino)ethyl methacrylate] (PCL-*b*-PDMAEMA) block copolymers by the addition of methanol to a unimer solution in THF at 25 °C. In this system, the crystalline core is composed by the PCL block and PDMAEMA forms the corona. BCPs with the shorter PDMAEMA block lengths and longer PCL blocks forms the most uniform platelets. Hexagonal shaped platelets were formed from longer PCL block, while the use of shorter PCL block leads to more lenticular geometry.

A similar effect was observed by Cha *et al*., who performed crystallization-driven self-assembly(CDSA) of metallo-polyelectrolyte block copolymers that contain cationic cobaltocenium amidoethyl methacrylate (PCoAE-MA) in the corona-forming block and polycaprolactone (PCL) as the crystallizable core-forming block (Scheme 1.3).[111] Electrostatic interactions originating between the cationic metalloblocks and crystallization of the PCL leads to the self-assembly of these amphiphilic block copolymers into two-dimensional platelet nanostructures in polar protic solvents. By varying the aspect ratio between the blocks, different 2D morphologies from elongated hexagons to diamonds can be obtained. The stability of these polymer 2D crystals to fragmentation depends on the ionic strength of the solution.

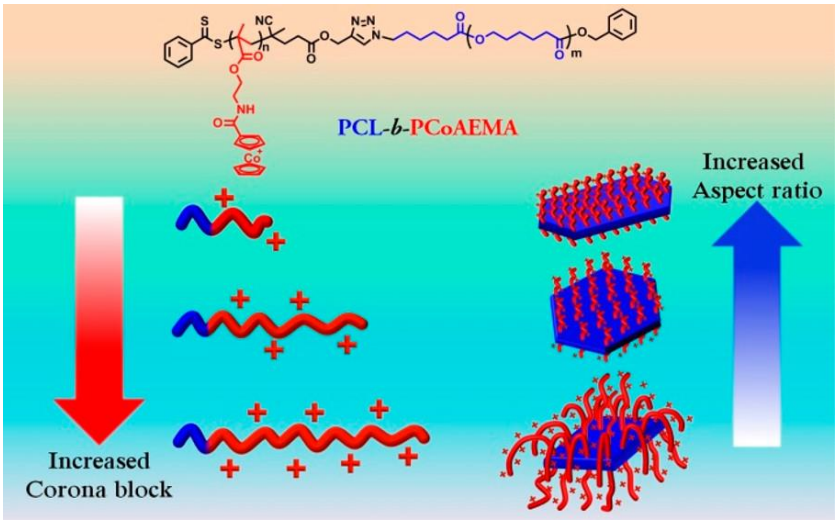

Scheme 1.3. Illustration of CDSA of PCL-*b*-PCoAEMA block copolymer to form different shape platelet nanostructures, depending on aspect ratio. Reprinted with permission from[111]. Copyright 2019 ACS Macro Letters.

The majority of BCPs with a short corona-forming block usually form planar structures by minimizing chain–chain repulsion and favoring lamellar over cylindrical morphologies,[106] but it is not a characteristic of all BCPs. Recently, it was shown that poly(ferrocenyldimethylsilane)-*b*-poly(2-vinylpyridine) (PFS-*b*-P2VP) BCPs with block ratios of 1:6 form narrow lenticular platelets rather than cylindrical micelles in the presence of THF, a common solvent for both blocks.[112] In this system, THF facilitates crystallization of the PFS core and favors the formation of lamellar platelet morphologies. Similar results were observed for PFS-*b*-P2VP BCPs, where initially formed spherical micelles transformed into lenticular platelets over time. Increasing the initial THF concentration higher than 30 % leads to an exclusive formation of platelets.[113]

The ability to spatially isolate functionality in 2D is also a very attractive target, but currently there are only a few reports on the preparation of multicompartment 2D nanostructures. In their work, Cheng *et al*. formed nanosheets with alternating rings of BCP and homopolymer by forming a poly(ethylene oxide)-*b*-polystyrene (PEO-*b*-PS) BCP single-crystal as seeds and subsequently adding PEO homopolymer and a “fresh portion” of BCP.[114] In 2013, Wooley *et al*. generated 2D structures with nanosegregated domains derived from the two BCPs using cooperative self-assembly of BCP blends.[115]

The seeded growth approach allows to create well-defined, low area dispersity 2D multicompartment structures with nanosegregated functionality. Experiments with platelet-forming PFS-based BCPs, PFS-b-

polyisoprene (PFS_{76}-*b*-PI_{76}), PFS-*b*-poly(dimethylsiloxane) (PFS_{114}-*b*-$PDMS_{81}$), and PFS-b-poly(methylvinylsiloxane) (PFS_{69}-*b*-$PMVS_{35}$) as short cylindrical crystallite seed micelles also showed that living CDSA can be used to form 2D structures. Obtained lenticular platelets had a low area polydispersity (<1.1) and a linear dependence with unimer-to-seed ratio, which indicates the living nature of the process.[92]

Recently, the fabrication of well-controlled and hierarchical colloidally stable PLLA-based diamond-shaped[116] or PFDMS-based rectangular structures,[117] including "patchy" platelet block co-micelles, was demonstrated (Figure 1.12). Seeded growth and living-crystallization-driven self-assembly processing approaches yields well-defined, low area dispersity two-dimensional (2D) structures. To bring a surface complexity into the system, the sequential addition of a different platelet-forming BCP with a common crystallizable part is needed. When the corona of the peripheral block in the 2D block co-micelles undergoes a cross-linking process, interior region can be dissolved in a good solvent, leading to the formation of novel, hollow assemblies.

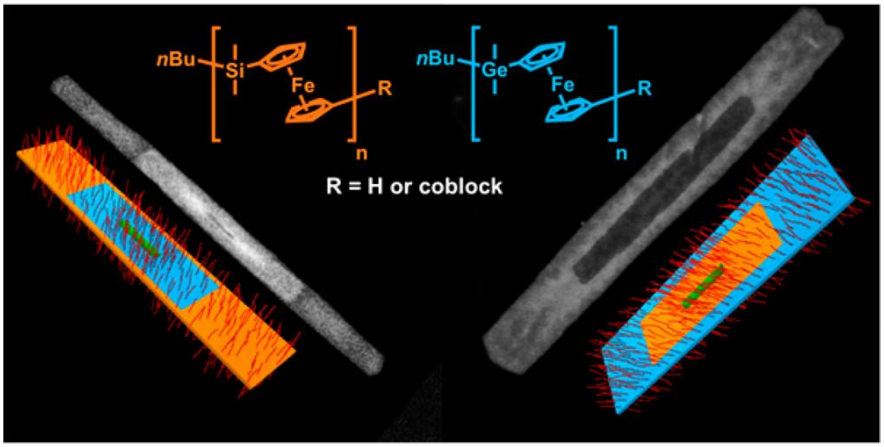

Figure 1.12. Schematic representation of "Patchy" platelet block comicelle formation by seeded heteroepitaxial growth of crystallizable polymer blends in two dimensions. Reprinted with permission from ref [117]. Copyright 2017 Journal of the American Chemical Society.

In 2017 Winnik and Manners went a step further and showed that the CDSA approach allows to have a control over both shape and surface functionality of block-copolymer 2D nanostructures.[118] These structures were obtained through seeded growth of phosphonium-terminated PFS homopolymers by 1D PFS-containing BCP 1D micelles. Thanks to electrostatic repulsion between the charged surfaces, which prevented stacking of crystalline lamellae, the obtained platelet structures were colloidally stable in solution. The shape of the initial seeds determines the shape of obtained 2D nanocrystals due to the memory effect. This leads to the formation of rectangular, diamond-shape or quasi-hexagonal disc-like platelets. Sequential addition of different PFS BCPs to seeds yields platelet block co-micelles with concentric regions of different coronal chemistry. Similar to previous work, spatially selective processing allows programmed disassembly and yield perforated or hollow rectangular morphologies.

1.4.3. Bio-based polymers

Besides synthetic polymer 2D materials, 2D organic biomaterials (2DOBM) based on the self-assembly of various biomolecules, including DNA,[119] RNA,[120] proteins,[121] peptides,[122] peptoids,[123] and other biopolymers,[124] also showed promising structures, functions, and applications.[125] A wide range of 2DOBM was produced *via* self-assembly processes, based on noncovalent interactions, such as hydrogen bonding, electrostatic interactions, hydrophobic interactions, π–π interactions, and van der Waals interactions.[126–128] The experimental conditions[129] and the chemical structure define the self-assembly process of 2DOBMs. The structure of 2DOBMs can be tailored from nanosheets to nanobelts, grids, films, membranes, arrays, and even 2D porous materials and the functions can be adjusted through further functionalization.

2DOBMs provide flexible structures and bio-functions, which promote their applications even beyond bio-related fields. Previously, peptoid nanosheets[130] and DNA origami[131] have been reported to be excellent building blocks for fabricating biosensors, 2D self-assembled amyloid peptide nanosheets have been reported as retrovirus carriers,[129] and tyrosine-based 2D peptide films have been used as molecularly tunable, self-repairable bio-catalytic platforms.[132] Also, 2DOBMs have exhibited potential applications in functional nanomaterials,[133] energy materials,[134] and environmental science.[135] For instance, DNA origami has been utilized as an effective light-harvesting system,[134] and self-assembled protein–carbon hybrid membranes have been applied for universal water purification.[135]

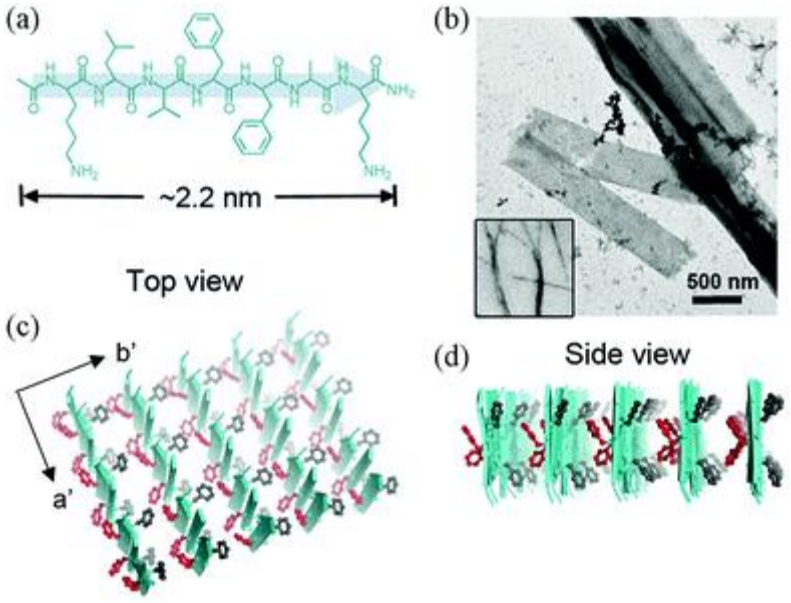

Figure 1.13. (a) Chemical structure of KLVFFAK. (b) TEM images of KLVFFAK nanosheets prepared from solution. Schematic model of the KLVFFAK nanosheet: (c) along the fibril axis and (d) along the zippering axis. Reprinted with permission from [129]. Copyright 2015 Proceedings of the National Academy of Science.

Self-assembly in solution is a straightforward and efficient strategy to form 2DOBMs. However, this process is highly sensitive to the molecular structure and solution conditions, such as concentration, type of solvent, temperature and pH.[129,136,137] It was demonstrated that biomaterials with one-dimensional 2D structures can be fabricated *via* molecular recognition and binding.[129,138,139] Dai *et al.* reported that the key amyloid-forming

segment (KLVFFAK) of Alzheimer's β-amyloid peptide (Aβ) could grow into amyloid nanosheets in sodium phosphate buffer.[129] In their study, the width of the formed nanosheets was over 200 nm and the thickness was determined to be 2.3 ± 0.2 nm. They found, that the peptide self-assembly was the major driving force in the antiparallel model by tuning the molecular structure of peptides (Figure 1.13). In addition, increasing concentration of NaCl or $MgCl_2$ leads to the thickening of the nanosheet from 0.2–0.4 to 0.6–1.0 μm. The reason for this is, that higher ionic strength prevents the repulsive interactions between the positively charged Lys–Lys contacts and thus improves the aggregation ability.

Various specific biomolecules can be used as building blocks for creating 2DOBMs, such as proteins, peptides, polymers and other biomolecules etc. The obtained 2DOBMs can be fine-tuned to yield nanostructures with tailored bio-functions.

Protein-based 2DOBMs. Protein–protein interactions and metal-coordination are efficient ways to facilitate the self-assembly of proteins into 2DOBMs. For example, Brodin *et al.* utilized a protein of Rosetta Interface Designed Cytochrome 3 (RIDC3) to self-assemble into 1D nanotubes and 2D nanosheets through Zn^{2+} and pH-coordination.[136,140] It was found that the morphology of the RIDC3-based self-assembled nanosheets depends on the concentration of Zn^{2+}, RIDC3 and the pH of the solution. In another study, Suzuki and co-workers found that the metal-mediated self-assembly of the C_4-symmetric L-rhamnulose-1-phosphate aldolase (RhuA) forms 2D protein lattices via metal-mediated biomolecular interactions.[10]

Peptide and peptoid 2DOBMs. Peptide- and peptoid-based polymers are attractive hybrid systems to design polymer-based 2DOBMs. Flood *et al.* designed peptoid nanosheets using an alternating pattern of ionic and hydrophobic monomers, which exhibited strong resistance to sound waves, freeze-drying and high organic solvent environments.[141,142] Zuckermann and co-workers demonstrated, that peptoid nanosheets can serve as scaffolds for molecular and protein recognition.[130,143] Hamley's group designed a novel aromatic dipeptoid by intermolecular π–π interactions for the fabrication of free-floating nanosheets in a water–acetonitrile mixture solution.[144] They designed diphenylalanine dipeptoid *via* capping the N terminal by acetic anhydride reaction on a resin (hereinafter reffered to as CapNFF). The subsequent assembly CapNFF in the mixture solution results in the formation of free-floating nanosheets. Nam *et al.* prepared free-floating 2D polymer nanosheets in solution by using two oppositely charged peptoid-based polymers.[123] Peptide-grafted hyperbranched polymer nanosheets, synthesized by Gao *et al.,* revealed prominent antibacterial properties.[145]

Polymer- or macromolecule-based 2DOBMs. Besides proteins, peptides and peptoids, other bio-based macromolecules can also form 2DOBMs. In the work of Vyborna *et al.* DNA-grafted supramolecular polymers (SPs) were designed by connecting a heptapyrenotide part with a DNA sequence *via* two different oligonucleotides.[146] Then the DNA-grafted SPs were self-assembled into nanoribbons. In a similar study, Yu *et al.* fabricated a 2D polymer network by using the self-assembly of a branched oligonucleotide that contained a benzene core, three identical arms and a photo-reactive anthracene.[147] Huang *et al.* reported the synthesis of a copolymer with poly-*para*-phenylene as backbone and poly(ethylene oxide) (PEO) as side chain, which can self-assemble into nanoribbons in THF-water solutions.[148] Li *et al.* fabricated collagen-like supramolecular nanofiber networks using 2-ureido-4[1*H*]-pyrimidone (UPy) modified glycerol molecule (UPy-Gly) by adjusting the pH in solution through π–π interactions and hydrogen bonding.[149]

An innovative direction to form 2DOBM by specific design of amino acid groups in peptides was proposed by Lin *et al.* In this study, the growth process to assemble peptide amphiphile F6C11 into free-standing nanosheets was thermodynamically driven and solution processable (Figure 1.14).[150] It was shown that absorption of enzymes enhanced the catalytic activity of the nanosheets. Utilization of the amino acids, particularly the aromatic groups, facilitates the β-sheet stacking.

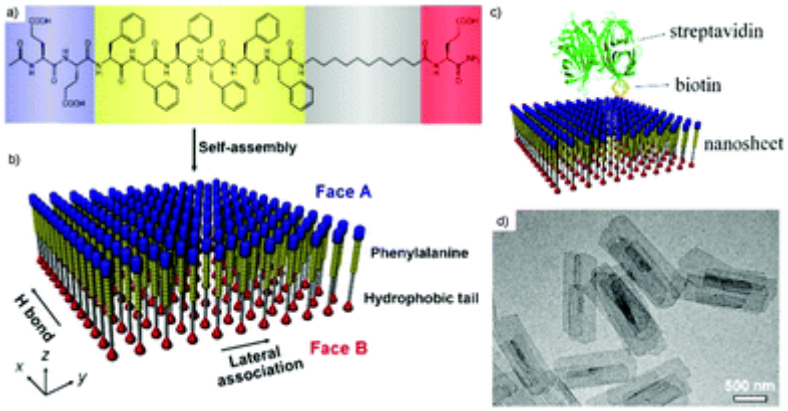

Figure 1.14. Molecular design and self-assembly of 2DOBMs. a) Schematic structure of the peptide amphiphile F6C11. b) Janus nanosheets obtained via self-assembly. (c) Adsorption of streptavidin on a nanosheet. (d) TEM image of biotin-displaying nanosheets. Reprinted with permission from ref. [150]. Copyright 2017 American Chemical Society.

Feng *et al*. used plant-derived materials to form polymer nanosheets with a high density of functional groups on the surface (Figure 1.15).[6] A supramolecular complex was created by attaching conjugated linoleic acid (CLA) moieties to a structure-directing tribasic aromatic core via hydrogen-bonding conjugates. The resulting structure self-assembles into a thermotropic, lamellar mesophase. Subsequent photo-cross-linking of the mesophase yields a polymeric material with tight connection of the lamellar mesophase structure. Extraction of the tribasic core and neutralization of the carboxyl groups by NaOH leads to the exfoliation of polymer nanosheets with a uniform thickness of ~3 nm and a large specific area decorated by negatively charged carboxylate groups. This strategy presents a way to fabricate 2D structures from renewable or sustainably derived materials via supramolecular self-assembly in a scalable manner.

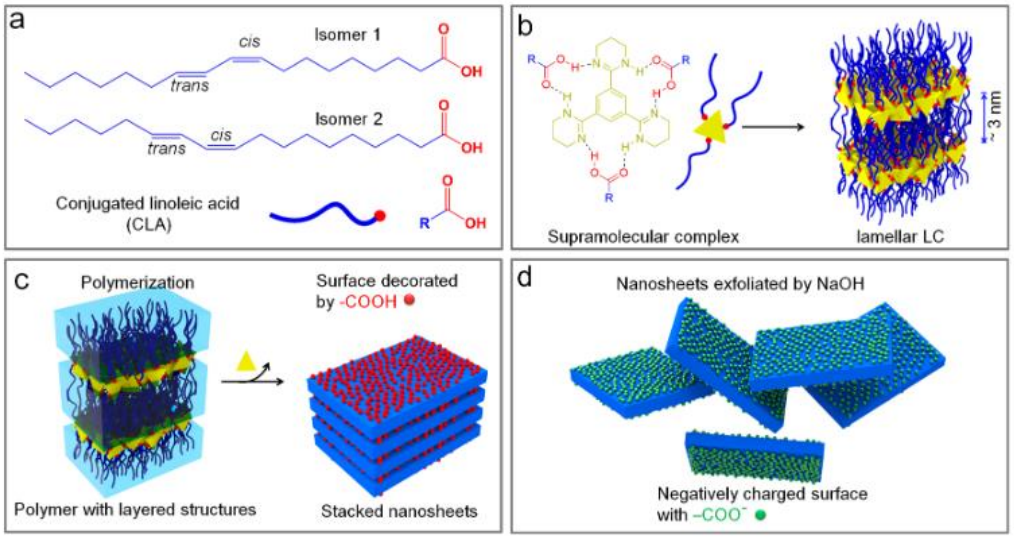

Figure 1.15. Preparation of polymer nanosheetes from vegetable oil-derived fatty acids. (a) Molecular structures of initial polymerizable octadecadienoic acids (CLA). (b) Formation of the lamellar mesophase from the supramolecular complex by hydrogen bonding between CLA and a template molecules. (c) Cross-linking polymerization of the lamellar mesophase to generate a polymer with layered nanostructures. Removing of the template molecules results in polymer nanosheets with surface-enriched−COOH groups. (d) Neutralization of carboxylic groups leads to formation of exfoliated polymer nanosheets with negatively charged surface. Reprinted with permission from[6]. Copyright 2017 Langmuir.

1.5. Conclusions and future outlook

The use of “bottom-up” synthetic approaches opens new ways to prepare 2D structures with nanometer-size thickness under mild synthetic conditions. These mild conditions are beneficial compared to the more popular methods using the “top-down” exfoliation strategy or to the often harsh reaction procedures during synthesis of inorganic materials with layered structures. The “bottom-up” approach allows not only to conduct all assembly processes in mild conditions in solution, but also to introduce homogeneous or segmented functionality into the resulting products. It is possible to form stable, free-standing 2D films in the absence of a dimension-confining template, moreover the obtained 2D structures have a high dimensional control over a large area.

Various small building blocks can be utilized for the construction of polymer 2D materials, including synthetic homopolymers, block copolymers and bio-based materials. That makes it possible to create an extensive variety of new 2D materials with interesting structural and physical properties that were previously inaccessible. A range of possible technological applications of functional 2D materials with enhanced structural control and complexity appears to offer promising opportunities for the future.

Nevertheless, all the methods for the production of 2D structures presented up to now only produce surfaces that are homogeneous in their functionalization or involve the use of complex block copolymer systems. A simple specific structuring of the surface with different functional groups could not be achieved with any of the

methods so far. This thesis presents a new platform for the fabrication of organic 2D nanoplatelets, which is based on the crystallization of polymers. The key element hereby is the crystallization of a polymer resulting in a lamellar polymer crystal – the 2D nanoplatelets. The dimension and surface functionality of the nanoplatelets can be adjusted versatile. In addition, the new method allows a structured surface functionalization with different functional groups for the first time.

2. Controlling the crystal structure of precisely spaced polyethylene-like polyphosphoesters

Tobias Haider,* Oksana Suraeva,* Miriam L. O'Duill, Julian Mars, Markus Mezger, Ingo Lieberwirth and Frederik R. Wurm

*These authors contributed equally

I was essentially responsible for the interpretation of the measurement results and based on this, I developed the model to explain the observed deviations from the theoretical values (Figure 2.7). I performed the controlled solution crystallization of the polymers and characterized their physical properties by SAXS, TEM and AFM, I also carried out the corresponding preparation of the samples for the physical measurements in bulk and supervised them. I wrote the part of the manuscript explaining the developed model with all values and deviations. Tobias Haider synthesized the "C30" and "C40" polymers. Hisaschi Tee synthesized the "C20" polymer. Julian Mars and Markus Mezger performed SAXS measurements of the polymers crystallized in bulk. Tobias Haider wrote the remaining parts of the manuscript.

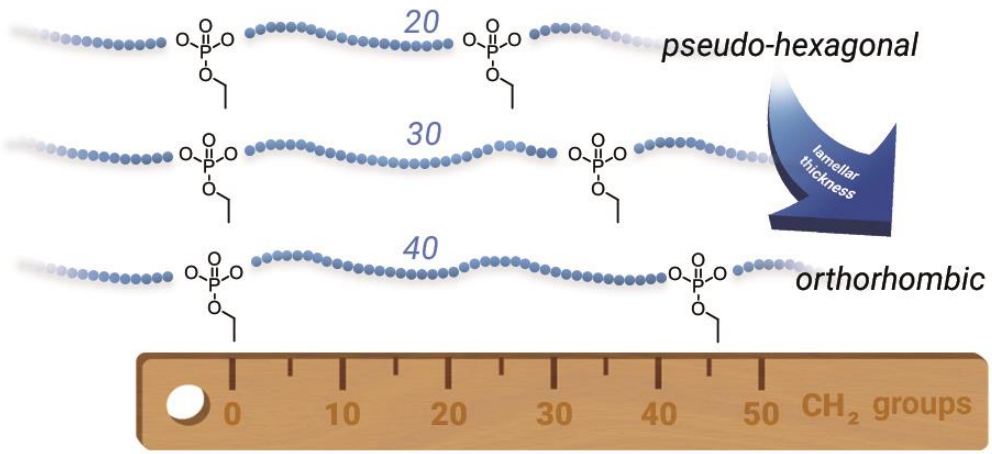

Keywords: polymer crystallization, crystal engineering, functional polymers, metathesis polymerization

2.1. Preface

In this chapter I will show the influence of the distance between the inserted defects on the properties of the polymer crystals. As shown in the chapter 1, we can engineer the polymer structure on the molecular level by introducing different “defects” in the polymer chain. This affects a number of properties, such as the melting point and the ability to undergo crystallization and it also introduces a functionality into the final composition. These changings depend on the nature and size of the incorporated groups and the frequency and equidistance of their distribution. This chapter concentrates on the frequency of included groups and how this parameter influences the properties and behavior of the polymer.

First, to evaluate the contribution of the length of aliphatic part between the defects, it is necessary to achieve equidistant distribution of them along the polymer chain. One of the most convenient ways to accomplish this is acyclic diene metathesis (ADMET) polymerization, developed by Wagener.[18] The main idea behind this method is, that monomers with a functional group in the middle and identical aliphatic parts with double bonds on the ends undergo metathesis reaction. As a result, the length of aliphatic part doubles and the functional groups are arranged equidistantly along the main chain.

Now, using ADMET as a tool to control the precision of inserted groups, we were changing distance between them. Three polymers with 20, 30 and 40 CH_2 groups between the inserted phosphate groups were synthesized. These defects are too bulky to be included in the crystal lattice during crystallization. Therefore, they are pushed out to the basal surface of polymer crystal and thus the length of aliphatic part between them determines the thickness of obtained 2D crystal. Combination of different characterization techniques, as TEM, AFM and SAXD showed perfect correlation between both crystal and lamellar thickness and the number of CH_2 groups between defects. Moreover, changing the distance between phosphate groups cause also the formation of different crystal structures. The polymer with 40 CH_2 groups reveals orthorhombic structure, similar to pure polyethylene and the reduction of the aliphatic segment leads to the formation of a pseudo-hexagonal crystal system.

In summary, we show that by varying just the number of CH_2 groups between the defects, it is possible to adjust the thickness of the obtained 2D crystals and change their crystal structure. In the following chapters I will show, how to form 2D polymer crystals with functional groups and how the choice of included groups together with the determined length of the aliphatic part define the properties and the possible applications of the final material.

2.2. Abstract

Understanding polymer crystallization is important for polyethylene-like materials. A small fraction of monomers with functional groups within the polyethylene chain can act as crystallization “defects”. Such defects can be used to control the crystallization behavior in bulk and to generate functional anisotropic polymer crystals if crystallized from a dilute solution. Due to their geometry, phosphate groups cannot be incorporated in the polyethylene lamellae and thus control chain folding and crystal morphology. Herein, the synthesis and crystallization behavior for three different long-chain polyphosphates with a precise spacing of 20, 30, and 40 CH2-groups between each phosphate group are reported. Monomers were prepared by esterification of ethyl dichlorophosphate with respective tailor-made unsaturated alcohols. Acyclic diene metathesis (ADMET) polymerization and subsequent hydrogenation were used to receive polyethylene-like polyphosphoesters with molecular weights up 23 100 g mol−1. Polymer crystallization was studied from the melt and dilute solution. Samples were characterized by differential scanning calorimetry (DSC), small-angle X-ray scattering (SAXS), wide-angle X-ray scattering (WAXS), transmission electron microscopy (TEM), and atomic force microscopy (AFM). A change in crystal structure from pseudo-hexagonal to orthorhombic was observed from the “C20” to the “C40” polymer. Melting points and lamellar thicknesses increased with the length of the aliphatic spacer from 51 °C (“C20”) to 62 °C (“C30”) and 91 °C (“C40”). Values for the long periods in bulk (3.1 nm for C20, 4.8 nm for C30, and 7.2 nm for C40) obtained by SAXS and TEM are in qualitative agreement. The thickness of the crystalline part obtained by AFM and TEM increased from about 1.0 nm (C20) to 2.0 nm (C30) to 2.9 nm (C40). Our systematic library of long-chain polyphosphates will allow designing anisotropic polymer colloids by crystallization from solution as functional and versatile colloid platform.

2.3. Introduction

Semi-crystalline polymers make up more than 50% of all commodity polymers consumed, with polyethylene (PE) being the most produced synthetic polymer today.[151] Tailoring the crystallinity as well as the size and shape of crystallites in polyethylene enables new possible applications. With so-called “defect engineering”, the crystallization of PE can be controlled by the synthesis of PE-derivatives with crystallization defects, *i.e.* side chains or bulky functional groups. Such “defects” can also be used for further chemical functionalization. Polymerization techniques that facilitate a precise distribution of the crystallization defects in the polymer backbone allow control over the crystal morphology including *e.g.* the lamellar thickness of the PE crystallites. Following this “defect engineering” approach, we present PE-like polyphosphates with distinctive spacing between the phosphate groups and elucidate the effect of the spacer length on the crystal structure and morphology of solution-grown polymer platelets and bulk-crystallized polymer crystals.

The crystallization of PE results from the van-der-Waals forces between parallel ordered aliphatic polymer chains and yields lamellar crystals. Finally, these lamellae arrange to larger structures and form spherulites.[152] Overall, PE crystallizes in an orthorhombic crystal structure.[153] Side-chains or additional functional groups along the polymer backbone can affect the crystallization: any bulky alkyl side groups (*e.g.* branching in low-density polyethylene (LDPE) and linear low-density polyethylene (LLDPE)) might be expelled from the crystalline to the amorphous phase, reducing the overall crystallinity.[154] At the same time, a high branch content

reduces the thickness of the lamellae, resulting in lower melting points compared to defect-free, linear PE.[155] The influence of branch length and the distribution of branching on the polymer chain on the overall crystal structure of precisely branched polyethylene have been studied by the group of Wagener.[17,18,74,156–159]

In contrast, functional groups incorporated into polyethylene can add new properties to the material: for instance, Mecking *et al.* recently reported ion-conducting PE-like polymers based on a sulfonate bearing polyester[160] and a telechelic polyethylene with terminal carboxylic acids,[161] respectively. Also, degradable PE mimics based on long-chain polyacetals[162,163] and polyorthoesters[164] had been reported. Different polymerization techniques enable the synthesis of PE-like polymers containing functional groups: long-chain polyesters, for instance, were obtained by polyesterification,[76,165] ring-opening metathesis copolymerization,[166] and acyclic diene metathesis (ADMET) polymerization.[167] In this work, we used ADMET polymerization, a polycondensation, which uses α,ω-dienes to produce linear polymers and allows the installation of precise branches or other functionalities in PE-like materials.[18]

As mentioned above, functional groups act as crystallization defects in the polyethylene chain, which can be used to control the thickness of the crystal lamellae. Whether the defects are incorporated in the lamellar crystal segment or not depends on the size and the flexibility of the functional group. Fan *et al.* reported that the crystal structure of polyethylene derivatives with aryl ether defects in the main chain (with a precise spacing of 20 CH_2 groups between each defect) was determined by the substitution pattern on the aromatic ring.[168] For *ortho*-substituted polymers, the aromatic crystallization defects were urged into the amorphous phase, while the defect in the *para*-substituted polymer was incorporated into the crystal with a remaining orthorhombic crystal structure like polyethylene. Similarly, poly(1,3-adamantylene alkylene)s synthesized by ADMET polymerization also crystallized in an orthorhombic crystal structure.[169] Due to the rigid adamantane defect, the black-folding of the polymer chain at adjacent reentry sites of the crystal lamellae is sterically impossible. In contrast, our group previously investigated the crystallization behavior of two different polyphosphates bearing a methyl and a phenyl side chain.[170] All bonds in the phosphate group are flexible, thus only the size of the defect had an impact on crystallization. The phosphate group with a methyl side chain was incorporated into the polymer crystal, which was not the case for the polyphosphate with a bulky phenyl side chain. Polyphosphates are potentially enzymatically degradable and enable further functionalization trough variation of the side chain.[171] Similarly to long-chain polyesters, long-chain polyphosphates were synthesized by ADMET, ring-opening metathesis (ROMP) polymerization or polytransesterification.[24,172] Due to the formation of pyrophosphate groups in side-reactions during the polytransesterification, we used ADMET polymerization as a reliable technique that provides a precise spacing between the phosphate groups.

Here, we present the synthesis of three PE-like polyphosphates with precise alkyl spacing of 20, 30, and 40 CH_2-units between each phosphate group. The phosphate groups are intended to act as crystallization defects, as they are expected to be expelled of the crystal lamellae. Thus, differences in *e.g.* lamellar thickness are expected to only rely on the length of the aliphatic spacer. We examined their influence on the thermal properties of the synthesized polymers by differential scanning calorimetry (DSC). Crystal structures and morphologies of the bulk polymers and solution-grown polymer platelets were determined by WAXS, SAXS, TEM, and AFM. The synthesized precise PE-like polyphosphates could, for example, represent a modular platform for anisotropic colloids with functional surfaces.

2.4. Results and discussion

Monomer synthesis, ADMET polymerization and hydrogenation

To vary the distance between the phosphate groups in PE-like materials, three α,ω-diene monomers were synthesized by esterification of ethyl dichlorophosphate with linear unsaturated alcohols containing a terminal double bond and a different number of methylene groups (Scheme 2.1). The chain length of the alcohol determines the spacer length between two phosphate groups in the polymer. For example, the polymerization of monomer **1**[173] with 22 carbons gives the "C20 polymer". In this way, polymers with a precise spacing of 20, 30, and 40 CH_2-groups between each phosphate group were prepared.

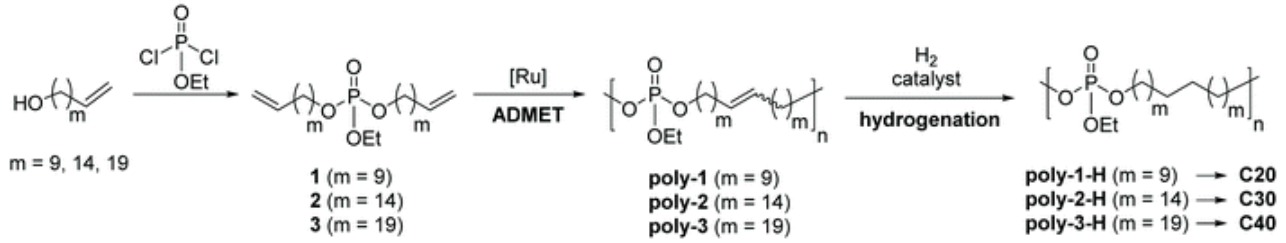

Scheme 2.1. Synthesis of phosphate diene monomers and their ADMET polymerization and hydrogenation.

ADMET polymerization was carried out with 1st generation Grubbs catalyst. In order to obtain high precision polymers with defined spacing between two defect groups, the 1st generation Grubbs catalyst is beneficial to the more reactive 2nd generation Grubbs catalyst and the Hoveyda–Grubbs catalysts, as it disfavors olefin isomerization.[174] Still, olefin isomerization can occur at elevated temperatures while using 1st generation Grubbs catalyst,[175] so care was taken to never exceed 85 °C during polymerization. Monomer **1** was polymerized in bulk at 65 to 85 °C for 48 h at reduced pressure to remove evolving ethylene. In contrast, ADMET polymerization of monomers **2** and **3** was carried out for 48 h in solution with 1-chloronaphthalene as a high-boiling solvent to enable agitation during the polymerization. The amount of solvent was kept low (concentration of polymer *ca.* 750 mg mL^{-1}) to prevent cyclization.[176] The obtained honey-like C20 polymer, **poly(1)**, revealed an apparent molecular weight M_w of *ca.* 23 100 g mol^{-1} (by SEC, M_w/M_n = 2.5). Both polymers **poly(2)** and **poly(3)** had a waxy appearance and apparent M_ws of *ca.* 15 400 and 12 100 g mol^{-1}, respectively (Table 2.1). In the ^1H NMR spectra, the resonances of the terminal olefins at 5.8 and 4.9 ppm vanished (**Figure 2.1**, **Figure 2.2**, **Figure *2.3*** top and middle) and new signals at 5.4 ppm were detected, which were assigned to the internal double bonds of the polymer.

Table 2.1. Long-chain polyphosphates by ADMET polymerization prepared in this study

Polymer	No. of CH_2 groups	M_n[a]/g mol^{-1}	M_w[a]/g mol^{-1}	M_w/M_n[a]	T_g[b]/°C	T_m[b]/°C	ΔH[b]/J g^{-1}	Crystallinity[c]/%
poly(1)	20	9300	23 100	2.5	−61	14	−35	n.d.
poly(2)	30	6000	15 400	2.6	n.d.	n.d.	n.d.	n.d.
poly(3)	40	4500	12 100	2.7	n.d.	n.d.	n.d.	n.d.
poly(1)-H	20	9900	23 100	2.3	−47	51	−71	24
poly(2)-H	30	5900	15 200	2.6	−39	62	−105	36
poly(3)-H	40	n.d.[d]	n.d.[d]	n.d.[d]	−38	91	−119	41

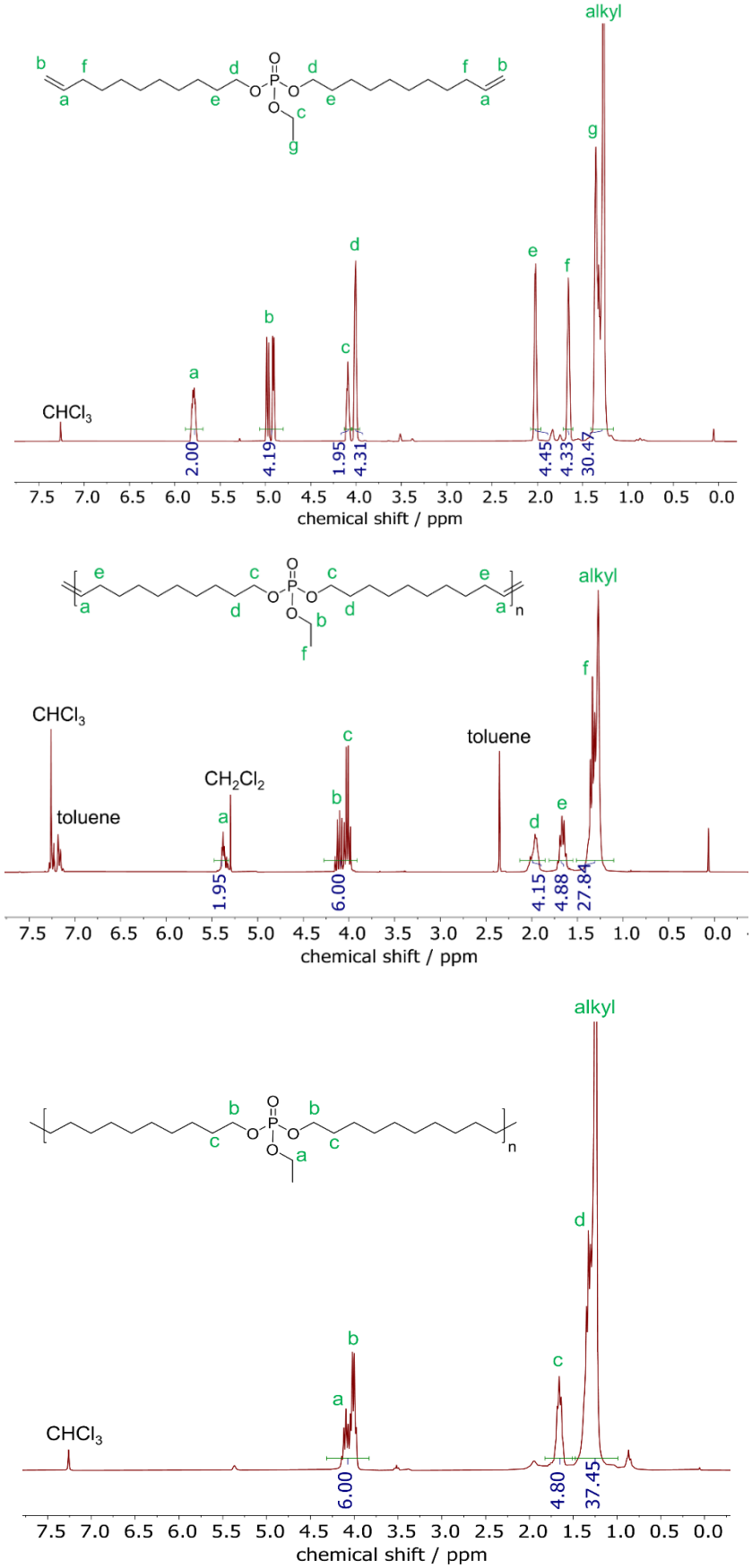

Figure 2.1. ^{1}H NMR spectrum of **1** (top), **poly(1)** (middle) and **poly(1)-H** (bottom) in $CDCl_3$ at 300 MHz at 298 K.

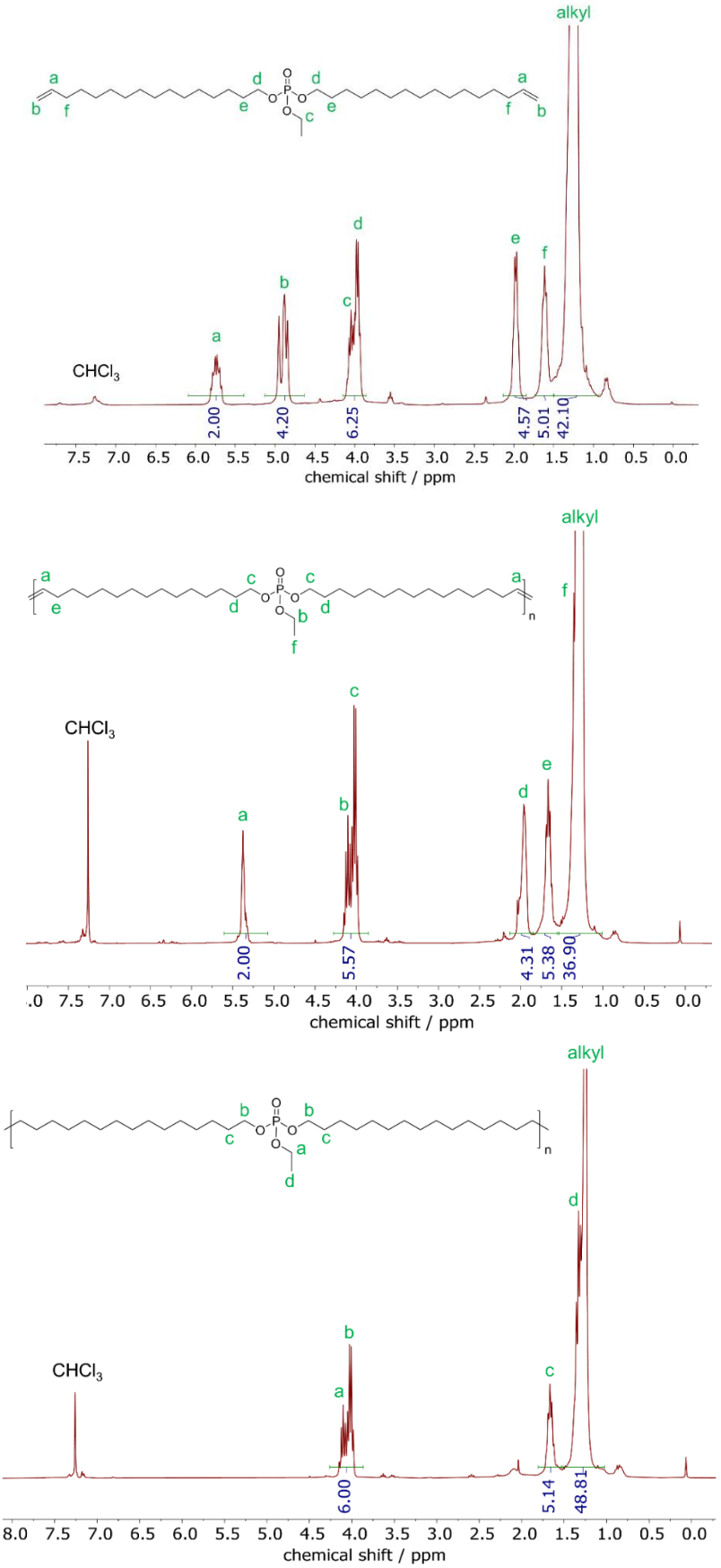

Figure 2.2. ^{1}H NMR spectrum of 2(top), **poly(2)** (middle) **and poly(2)-H** (bottom) in $CDCl_3$ at 300 MHz at 298 K.

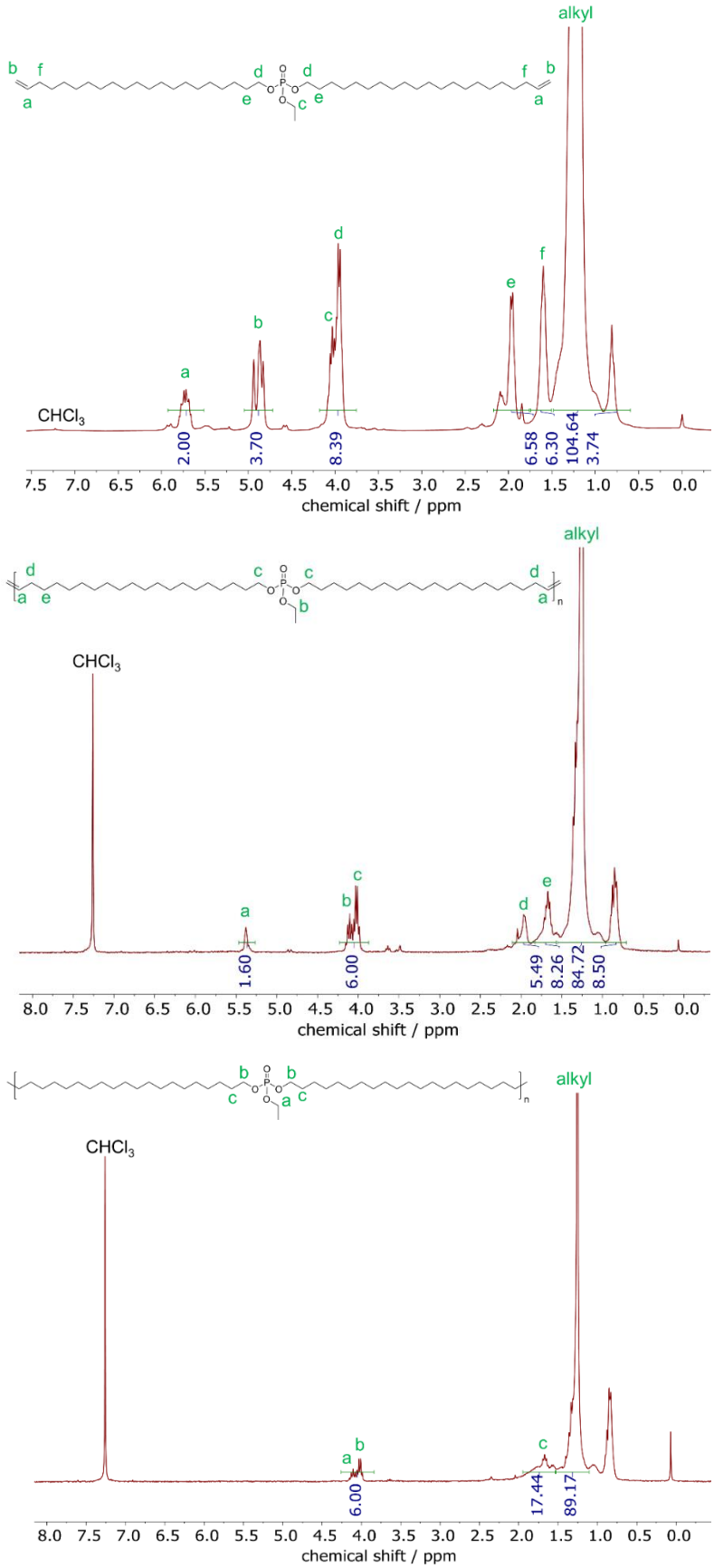

Figure 2.3. ^{1}H NMR spectrum of **3** (top), **poly(3)** (middle) and **poly(3)-H** (bottom) in $CDCl_3$ at 300 MHz at 298 K.

To obtain PE-like materials, we performed hydrogenation of the polymers with either Pd/C or the Fischer carbene derivative of Grubbs catalyst 1st generation.[177] The disappearance of the double bond signal at 5.4 ppm in the ^{1}H NMR spectra after the reaction confirmed the complete hydrogenation of the polymers **Figure 2.1**, **Figure 2.2**, **Figure *2.3*** bottom). For **poly(3)-H**, a signal at 0.9 ppm in the range of $-CH_3$ groups is detectable, most likely indicating the presence of ethyl dihenicosyl phosphate, a side product during monomer synthesis. Molecular weights of **poly(1)-H** and **poly(2)-H** were determined by SEC in THF *vs.* polystyrene standards and are following the values of the respective unsaturated polymers (**Figure 2.4**). SEC measurements of **poly(2)-H and poly(3)-H** in THF were not possible due to the insolubility of the hydrogenated polymer in the solvent for SEC.

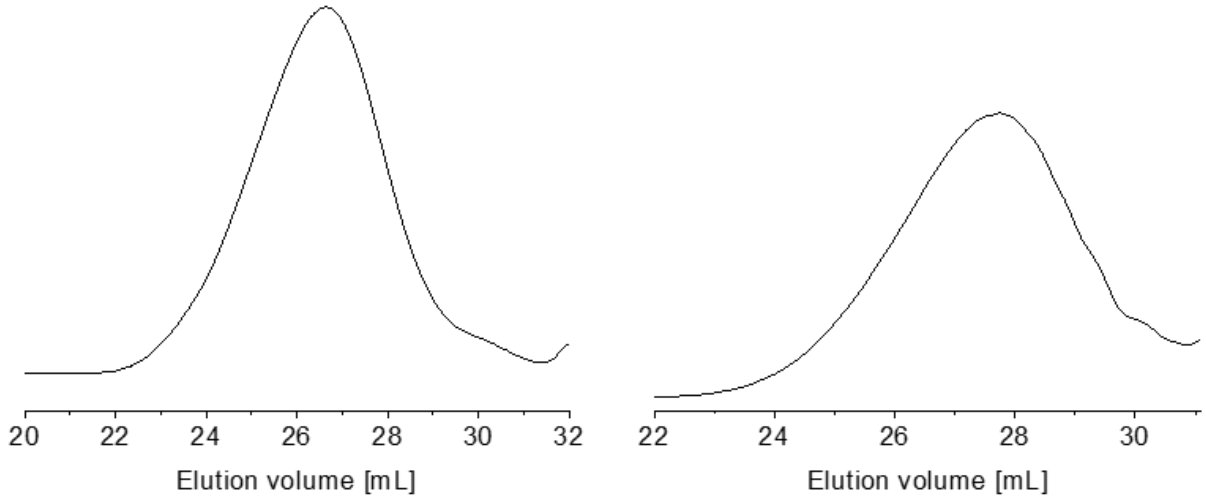

Figure 2.4. SEC elugrams of **poly(2)** (left) and **poly(3)** (right) in THF

Solid-state characterization

In contrast to the oily or waxy unsaturated polymers, all hydrogenated polymers were solid at room temperature. All polymers showed a brittle deformation behavior and with an increasing length of the aliphatic spacer, the polymeric materials became harder. By differential scanning calorimetry (DSC), the melting points and the crystallinity of polymers **poly(1)-H** to **poly(3)-H** were determined. Theoretically, the lamellae thickness of the PE-like crystallite is expected to increase with an increase in the length of the aliphatic chain (equals a decrease in the number of crystallization defects) resulting in higher melting points according to the Gibbs–Thompson equation. As expected, the melting points increased from 51 °C for **poly(1)-H** to 62 °C for **poly(2)-H** up to 91 °C (**poly(3)-H**) (Figure 2.5. DSC thermograms of poly(1)-H (left), poly(***2)-H*** *(middle) and* ***poly(3)-H*** *(right) (*exo *up, heating and cooling rate 10 K min^{-1} (second run)).* At the same time, the melting enthalpies ΔH_m increased from −71 to −105 and −119 J g^{-1} (Table 2.1). By comparing ΔH_m to ΔH of theoretical 100% crystalline polyethylene (ΔH_m = 293 J g^{-1}), the crystallinity of the synthesized polymers was estimated.[178] Values for the semi-crystalline polyphosphates ranged from 24% to 41% (Table 2.1). Glass transition temperatures (T_g) were below room temperature, ranging from −47 °C to −38 °C. In the DSC thermogram of **poly(3)-H**, an additional melting process at 80.5 °C was visible, which overlapped with the main melting peak

at 91 °C. The pre-melting peak might be explained either by the presence of polymorphism or by co-crystallization of long-chain impurities that could not be entirely removed during monomer synthesis and polymer work-up. Additionally, melting and recrystallization cannot be excluded as a reason for the additional melting peak. In general, the melting endotherms broadened from the C20 to the C40 polymer, indicating a larger distribution in crystallite sizes for **poly(3)-H** and **poly(2)-H** compared to **poly(1)-H**. This may be explained by an increasing molar mass distribution from C20 to C40 as well as a decreasing weight average molecular weight (M_w).

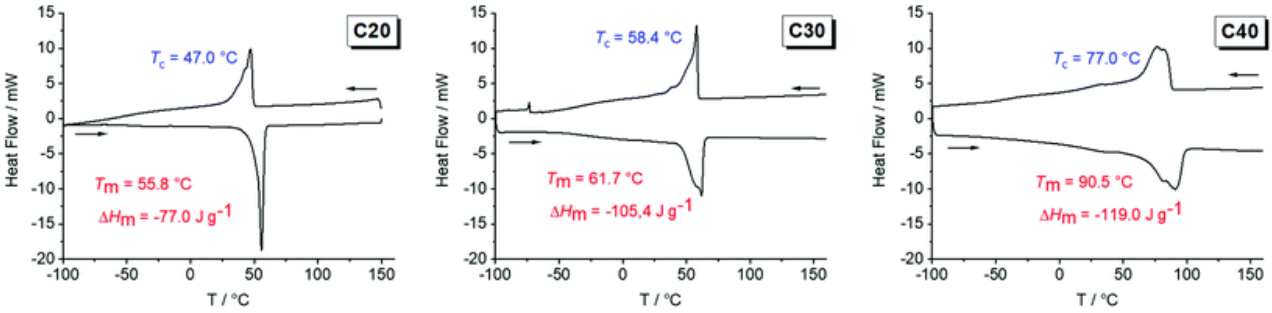

Figure 2.5. DSC thermograms of **poly(1)-H** (left), **poly(2)-H** (middle) and **poly(3)-H** (right) (*exo* up, heating and cooling rate 10 K min^{-1} (second run)).

The crystal morphologies of the polyphosphates were investigated by wide and small-angle X-ray scattering, atomic force microscopy, and transmission electron microscopy. Scheme 2.2 summarizes the information which is provided by each method. As all hydrogenated polyphosphates were party crystalline, the bulk material consists of crystalline and an amorphous regions. Both, solution-grown and melt-grown crystals were studied. By SAXS and TEM the thickness of the long period, including both regions, can be determined from the melt-crystallized polymers. The thickness of the lamellar crystal can be obtained by AFM (solution-grown crystals) and TEM (melt-grown crystals), while the crystal structure within the lamellae is measured by WAXS (melt-grown crystals), yielding the lattice constants.

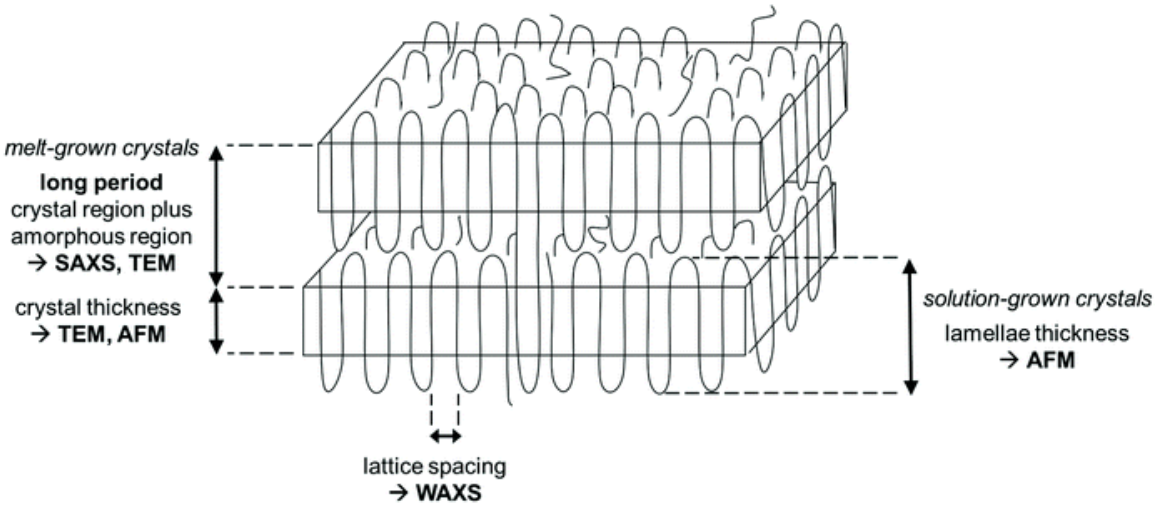

Scheme 2.2. General schematic representation of polymer crystallization and information about the morphologies of semi-crystalline polymers in the bulk or of solution-grown crystals obtained by SAXS, WAXS, AFM, and TEM.

To investigate the crystal structure of the different polymers, X-ray diffraction (XRD) measurements were performed. The WAXS patterns indicated a change in the crystal structure, as the length of the aliphatic spacer was increased (Figure 2.6). The XRD diffractogram of **poly(1)-H** revealed a single peak at 21.5°, confirming a pseudo-hexagonal crystal structure.[179] In contrast, the crystal structure of **poly(3)-H** was found to be orthorhombic with two distinct reflections at 21.6° and 23.8°, similar to linear polyethylene.[180] For **poly(2)-H**, two overlapping reflections at 21.2° and 23.1° indicate a transition from the pseudo-hexagonal and the orthorhombic crystal structure. Comparing the different polymers, the intensity of the amorphous halo increases with the number of defects in the polyethylene chain from **poly(3)-H** to **poly(1)-H**, which is in agreement with the literature.[155]

SAXS measurements show peaks at scattering vectors of 2.05, 1.27, and 0.87 nm^{-1} for the polymers with 20, 30, and 40 CH_2, respectively (Figure 2.6B). Values for the long period $D = 2pi/q_0$ were estimated from the scattering vector q_0 at the peak maximum. For the polymers **poly(1)-H** with 20 CH_2 groups and **poly(3)-H** with 40 CH_2-groups, the long period was 3.1 nm and 7.2 nm, respectively. In combination with the crystallinity extracted from the DSC data, the crystal thickness can be calculated from the long period obtained from SAXS (Table 2.2). Additionally, the topography of solution-grown crystals was measured by AFM. From these measurements, the lamellar thickness was extracted, yielding thicknesses of 3.6 nm for **poly(1)-H** (20 CH_2), 4.9 nm for **poly(2)-H**, and 7.0 nm for **poly(3)-H**. Remarkably, these thicknesses of solution-growth polymers correlate well with the long period of bulk polymers obtained by SAXS (Figure 2.7).

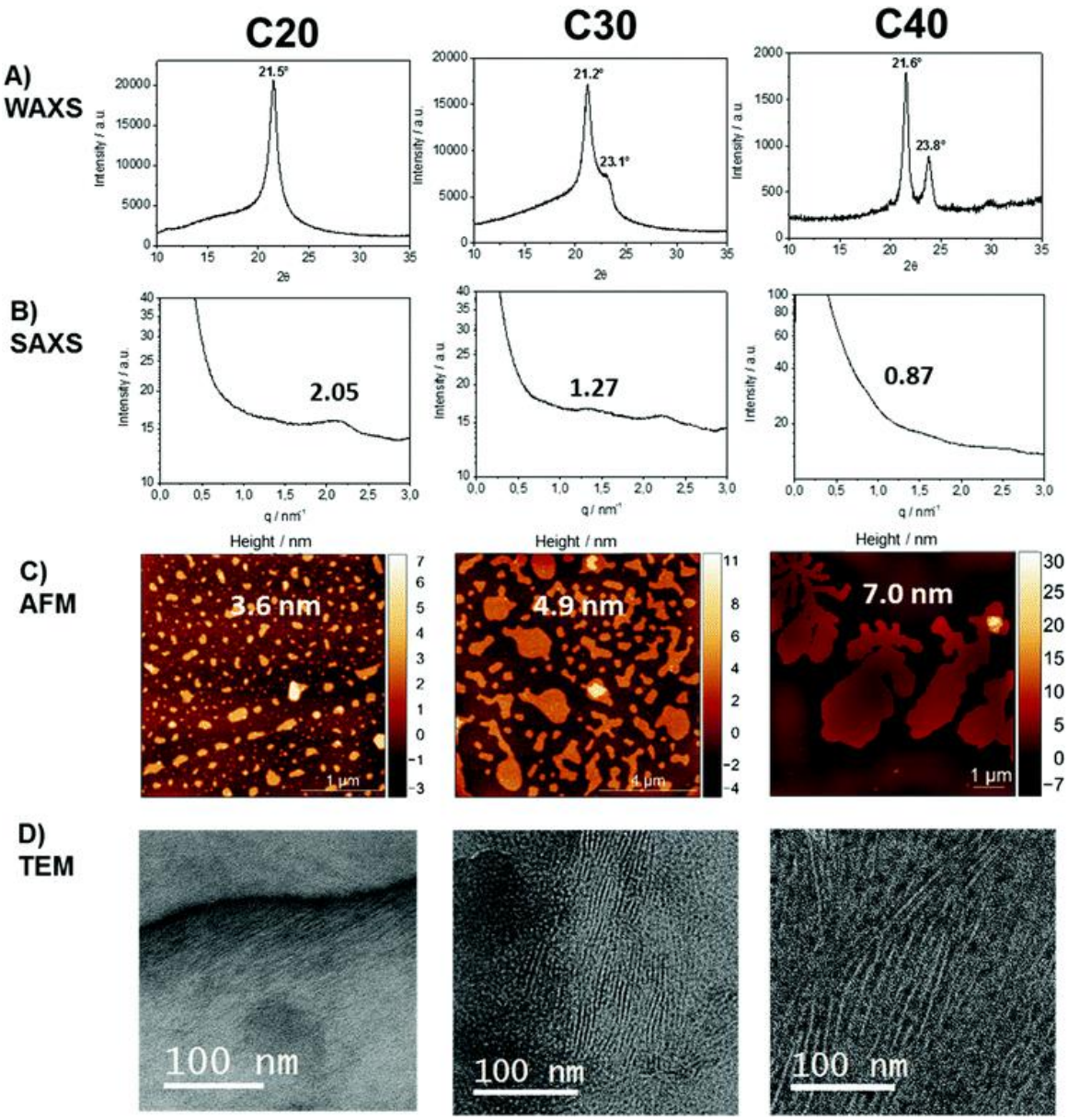

Figure 2.6. Solid-state characterization of polyethylene-like PPEs. (A) Wide and (B) small X-ray diffractograms; (C) atomic force microscopy images; (D) and corresponding lamellar morphologies visualized by TEM of **poly(7)-H** (left), **poly(8)-H** (middle) and **poly(9)-H** (right). The micrographs display a cross-section perpendicular to the lamellae, so the crystal- and amorphous thickness of the crystals is visualized. WAXS, SAXS, and TEM data were obtained from bulk polymer samples, AFM measurement from solution-grown crystals.

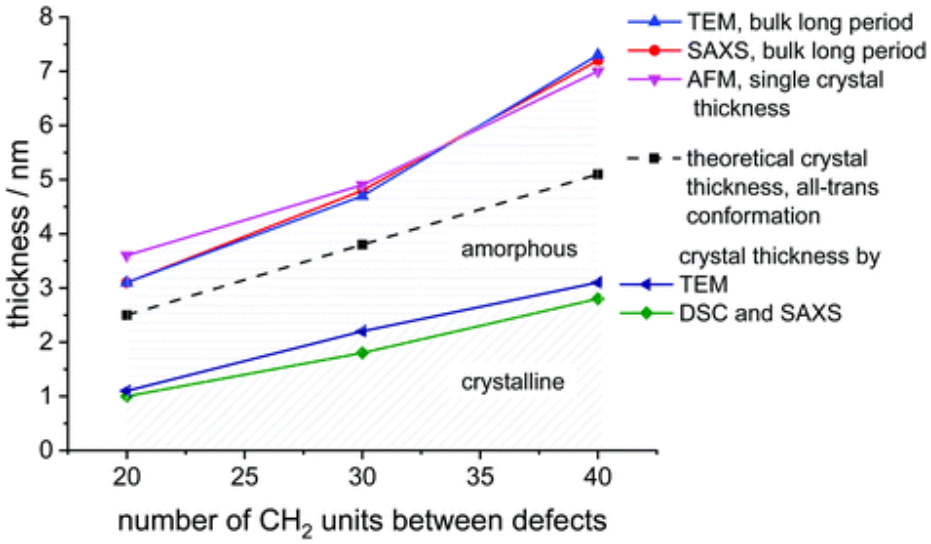

Figure 2.7. Graphical representation of crystal parameters for PE-like PPEs determined by different methods (data listed in Table 2.2).

Table 2.2. Thickness of polymer lamellae of solution-grown polymer platelets and bulk polyphosphates with varying distance between the phosphate groups determined by wide and small X-ray diffractograms, AFM, and TEM (values in nm)

Method	C20	C30	C40
Theoretical crystal thickness All-trans formation, nm	2.5	3.8	5.1
SAXS Bulk long period, nm	3.1	4.8	7.2
TEM Bulk long period, nm	3.1	4.7	7.3
AFM Single crystals thickness, nm	3.6	4.9	7.0
Thickness of crystalline part from **DSC** and **SAXS**, nm	1.0	1.8	2.8
Thickness of crystalline part from **TEM**, nm	1.1	2.2	3.1

In order to visualize the lamellar structure of the different polymers, additional TEM examinations have been performed (Figure 2.6D). Here, the bulk crystallized polymer was sectioned to achieve a cross-section perpendicular to the crystals. Due to the RuO_4 staining, the amorphous regions show a darker contrast compared to the crystal region. The micrographs allow determining the crystal thickness as well as the long period. All values obtained by WAXS, SAXS, AFM, and TEM measurements (Figure 2.6) are listed in Table 2.2. Theoretically, a fully crystalline polyethylene segment of 20 CH_2 groups in an all-trans conformation would have a length of 2.5 nm. Accordingly, 30 CH_2 groups stretch to 3.8 nm and 40 CH_2 groups to 5.1 nm. The theoretical crystal thickness is displayed in Figure 2.7 (dashed line). TEM measurements of stained sections of annealed polymer samples provided the crystal thickness for the bulk crystallization with 1.1, 2.2, and 3.1 nm for polymers with 20, 30, and 40 CH_2-groups, respectively. As these values are lower than the theoretical numbers, it is likely that despite some incorporated defects, also a considerable part of the CH_2-groups was necessary for the formation of the reentry of the chain to the crystal. This correlates well as the crystallinity of

the PPEs was calculated to be between 26 and 41% (assuming ΔH_m for PE) and increase with increasing spacer length.

The combination of complementary methods, including WAXS, SAXS, AFM, and TEM helps to understand the crystallization of all three polymers and to elucidate the differences between their crystal structures and morphologies. Theoretically, an addition of every 20 CH_2 groups in aliphatic segment in the ideal case would lead to an increase of the lamellae thickness by 2.5 nm. However, the obtained difference was determined as 4.1 nm instead of 2.5 nm and cannot be explained by the difference in the length of polymer chain segments alone. The combination of the density of crystal packing and the amorphous/loop region might be a reason for the inconsistent values. Also, the data indicates, that there is not necessarily a perfect arrangement with an adjacent reentry model, but instead a part of polymer chain segments might be expelled to the amorphous phase during the bulk crystallization, yielding a considerable amount of random reentry.[181] By extrapolation of the crystal thickness data to shorter aliphatic length, we can theoretically evaluate the minimal number of CH_2-units that are necessary to form crystalline parts in the polymer. From Figure S2.48 we obtain a spacer length of 9 CH_2-units. For polymers with less CH_2 units between the defects, the length of the aliphatic part would not be enough for both loop formation and PE crystallization.

There are different models of polymer chain arrangement depending on the polymer structure and crystallization conditions. In bulk, polymer chains are rather folding according to a random reentry or the so-called “switchboard” model.[41,182] This model was first proposed by Flory and recently confirmed for a number of semi-crystalline polymers,[183] consists of chains randomly folding back into the same lamella or participating in adjoining lamellae. However, for solution-grown single monolayer polymer crystals, the most preferable chain-folding model is the adjacent reentry. This model is characterized by a sharp phase boundary between the crystal and the amorphous phase. The position of reentry of the chains is the adjacent neighbor with only a few exceptions due to multiple nucleations and chain-end defects.[184] Figure 2.7 summarizes the measured thickness ratios of the crystal lamellae graphically. The theoretical thickness of an all-trans configuration is indicated as the dashed line. It is noticeable that the measured lamellar thickness is greater than the theoretically achievable value. In determining the theoretical thickness, however, we have disregarded the phosphate groups, which could at least be the first attempt at an explanation. However, this does not explain the increase in thickness difference found in the C40 polymer. This observation applies both to bulk and solution-grown crystals. Hence, the increased thickness of the long period of the crystals is a strong indication, that even the solution grown crystals still contain some part of random reentry folds. As has been shown by NMR[181,185–187] and AFM[188] solution grown crystals can have up to 10%, whereas melt grown crystals exhibit up to 35% of random reentry folds. In the case of the PPEs synthesized in this work, we can therefore assume that a certain amount of random reentry folding is also present in the solution-grown crystals. Hence, several segments are expelled from the crystal phase and contribute to a thickening of the amorphous phase. This explains, why even solution-grown crystals exhibit lamellar thicknesses larger than expected for the respective defect distance. In general, the obtained values for lamellar thickness from AFM and SAXS techniques show only minor differences, although the crystals were prepared following different procedures in bulk and solution. Thus, we can claim that the phosphate defects confine the lamellae thickness, regardless of the way of crystallization.

2.5. Experimental section

Materials

All available reagents were purchased from Sigma Aldrich, Alfa Aesar, Acros Organics or TCI and were used without further purification unless otherwise stated. Deuterated solvents were purchased from Sigma Aldrich.

Instrumentation and characterization techniques

Thin-layer chromatography (TLC) was performed using Merck aluminum-foil baked plates coated with Kieselgel 60 F245. The products were visualized using UV fluorescence (254 nm) or potassium permanganate stain. Flash column chromatography was performed over Merck silica gel C60 (40–60 µm) using eluent systems as described for each experiment. Size exclusion chromatography (SEC) measurements were performed in THF on an Agilent Technologies 1260 instrument consisting of an autosampler, pump, and column oven. The column set consists of 3 columns: SDV 10^6 Å, SDV 10^4 Å, and SDV 500 Å (PSS Standards Service GmbH, Mainz, Germany), all of 300 × 8 mm and 10 µm average particle size were used at a flow rate of 1.0 mL min^{-1} and a column temperature of 30 °C. The injection volume was 100 µL. Detection was accomplished with an RI detector (Agilent Technologies). The data acquisition and evaluation were performed using PSS WINGPC UniChrom (PSS Polymer Standards Service GmbH, Mainz, Germany). Calibration was carried out by using polystyrene provided by PSS Polymer Standards Service GmbH (Mainz, Germany). For nuclear magnetic resonance (NMR) analysis ^{1}H, ^{13}C and ^{31}P NMR spectra of the monomers were recorded on a Bruker AVANCE III 300, 400, 500, or 700 MHz spectrometer. All spectra were measured in $CDCl_3$ at 298 K. The spectra were calibrated against the solvent signal and analyzed using MestReNova 14.1.0. (Mestrelab Research S.L). The thermal properties of the synthesized polymers have been measured by differential scanning calorimetry (DSC) on a Mettler Toledo DSC 823 calorimeter. Three scanning cycles of heating/cooling were performed in a nitrogen atmosphere (30 mL min^{-1}) with a heating and cooling rate of 10 °C min^{-1}. The heating rate was 10 °C min^{-1} in a range of temperatures between −100 and 180 °C. Wide-angle X-ray scattering (WAXS) measurements on powder diffractometers with Cu radiation (wavelength 1.5418 Å) were performed using a Philips PW1820 for **poly(1)-H** and a Rigaku SmartLab for **poly(2)-H** and **poly(3)-H**. Small-angle X-ray scattering (SAXS) experiments were performed on a home-built instrument.[189] The crystal morphology, thickness, and crystal structure were determined using an FEI Tecnai F20 transmission electron microscope operated at an acceleration voltage of 200 kV. Bright-field (BF) and energy-filtered transmission electron microscopy (EFTEM) techniques were used for measurements. AFM measurements were performed using a Dimension Icon FS with tapping mode. For the measurements, one droplet of the dispersion containing the solution-grown crystals was dropped onto a freshly cleaved mica substrate, and excess liquid was blotted off with the edge of a filter paper.

Sample preparation

Both solution- and melt-crystallization methods were used for sample preparation. To prepare solution-grown crystals, the polymer was dissolved in hot *n*-octane at a concentration of 0.05 wt%. The solution was kept in a temperature-controlled oil bath, whereby the change of the temperature was controlled by the change of the oil bath. After full dissolution, the solution was slowly cooled down to room temperature for crystallization.

Afterwards, one droplet of the dispersion was dropped onto a carbon-coated grid for further TEM measurement.

For the melt-grown crystals, the samples were annealed in the oven at the temperature 5 degrees below the melting point for 2 days and slowly cooled down to room temperature. For TEM examination the melt crystallized bulk samples were prepared using ultramicrotomy. The samples were embedded in epoxy resin and subsequently sectioned at room temperature using a Leica ultracut UCT. To decrease the compression of the sample, a 35° DiATOME ultrasonic oscillating diamond knife was used for sectioning. The thin sections were collected on the copper grids and subsequently RuO_4 stained for 24 h.

Synthetic procedures

Polymer synthesis

Procedure for ADMET polymerization in bulk (poly(1))

Monomer **1** (30 g, 0.16 mol) and the Grubbs catalyst 1st generation (0.3 mol%) were mixed in a vacuum reactor with a mechanical stirrer under an argon atmosphere. The polymerization was carried out at reduced pressure to remove the evolving ethylene, first with a membrane pump at 50 mbar for 5 h, then with an oil pump (0.07 mbar) at 65 °C for 1 h and 85 °C for 48 h. The crude mixture was allowed to cool down to room temperature, then dissolved in CH_2Cl_2 and treated with tris-(hydroxymethyl) phosphine (10 eq. with respect to the catalyst) and 2 mL of Et_3N to form a water-soluble ruthenium complex.[190] After stirring for 1 h water was added in the same volume to the organic phase and the solution was stirred overnight. The organic layer was washed twice with a mixture of 100 mL 5% aqueous HCl and 100 mL brine and then washed twice with brine. The aqueous layer was extracted with ethyl acetate several times. The organic phase was dried over sodium sulfate (Na_2SO_4), filtered, and dried at reduced pressure. (yield: 93%). **^{1}H NMR** (250 MHz, $CDCl_3$) δ = 5.53–5.27 (m, 2H), 4.21–3.90 (m, 6H), 2.13–1.85 (m, 2H), 1.75–1.53 (m, 2H), 1.48–1.16 ppm (m, 27H). **^{13}C NMR** (125 MHz, $CDCl_3$): δ = 130.32, 130.30, 130.26, 129.87, 129.83, 129.79, 67.65, 63.58, 32.61, 30.30, 29.65, 29.62, 29.49, 29.43, 29.38, 29.16, 25.46, 16.17 ppm. **^{31}P NMR** (202 MHz, $CDCl_3$): δ = −0.71 ppm.

Procedure for ADMET solution polymerization (poly(2)/poly(3))

A 25 mL Schlenk tube was charged with the monomer (230 mg) and 1-chloronapthalene as a solvent (300 µL, *ca.* 150 wt%). The solution was degassed by three consecutive Argon/vacuum cycles. Grubbs catalyst 1st generation (6.5 mg, 0.02 eq.) was added under an Argon stream and the Schlenk tube was placed in an oil bath at 60 °C. High vacuum (2×10^{-2} mbar) was applied to remove the evolving ethylene and the solution was kept stirring overnight. After 17 h, the brown reaction mixture solidified and was dissolved in 300 µL 1-chloronaphthalene before the addition of a second portion of the Grubbs catalyst. After another 24 h at 60 °C and 2×10^{-2} mbar, the reaction mixture was cooled to room temperature and 100 µL ethyl vinyl ether were added to cleave the catalyst of the polymer chain and 1 mL CH_2Cl_2 to dissolve the polymer. Precipitation into methanol gave a solid but soft polymer of light brown color.

Poly(2)

Yield: 142 mg, 65%.

^{1}H NMR (300 MHz, $CDCl_3$) δ = 5.37 (m, *J* = 6.7, 5.3 Hz, 2H), 4.06 (m, 6H), 1.98 (m, 4H), 1.67 (m, 4H), 1.53–1.03 (m, 47H). **^{13}C NMR** (75 MHz, $CDCl_3$) δ = 130.33, 118.16, 67.68, 63.60, 32.62, 30.31, 29.96, 28.84, 25.46, 16.17. **^{31}P NMR** (121 MHz, $CDCl_3$): δ = −0.70 ppm.

Poly(3)

Yield: 109 mg, 76%.

^{1}H NMR (300 MHz, $CDCl_3$) δ = 5.37 (m, 2H), 4.07 (m, 6H), 2.14–1.85 (m, 4H), 1.67 (m, 4H), 1.52–1.01 (m, 59H), 0.85 (m, 8H). **^{31}P NMR** (121 MHz, $CDCl_3$): δ = −0.70 ppm.

Poly(1)-H

A Schlenk flask was charged with **poly(1)** and dissolved in toluene (*ca.* 12 wt%). The air was removed by reduced pressure and flushed with argon. 10 wt% of 5% Pd/C catalyst was added followed by removing the argon by reduced pressure and flushing with hydrogen by a balloon. Then *via* septum and syringe hydrogen was bubbled into the solution. Hydrogenation was then performed with a hydrogen balloon under vigorous stirring at room temperature until NMR showed no signals of double bonds. The solution was filtered over Celite and the polymer was obtained as a solid after solvent evaporation with a yield of 89%. **^{1}H NMR** (300 MHz, $CDCl_3$, 298 K): δ = 4.23–3.91 (m, 6H, –OPO3–C*H*2–), 1.82–1.58 (m, 4H –OPO3–CH2–C*H*2–), 1.31–1.22 ppm (m, 37H). **^{13}C NMR** (176 MHz, $CDCl_3$, 24 °C): δ = 67.73, 63.65, 30.37, 29.78, 29.73, 29.68, 29.23 25.53, 16.23 ppm. **^{31}P NMR** (283 MHz, $CDCl_3$, 298 K): δ = −0.74 ppm.

Poly(2)-H

Poly(2) (120 mg) was dissolved in 10 mL toluene in a glass vessel. Argon was bubbled through the solution for 5 min to degas the solution before the addition of 10wt% Pd/C (30 mg). Then the glass vessel was charged into a 250 mL ROTH autoclave and the system was flushed twice with hydrogen. The hydrogenation was performed at 50 °C and 60 bar H_2 for 40 h. After filtration with a Merck Teflon filter, the solvent was removed under reduced pressure to yield the off-white polymer with a yield of 88%. **^{1}H NMR** (300 MHz, $CDCl_3$) δ = 4.06 (m, 6H), 1.67 (m, 4H), 1.52–1.07 (m, 55H). **^{13}C NMR** (75 MHz, $CDCl_3$) δ = 118.17, 67.69, 63.60, 30.31, 30.07, 29.37, 29.17, 25.46, 16.16. **^{31}P NMR** (121 MHz, $CDCl_3$): δ = −0.72 ppm.

Poly(3)-H

The hydrogenation was performed under homogenous conditions using a Grubbs catalyst 1st generation modified with ethyl vinyl ether as the catalyst.[177] In a glass vessel, **poly(9)** (76 mg) was dissolved in 10 mL toluene, then Argon was bubbled through the solution for 5 min. Upon addition of the catalyst (15 mg), the solution changed its color to orange. The hydrogenation was performed in a 250 mL ROTH autoclave. The system was flushed twice with hydrogen, afterwards the hydrogenation was performed at 60 °C and 80 bar H_2 overnight. After 14 h, the completion of the reaction was confirmed by ^{1}H NMR. The now dark brown solution was concentrated *in vacuo* before precipitating into cold methanol to yield an off-white solid material (80% yield). **^{1}H NMR** (300 MHz, $CDCl_3$) δ = 4.07 (m, 6H), 1.84–1.48 (m, 4H), 1.45–1.08 (m, 63H), 0.97–0.68 (m, 12H). **^{31}P NMR** (121 MHz, $CDCl_3$) δ = −0.71.

2.6. Conclusion

We report on a “defect engineering” approach using PE-like polyphosphates with varying amount of phosphate defects in the aliphatic polymer backbone to control the crystal structure and lamellar thickness of polymer crystals. Three different *α*,*ω*-diene monomers with identical phosphate groups but different aliphatic spacer length were synthesized for acyclic diene metathesis polymerization. Linear polyphosphates with 20, 30, or 40 CH_2-groups between phosphate groups were obtained after polymerization. Post-polymerization hydrogenation yielded solid, polyethylene-like materials. The polymers were crystallized both in bulk and from solution. With the phosphate side chain being identical for all three polymers, differences in crystal structure and morphology as well as thermal properties relied only on length of the aliphatic spacers. Melting temperatures increased with increasing length of the aliphatic spacer segment up to 91 °C for the polymer with 40 methylene groups. A change from a pseudo-hexagonal to an orthorhombic crystal structure was observed by WAXS with a decrease of phosphate defects in the polymer chains, i.e. increasing similarity to polyethylene. A combination of WAXS, SAXS, AFM, and TEM revealed an increase in lamellar and crystal thickness with increasing length of the aliphatic spacer. Following our synthesis approach, different functionalities could be added to the polymers by varying the side chain of the phosphate group in the future. The synthesized PE-like polyphosphates with precisely engineered lamellar crystals thicknesses show potential for applications where distinct spacing on a nanometer scale is advantageous, e.g. for electronics, or as highly functional and anisotropic polymer colloids.

3. How to form conductive 2D platelets using precise thiophene-based polymers

Oksana Suraeva, Beomjin Jeong, Kamal Asadi, Frederik R. Wurm, Katharina Landfester, Ingo Lieberwirth

This chapter is based on unpublished results.

I designed, synthesized and analyzed all monomers and polymers, performed TEM measurements and wrote the manuscript. Beomjin Jeong performed conductivity experiments, and together with Kamal Asadi partly wrote the part about evaluation of conductivity measurements.

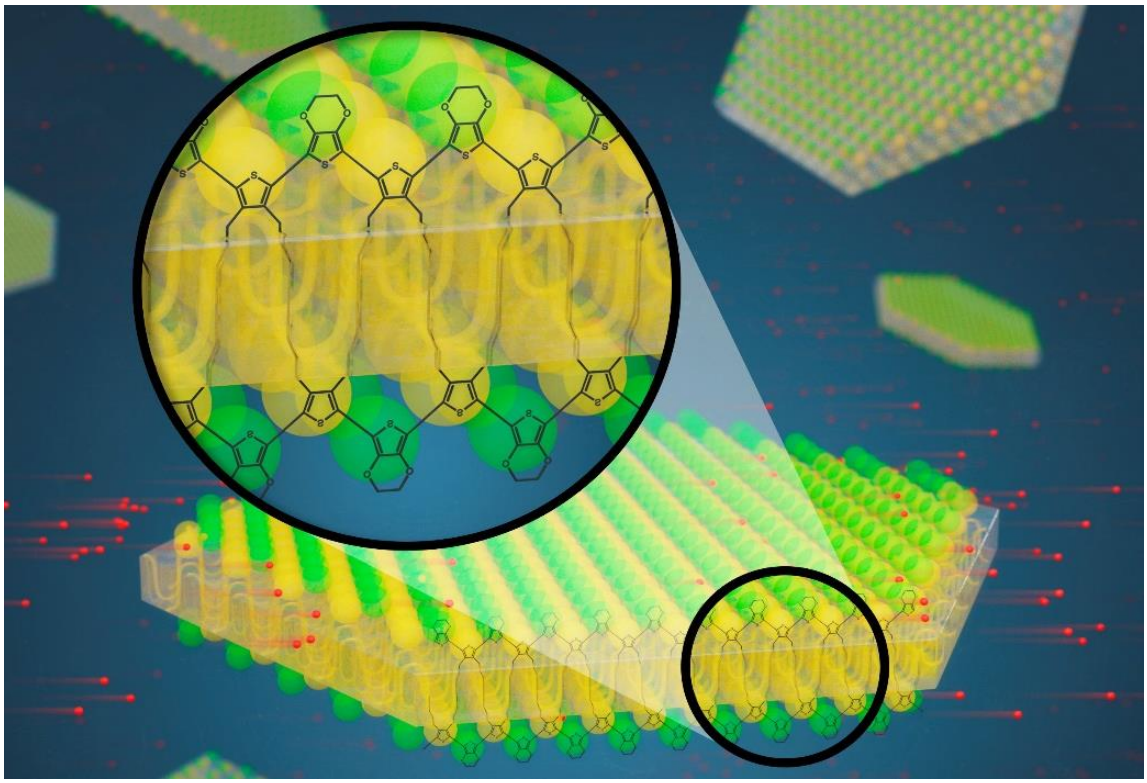

Keywords: Acyclic diene metathesis polymerization, ADMET, conducting polymers, thiophene, polymers, defect engineering

3.1. Preface

In the following chapter I will show the importance of the chemistry of the inserted functional groups. As already shown in the previous chapter, we can insert functional groups into the polyethylene main chain in a targeted manner and with molecular precision. In principle, any functional group is possible for this synthesis. I would like to mention here once again that the distribution of functional groups within the polyethylene chain is absolutely equidistant due to the ADMET synthesis. As already shown in chapter 2, the molecular architecture - especially the distance between the inserted groups - determines the thickness of the crystal lamellae, which are formed after crystallization.

Here I show how the chemical nature of the inserted functional groups can be exploited to create specific physical properties. For this purpose I have synthesized a polyethylene with evenly distributed thiophene groups. After crystallization, these thiophene groups are expressed on the basal surface of the crystal lamellae, as already presented in the other system. Thiophene is a conjugated molecule which becomes conductive after polymerization. Therefore, when I polymerize the thiophene on the crystal surface, I obtain 2D nanocrystals with a conductive surface. This shows that the choice of the incorporated group will ultimately determine the functionality of the material.

For these investigations I developed the synthesis and prepared two polymer systems, one with a spacing of 20 CH_2 units and one with a spacing of 38 CH_2 units. The characterization of the synthesized polymers showed that the variant with the short spacing has a melting temperature in organic solvent close to room temperature, which makes it unpracticable to perform any crystallization and modification experiments. Therefore I focused exclusively to the polymer with a distance between the thiophene groups of 38 CH_2 between the thiophene units.

As already mentioned, the goal in this chapter was to produce polymer crystals with a conductive surface by polymerizing the thiophene groups on the surface. It turned out that due to the arrangement during crystallization, the thiophene groups are too far away from each other to form a conjugated bond by a simple polymerization reaction. I have solved this problem by filling the large distance between the thiophene groups on the surface of the crystal by forming bonds with 3,4-Ethylenedioxythiophene (EDOT) – another thiophene-based molecule, capable to exhibit conductive properties upon polymerization. Using this approach, I demonstrate that the thiophene groups on the surface of the polymer crystal are still chemically active and able to undergo modifications to create a conductive surface on the 2D nanocrystals.

3.2. Abstract

We developed a simple way to create 2D conductive nanostructures with dielectric core and conductive surfaces based on polyethylene with in-chain thiophene groups. Generally, thiophene-based polymers show great conductive properties, but possess a poor processability. Here, we use the crystallization of a polyethylene chain with precisely distributed thiophene groups as the platform for a self-organization of a lamellar structure. During crystallization, thiophene groups are expelled to the crystal surface. Subsequent copolymerization with 3,4-Ethylenedioxythiophene (EDOT) molecules finally yields 2D platelets with a conductive surface. The electric properties of the surface are demonstrated by conductivity measurements. Given the molecular structure of the polymer, it can be assumed that the conductive layer consists of only one monoatomic layer of polymerized thiophene. We thus show a new way to create an ultra-thin, conductive surface on a polymer surface in just a few steps. Hence, the method presented here opens up a wide range of possibilities to produce complex, nanoscale electronic structures for microelectronic applications.

3.3. Introduction

Conductive polymers combine the mechanical advantages of polymers with the electronic properties of metals and semiconductors, which makes them valuable in electronic and optical industry.[191–193] One of the most common organic molecules to obtain conductive material is thiophene and its derivatives, because of their good electrical and chemical properties and environmental stability (both to oxygen and to moisture).[194] However, the conjugated backbone of un-substituted polythiophenes is typically rigid and results in poor processability.[195] To obtain control over the nanostructure and to increase the processability of thiophene containing materials, two different approaches have been described in the literature. The first approach utilizes the self-assembly of a polymer system to form a nanoscopic template.[196] Subsequently, a conductive polymer like polythiophene is grafted upon this template. The resulting nanostructures thus formed have a dielectric core, but the surfaces show only a partial conductivity. The other approach aims to generate a polymeric material with bulk conductivity first.[197] Subsequently, this conductive polymer is attached to a dielectric layer, which involves several additional steps.

Here, we demonstrate a unique method to generate 2D polymer nanoplatelets with conductive surfaces. To achieve this, we utilize the crystallization driven self-assembly of a precisely synthesized polyethylene-based polymer with in-chain thiophene groups. We use acyclic diene metathesis (ADMET) polymerization[18] to synthesize the necessary polymer. This approach allows us to generate an equidistant distribution of functional groups along the polymer backbone.[198,199] We designed the polymer architecture in a way, so that the crystallization of this polymer automatically yields the desired 2D nano platelets with the thiophene groups arranged exclusively on their surface. Although the thiophene groups are arranged with crystal perfection on the surface, their intramolecular distance is too large to allow for charge carrier transport. Hence, to achieve the final surface conductivity of these nano platelets, we copolymerize the surface protruding thiophene groups with 3,4-Ethylenedioxythiophene (EDOT). The resulting 2D nano platelets thus designed show a significant increase of conductivity after this copolymerization.

3.4. Results and discussion

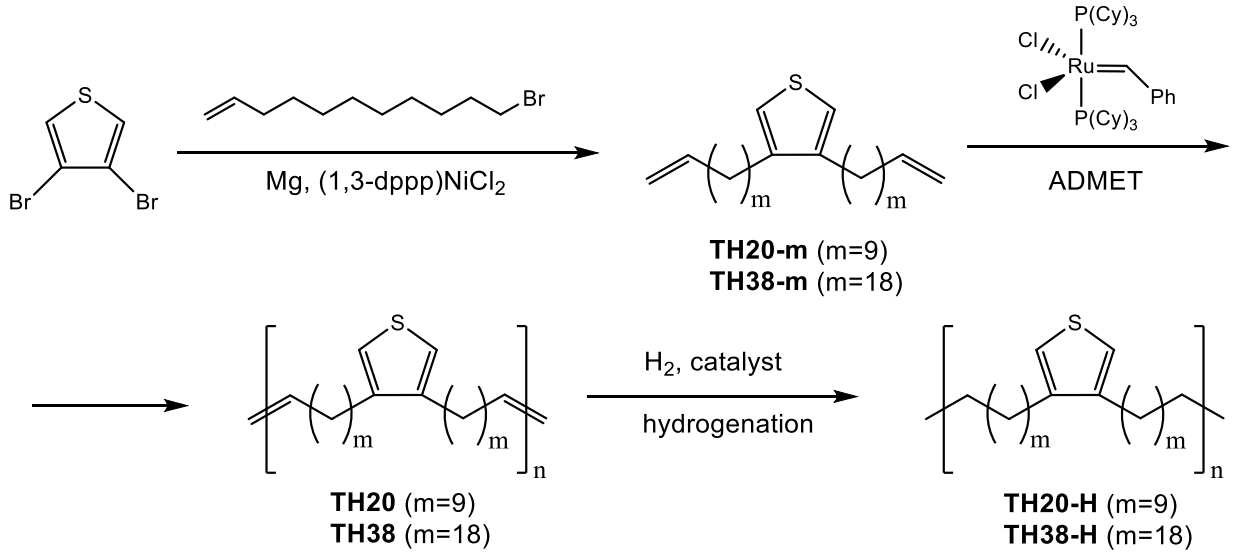

Scheme 3.1. Synthesis of thiophene diene monomers with different length of the aliphatic spacers and the ADMET polymerization and hydrogenation.

Two polyethylene-like polymers carrying precisely spaced thiophene units were prepared by ADMET polymerization. The distance between the thiophene groups was adjusted to either 20 or 38 methylene units, which should influence the thermal properties of the resulting polymers. The monomers TH20-m and TH38-m for ADMET polymerization were prepared accordingly to Scheme 3.1 in THF with excess of 11-bromo-1-undecene or 18-bromo-1-octadecene respectively. After column chromatography the structure of TH20-m and TH38-m was confirmed by NMR and mass-spectroscopy (**Fehler! Verweisquelle konnte nicht gefunden werden.**Figure 3.1 top, Figure 3.2 top,**Fehler! Verweisquelle konnte nicht gefunden werden.** top, Figure 3.4 top, Figure 3.5 and**Fehler! Verweisquelle konnte nicht gefunden werden.** Figure 3.6). Peaks with masses 388.1 and 585.9 are responsible for di-substituted thiophene derivatives. The terminal olefin protons were detected at 4.9 and 5.7 ppm and the terminal olefin carbon signal at 139.3 and 114.1 ppm from ^{1}H and ^{13}C spectra, respectively, indicating that alkylation reaction was successful.

The ADMET polymerization of TH20-m and TH38-m was carried out in the bulk using 1% of Grubbs first generation catalyst. Instead terminal double bond multiplets at 4.9 and 5.7 ppm, a new internal double bonds multiplet at 5.30 ppm was detected on ^{1}H spectra after ADMET polycondensation (Figure 3.1 middle, Figure 3.3 middle). In the ^{13}C NMR spectra, the resonances of the terminal olefins vanished (Figure 3.2 middle, Figure 3.4 middle) and new signal at 130.4 ppm was detected, which was assigned to the internal double bonds of the polymer.

Internal double bonds in TH-20 and TH38 were hydrogenated in the presence of Grubbs catalyst 1st generation modified with ethyl vinyl ether as the catalyst. Structures of successfully hydrogenated polymers TH20-H and TH38-H were confirmed by NMR spectroscopy. Comparison of the polymers before and after hydrogenation reveals the disappearance of the double bond resonances at 5.30 ppm for ^{1}H spectra and at 130.4 ppm for ^{13}C NMR spectra, confirming successful hydrogenation of the polymers (Figure 3.1, Figure 3.2, Figure 3.3, Figure 3.4 bottom).

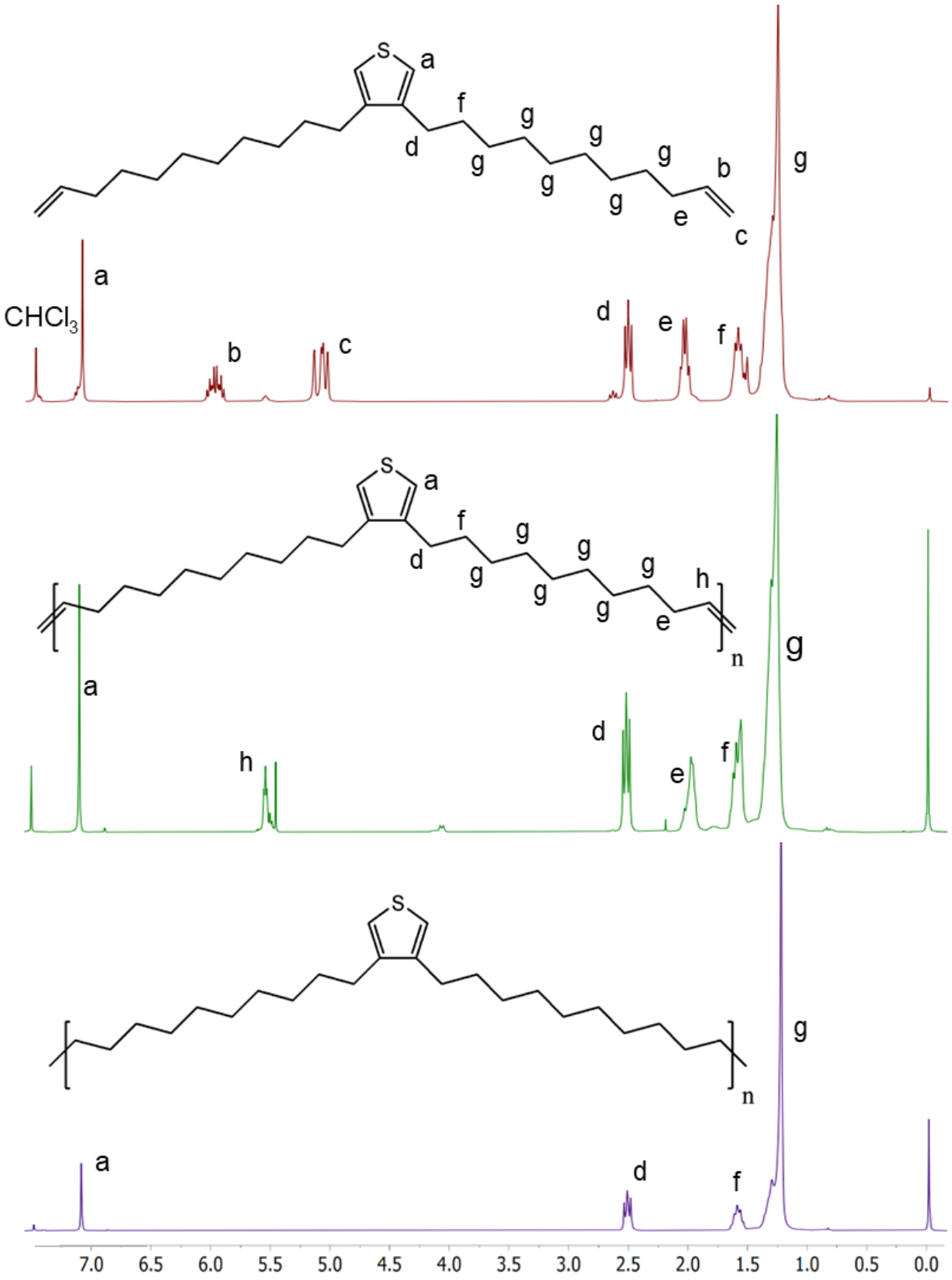

Figure 3.1. ^{1}H NMR spectra of **TH20-m, TH20 and TH20-H**

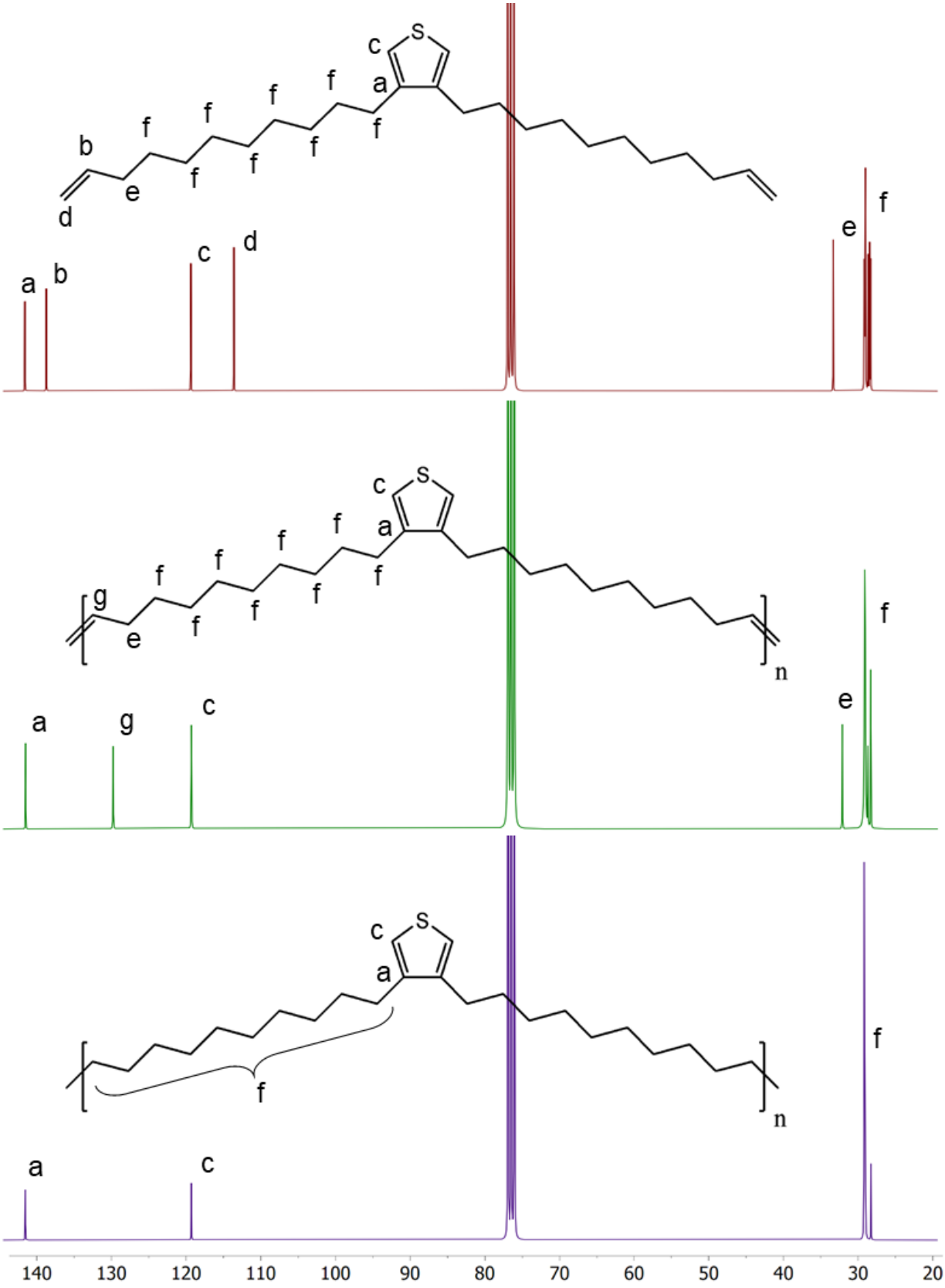

Figure 3.2. ^{13}C NMR spectra of **TH20-m, TH20 and TH20-H**

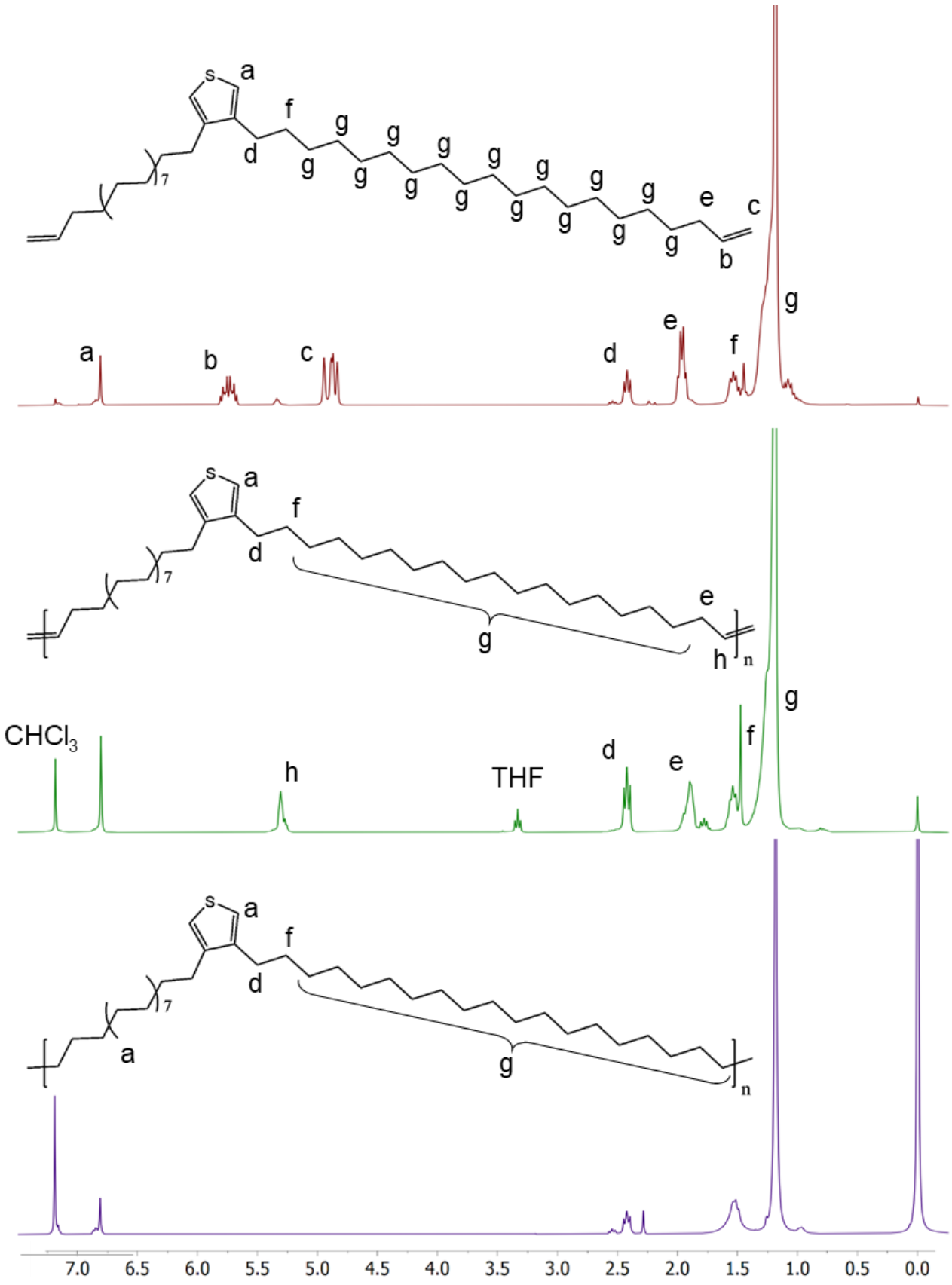

Figure 3.3. ^{1}H NMR spectra of **TH38-m, TH38 and TH38-H**

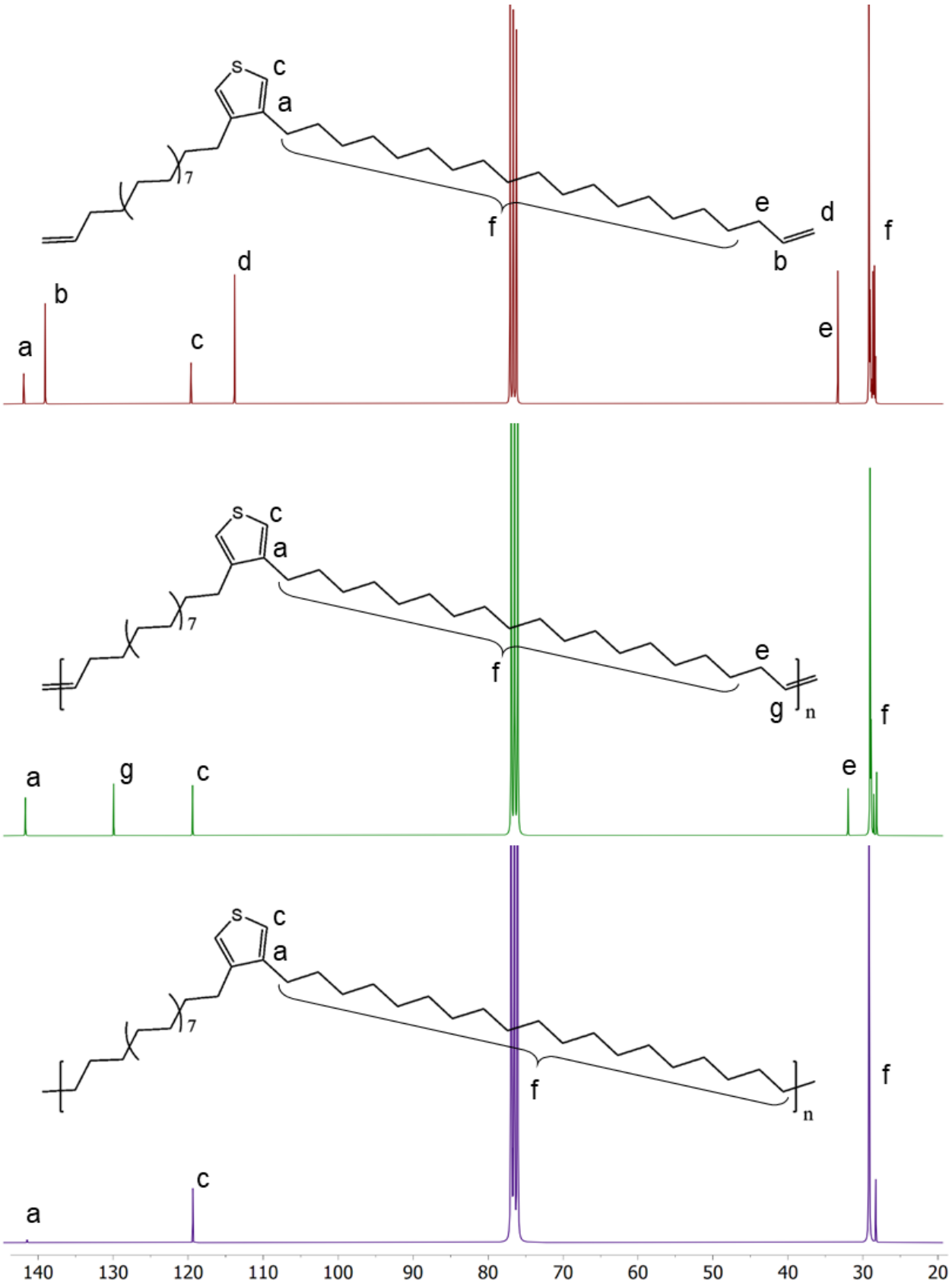

Figure 3.4. ^{13}C NMR spectra of **TH38-m, TH38 and TH38-H**

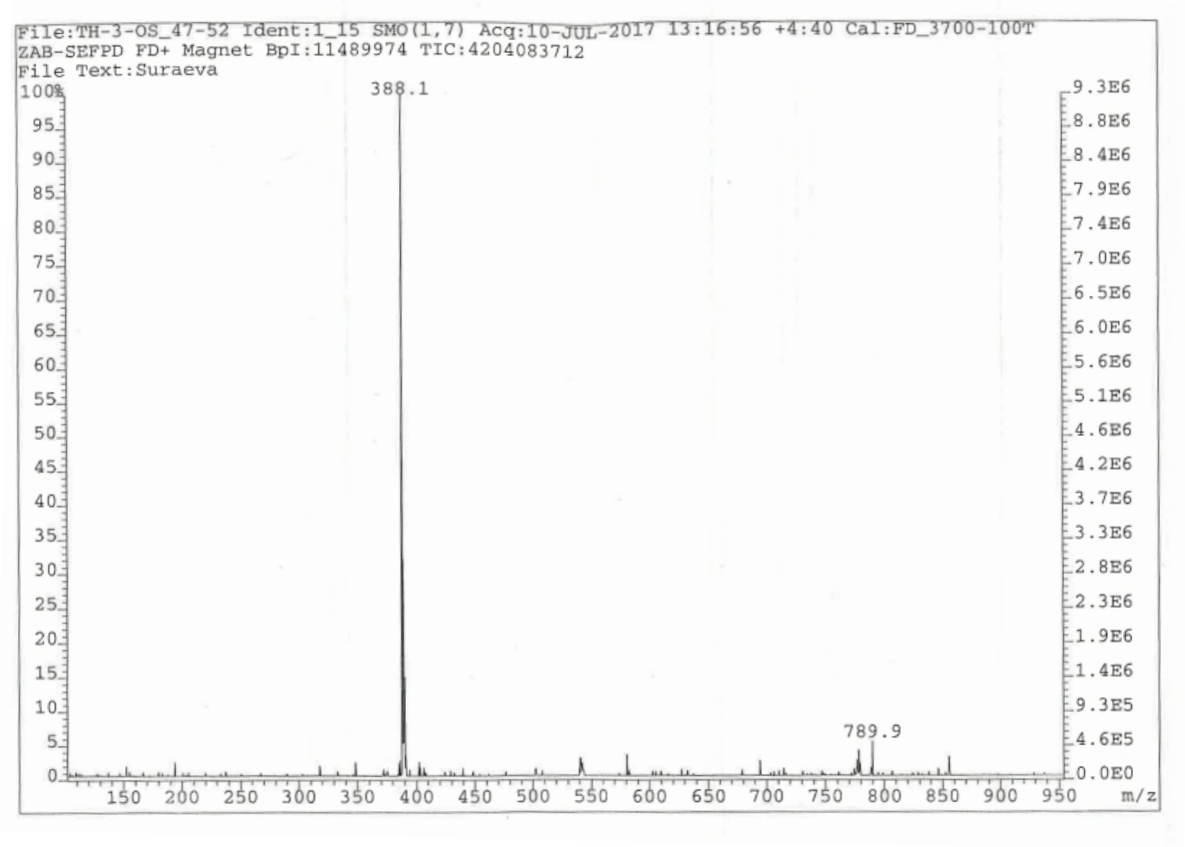

Figure 3.5. Mass-spectrum of monomer TH20-m

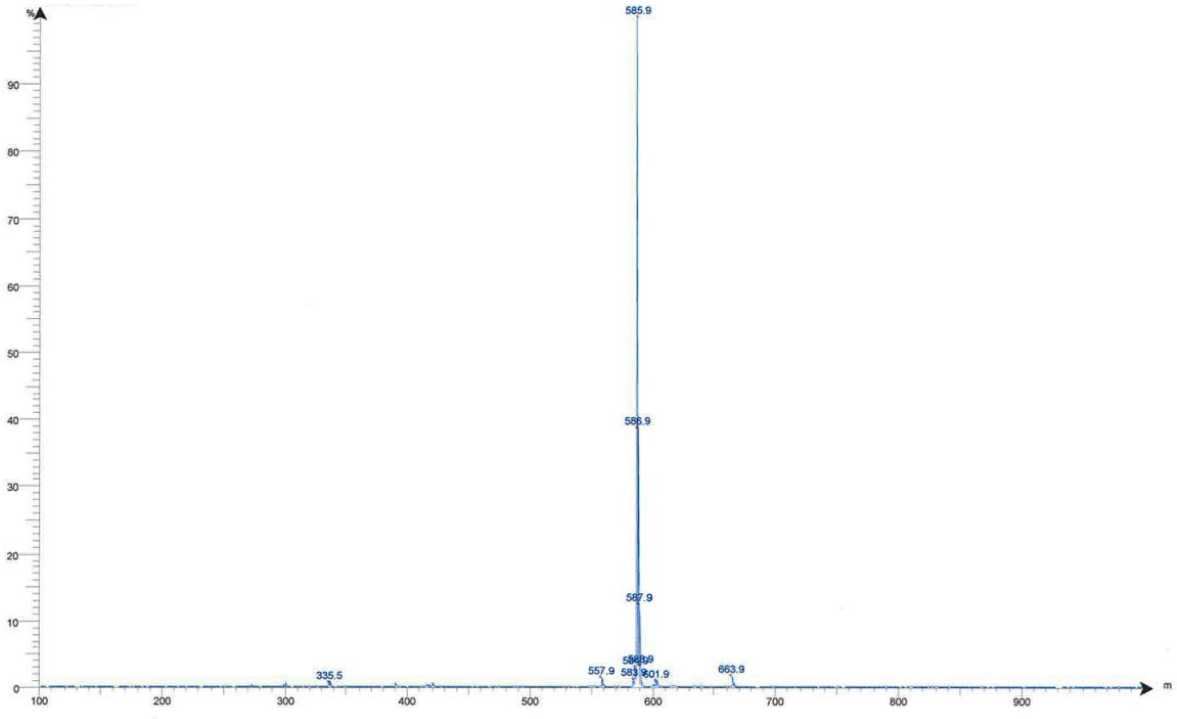

Figure 3.6. Mass-spectrum of monomer TH38-m

Molecular weights of TH20-H and TH38-H were determined by SEC in THF vs. polystyrene standards and were in accordance with the values of the respective unsaturated polymers (Figure 3.7, Figure 3.8). The obtained TH20-H and TH38-H revealed an apparent molecular weight M_w of ca. 23,400 g mol^{-1} (by SEC, M_w/M_n = 2.2) for TH20-H and 6,300 g mol^{-1} (by SEC, M_w/M_n = 1.7) for TH38-H. Due to the low solubility of the sample with 38 CH_2 units probably a lower degree of polymerization was achieved.

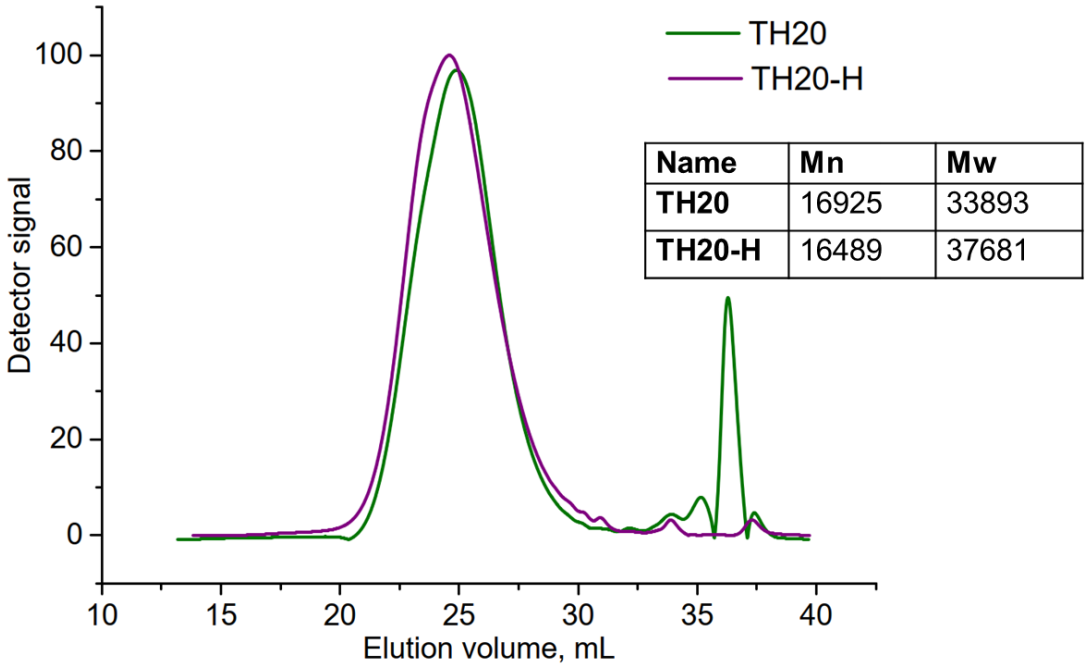

Figure 3.7. GPC curves of unsaturated polymer TH20 (green), and polymer TH20-H (purple) after hydrogenation

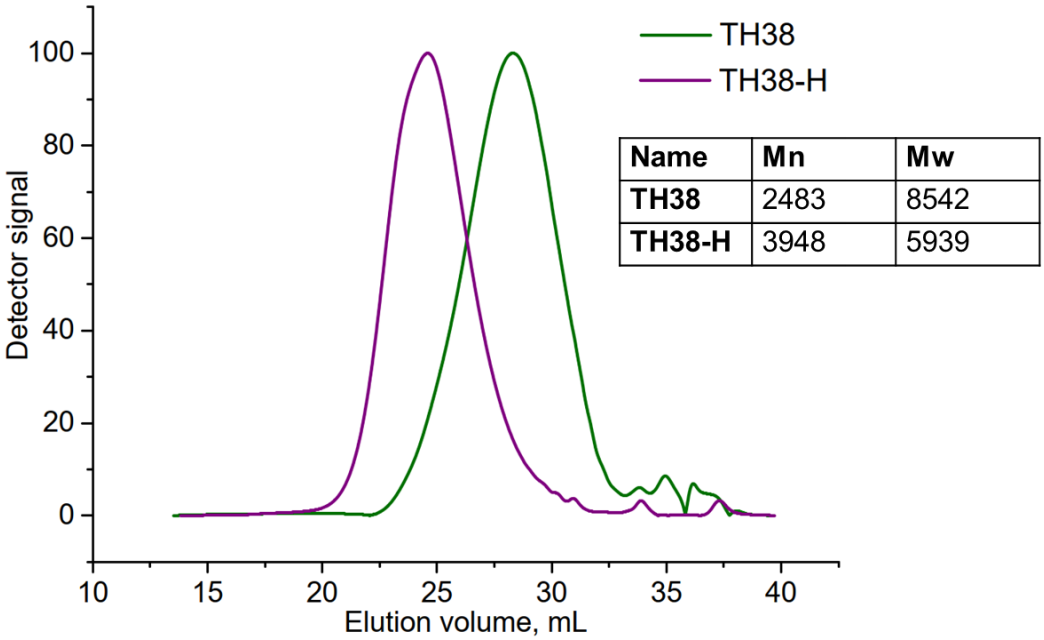

Figure 3.8. GPC curves of unsaturated polymer TH20 (green), and polymer TH20-H (purple) after hydrogenation

Solid State Characterization. . Both, the non-hydrogenated and the hydrogenated polymers were able to crystallize, as shown by the DSC thermograms in Figure 3.9 and Figure 3.10. The hydrogenation increased the melting temperature T_m from -36 to 56 °C for TH20 and from 50 to 77°C for TH38 as the internal cis-double bonds act as crystallization defects in the unsaturated polymer structures.

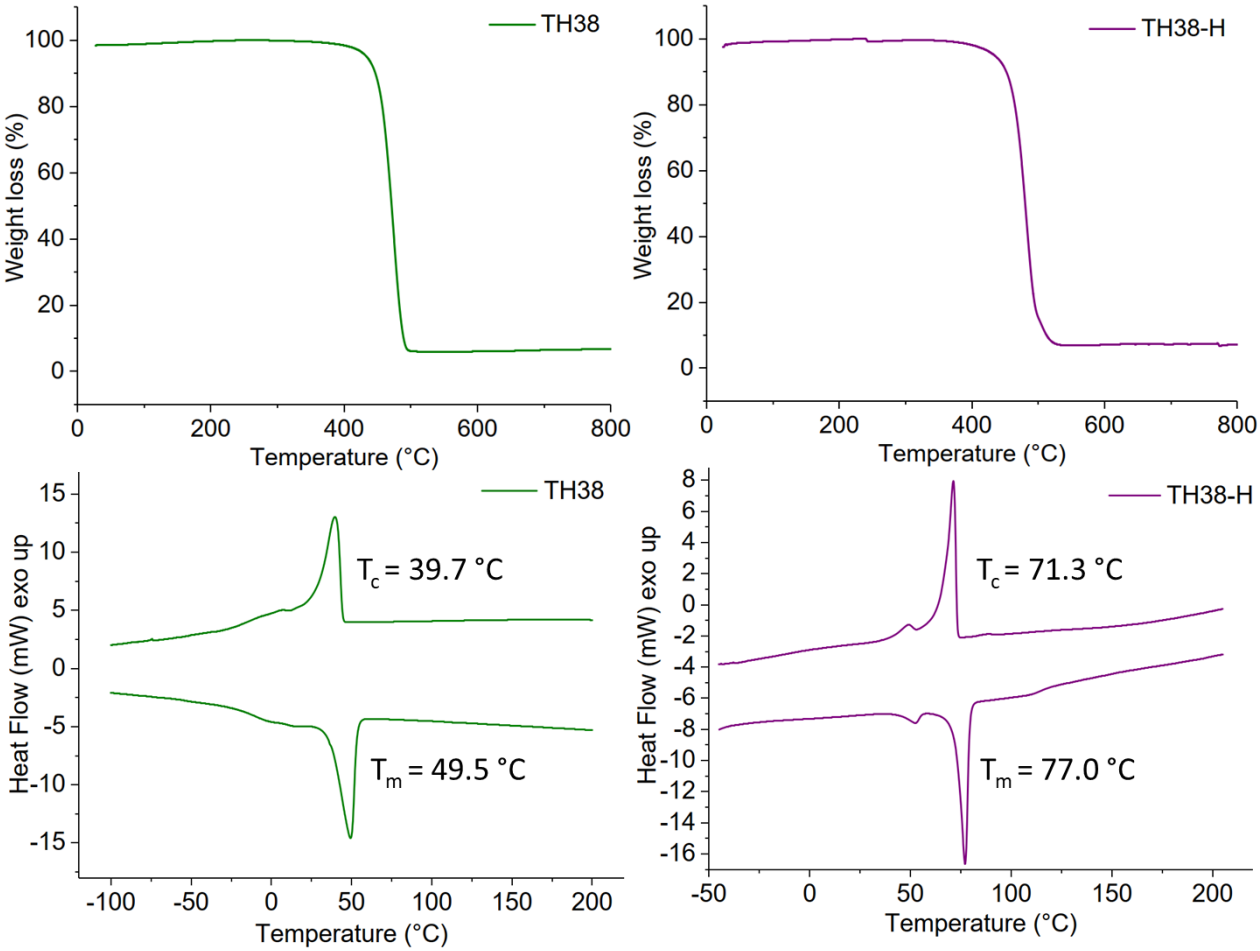

Figure 3.9. TGA (top) and DSC (bottom) thermograms of unsaturated polymer TH38 (left) and the product after hydrogenation TH38-H (right). The hydrogenation has no significant influence on the decomposition temperature, both materials are thermally stable up to approximately 500 °C. The thermal properties of the crystal, on the other hand, significantly change after the hydrogenation. The melting temperature T_m increases by 27 °C and the crystallization temperature T_c increases by 31 °C. This effect is attributed to the fact, that the unsaturated bond in the center of the aliphatic part acts as defect for the crystallization and hence reduces the melting- and crystallization temperature.

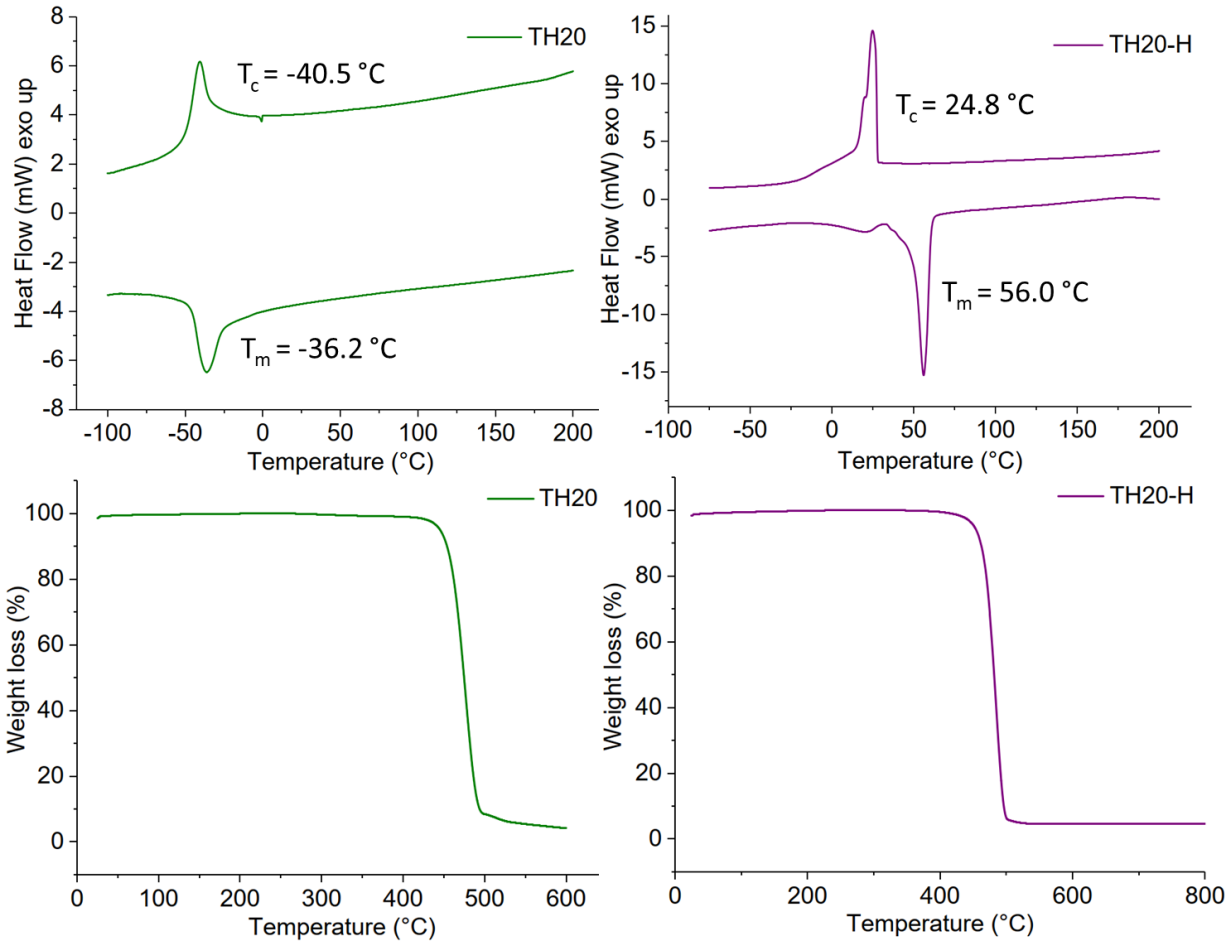

Figure 3.10. DSC thermograms of unsaturated polymer TH20 and product after hydrogenation TH20-H.

By elongating the aliphatic spacer between the thiophene units, the frequency of crystallization-defects is reduced, which resulted in increased melting temperatures. As the solution crystallization temperature of the TH20-H polymer was relatively low (39°C), the further electrochemical polymerization experiments were carried out exclusively with the TH38-H polymer.

The crystal structure of TH38-H lamellar crystals was determined by TEM and WAXS measurements. TEM measurement (Figure 3.11A) revealed hexagonal shaped crystals. The SAED diffraction pattern proved an orthorhombic structure, with an orthorhombic lattice plane of 4.18 Å for the (110) and 3.75 Å for the (200). This results in the orthorhombic lattice constants of a = 7.5 Å and b = 5.1 Å, which were slightly larger than for conventional polyethylene with a = 7.4 Å and b = 4.9 Å.

In the WAXS pattern (Figure 3.11B) distinct (110) and (200) Bragg reflections at 2θ = 21.2° and 23.3°, were observed, which correspond to a lattice distance of 4.2 Å and 3.8 Å, respectively.

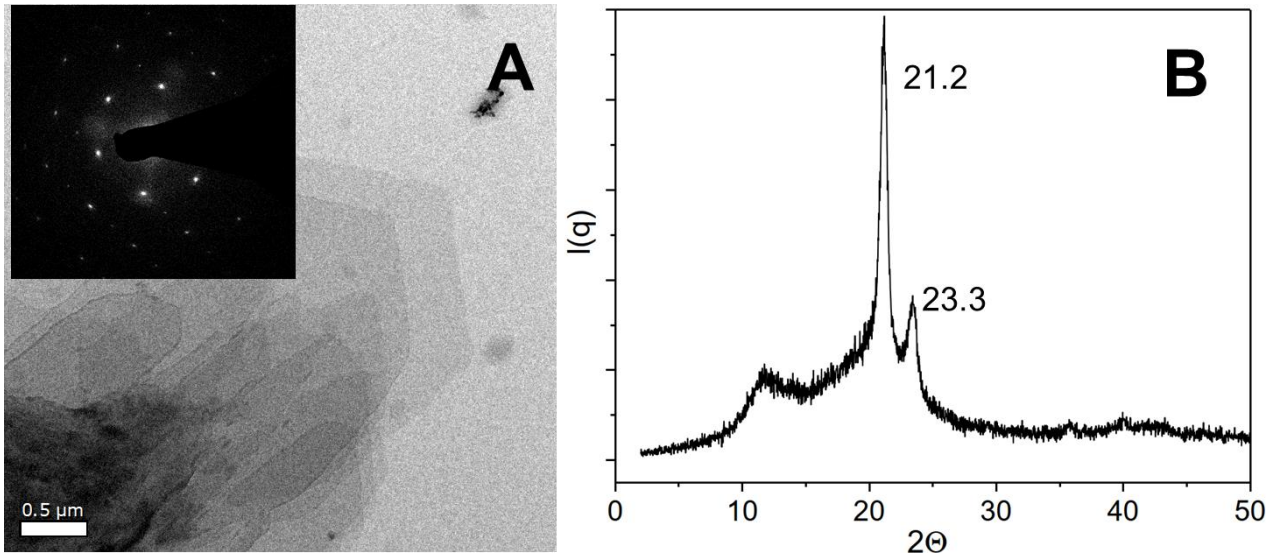

Figure 3.11. (A) TEM bright-field micrograph and selected area electron diffraction pattern (inset) of solution grown single crystal of polymer TH38-H from n-octane. The diffraction spots reveals an orthorhombic crystal structure with a lattice distance of 4.18 Å for (110) and 3.75 Å for (200). Assuming an orthorhombic crystal lattice, the lattice constants are a = 7.5 Å and b = 5.1 Å. (B) Wide-angle X-ray scattering of polymer TH38-H corroborates this finding with the two crystal peaks corresponding to a lattice distance of 4.2 Å and 3.8 Å, respectively.

Electrochemical polymerization.

To achieve conductive properties, a covalent bond between thiophene groups is necessary to form a conjugated oligomer or polymer.[200] For the electrochemical polymerization of the initial polymer two distinct approaches were chosen – in homogeneous solution or "on-surface" of the 2D nanoplatelets after they had been crystallized from a dilute solution. First, electrochemical polymerization in solution (Scheme 3.2 A), was performed using anhydrous chloroform as a solvent. This experiment was necessary to check, whether the thiophene groups in the polymer backbone can react with each other despite their relatively low abundance. The polymer was completely soluble in chloroform and during the polymerization agglomeration occurred. After 24 h, a dispersion of black and almost insoluble polymer particles was obtained due to the intra- and intermolecular crosslinking of the thiophene units. Visualization of the dispersion via TEM proved the formation of particles with diameters of ca 250 nm (Figure 3.13B left). The random crosslinking hinders formation of continuous conductive layer. Therefore, the polymerized product did not show a significantly increase in conductivity and probably only dimers or very short oligomers had been formed during the reaction (Figure 3.13C left). It is well known for thiophene polymers, that during polymerization in solution the solubility drastically decreases which practically impedes processing and exploitation of the final product.[201] DSC measurement of the randomly cross-linked polymer (Figure 3.13D left) reveals only minor glass transition temperature peak at 55°C, which in good agreement with polythiophene polymers.[202]

Instead of utilizing the in-chain thiophene groups in solution, we crystallized the polymer prior to the thiophene polymerization from a dilute solution to prepare anisotropic polymer nanoplatelets with expelled thiophene units to their surface as previously proven for structurally similar polyphosphoesters. Although the lamellar crystals are supposed to have the thiophene groups at their surface, they were non-conductive (Figure 3.12C

left column).[19] To achieve conductivity, the thiophene groups need to be covalently bonded, e.g. by polymerization on the crystal surface (Scheme 3.2).

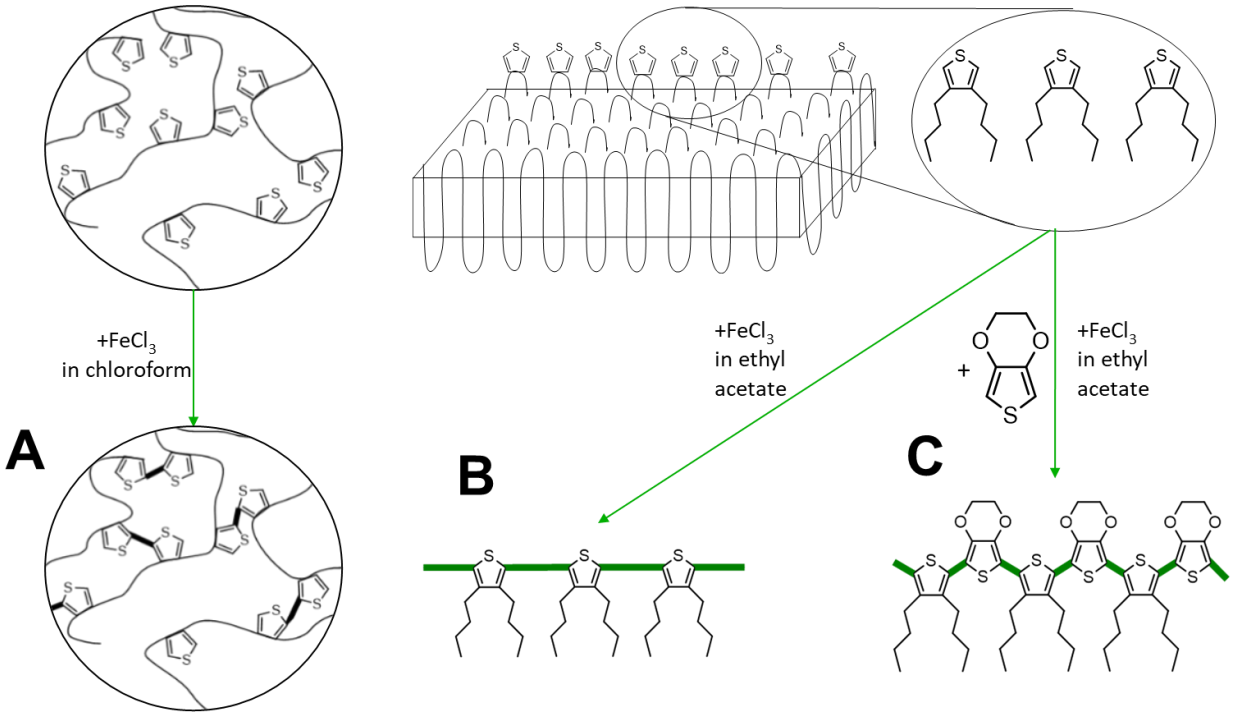

Scheme 3.2. Reaction scheme of the electrochemical polymerization of TH-38H. The thiophene groups are expelled to the lateral surface of the lamellar polymer crystal. The distance between the thiophene groups is too large to allow charge transport. Accordingly, the thiophene groups need to be polymerized to achieve surface conductivity. The electrochemical polymerization can be done in presence of FeCl3 (A) or with a mixture of $FeCl_3$ and EDOT (B). When the electrochemical polymerization is performed with dissolved TH-38, insoluble particles precipitate due to uncontrolled crosslinking (C).

For the polymerization of the thiophene groups on the crystal surface, we have to take care that the crystals are not destroyed, *e.g.* by melting or dissolution during the process. Hence, the oxidative polymerization of the thiophene groups was carried out in cooled ethyl acetate, which allowed to conserve the polymer crystals, in the presence of $FeCl_3$ as a catalyst (Scheme 3.2B).[203] After 24 h, the color of the dispersion turned light brown, which indicated the partial oxidation of $FeCl_3$. The TEM measurement reveals, that the TH-38 crystals stayed intact (Figure 3.13B right), but the electrical conductivity did not show a marked increase as compared to the initial nanoplatelets (Figure 3.13C right).

The lack of conductivity after reaction with $FeCl_3$ can be explained by the arrangement of the thiophene groups on the crystal surface. Assuming an orthorhombic crystal structure of the TH-38 (with lattice constants a =7.5 Å and b = 5.1 Å), the minimal thiophene-to-thiophene distance is 9.1 Å (in (110) direction). Hence, several additional molecules may be necessary to bridge the thiophene units. Thus, it is likely that thiophene groups

only react to a low extend in the amorphous parts but could not generate conjugated bonds on the surface of the crystals.

To covalently bond thiophene units on the crystal surface with each other, we added EDOT as a comonomer which should bridge the distance between the thiophene groups on the crystal surface (Scheme 3.2C). By copolymerization with EDOT as linker between the thiophenes conductive behavior on the crystal surface should be feasible. Also during the copolymerization special care was taken that the TH-38 nanoplatelets were not destroyed, which was proven by TEM imaging after the polymerization (Figure 3.12B right). From the TEM images only nanoplatelets were observed without any additional visible impurities, indicating the successful copolymerization on the surface on the crystals. In addition, the sample proved a substantial increase in conductivity, with a current level of $2.7X10^{-9}$ A at 1 V and $4.7X10^{-7}$ A at 20 V. Thus, it is likely that EDOT copolymerized with the thiophene groups "on surface" (Figure 3.12C right). As shown in Figure 3.14, the current level was linearly proportional to the applied voltages at the low bias regime, revealing the Ohmic nature of conduction through the poly(EDOT-*co*-TH-38) surface layer.[204] Observation of an Ohmic behavior is indicative for good contact formation between the Au electrodes and the thiophene-EDOT surface of the 2D conductive crystals. Besides the desired copolymerization between the thiophene groups of TH-38 and EDOT, also the homopolymerization of EDOT to form poly(3,4-ethylenedioxythiophene (PEDOT) might occur. After the polymerization, the crystals were purified by centrifugation to remove $FeCl_3$ and PEDOT, which might have formed as a side product. Then, the platelets were visualized by TEM; from the TEM imaging, no additional polymer nanoparticles or aggregates could be visualized, which hints that no homopolymer was present after workup. In addition, DSC measurements did not show signs of PEDOT. In order to prove, that observed conductivity resulted from the formation of bond between thiophene groups in polymer chain and EDOT, but not only due to formation of PEDOT, which might even not be detectable by DSC measurements, we performed a control experiment with polymer nanoplatelets carrying no thiophene groups. We prepared similar nanoplatelets using a long-chain polyphosphoester.[170] This polyethylene-like polymer carries 20 methylene groups between phosphate units and our previous findings proved that they form very similar nanoplatelets when crystallized from a dilute solution. The nanoplatelets were prepared accordingly and EDOT and FeCl3 were added to initiate the polymerization. As the phosphate units cannot generate a copolymer with EDOT only homopolymerization is possible. After the reaction, we purified the nanoplatelets in the same way and measured their conductivity but, importantly, we did not observe an increased conductivity (Figure 3.15). Together, these experiments prove that we were able to prepare 2D nanoplatelets from polyethylene-like polymers carrying thiophene units on their surface and that conductivity on the crystal surface was achieved by copolymerization with EDOT in dispersion.

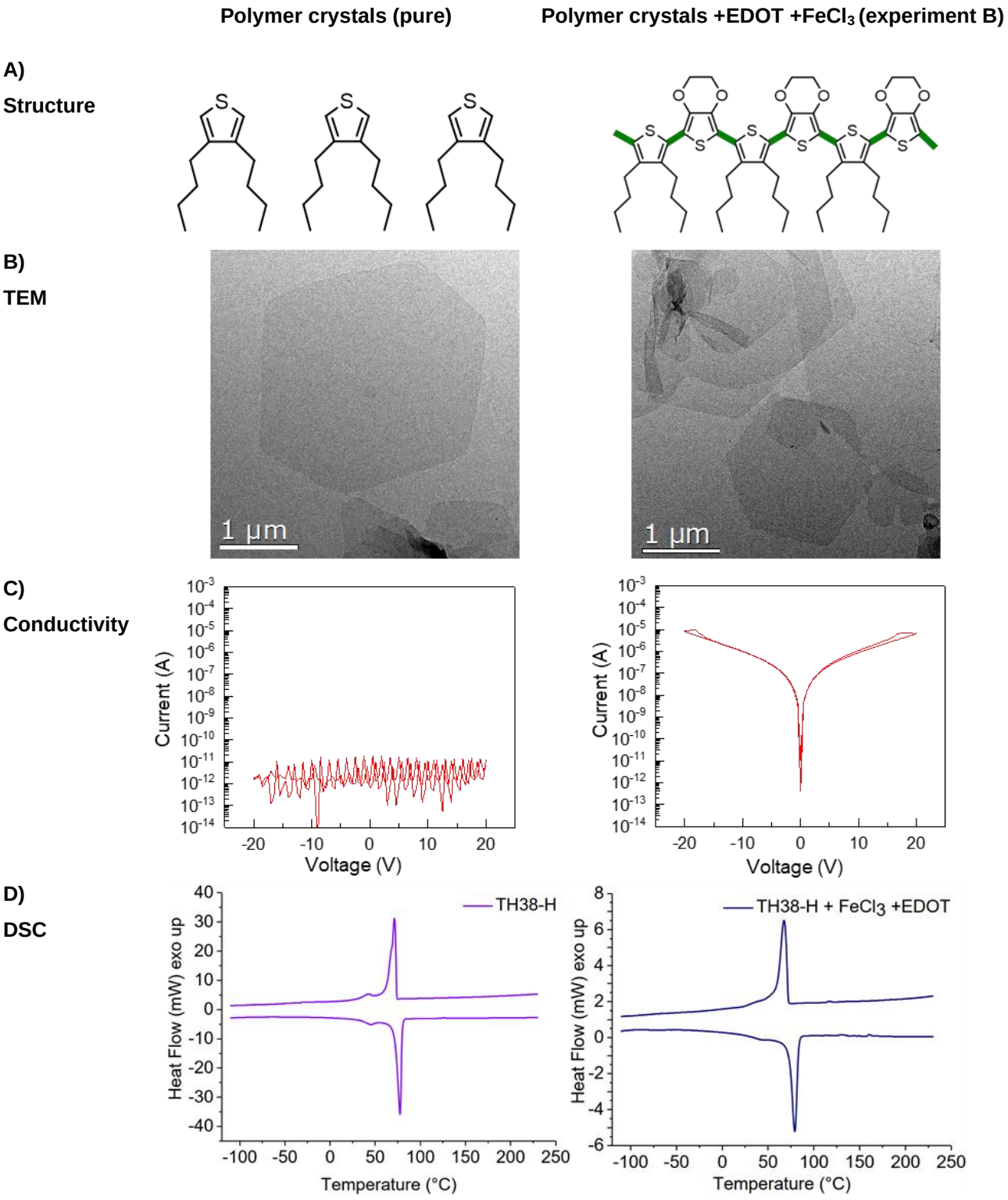

Figure 3.12. Structure (A), TEM bright-field micrograph (B), conductivity (C) and DSC thermograms (D) of polymer TH38-H before (left) and after electrochemical polymerization in crystal state with addition of EDOT (right).

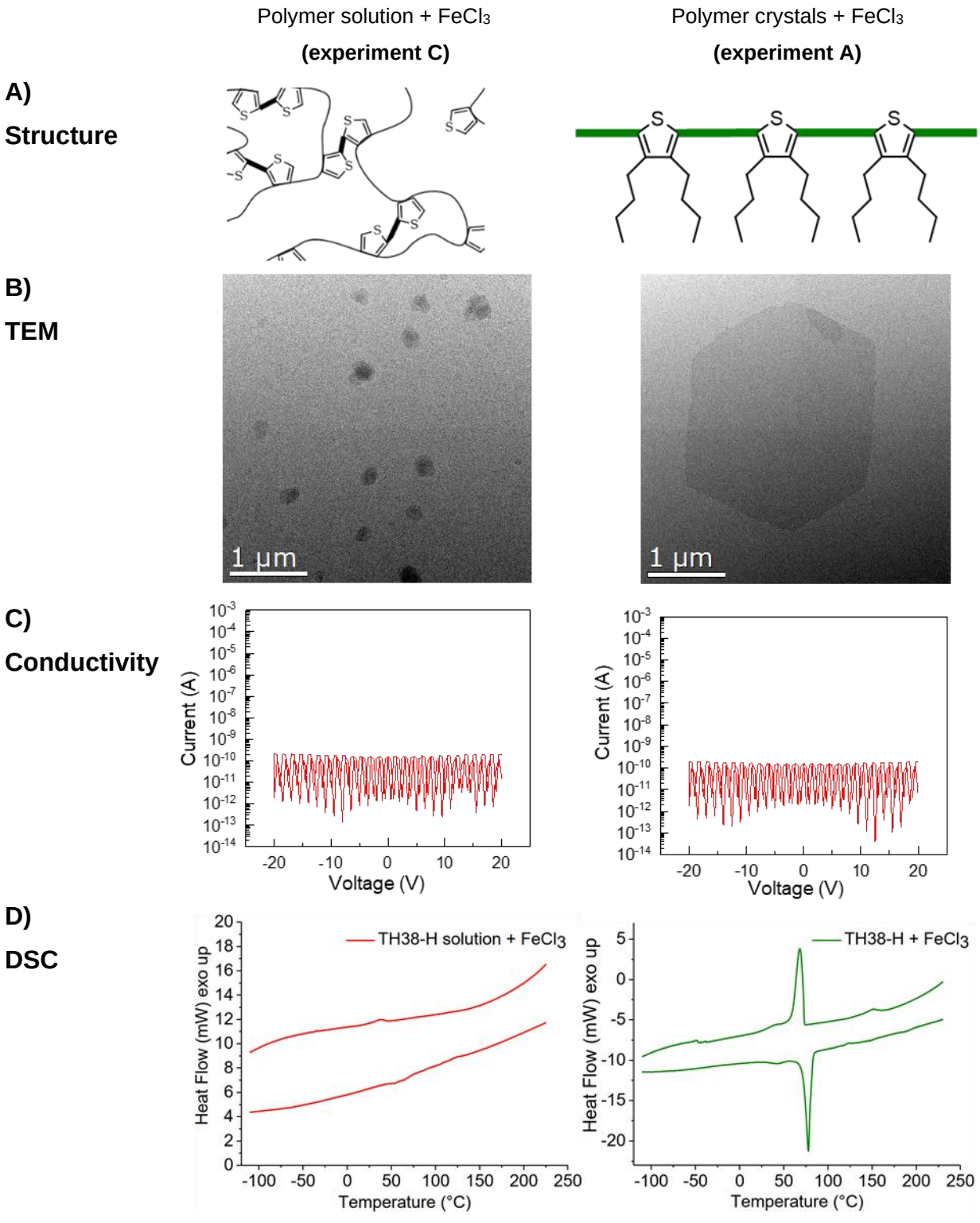

Figure 3.13. Structure (A), TEM bright-field micrograph (B), conductivity (C) and DSC thermograms (D) of polymer TH38-H after electrochemical polymerization in solution (left) in crystal state (right)

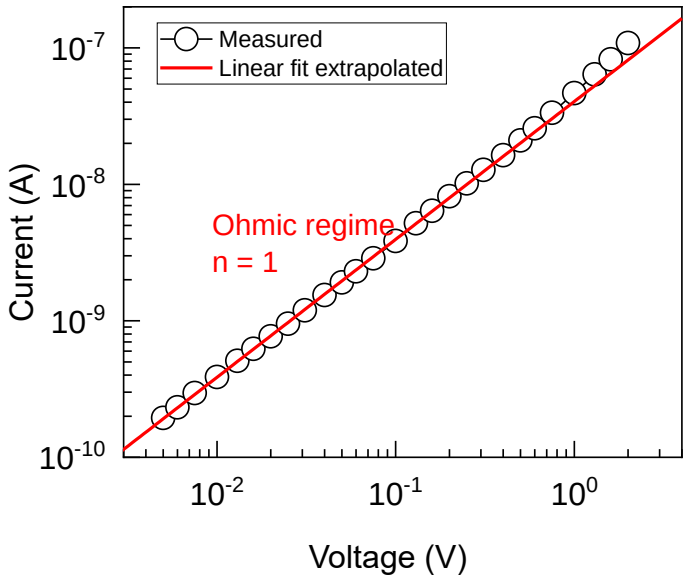

Figure 3.14. Log I-Log V plot at low bias regime to prove Ohmic electrical conduction of the polymer TH38-H after electrochemical polymerization in crystal state with addition of EDOT

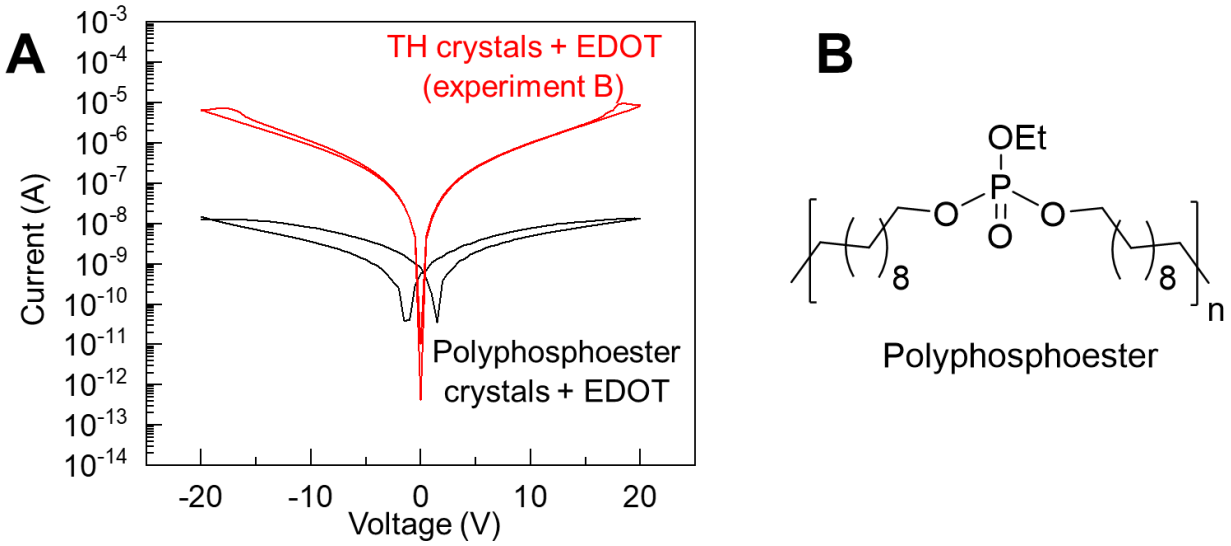

Figure 3.15. (A) "Negative control" experiment. Polyphosphoester crystals after reaction with EDOT in the presence of $FeCl_3$ (black curve) do not reveal conductivity compare to thiophene crystals with conductive surface (red curve). (B) Chemical structure of polyphosphoester polymer.

3.5. Experimental Section

Experimental

Solvents were purchased from Acros Organicsc and Sigma Aldrich and used as received, unless otherwise stated. 3,4-dibromothiophene, 11-bromo-1-undecene, 18-bromo-1-octadecene, 3,4-Ethylenedioxythiophene (EDOT), (1,3-dppp)$NiCl_2$, Mg, I_2, $CaCl_2$, $MgSO_4$, HCl, ethyl vinyl ether, were used as received from Acros Organics and Sigma Aldrich. The 1st generation Grubbs catalyst was purchased from Sigma-Aldrich and stored under argon atmosphere. Deuterated solvents were purchased from Acros Organics and Carl Roth Chemicals.

Instrumentation

Thin layer chromatography (TLC) was performed using Merck aluminium-foil baked plates coated with Kieselgel 60 F245. The products were visualized using UV fluorescence (254 nm) or potassium permanganate stain. Flash column chromatography was performed over Merck silica gel C60 (40-60 µm) using eluent systems as described for each experiment.

^1H and $^{13}C\{H\}$ NMR spectra were acquired on a 300 MHz Bruker system. The temperature was kept at 298.3 K and calibrated with a standard 1H methanol NMR sample using Topspin 3.0 (Bruker). $^{13}C\{H\}$ NMR spectra were referenced internally to solvent signals. The $^{13}C\{H\}$ NMR (101 MHz) measurements were obtained with a 1H power gate decoupling method using 30° degree flip angle. All spectra were measured in $CDCl_3$ at 298 K. The spectra were calibrated against the solvent signal and analyzed using MestReNova 14.1.0. (Mestrelab Research S.L).

Mass spectrum acquisitions were conducted on an Advion expression^L compact mass spectrometer (CMS) by using the atmospheric solids analysis probe (ASAP) technique. All spectra were acquired in the positive ion reflectron mode, *m/z* range from 10 to 2000 *m/z*, and acquisition speed 10000 *m/z* units s^{-1}. The obtained spectra were analyzed by using Advion CheMS Express software version 5.1.0.2

Wide-Angle X-ray Diffraction WAXD patterns of the precision PEs were obtained on a Philips PW 1820 diffractometer (scattering angle $2° \leq 2\theta \leq 60°$, 0.02° step size), using Cu Kα radiation (λ = 1.5418 Å) as X-ray source.

Gel-permeation chromatography (GPC) measurements were carried out in THF, with 1 g L^{-1} sample concentration. Sample injection was performed by a 717 plus auto sampler (Waters) at 30 °C (THF). Flow was 1 mL min^{-1}. Three SDV columns (PSS) with the dimensions 300 × 80 mm, 10 µm particle size and pore sizes of 106, 104, and 500 Å were employed. Detection was accomplished with DRI Shodex RI-101 detector (ERC) and UV−vis S-3702 detector (Soma). Calibration was carried out using polystyrene standards provided by Polymer Standards Service.

Differential Scanning Calorimetry (DSC). Thermal analysis was carried out using a Mettler-Toledo DSC 822. Three scanning cycles of heating/cooling were performed in a nitrogen atmosphere (30 mL/min) with a heating and cooling rate of 10 °C min^{-1} in a temperature range between -50 and 250 °C for polymers TH20, TH20-H, TH38, TH38-H and between -120 and 250 °C for all samples before and after electrochemical polymerization.

Thermal Gravimetric Analysis (TGA) was measured on a Mettler Toledo ThermoSTAR TGA/SDTA 851-Thermowaage in a nitrogen atmosphere. The heating rate was 10 °C min^{-1} in a temperature range between 25 and 900 °C.

Transmission Electron Microscopy (TEM). A FEI Tecnai F20 transmission electron microscope operated at an acceleration voltage of 200 kV was used to determine the crystal morphology and crystal structure. Bright field (BF) and parallel beam nano-electron diffraction (NBED) were used for measurements.

Conductivity measurement: glass substrates were sequentially cleaned by detergent, acetone, and 2-propanol by sonication for 5 min. each and then dried. Polymers TH38-H, A and B (Scheme 3.2) was crystallized on the substrate from hot ethyl acetate, dispersion of polymer C (Scheme 3.2) was applied on the substrate without additional preparation. Au electrodes were deposited on the dried films by thermal evaporation through shadow masks with a rate of 1 Å/s under high vacuum of 10^{-7} mbar. The spacing between the electrodes amounted to 20 µm, the electrode width was 10,000 µm. Current (I)-voltage (V) measurement was performed by Keithley 4200A semiconductor parameter analyzer in a vacuum probe station under 10^{-5} mbar.

Synthesis of Grignard reagent and ADMET diene monomers TH20-m and TH38-m

All reactions have been carried out under argon atmosphere. Into a flame-dried 25 mL 3-neck round-bottom flask, equipped with reflux and tube with $CaCl_2$ on the top neck and connected with argon line on left neck, magnesium metal pellets were added (0,34 g, 14.2 mmol, 3.45 eq) and a magnetic stirrer. After 10 minutes, one iodine crystal and 10 mL of THF were added. The mixture was heated to 40°C and the first halide of the alkyl bromides, i.e. 11-bromo-1-undecene (1,49 mL, 6.8 mmol, 1.5 eq) for TH20-m or 18-bromo-1-octadecene (2.25 g, 6.8 mmol, 1.5 eq) for TH38-m, were added. The reaction mixture slowly changed its color to dark blue, then add the second half of the respective alkyl halide was added. The mixture was allowed to stir until almost the whole magnesium metal pellets disappeared (ca. 30-40 minutes). After that, a solution of 3,4-dibromothiophene (1) (0.5 mL, 4.5 mmol, 1.0 eq) in 10 mL THF was added, followed by (1,3-dppp)$NiCl_2$ (0.12 g, 0.2 mmol, 0.05 eq). The reaction mixture was stirred at room temperature overnight and then poured into a mixture of water and hydrochloric acid. The aqueous layer was extracted with ether twice; combined organic phases were dried over anhydrous $MgSO_4$, filtered and dried under reduced pressure.

The product was purified by column chromatography over silica gel eluting with petroleum ether to give 3 as pale yellow oil. Yield 73% for TH20-m and 75% for TH38-m. ^{1}H NMR TH20-m (Figure 3.1 top) (CDCl3, δ): 6.81 (s, 2H), δ 5.73 (ddt, 2H), 4.94−4.84 (m, 4H), 2.45-2.40 (t, 4H), 2.00−1.92 (m, 4H), 1.57−1.52 (m, 4H), 1.28 (br s, 24H).^{13}C NMR TH20-m (Figure 3.2 top) (CDCl3, ppm): 142.11, 139.25,119.89, 114.12, 33.82, 29.67-28.82.

^{1}H NMR TH38-m (Figure 3.3 top) (CDCl3, δ): 6.81 (s, 2H), δ 5.73 (ddt, 2H), 4.94−4.84 (m, 4H), 2.45-2.40 (t, 4H), 1.97−1.88 (m, 4H), 1.59−1.54 (m, 4H), 1.28 (br s, 52H). ^{13}C NMR TH-38-m (Figure 3.4 top) (CDCl3, ppm): 142.12, 139.28, 119.87, 114.07, 33.84, 29.71 - 28.82.

GSMS (EI) for TH20-m (Figure 3.5): calcd for $C_{26}H_{44}S$: 388.7 (M), found: 388,1 (M). m/e: 789.9 GSMS (EI) for TH38-m (Figure 3.6): calcd for $C_{26}H_{44}S$: 585.1 (M), found: 585.9 (M). m/e: 663.9, 601.9, 587.9, 586.9, 583.9, 557.9, 335.5

Procedure for ADMET bulk polycondensation TH20 and TH38

Monomer TH20-m (0.7 g, 1.80 mmol, 1 eq) or monomer TH38-m (0.6 g, 1.026 mmol, 1 eq) was charged into a flame-dried 25 mL flask in CH_2Cl_2 (2 mL) and the solution was stirred for 5 min at room temperature under argon. Then, 1st generation Grubbs catalyst (0.01 eq) was added to this solution under an argon atmosphere. After the addition of the catalyst, the reaction mixture was stirred for 1 h at room temperature under argon flow and then evacuated to 5 x 10^{-2} mbar for 2 h, at 40 °C for 2 hours, at 60 °C for 5 h and at 80 °C for 10 h to remove ethylene and remaining solvent. . The reaction mixture was cooled to room temperature and the catalyst was terminated by adding ethyl vinyl ether (1 mL in 2 mL of CH_2Cl_2), followed by 30 min stirring at room temperature. The reaction mixture of was precipitated into methanol (100 mL). A brown, highly viscous polymer (4) was obtained after removal of the solvent in vacuo (Yield: 73 %). ^{1}H NMR TH20 (Figure 3.1 middle) (CDCl3, δ): 6.81 (s), δ 5,33-5,23 (m), 2.44-2.39 (t), 1.96−1.86 (m), 1.59−1.50 (m), 1.26 (br s, backbone). ^{13}C NMR TH20 (Figure 3.2 middle) (CDCl3, δ): 142.11, 130.38, 119.89, 33.66, 29.66-28.85. ^{1}H NMR TH38 (Figure 3.3 middle) (CDCl3, δ): 6.81 (s), δ 5,32-5,26 (m), 2.45-2.40 (t), 1.97−1.86 (m), 1.59−1.51 (m), 1.26 (br s, backbone). ^{13}C NMR TH-38 (Figure 3.4 middle) (CDCl3, ppm): 142.11, 130.36, 119.87, 32.63, 29.72-28.82.

Hydrogenation of polymer TH20

The hydrogenation was performed using a Grubbs catalyst 1st generation modified with ethyl vinyl ether as the catalyst.[177] In a glass vessel, TH20 (500 mg) was dissolved in 10 mL THF and argon was bubbled through the solution for 5 min. Upon addition of the catalyst (1% mol), the solution changed its color to orange. The hydrogenation was performed in a 250 mL ROTH autoclave. The system was flushed twice with hydrogen, afterwards the hydrogenation was performed at 40 °C and 70 bar H_2 for 2 days. Dark brown solution was concentrated in vacuo before precipitating into cold methanol to yield an off-white solid material (80% yield). ^{1}H NMR (Figure 3.1 bottom) (CDCl3, δ): 6.81 (s), 2.45-2.439 (t), 1.59−1.51 (m), 1.26 (br s, backbone). ^{13}C NMR (Figure 3.2 bottom) (CDCl3, δ): 142.11, 19.86, 29.73 -28.82.

Hydrogenation of polymer TH38

The hydrogenation was performed using a Grubbs catalyst 1st generation modified with ethyl vinyl ether as the catalyst. In a glass vessel, TH38 (300 mg) was dissolved in 10 mL toluene and argon was bubbled through the solution for 5 min. Upon addition of the catalyst (1% mol), the solution changed its color to orange. The hydrogenation was performed in a 250 mL ROTH autoclave. The system was flushed twice with hydrogen, afterwards the hydrogenation was performed at 50 °C and 65 bar H_2 overnight. Dark brown solution was concentrated in vacuo before precipitating into cold methanol to yield an off-white solid material (80% yield). ^{1}H NMR (Figure 3.3 bottom) (CDCl3, δ): 6.81 (s), 2.45-2.40 (t), 1.97−1.86 (m), 1.59−1.51 (m), 1.26 (br s, backbone). ^{13}C NMR (Figure 3.4 bottom) (CDCl3, δ): 142.11, 119.87, 29.72 - 28.82.

Electrochemical polymerization. All experiments were performed under an argon atmosphere.

In dispersion of nanoplatelets: $FeCl_3$ (0.11 g, 0.68 mmol, 4 eq) was dissolved in 10 mL dry ethyl acetate and cooled to 0°C in an ice bath. TH38 (0.1 g, 0.17 mmol, 1eq) was dissolved in 5 mL ethyl acetate, heated up to 70°C and cooled down to room temperature within 30 minutes to form polymer platelets. Obtained dispersion

was cooled to 0°C and added dropwise to the $FeCl_3$ solution. Subsequently, the mixture was stirred for 2 h at 0°C, then warmed up to room temperature and stirred for 24h and precipitated into 80 mL of methanol.

In solution: $FeCl_3$ (0.11 g, 0.68 mmol, 4 eq) was dissolved in 10 mL dry $CHCl_3$ and cooled to 0°C in an ice bath. TH38 (0.1 g, 0.17 mmol, 1eq) was dissolved in 5 mL $CHCl_3$, cooled to 0°C and added dropwise to the solution. This mixture was stirred for 2 h at 0°C, then warmed up to room temperature and stirred for 24h and finally precipitated into 80 mL of methanol.

In dispersion of nanoplatelets with EDOT: $FeCl_3$ (0.11 g, 0.68 mmol, 4 eq) was dissolved in 10 mL dry ethyl acetate and solution was cooled down to 0°C in an ice bath. TH38 (0.1 g, 0.17 mmol, 1eq) was dissolved in 5 mL ethyl acetate, heated up to 70°C and slowly cooled down to room temperature to form polymer crystals. EDOT (0.04 mL, 0.37 mmol, 1.1 eq) was added to the polymer crystal dispersion. The mixture was cooled to 0°C and added dropwise to the $FeCl_3$ solution. After several minutes the color of reaction mixture turned dark blue. The mixture was stirred for another 2 h at 0°C, then warmed up to room temperature and stirred for 24h before precipitation in methanol.

Negative control experiment: $FeCl_3$ (0.11 g, 0.68 mmol, 4 eq) was dissolved in 10 mL dry ethyl acetate and solution was cooled down to 0°C in an ice bath. A structurally similar polyphosphoester (Chapter 2 and ref.[19]) (0.11 g, 0.17 mmol, 1eq) was dissolved in 5 mL ethyl acetate, heated up to 70°C and slowly cooled down to room temperature to form polymer crystals. EDOT (0.04 mL, 0.37 mmol, 1.1 eq) was added to the polymer crystal dispersion and then cooled to 0°C and added dropwise to the $FeCl_3$ solution.

After several minutes the color of the reaction mixture turned dark blue indicating the polymerization of EDOT. The mixture was stirred at 0°C for 2 h, then warmed up to the room temperature and stirred for 24h and precipitated into methanol.

3.6. Conclusion and outlook

We demonstrated a new method to generate polymer 2D lamellar nanoplatelets with a conductive surface. By crystallizing polyethylene-derivatives from a dilute solution that carry thiophene groups with a precise, equidistant distribution along their backbone, lamellar crystals with a constant thickness and a thiophene surface functionalization were obtained (nanoplatelets). The thiophene groups, expelled from the crystal surface, were copolymerized with EDOT, yielding a conductive surface. This is a new, versatile concept exploiting the crystallization of a polyethylene-derivative with build-in in-chain functional groups to spatially control conductivity on the surface of nanoplatelets. Because the crystallization from solution can be easily controlled, a combination of polymers, doped with different functional groups, can be co-crystallized and will yield a nanostructured polymer crystal with a local control of the chemical groups on the surface. Accordingly, this new method has the potential to serve as a versatile concept to achieve nanostructured surface functionalization, not only for microelectronic applications. By chemically tailoring the polymer, a versatile spectrum of functionalities can be placed on the surface of the crystal nanoplatelets.

.

4. Vitamin C loaded polyethylene: synthesis and properties of precise polyethylene with vitamin C defects via acyclic diene metathesis polycondensation

Oksana Suraeva, Carole Champanhac, Volker Mailänder, Frederik R. Wurm, Henning Weiss, Rüdiger Berger, Markus Mezger, Katharina Landfester, and Ingo Lieberwirth

Based on "*Macromolecules*, **2020**, *53*, 2932-2941." Copyright 2020 American Chemical Society. Open access provided.

I designed, synthesized and analyzed all polymers, performed crystallization experiments, degradation and free radical scavenging tests and wrote the manuscript. Henning Weiss performed SAXS measurements. Rüdiger Berger performed AFM measurements. Viability and cell uptake experiments were performed by Carole Champanhac.

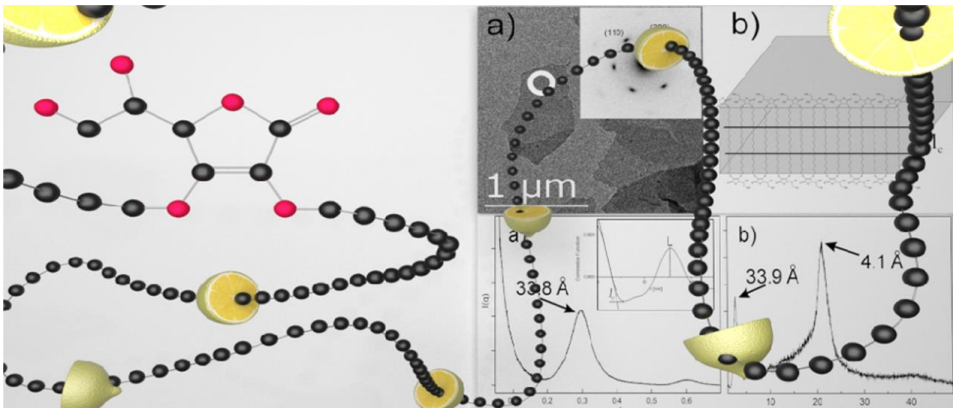

Keywords: Acyclic diene metathesis polymerization, ADMET, free radical scavenging, vitamin C, polymers, defect engineering

4.1. Preface

In this chapter I introduce a biologically active molecule – ascorbic acid – as a defect in the polymer chain. Ascorbic acid, also known as vitamin C, is an essential nutrient, required for the functioning of several enzymes, important for the immune system and possesses antioxidant properties, what raises the attention of various bio-directed research areas to this molecule. Accordingly, there is a demand to preserve the bio-active properties of the vitamin C molecule after the introduction to polymer-based systems and I will show how my approach fulfills these requirements.

Initially, inspiration to introduce ascorbic acid molecule in the polymer chain came from the work of Luleburgaz *et al*.,[205] who created an unsaturated polymer loaded with vitamin C groups. I improved this idea and went further by increasing the distance between the defects and subsequent hydrogenation of the polymer, so it can crystallize. The ADMET approach yields equidistant defects in the polyethylene chain. Hence, after crystallization I got nice 2D crystals with a surface that is homogeneously covered by vitamin C groups. These groups are available for further reactions.

The bioactivity of vitamin C molecules retains even after substitution of two hydroxy groups, which is proved by several observations. First, in contrast to pure polyethylene, the vitamin C containing polymer shows hydrolytic degradation in the presence of sodium hydroxide both in solution and in crystal state. The latter is an additional evidence, that the vitamin C groups are expelled to the crystal surface, otherwise the NaOH molecules would not be able to reach the vitamin C groups. Moreover, the vitamin C polymer crystals show free-radical scavenging properties. Hence, I also investigated the cell uptake of the crystals. For this purpose, the available hydroxy groups were labeled with fluorescent dyes, confirming at the same time that incorporated defects / vitamin C groups keep their functionality. The fluorescent labeld 2D crystals show a high cell uptake with no cytotoxicity. Hence, the vitamin C loaded polyethylene can be used for biomedical applications.

In summary, this chapter shows that the incorporation of defects not only provides certain functional groups in the final system, but also that the properties of the initial defect group molecules can be preserved and transferred to the polymer structure. Despite this approach yields a convenient tool to create polymer 2D crystals with any specific properties, it only generates 2D structures with a homogeneous surface. In the following chapter I will develop the idea further to achieve local control of surface functionality.

4.2. Abstract

A polyethylene-like polymer with an in-chain vitamin C group was synthesized by olefin metathesis polymerization. Here, we describe both the synthesis and a comprehensive physical characterization. Because of the olefin metathesis synthesis, the vitamin C groups are equidistantly arranged in the polyethylene (PE) main chain. Their separation was adjusted to 20 CH2 units. After hydrogenation, a semicrystalline polymer is obtained that is soluble in polar solvents. Because of its size and steric effect, the vitamin C acts as a chain defect, which is expelled from the crystal lattice, yielding a lamellar crystal with a homogeneous thickness corresponding to the interdefect distance. The physical properties were examined by various methods including differential scanning calorimetry, X-ray scattering, and transmission electron microscopy. We show that vitamin C retains its radical scavenger properties despite being incorporated into a polyethylene chain. Furthermore, we demonstrate that it is degrading in alkaline conditions. To complete its suitability as a biocompatible material, cytotoxicity and cell uptake experiments were performed. We show that the polymer is nontoxic and that it is taken up in nanoparticular form via endocytosis processes into the cytoplasm of cells.

4.3. Introduction

The material class of polymers is characterized, among other things, by the fact that the properties and functionality of the material can be specifically adjusted via the macromolecular architecture. The combination of different molecules by means of polymerization to form a macromolecule, for example, offers an almost innumerable amount of possible new polymers. Thus, it is possible to specifically design a polymer with a certain property or functionality. This can be achieved by transferring the functionality of a specific molecule to the polymer during polymerization.[206–208]

Most fossil and bio-based polymers contain certain defects, such as chain ends, pendant groups, or branches; the latter two are typically randomly distributed along the polymer chain. The random defect distribution makes it difficult to estimate the influence of defects on the properties of the polymer. Of course, this also applies to polymers that contain functional groups. Here, too, the functional groups are randomly distributed in the main chain. Accordingly, a further aspect in the tailor-made design of a polymer with correspondingly planned properties is the positioning of the functional groups in the main chain of the polymer. In contrast to most other polymerizations, acyclic diene metathesis polymerization (ADMET) is characterized by the fact that the functional groups are integrated into the polymer chain at a precisely defined distance. ADMET polymerization is a unique strategy for preparing polymers with precise control over the molecular structure.[199] It is a step-growth polymerization driven by the release of a condensate, usually ethylene. Furthermore, ADMET offers synthetic routes to perfectly linear polyethylene and to a variety of alkyl branched and functionalized polyethylenes that have precisely placed pendant groups along the hydrocarbon backbone.[26,209,210] If the length of the segments and the periodicity of their placement are precisely controlled, crystallization will result in well-defined and predictable morphologies with lamellar polymer crystals of precisely adjusted lamellar thickness.[164,211] Depending on the size of the defect group, it is either integrated into the crystal lattice or expelled from the crystal to the basal surface of the lamella during crystallization. The first effect is expected for defects smaller than propyl, whereas more bulky defects are expected to be expelled to the surface of the

lamellar crystal. The latter allows to generate well-defined structures in which the defect groups are regularly arranged on the surface of a thin, lamellar crystal. As a result, it is possible to control their spatial arrangement simply by crystallization.

Based on the above-mentioned aspects, it should therefore be possible to incorporate a biologically active small molecule into the chain of a polymer. In biological systems, vitamin C plays the role of an effective antioxidant.[212] The biochemical functions of vitamin C, especially its antiviral and antitumor properties, are of increasing interest.[213] However, the use of vitamin C is limited by its physical and chemical instability. It is highly unstable and very easy to get oxidized and changes to dehydroascorbic acid when exposed to light, air, and elevated temperature.

The introduction of vitamin C into the polymer structure not only brings functional groups into the obtained product, but it is expected to be bioactive and provides free radical scavenging properties, which can prevent biomolecules such as proteins, DNA, and lipids from damage.

In this work, we synthesize a new polyethylene-mimic polymer with equidistantly distributed vitamin C groups as a defect in the polymer main chain. Vitamin C presents several electrophilic groups. It contains four hydroxyl groups in positions 2, 3, 5, and 6 with different acidities allowing acid–base reactions. The −OH in position 3 is the more acidic one (*pKa* = 4.2), while the hydroxyl in position 2 has a *pKa* of 11.6, and those in positions 5 and 6 behave as secondary and primary alcohol (*pKa* ≈ 17 and 16, respectively).[214] Initial protection of two hydroxyl groups in positions 5 and 6 is necessary to decrease hydrophilicity of l-ascorbic acid for further modification.

From synthesis, we obtain an amphiphilic, semicrystalline material. Final deprotection reveals hydroxyl groups capable of further modifications. The thermal properties and the crystal structure of the polyethylene-like polymer have been studied as well as the degradation and free-radical scavenging properties. Because of the bio-based synthetic approach and potential biological relevance of the obtained material, we tested the biocompatibility of the polymer by assessing the toxicity of the pure polymer and investigated cellular uptake.

4.4. Results and Discussion

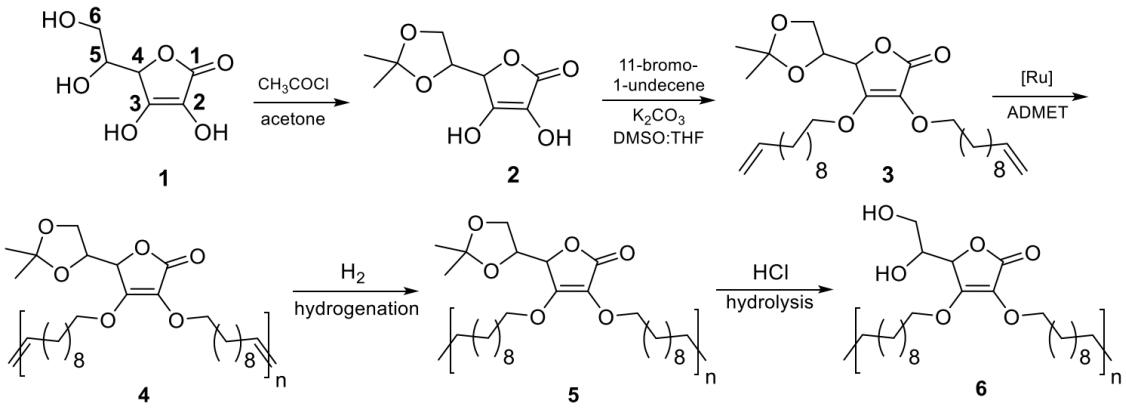

Scheme 4.1. Synthetic Procedure for α,ω-Diene Functionalized l-Ascorbic Acid 3 and Its ADMET Polymerization

Monomer and Polymer Synthesis (*Scheme 4.1*)

For the preparation of the ADMET monomer **3**, ascorbic acid **1** was protected first as acetonide. Vitamin C was dissolved in an excess of acetone containing catalytic amounts of acetyl chloride. The acetonide **2** crystallized directly from the reaction in yields of 80–85%. The speed of this reaction depends on the temperature: at 0 °C even after several hours stirring no changes were detected (**Figure *4.1***); after 4 h at room temperature the appearance of peaks at 4.06, 4.20, 4.49, and 4.81 ppm in the ^{1}H NMR spectrum is indicative of acetonide. After stirring the reaction mixture overnight at 40 °C, we obtained the almost fully protected form of L-ascorbic acid.

The monomer **3** for ADMET polymerization was prepared according to Scheme 4.1 in a mixture of DMSO/THF with excess of 11-bromo-1-undecene. After column chromatography the structure of **3** was confirmed by NMR spectroscopy and mass spectrometry (Figure 4.2 and Figure 4.3) (peak with mass 521.0 originated for the disubstituted acetonide form of L-ascorbic acid). The terminal olefin protons were detected at 4.9 and 5.7 ppm and the terminal olefin carbon signal at 139.2 and 114.2 ppm from ^{1}H and ^{13}C NMR spectra, respectively, indicating that the alkylation reaction was successful (Figure 4.4).

Polymerization of **3** was conducted in the bulk in the presence of 1% of Grubbs first-generation catalyst. Instead of terminal double bonds, multiplets at 4.9 and 5.7 ppm, a new internal double bond multiplet at 5.30 ppm was detected in ^{1}H NMR spectra after ADMET polycondensation. Internal double bonds in **4** were hydrogenated in the presence of palladium hydroxide on activated charcoal. The structure of successfully hydrogenated polymer **5** was confirmed by NMR spectroscopy (Figure 4.3 and Figure 4.4).

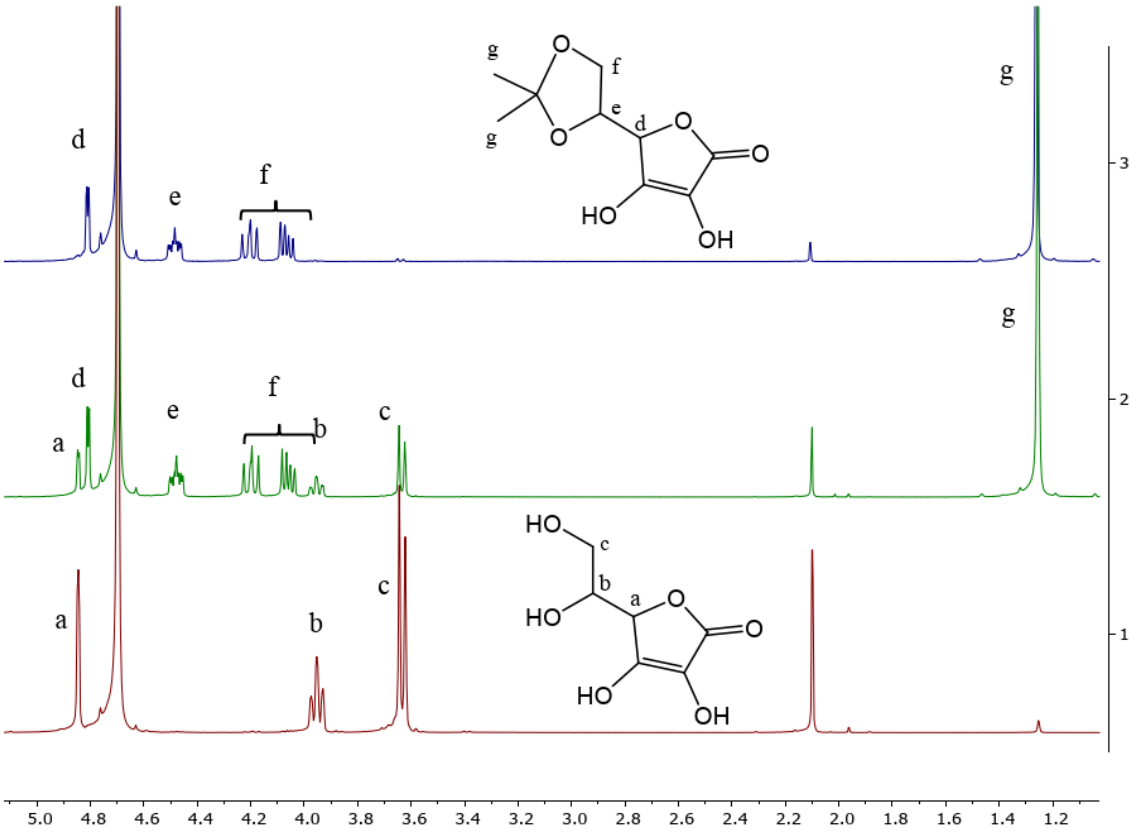

Figure 4.1. [1]H NMR spectra of protection reaction of initial vitamin C molecule **1** to its protected form of acetonide **2**

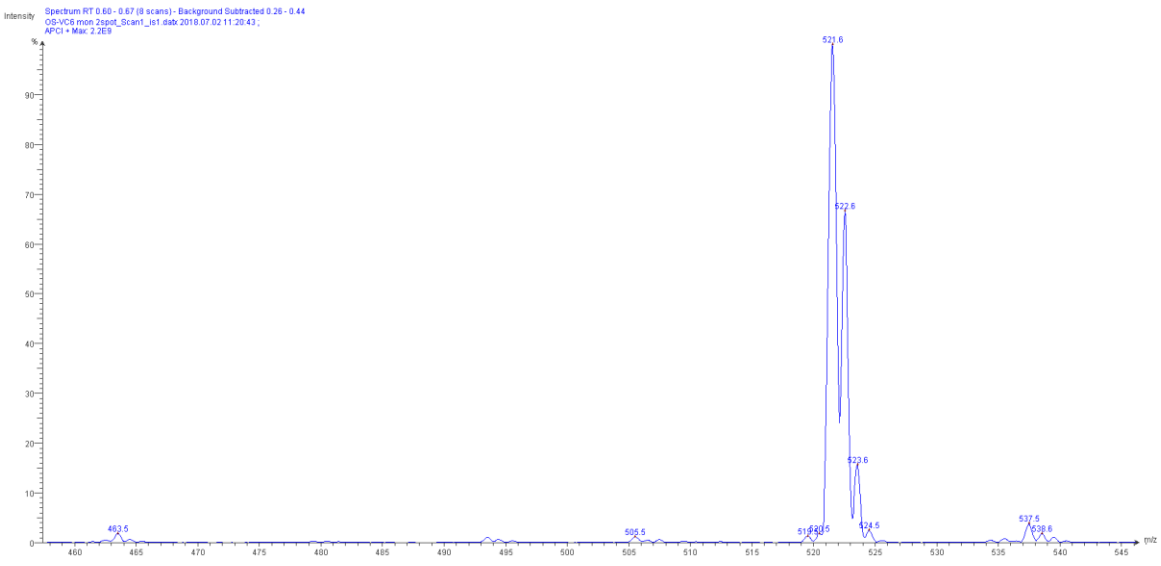

Figure 4.2. Mass-spectrum of monomer **3**

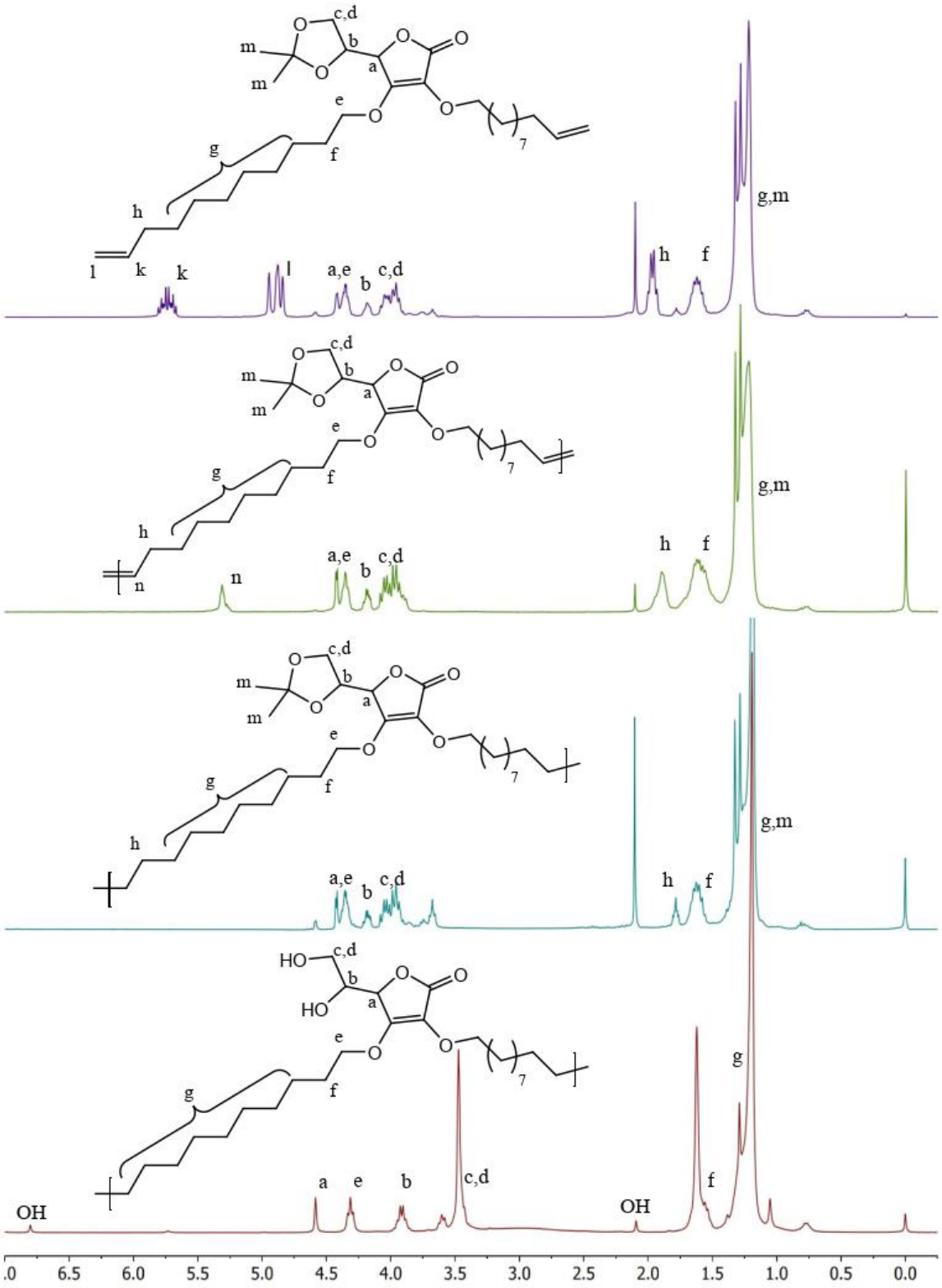

Figure 4.3. [1]H NMR spectra of **3, 4, 5** and **6**

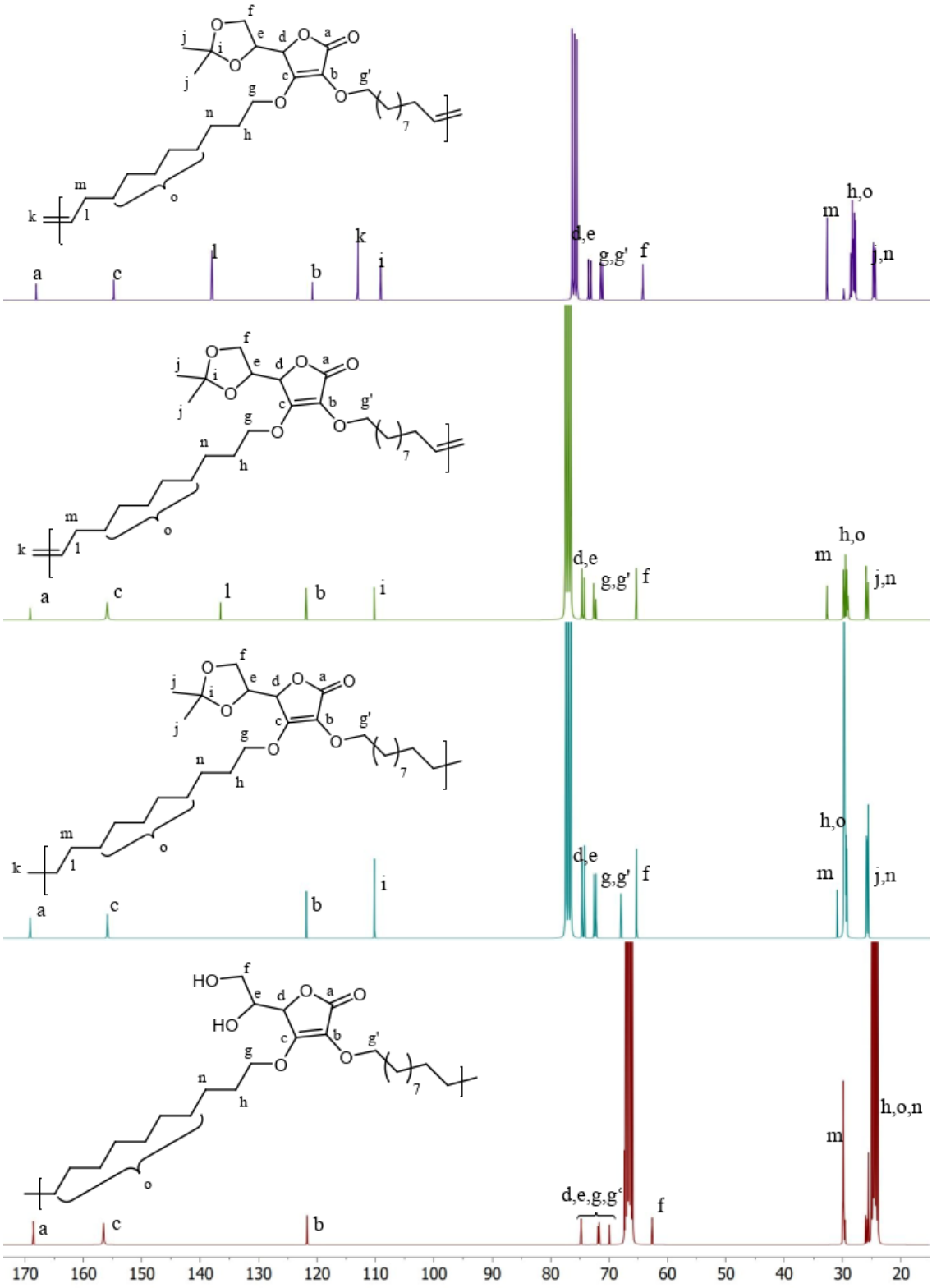

Figure 4.4. ^{13}C NMR spectra of **3, 4, 5** and **6**

Comparison of the ^{13}C NMR spectra of monomer before polymerization and polymer after hydrogenation (Figure 4.4) shows signals at 139.1, 114.12, and 33.8 ppm (l, k, and m peaks in ^{13}C NMR spectra, respectively),

which proves that the terminal double bonds in the monomer disappeared after polymerization, changed to internal olefins, and vanished from the spectra after hydrogenation.

The hydrolysis of the ketal groups in polymer **5** was achieved in THF by the addition of HCl solution. The structure of deprotected poly(vitamin C) **6** with functional OH groups was confirmed by ^{1}H and ^{13}C NMR spectroscopy. In the ^{13}C NMR spectra (Figure 4.4), the peak at 110.2 ppm was completely removed; in ^{1}H NMR spectra the methine and methylene protons next to hydroxyl groups at 3.6–4.6 ppm have shifted to positions, corresponding to the expected structure of product **6**, which is similar to initial L-ascorbic acid before modifications. The ^{13}C NMR spectra of polymer **6** reveal vitamin C ring peaks at 121.0, 155.4, and 168.2 ppm (Figure 4.4, peaks a, b, and c), which confirm that hydrogenation conditions are mild enough and the eneone within the vitamin C moiety survived the process.

By comparing GPC elugrams of polymers **4** and **6**, we observed a slight shift to a lower molecular weight region since the removal of the ketal group causes the smaller hydrodynamic volume (Figure 4.5).

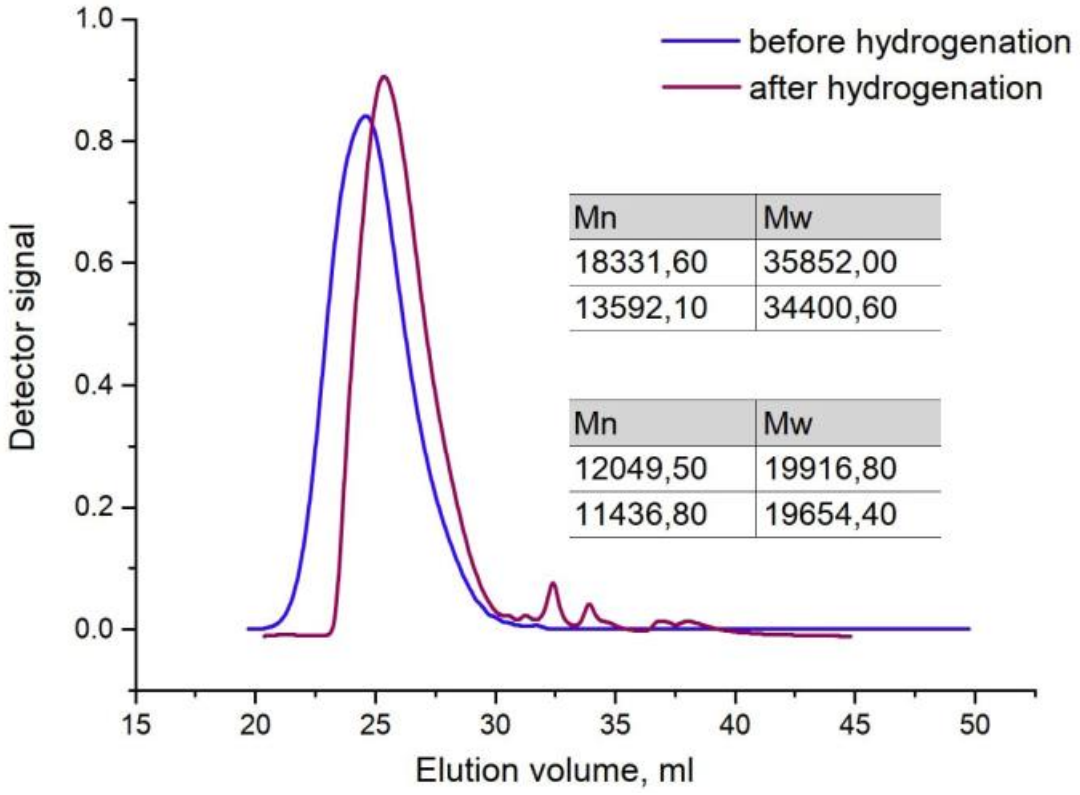

Figure 4.5. GPC curves of unsaturated polymer 4 (blue), and polymer 6 (purple) after hydrogenation and deprotection.

The unsaturated polymer **4** synthesized in this study was obtained as a highly viscous, sticky material, while the hydrogenated polymer **5** and its deprotected form **6** were solids.

Solid-State Characterization

Table ***4.1*** summarizes the thermal and molecular properties of polymers **4** and **6** synthesized in this study. Both the non-hydrogenated and the hydrogenated polymers can crystallize, as shown by the DSC thermograms in Figure 4.6. The hydrogenation of **4** to **6** leads to a shift of the main melting temperature T_m from 29 to 99 °C and an increase in the melting enthalpy from ca. −37 to −43 J g^{-1}. Correspondingly, the crystallization temperature T_c increases from 9 to 91 °C upon hydrogenation. The glass transition temperature T_g for both polymers could not be explicitly read from the DSC thermograms. The melting and crystallization temperatures of polymer **6** are remarkably high, especially considering that the molecular chain has a defect concentration of 1/20. Common PE shows a melting temperatures around 130 °C with a molecular defect concentration well below 1%.[45] Precision polymers with pure aliphatic pendant groups placed every 20 CH_2 units along the chain show melting temperatures ranging from 63 °C for a methyl branch down to ~12 °C for larger branches like propyl.[17] For similar polymers containing in-chain aromatic or other bulky defects remarkably higher melting temperatures have been observed as well.[173,215,216] The vitamin C substituted polymer **6** is similar to the arylene ether polymer with the defect group substituted in the ortho-position reported by Song *et al*., which exhibited a melting temperature of 81.7 °C.[168]

	M_n[a]	M_w[a]	$Đ$[a]	T_m[b]	T_c[b]	ΔH_m[b]	ΔH_c[b]
polymer	*(g mol^{-1})*	*(g mol^{-1})*		*(° C)*	*(° C)*	*(J g^{-1})*	*(J g^{-1})*
polymer 4	18,300	35,800	2.0	29.3	9.5	-37.0	30.6
polymer 6	12,050	19,900	1.7	99.4	90.6	-42,9	45,6

[a]Determined by SEC in THF vs polysterene standard**.**

[b]Determined by DSC.

Table 4.1. Molecular Weights and Thermal Properties of the Unsaturated and the Deprotected and Hydrogenated Polymer

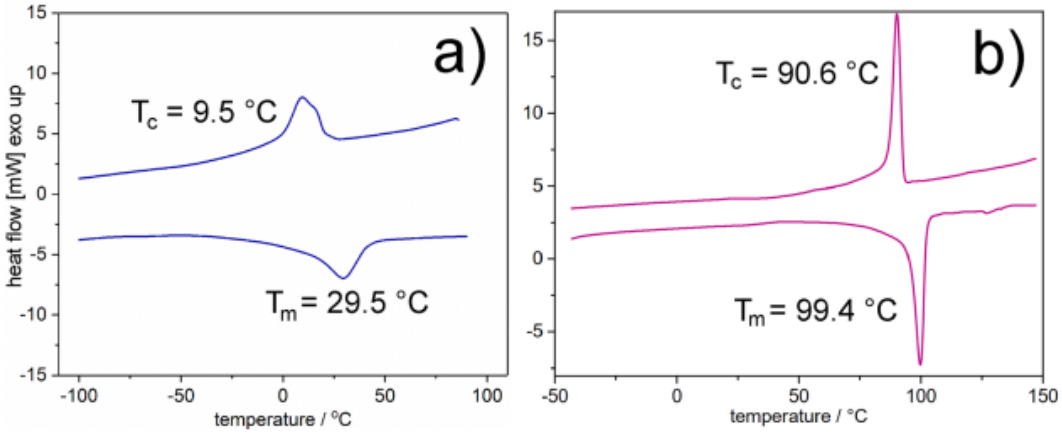

Figure 4.6. DSC thermograms of polymers 4 and 6. The hydrogenation of polymer 4 to polymer 6 results in a significant shift of crystallization and melting temperature of ~70 °C. This has to be attributed to the elimination of the central double bond which acts as an additional defect for the crystallization.

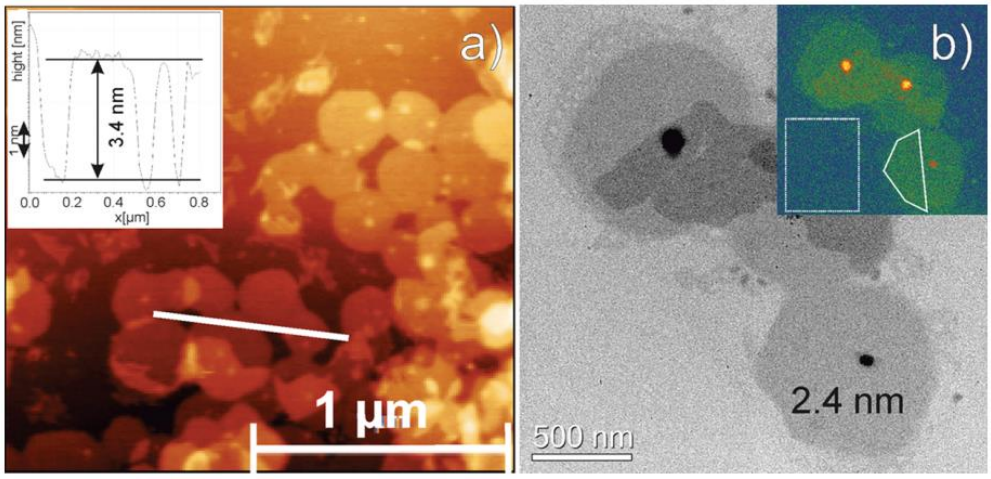

Figure 4.7. Thickness of solution grown single crystals of polymer 6. (a) AFM topography yields a lamellar thickness of 3.4 nm (inset: height profile along the indicated line). (b) EFTEM micrograph and thickness map (inset) yielding a lamellar thickness of 2.4 nm. The annotated areas indicate the positions used for the thickness measurement of the carbon substrate and the single crystal.

For crystallization and the formation of a crystal lattice, the vitamin C group represents a bulky defect that cannot be incorporated into the crystal lattice and is therefore expelled to the basal surface of the crystal. However, the ortho-substituted vitamin C groups promote an adjacent reentry of the PE chains at the crystal surfaces. Consequently, the lamellar thickness is limited by the precise alkyl spacing of 20 CH_2 units, which amounts to a total length of 20 × 0.127 nm = 2.5 nm for C_{20} alkyl chains in the all-trans configuration. Figure 4.7 shows measurements of solution grown single crystals of polymer **6** by AFM and EFTEM. From AFM topography we extracted a crystal thickness of ~3.4 nm, which corresponds to a distance given by 20 CH_2 units and 2 vitamin C molecules situated at the top and bottom of the crystal. EFTEM yields a thickness of 2.4 nm. The latter is very close to the expected lamellar thickness formed by 20 CH_2 units in the all-trans configuration. Possibly the electron beam damage during the TEM measurement leads to a loss of the vitamin C molecules, and only the polymer crystal bulk remains.

The above-mentioned thicknesses have been measured on solution grown single crystals whereas the thermal characterization was done by using melt crystallized samples. Accordingly, X-ray scattering measurements of annealed polymer **6** have been performed to better correlate the thermal data to the underlying crystal structure. Prior to the X-ray measurements, the polymer was annealed at 80 °C for 5 h. Figure 4.8 shows the data obtained by small- and wide-angle X-ray scattering.

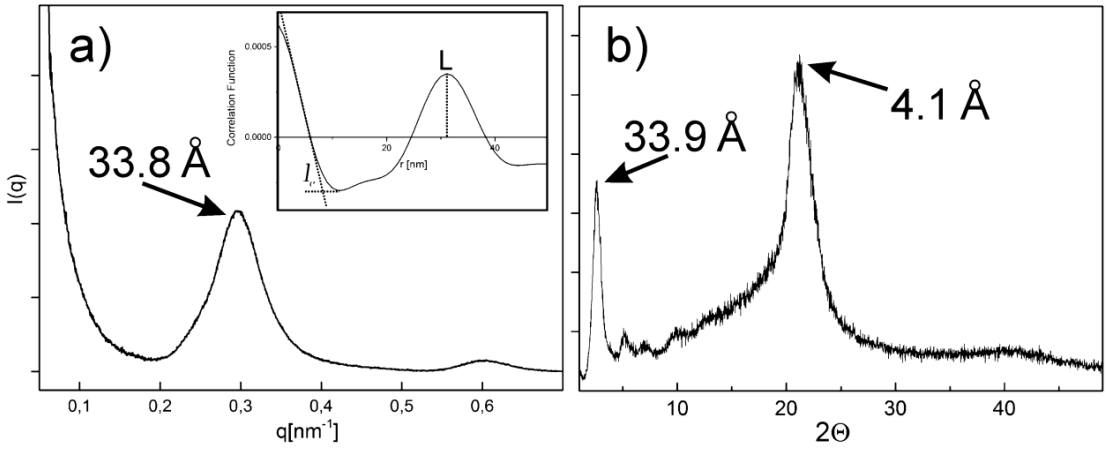

Figure 4.8. (a) SAXS data with the corresponding correlation function (inset) and (b) WAXS measurements of polymer 6.

At small angles, a peak corresponding to a long period of 33.9 Å is found in the SAXS and WAXS patterns. Moreover, in the WAXS pattern (Figure 4.8b) a broad peak with 4.1 Å lattice plane distance represents in-plane reflections of the PE crystal. PE crystallizes in an orthorhombic unit cell which gives rise to distinct (110) and (200) Bragg reflections at 2θ = 21.7° and 24°, respectively. When the polymer crystallizes in a pseudohexagonal crystal structure, the (110) and the (200) peaks coincide, yielding one peak around 2θ ≈ 21°.[217] Furthermore, using Equation 2, we determined the crystallinity of polymer **6** to be X_{vol} = 27% from the WAXS measurement.

The SAXS pattern shows a dominant peak at a long spacing period of 33.8 Å (q = 0.29 nm^{-1}). A weaker, second-order peak is observed at q = 0.59 nm^{-1}. The long spacing period of 33.8 Å is comparable to the length of 25.4 Å for an all-trans C20 alkyl chain plus the size of two vitamin C groups as measured by AFM. Albeit weak, the clear presence of the second-order peak indicates that the interface between the amorphous and crystalline region is rather sharp. Apparently, the equidistant spacing between the vitamin C defects in the PE main chain significantly reduce fluctuations of the lamella periodicity, commonly suppressing the second-order signal. Using Equation 4 in combination with the crystallinity obtained from WAXS, we obtained a lamellar crystal thickness l_c = 8 Å. The pair correlation function extracted from the SAXS data (inset in Figure 4.8a) shows similar results. According to this, the long period is L = 31.0 Å, and the layer thicknesses are 23 and 8 Å. As already extracted from the crystallinity measurement, the 8 Å periodicity has to be attributed to the "neat" crystal thickness l_c, whereas the 23 Å periodicity is more likely the thickness of the amorphous layer. However, the shape of the resulting correlation function is not ideal, and therefore these results should be treated with some caution. In conclusion, these data from the melt-grown polymer **6** indicate that in between two defects only a few CH_2 groups seem to crystallize. Hence, together with the vitamin C groups a significant fraction of them are excluded from PE crystal lamella and form the amorphous phase. Because of ortho-substitution and the steric effect of vitamin C defect groups, they cannot be included into the crystal phase, which prevents formation of thick lamellae.

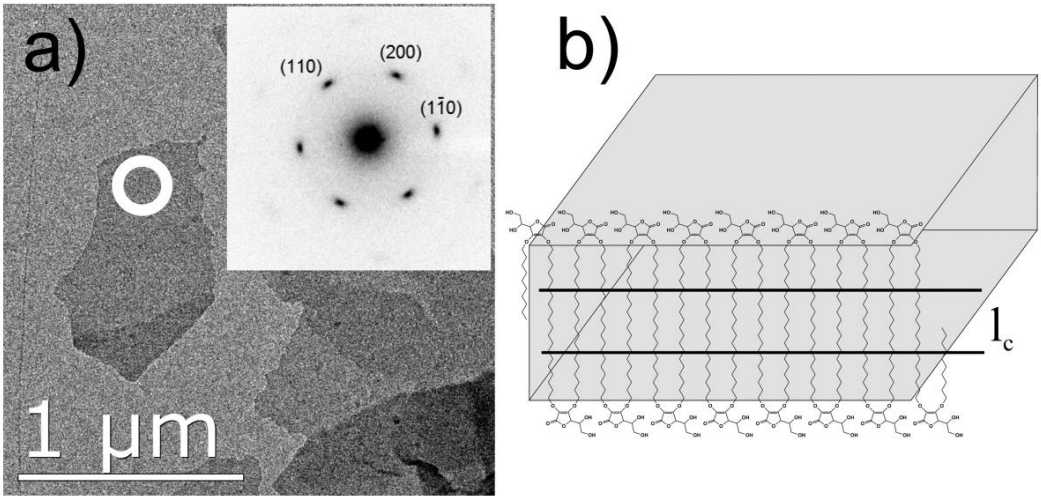

Figure 4.9. (a) TEM bright-field micrograph and selected area electron diffraction pattern (inset) of solution grown single crystal of polymer 6 from ethyl acetate solution. The diffraction spots reveal a nearly perfect quasi-hexagonal crystal structure with a lattice distance of 4.16 Å for (110) and 4.10 Å for (200). Assuming an orthorhombic crystal lattice, the lattice constants for polymer 6 are a = 8.2 Å and b = 4.8 Å. The schematic molecular model for the lamellar crystal is shown in (b). When assuming an adjacent reentry, the vitamin C groups are expelled from the crystal to the lamellar basal planes. The perfectly crystalline layer makes up only a small part of the entire lamella, as indicated by *lc*.

Complementary to the WAXS pattern measured on a melt-crystallized sample, the crystal structure of the lamellar crystals was also determined by electron diffraction of solution grown single crystals (Figure 4.9a). The SAED diffraction pattern shows a nearly perfect hexagonal structure, with an orthorhombic (110) lattice plane of 4.16 and 4.10 Å for the (200). This results in the orthorhombic lattice constants of *a* = 8.2 Å and *b* = 4.8 Å. With *a*/*b* = 1.71 the ratio is close to the theoretical value of 1.73 for a hexagonal structure. The lattice constant in the *c*-direction cannot be determined from this measurement. As already observed for other similar PE crystal systems with random incorporation of molecular defects, the crystal lattice inflates preferably in the *a*-direction of the orthorhombic unit cell.[218] Combining all the structural data we have achieved, we can propose a structural model of the vitamin C polymer crystal. The distortion of the vitamin C groups on the crystal surface is so massive that a crystalline structure is only formed over a thickness of 8 Å in the interior of the lamellae. This refers to a perfect crystal thickness of only three all-trans CH_2–CH_2 units. Adjacent, the reorganization with regards to the basally located vitamin C groups takes place in a 11.5 Å layer on both sides of the crystal. Finally, the vitamin C group is sitting on the fold surface of the crystal (Figure 4.9b).

With such a small thickness of the perfect crystalline region, one should expect a much lower melting temperature for the hydrogenated polymer (polymer **6**) according to the Gibbs–Thomson equation.[219] However, a relatively high melting temperature in the range of 90 °C is observed. Comparatively similarly high melting temperatures with the same molecular defect density (20 CH_2 groups between the functional groups) were also observed for hydroxyl[220] and ester functions.[76,221,222] It can be assumed that the high melting point is due to the interaction of the functional groups on the basal surface of the lamellar crystals.[223]

Decomposition and Degradation

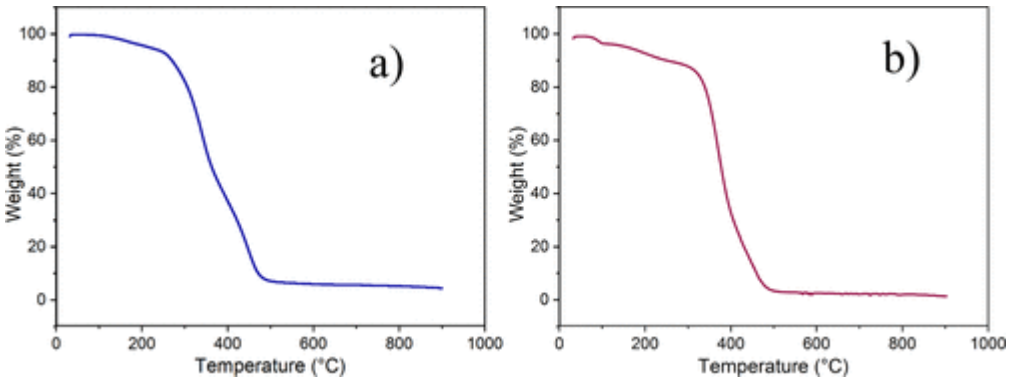

Figure 4.10. TGA thermograms of (a) the unsaturated polymer **4** and (b) the saturated polymer **6**. There is no significant influence of the hydrogenation on the thermal decomposition characteristics of both polymers.

The thermal stabilities of polymers **4** and **6** proved to be very similar and were evaluated by thermogravimetry under a nitrogen atmosphere with a heating rate of 10 K min^{-1}. The onset of the main decomposition was detected at ca. 300 °C and reaches its maximum weight loss at 500 °C (Figure 4.10). This main thermal decomposition profile is comparable to the TGA of PE.[224]

Slight mass loss was observed for both samples at temperatures below 300 °C, which might be attributed to the release of water. As the melting temperature of the final polymer **6** is well below the onset temperature, it can be processed like a Thermoplast without chemical alteration.

Accordingly, this polymer could be a promising material for biomedical applications because, on the one hand, it already offers a bioactive component due to the built-in vitamin C group and, on the other hand, it should have the biocompatible properties of PE. For this reason, we have investigated the degradation and antioxidative properties as well as the biocompatibility of the polymer.

Hydrolytic Degradation

The accelerated hydrolysis of the vitamin C-containing polymer was performed in acidic and basic conditions. Under basic conditions, degradation of the polymer backbone was observed and proven by GPC (Figure 4.11) and NMR (Figure 4.12) measurements. Comparison of the ^{1}H NMR spectra of polymer under basic conditions before after degradation reveals the L-ascorbic acid ring signals at 3.8–4.7 ppm, which vanished from the spectra after degradation to confirm the success of the process.

To assess degradation kinetics, the polymer was treated with different amounts of NaOH. Even in the experiment with the mildest condition (sample 4 in Table 4.2), degradation takes place (Figure 4.11). Moreover, it is remarkable that the polymer can also be degraded in its crystal state (sample 1 in Table 4.2). This indicates that in the crystal structure the vitamin C groups are accessible for degradation attacks and accordingly are placed on the crystal surface rather than in the crystal bulk. Or, in other words, if the size of the defect is small enough to be incorporated in the crystal lattice, the degradation rate of the long-chain polyacetals would decrease with increasing length of the methylene sequences.[225] That makes it beneficial

to aim for polymer structures with big defects, forming functional surfaces which are accessible for degradation or capable for functionalization.

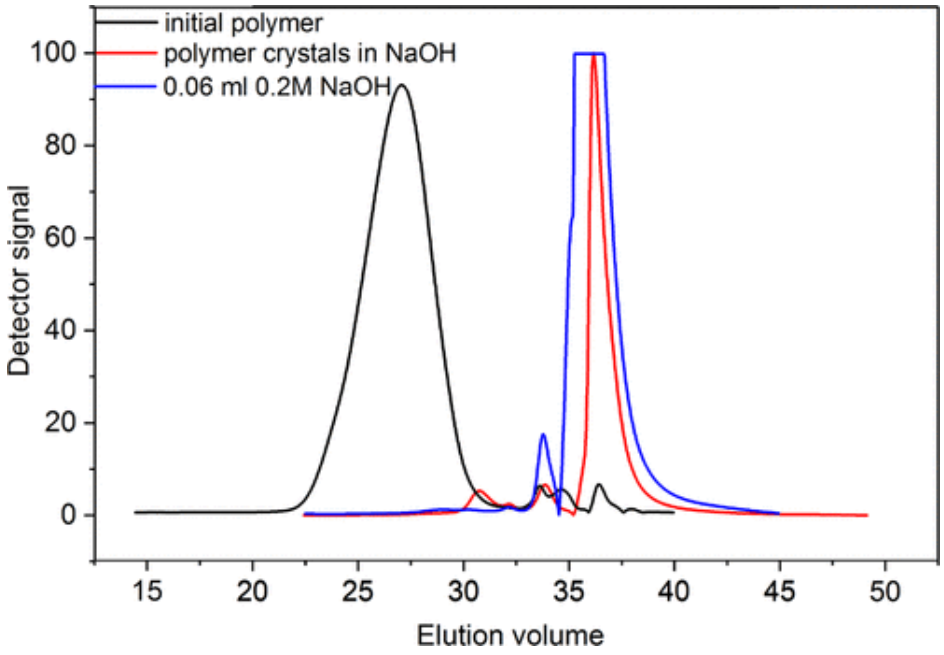

Figure 4.11. GPC elugrams of polymer **6** (black) and products of degradation in the presence of sodium hydroxide: polymer crystals in 1 M water solution NaOH (red) and a mixture of 0.1 mg of polymer solution and 0.06 mL of 0.2 M NaOH in 0.5 mL of THF (blue).

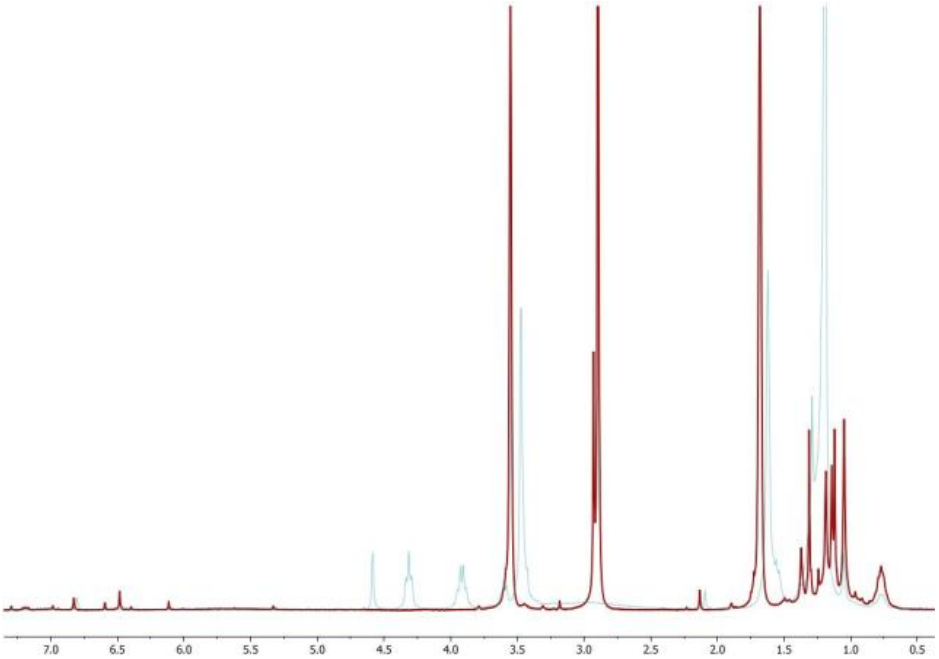

Figure 4.12. ^{1}H NMR spectra of final polymer 6 (blue) and product of degradation (red)

Sample N	*Polymer, **mg***	*NaOH mg*	*THF mL*	*H_2O mL*	*Time h*
1	10.0	4	-	2	10
2	5.0	4	0.5	0.05	0.5
3	5.0	2	0.5	0.05	0.5
4	5.0	0.4	0.5	0.06	0.5

Table 4.2. Degradation of Polymer 6 in the Presence of NaOH under Different Conditions: in Polymer Solution (Samples 2–4) and in Crystal State (Sample 1)

Free Radical Scavenging Properties

The DPPH (2,2-diphenyl-1-picrylhydrazyl hydrate) free radical method is an antioxidant assay based on electron transfer that produces a violet solution. This organic nitrogen-centered free radical, stable at room temperature, reduces to its colorless nonradical form while interacting with antioxidants.

The final polymer **6** crystals (0.5 mg) were added to DPPH (0.05 mg mL^{-1}) solution in THF and kept for 30 min in the dark or heat up for 5 min with a heat gun.

The color of the mixture of DPPH with free radical scavenger vanishes upon heating with a heat gun after 1 min, while the color of pure DPPH solution stays purple even after 5 min of heating with the heat gun. The same result was observed after keeping the samples in the dark for 30 min. For the sample with DPPH solution no difference in the color was detected, but the solution with addition of final hydrogenated polymer turned slightly yellow (Figure 4.13). Besides, another quite remarkable observation was made by using the protected monomer. A similar experiment was done using the protected monomer without hydroxyl groups instead. Even in this case the reaction and the color change indicate the free radical scavenging potential. We assume that in this case not only hydroxyl groups, typically responsible for radical scavenging process, but also the one of protons next to the oxygen in the polymer chain act as radical scavenger.

The property that polymer **6** can be used as a radical scavenger makes it interesting to use it as a material for encapsulating sensitive drugs. The first prerequisite for using it in nanomedicine is that the polymer or polymer crystals can be transferred to a stable, aqueous dispersion. The particle size was determined by TEM measurements (Figure 4.7) on the one hand and by DLS (Figure 4.14) on the other. The mean crystallite size is ~500 nm (TEM), and the hydrodynamic radius is 215 nm (DLS). Furthermore, the polymer should not prove to be toxic and should also be taken up by cells. Hence, for the cell experiments, the solution crystallized polymer **6** crystals were successfully transferred to an aqueous phase to check cell toxicity and cell uptake.

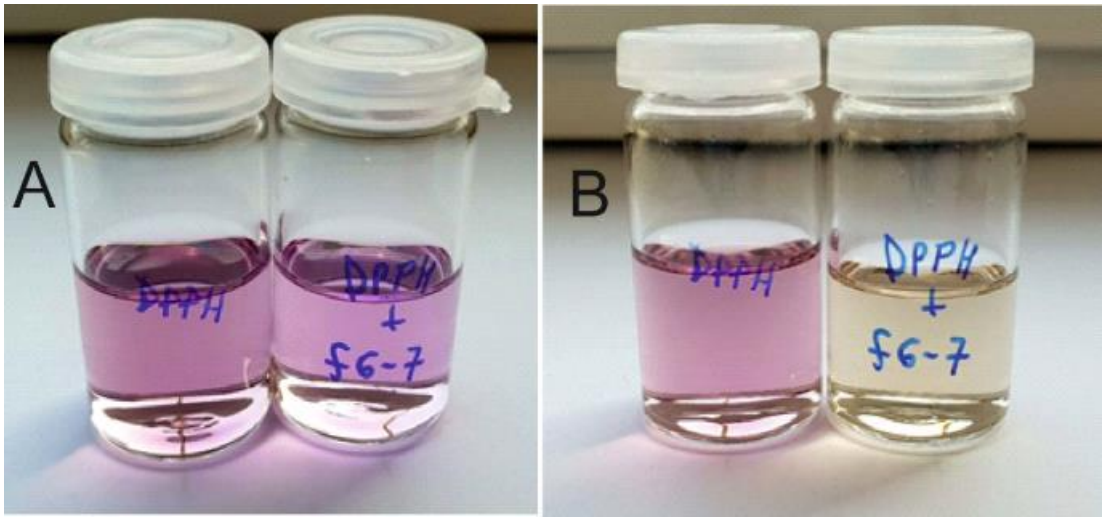

Figure 4.13. Color comparison between DPPH solution (A) and DPPH solution with addition of vitamin C containing polymer 6 (B)

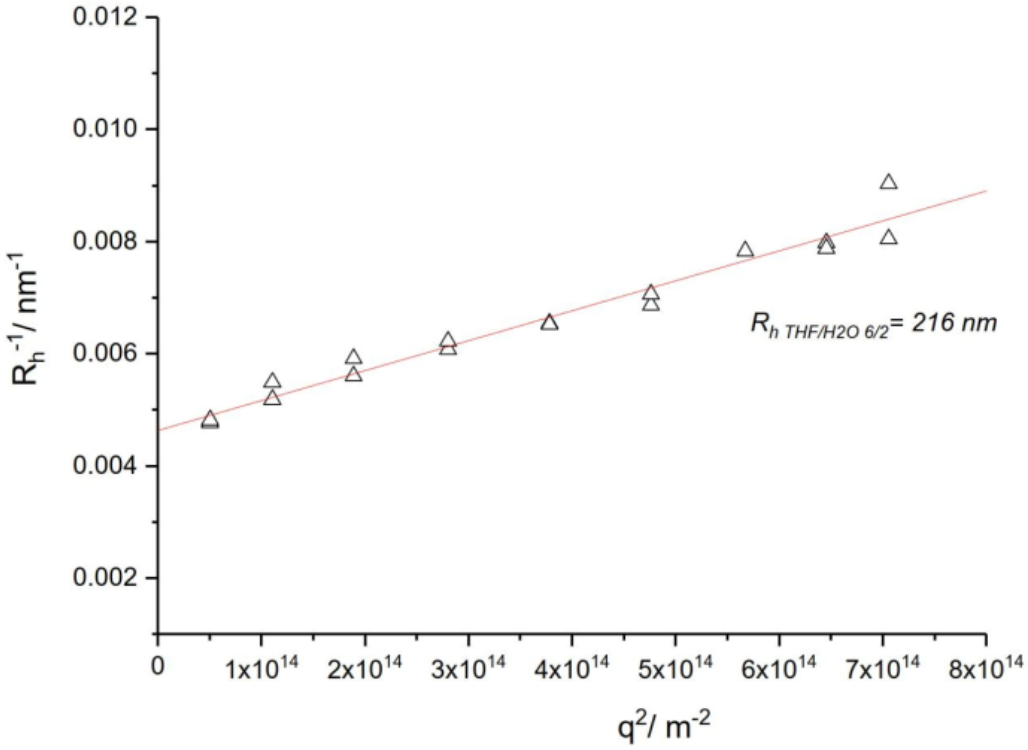

Figure 4.14. Hydrodynamic radius of the micelles derived by dynamic light scattering (DLS) measurement.

Viability and Cell Uptake

As a potential biological relevant material, we tested the biocompatibility of the polymer by assessing the toxicity of the pure polymer with HeLa cells and 3T3 fibroblasts. A good cell viability was obtained even with the highest concentration of 50 µg mL^{-1} tested for both cell lines (Figure 4.16A). The slight increase of the cell

viability for the 3T3 cells was not significant. The control experiment was done using DMSO. As expected in the presence of 10% DMSO, the cells were dying and only about 5–10% of the cells were alive after 24 h.

To assess the biological importance of the material further, the dye Cy5 cyanine was covalently attached to the polymer via esterification reaction. The labeled polymer was then crystallized, and the nanocrystals were incubated to the cells to determine their uptake potential. We observed that depending on the incubation medium, the results are different. In the presence of 10% FBS in the medium, HeLa cells internalized the nanocrystals to a large extent (Figure 4.16C or Figure 4.17. *Cellular uptake of Cy5-labeled VC06 polymer by HeLa cells was determined by confocal microscopy. The cells were incubated for 4h at 37°C in the absence of protein (A, B), or presence of 10% FBS (C, D) or 10% human serum (E, F). The nanocrystals are represented in red and the cell membrane in green. The overlay is displayed in orange. The scale bar represent 10 µm***Fehler! Verweisquelle konnte nicht gefunden werden.Fehler! Verweisquelle konnte nicht gefunden werden.**C, D). For 3T3 cells, the nanocrystals remain preferably in the membrane with a limited fraction entering the cell (Figure 4.16B or **Fehler! Verweisquelle konnte nicht gefunden werden.**Figure 4.18. *Cellular uptake of Cy5-labeled VC06 polymer by 3T3 cells was determined by confocal microscopy. The cells were incubated for 4h at 37°C in the absence of protein (A, B), or presence of 10% FBS (C, D) or 10% human serum (E, F). The nanocrystals are represented in red and the cell membrane in green. The overlay is displayed in orange. The scale bar represent 10 µm.*C, D). Based on flow cytometry data (Figure 4.15), the polymer nanocrystals are favored by 3T3 cells with a noticeable increased uptake. In the absence of protein, the nanocrystals tended to aggregate; thus, very limited cell uptake was observed. Finally, in the presence of 10% human serum, an unfavorable protein layer adsorbed on the nanocrystal surface could explain the low uptake by the cells.

Overall, the polymer interacts with the cells and can be internalized by them. The polymer is not toxic to the cells, making it a promising new material for biomedical applications. However, we have not yet checked for any positive effect of the vitamin C polymer on biological systems like cells.

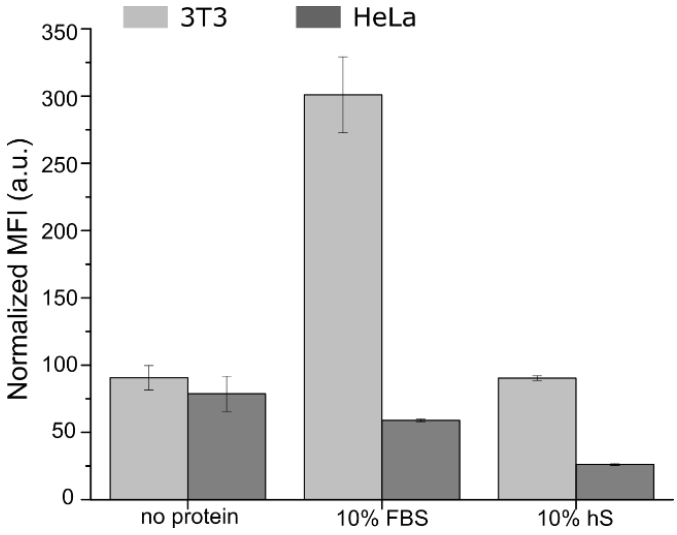

Figure 4.15. Cellular interaction between HeLa (A) and 3T3 (B) cells after 4h incubation with 25µg/mL labeled VC polymer nanocrystals. The nanocrystals were added with the cells in medium containing no protein, or 10% FBS, or 10% human serum. The error bar represents the standard deviation between the mean of a triplicate.

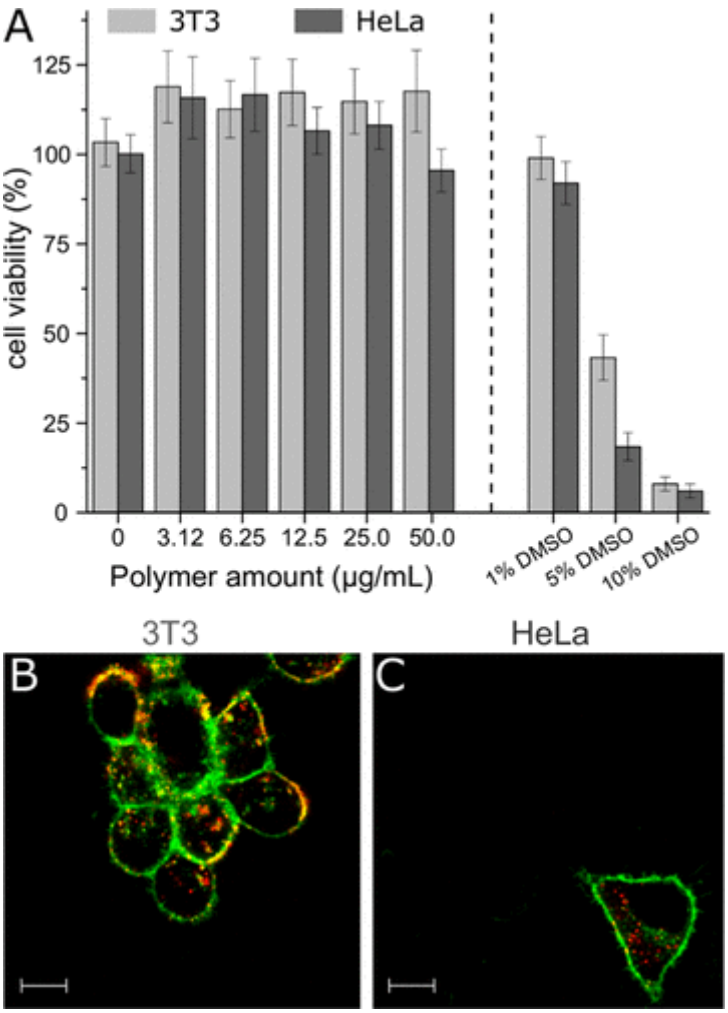

Figure 4.16. Interaction between vitamin C polymer and a biological sample. (A) Cytotoxicity of the nanocrystals after 24 h incubation in cell culture media tested on HeLa and 3T3 cells. DMSO was used as positive control. The error bars represent the standard deviation of the mean of a sextuplet. Cellular uptake of Cy5 nanocrystals (B, C) after 4 h incubation at 37 °C was determined by confocal laser microscopy. 3T3 cells (B) and HeLa cells (C) were tested. The cell membrane is represented in green, and the scale bar represents 10 µm.

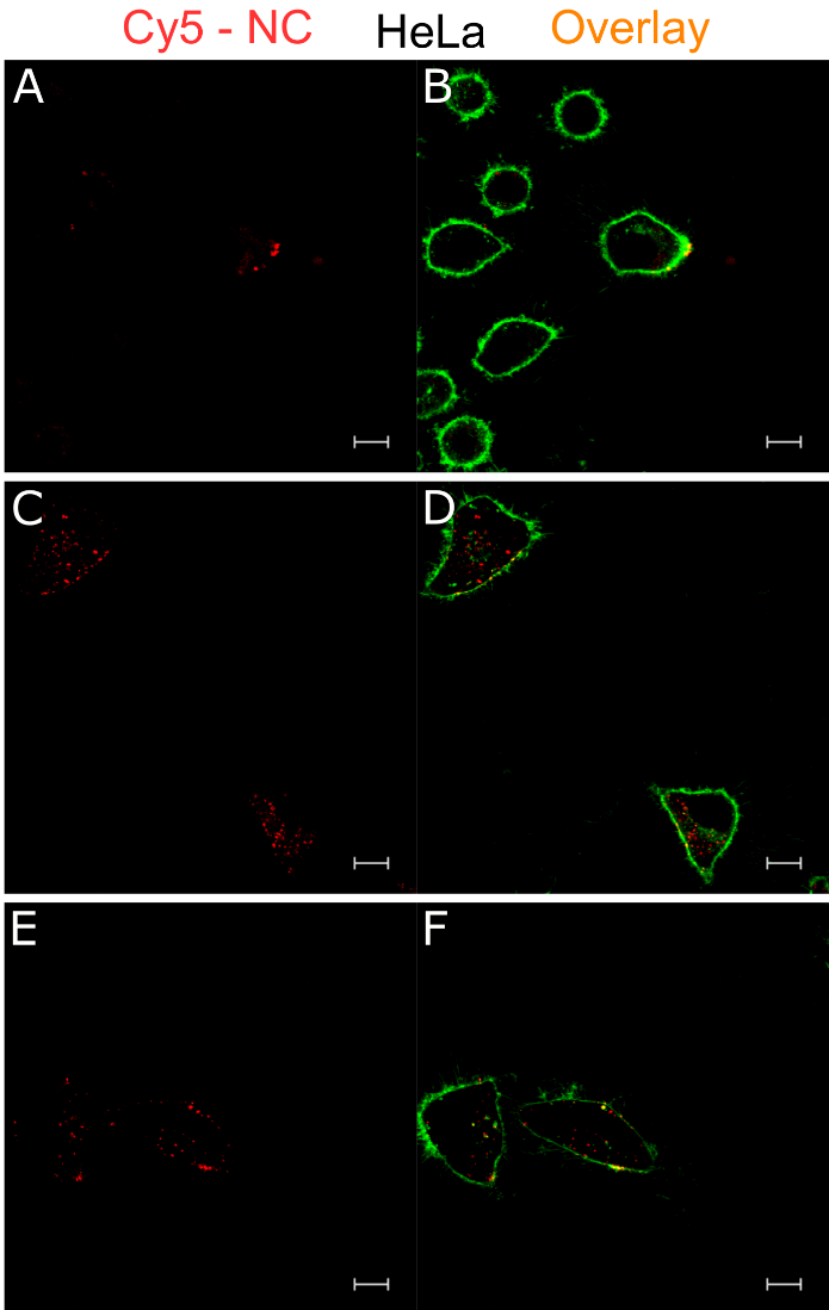

Figure 4.17. Cellular uptake of Cy5-labeled VC06 polymer by HeLa cells was determined by confocal microscopy. The cells were incubated for 4h at 37°C in the absence of protein (A, B), or presence of 10% FBS (C, D) or 10% human serum (E, F). The nanocrystals are represented in red and the cell membrane in green. The overlay is displayed in orange. The scale bar represent 10 µm

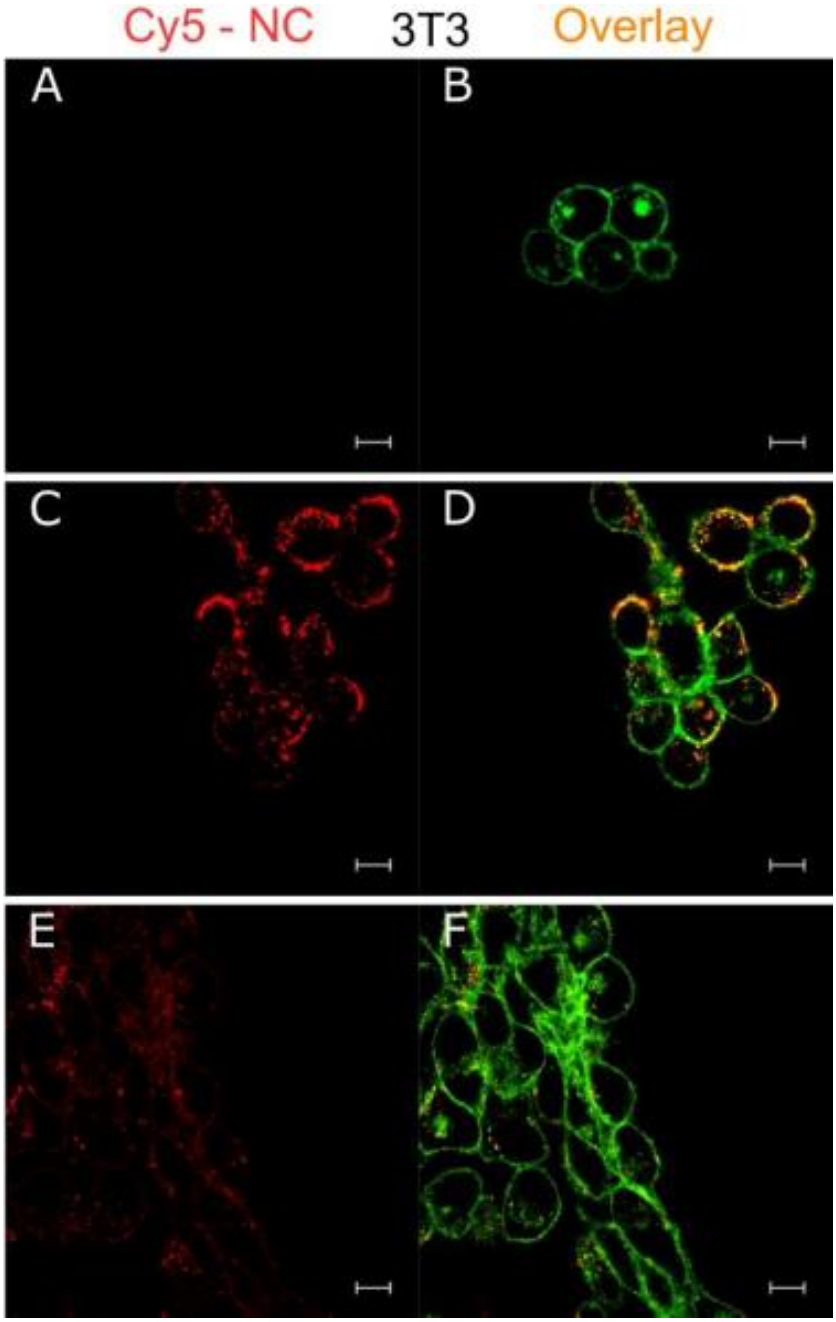

Figure 4.18. Cellular uptake of Cy5-labeled VC06 polymer by 3T3 cells was determined by confocal microscopy. The cells were incubated for 4h at 37°C in the absence of protein (A, B), or presence of 10% FBS (C, D) or 10% human serum (E, F). The nanocrystals are represented in red and the cell membrane in green. The overlay is displayed in orange. The scale bar represent 10 µm.

4.5. Experimental Section

Materials

Solvents and all commercially available reagents were purchased from Acros Organics and Sigma-Aldrich and used as received, unless otherwise stated. The first-generation Grubbs catalyst was purchased from Sigma-Aldrich and stored under an argon atmosphere. Deuterated solvents were purchased from Acros Organics and Sigma-Aldrich. All solvents were dried by using molecular sieves for at least 24 h. Chloroform-*d* was stored over activated 3 Å molecular sieves and anhydrous sodium carbonate to quench residual acid.

Cell lines and buffer: HeLa (human cervix adenocarcinoma (CCL-2)) cells were purchased from American Type Culture Collection (ATCC) and maintained in Eagle's Minimum Essential Medium (EMEM). NIH/3T3 (murine fibroblast (CRL-1658)) cells were purchased from ATCC and maintained in Dulbecco's Modified Eagle's Medium (DMEM). All media were supplemented with fetal bovine serum (10% v/v (Gibco)) and penicillin–streptomycin (100 UI/mL (Gibco)). All cells were cultured at 37 °C in a 5% CO_2 atmosphere. To prevent mutation of the cells, passaging was kept below 30.

Instrumentation

NMR Spectroscopy

^{1}H and ^{13}C NMR spectra were acquired on a 300 MHz Bruker system. The temperature was kept at 298.3 K and calibrated with a standard ^{1}H methanol NMR sample by using a Topspin 3.0 (Bruker). ^{13}C {H} NMR spectra were referenced internally to solvent signals. The ^{13}C {H} NMR (101 MHz) measurements were obtained with a ^{1}H powergate decoupling method using 30° flip angle. All spectra were processed with a MestReNova 12.0.1-20560.

Mass Spectrometry

Mass spectrum acquisitions were conducted on an Advion expression^{L} compact mass spectrometer (CMS) by using the atmospheric solids analysis probe (ASAP) technique. All spectra were acquired in the positive ion reflectron mode, *m/z* range from 10 to 2000 *m/z*, and acquisition speed 10000 *m*/*z* units s^{-1}. The obtained spectra were analyzed by using Advion CheMS Express software version 5.1.0.2

Differential Scanning Calorimetry (DSC)

Thermal analysis was performed using a Mettler-Toledo DSC 822. For nonisothermal crystallization, the samples were heated well above the melting point and kept at this temperature for 10 min. Unsaturated polymer sample 4 was then cooled at a rate of 10 K min^{-1} to −140 °C and heated again at the same rate to 90 °C. Saturated polymer sample 6 was then cooled at a rate of 10 K min^{-1} to 0 °C and heated again at the same rate to 120 °C. The second run melting curve was used for determining the melting enthalpy (ΔH_m) and T_m.

X-ray Diffraction

Wide-angle X-ray diffraction (WAXD) patterns of the precision PEs were obtained on a Philips PW 1820 diffractometer (scattering angle 2° ≤ 2θ ≤ 60°, 0.02° step size) using Cu Kα radiation (λ = 1.5418 Å) as the X-

ray source. The crystallinity (X_c^{WAXD}) of PEs with pseudohexagonal crystal phase was determined from the WAXD patterns as

$$X_c^{WAXD} = \frac{A_c}{A_c + A_a} \quad (1)$$

where A_c refers to the integrated area of the Bragg reflections from the PE crystal and A_a to the amorphous halo. The corresponding bulk volume fraction crystallinity X_{vol} can be calculated from X_c^{WAXD}:

$$X_{vol} = \frac{\rho_a}{\rho_c / X_c^{WAXD} - \rho_c + \rho_a} \quad (2)$$

where ρ_c and ρ_a are the densities of the crystalline and amorphous phases. The amorphous phase also contains vitamin C molecules. But since in this case the density ρ_a is not known, we assume the values for PE (ρ_c = 1.000 g cm^{-3} and ρ_a = 0.855 g cm^{-3}).[226]

Small-angle X-ray scattering (SAXS) data were measured at room temperature in transmission geometry on a free-standing polymer foil (Rigaku MicroMax 007 X-ray generator with Cu anode, Osmic Confocal Max-Flux curved multilayer optics, λ = 0.154 nm). Scattered intensities were recorded on an online image plate detector (Mar345, MarResearch) at a sample–detector distance of 2.2 m calibrated with silver behenate. Background noise was removed by a Laplace filter based masking algorithm. The scattering pattern $I(q)$ vs momentum transfer $q = 4\pi/\lambda \sin(\theta)$ was obtained by radial averaging of the 2D-scattering patterns. The long period L^{SAXS} can be estimated from the position q_0 of the scattering maxima in the SAXS patterns:

$$L^{SAXS} = 2\pi / q_0 \quad (3)$$

The lamellar crystal thickness (l_c) can then be calculated from the long period L^{SAXS} and bulk volume fraction crystallinity X_{vol} based on the equation

$$l_c = L^{SAXS} \times X_{vol} \quad (4)$$

To extract additional structural data, the pair correlation function was calculated from the Lorentz-corrected SAXS patterns by using the SAXSDAT software.[227]

Thermal Gravimetric Analysis (TGA)

TGA was measured on a Mettler Toledo ThermoSTAR TGA/SDTA 851-Thermowaage in a nitrogen atmosphere. The heating rate was 10 °C min^{-1} in a temperature range between 25 and 900 °C. Gel-permeation chromatography (GPC) measurements were performed in THF at a sample concentration of 1 g L^{-1}. Sample injection was performed by a 717 plus autosampler (Waters) at 30 °C. The flow was 1 mL min^{-1}. Three SDV columns (PSS) with the dimensions 300 × 80 mm^2, 10 µm particle size, and pore sizes of 106, 104, and 500 Å were employed. Detection was accomplished with a DRI Shodex RI-101 detector (ERC) and a UV–vis S-3702 detector (Soma). Calibration was performed using polystyrene standards provided by Polymer Standards Service.

Transmission Electron Microscopy (TEM)

A FEI Tecnai F20 transmission electron microscope operated at an acceleration voltage of 200 kV was used to determine the crystal morphology, thickness, and crystal structure. Bright field (BF), parallel beam nanoelectron diffraction (NBED), and energy-filtered transmission electron microscopy (EFTEM)[228] were used for measurements. To study the crystallization behavior, hydrogenated polymer **6** was dissolved in hot ethyl acetate and crystallized slowly during cooling from solution or dissolved in tetrahydrofuran (THF) and crystallized by adding dropwise deionized water while gently stirring.

Radical Scavenging Test

The radical scavenging ability of the conducting polymers, and their monomers, is assessed through their reaction with stable *α,α*-diphenyl-β-picrylhydrazyl (DPPH) radicals. Radical scavenging activities were assessed on the basis of the capacity of the compounds to scavenge the stable DPPH free radical by using the methodology of Brand-Williams *et al*.[229] DPPH typically extracts a proton to form DPPHH during the reaction. Polymer solution (5 mg in 0.1 mL of THF) was added to 3.9 mL of 6×10^{-5} M DPPH free radical in THF, vortexed, and left to stand for 30 min at room temperature.

Atomic Force Microscopy (AFM)

To measure the lamellar thickness, AFM measurements were performed (Bruker, Dimension Icon, operated in peak force mode) using OLTESPA probes (nominal spring constant 2 N/m) in ambient conditions. The samples were prepared by dropping 5 µL of the dispersion containing the solution grown crystals onto a freshly cleaved mica substrate. Then the excess liquid was blotted off with the edge of a filter paper.

Quantification of the Cellular Uptake by Flow Cytometry

The cells were seeded as a triplicate in 24-well plates 1 day before the experiment. The nanocrystals (13.3 µL at 1.4 g L^{-1}) were dispersed in a medium without serum, or a medium with 10% fetal bovine serum, or a medium with 10% human serum to a final concentration of 25 µg mL^{-1}. The cells were washed, and 1.0 mL of the fluorescently labeled nanocrystal dispersion was added to the cells and incubated for 4 h at 37 °C in a 5% CO_2 atmosphere. Then, the supernatant was removed, and the cells were washed three times with PBS. They were recovered with a 1X trypsin solution and washed with PBS. They were then incubated for 20 min at RT with Zombie Aqua (according to the manufacturer's recommendation). The cells were washed with PBS and suspended in 500 µL of PBS before analysis. Twenty thousand events were recorded on an Attune NxT flow cytometer using three lasers (violet (λ_{exc}: 405 nm/λ_{em}: 440 nm), blue (λ_{exc}: 488 nm/λ_{em}: 590 nm), and red (λ_{exc}: 638 nm/λ_{em}: 670 nm)). The dead cells were excluded from the cell population based on their Zombie Aqua staining. Each sample was tested at least twice to ensure the reproducibility of the experiment.

Verification of the Cellular Uptake by Confocal Laser Scanning Microscopy

The cells were seeded in 8-well Ibidi dishes 1 day before the experiment. The nanocrystals were dispersed in a medium without serum, or a medium with 10% fetal bovine serum, or a medium with 10% human serum to a final concentration of 12.5 µg mL^{-1}. The cells were washed, and 250 µL of the nanocrystal solution was added to the cells and incubated for 4 h at 37 °C in a 5% CO_2 atmosphere. Then, the supernatant was removed,

and the cells were washed three times with PBS. Next, the cell membrane was stained with a Cell Mask Deep Red solution or a Cell Mask Green for 5 min at room temperature (RT). The cells were washed once before imaging. Depending on the dye combination applied for staining, two channels were set up: an argon laser was used to detect the Cell Mask Green (λ_{exc}: 488 nm/λ_{em}: 520–560 nm), a DPSS diode was used to detect the CY3 dye (λ_{exc}: 561 nm/λ_{em}: 580–620 nm), and a HeNe laser was used for the Cy5 dye or the Cell Mask Deep Red staining (λ_{exc}: 633 nm/λ_{em}: 660–680 nm). The images were acquired by using the 63× oil objective of a Leica LSM5 instrument.

Cell Viability Assay

Cytotoxicity was determined by using the CellTiter 96 Aqueous One Solution Cell Proliferation Assay (Promega), following the procedure recommended by the manufacturer.[230] HeLa and NIH/3T3 cells were seeded in triplicate on a 96-well plate and grown overnight in 120 µL of complete media. The next day, 100 µL of media solution was removed. The cells were incubated with 100 µL solutions of 50, 25, 12.5, 6.25, and 3.125 µg L^{-1} pure polymer (VC06) nanocrystals in complete DMEM medium for 24 h at 37 °C. After removal of the media, MTS reagent (20 µL) diluted in 100 µL of media was added and incubated for 2 h. The absorbance (490 nm) was recorded by a plate reader, and the viability was determined as described by the manufacturer.

Synthesis

*Synthesis of 5,6-*O*-Ispropylidene-*L*-ascorbic Acid (2). 5,*

6-*O*-Isopropylidene-L-ascorbic acid (**2**) was prepared according to a previously published procedure.[231] ^{1}H NMR ($CDCl_3$, δ): 4.69 (s, 1H, OCH_2CHOCH), 4.24 (m, 1H, OCH_2CHOCH), 4.09 (m, 1H, OCH_2CHOCH), 3.88 (m, 1H, OCH_2CHOCH), 1.25 (s, 6H, CCH_3).

*Synthesis of 10-(Dec-9-en-1-yloxy)-5-(2,2-dimethyl-1,3-dioxolan-4-yl)-3-(pent-4-en-1-yloxy)furan-2(5*H*)-one (3)*

5,6-Isopropylidene-L-ascorbic acid (**2**) (2.00 g, 9.0 mmol, 1.0 equiv) and K_2CO_3 (3.18 g, 23.0 mmol, 2.5 equiv) were dissolved in 34 mL of a DMSO/THF (9:8) mixture. The reaction mixture was stirred for 10 min at room temperature, and 11-bromo-1-undecene (5.05 mL, 23.0 mmol, 2.5 equiv) was dissolved in 17 mL of DMSO/THF (9:8) and added dropwise to this mixture before left to stir at RT for 4 h. The reaction mixture diluted with water and extracted with ethyl acetate. The organic layer was thoroughly washed with water, and combined organic phases were dried over anhydrous Na_2SO_4; the solvents were removed under reduced pressure. The product was purified by column chromatography over silica gel eluting with ethyl acetate/hexane (1:4) to give **3** as pale yellow oil. Yield: 70%. ^{1}H NMR ($CDCl_3$, δ): 5.73 (m, 2H, C<u>H</u>=CH_2), 4.88 (m, 4H, CH = C<u>H</u>$_2$), 4.42 (s, 1H, $OCH_2CHC\underline{H}O$), 4.36 (m, 2H, $OC\underline{H}_2CHCHO$), 4.18 (m, 1H, $OCH_2C\underline{H}OCH$), 4.04 (m, 2H, $OCH_2CH_2CH_2$), 3.96 (m, 2H, $OCH_2CH_2CH_2$), 1.96 (m, 4H, $CH_2C\underline{H}_2CHCH_2$), 1.63 (m, 4H, $OCH_2C\underline{H}_2CH_2$), 1.33 (s, 3H, $CC\underline{H}_3$), 1.29 (s, 3H, $CC\underline{H}_3$), 1.22 (br s, 20H). ^{13}C NMR ($CDCl_3$, δ): 169.3 (O–C–<u>C</u>=O), 156.0 (O–CH–CH–<u>C</u>–O), 139.2 (CH_2=<u>C</u>H–CH_2−), 121.9 (O–<u>C</u>–C=O), 114.2 (<u>C</u>H_2=CH–CH_2−), 110.2 (CH_3–<u>C</u>–O–CH_2), 74.7 (O–<u>C</u>H–CH–C–O), 74.2 (O–CH–<u>C</u>H–C–O), 72.6, 72.2 (C–O–<u>C</u>H_2–CH_2), 65.3 (O–CH_2–CH–O), 33.8 (CH_2=CH–<u>C</u>H_2−), 29.8, 29.5, 29.1, 28.9 (backbone, −<u>C</u>H_2−), 25.9, 25.8, 25.6, 25.5 (<u>C</u>H_3−). CMS (EI): calcd

for $C_{19}H_{28}O_6$: 521.0 (M+); found: 521.5 (M+). *m/e*: 537.4, 524.5, 523.5, 522.5, 521.5, 519.4, 505.4, 464.4, 463.4, and 420.4.

Representative Procedure for ADMET Bulk Polycondensation (4)

3 (0.55 g, 1.40 mmol, 1 equiv) was charged into a flame-dried 25 mL flask in CH_2Cl_2 (2 mL), and the solution was stirred for 5 min at room temperature under nitrogen; first-generation Grubbs catalyst (0.01 equiv) was then added to this solution under a nitrogen atmosphere. After the addition of the catalyst, the reaction mixture was stirred at room temperature under nitrogen flow and then exposed to an intermittent vacuum to remove ethylene and remaining solvent. After that, the polymerization temperature was increased and kept at predetermined temperatures (40, 60, and 80 °C) with different time intervals until the magnetic stirrer stopped due to the high viscosity. The reaction mixture was cooled to room temperature, and the catalyst was quenched by adding ethyl vinyl ether (1 mL in 2 mL of CH_2Cl_2), followed by 30 min stirring at room temperature. The reaction mixture was precipitated in methanol (100 mL) and decanted. Brown solid polymers were obtained after removal of the solvent. ^{1}H NMR ($CDCl_3$, δ): 5.31–5.26 (m, 2H, C<u>H</u>=C<u>H</u>), 4.42 (s, 1H, $OCH_2CHC\underline{H}O$), 4.36 (m, 2H, $OC\underline{H}_2CHCHO$), 4.18 (m, 1H, $OCH_2C\underline{H}OCH$), 4.04 (m, 2H, $OCH_2CH_2CH_2$), 3.96 (m, 2H, $OCH_2CH_2CH_2$), 1.96 (m, 4H, $CH_2C\underline{H}_2CHCH_2$), 1.63 (m, 4H, $OCH_2C\underline{H}_2CH_2$), 1.33 (s, 3H, $CC\underline{H}_3$), 1.29 (s, 3H, $CC\underline{H}_3$), 1.22 (br s, 24H). ^{13}C NMR ($CDCl_3$, δ): 165.6 (O–C–<u>C</u>=O), 156.0 (O–CH–CH–<u>C</u>–O), 130.3 (<u>C</u>H═<u>C</u>H), 121.9 (O–<u>C</u>–C═O), 110.2 (CH_3–<u>C</u>–O–CH_2), 74.7 (O–<u>C</u>H–CH–C–O), 74.2 (O–CH–<u>C</u>H–C–O), 72.6, 72.3 (C–O–$\underline{C}H_2$–CH_2), 65.3 (O–$\underline{C}H_2$–CH–O), 32.6 (CH═CH–$\underline{C}H_2$−), 29.8, 29.5, 29.2, 29.1 (backbone, −$\underline{C}H_2$−), 25.9, 25.6 ($\underline{C}H_3$−).

Hydrogenation of Polymer 5

Polymer **4** (∼0.53 g) was dissolved in 3–4 mL of THF and charged into a flame-dried 25 mL Schlenk flask with stir bar in it. After two cycles nitrogen–vacuum catalyst palladium on charcoal (10 mol %) was added under a nitrogen atmosphere, and vacuum–nitrogen cleaning was repeated to remove the remaining air. Under vacuum conditions, a balloon with hydrogen was connected. It was stirred at room temperature for 3 days. To purify the product, it was filtered through a Celite 503 using excess of THF, and then the solvent was removed under reduced pressure. A black solid polymer was obtained after removal of the solvents.

Hydrolysis of Polymer 6

Polymer **5** (0.51 g) was dissolved in 25 mL of THF; then 5 mL of 1 M HCl solution was added, and the reaction mixture was stirred at 40 °C overnight. Solvents were evaporated under reduced pressure, and then the crude product was dissolved in a minimal amount of THF and precipitated in methanol. A light-brown solid polymer, soluble in THF and DMSO, was obtained after drying. ^{1}H NMR (d-THF, δ): 4.59 (s, 1H, $HOCH_2CHC\underline{H}O$), 4.31 (m, 2H, $OC\underline{H}_2CH_2CH_2$), 3.97–3.88 (m, 2H, $HOC\underline{H}_2CHCHO$), 3.60 (m, 1H, $HOCH_2C\underline{H}CHO$), 1.56 (m, 4H, $OC\underline{H}_2CH_2CH_2$), 1.19 (br s, 24H). ^{13}C NMR (d-THF, δ): 168.8 (O–C–<u>C</u>═O), 156.8 (HO–CH–CH–<u>C</u>–O), 121.9 (O–<u>C</u>–C═O), 75.0 (HO–CH–<u>C</u>H–C–O), 72.0, 71.8 (C–O–$\underline{C}H_2$–CH_2), 70.1 (HO–<u>C</u>H–CH–C–O), 62.8 (HO–$\underline{C}H_2$–CH–O), 30.0, 29.7, 26.2, 25.9, 25.7 (backbone, −$\underline{C}H_2$−).

Fluorescent Labeling

Polymer **6** (22.73 mg) was dissolved in 5 mL of THF; 0.06 mg of 4-(dimethylamino)pyridine (DMAP) and dye (1.2327 mg of Cy-3 or 1.2978 mg of Cy-5) were added and dissolved in 0.3 mL of dichloromethane. Then the

mixture was cooled to 0 °C; afterward, 1.0316 mg of dicyclohexylcarbodiimide (DCC) was added. The mixture was stirred at room temperature over 2 days. Excess of water with two drops of hydrochloric acid was added. For the purification, the product was washed twice with deionized water and precipitated by a centrifuge. Colored polymer crystals, soluble in THF and DMSO, were obtained after drying.

4.6. Conclusion

This work reports on the synthesis of a polyethylene-like polymer with a vitamin C group built into the main chain. Because of the ADMET polymerization, the vitamin C is arranged equidistantly with a distance of 20 CH_2 groups. This polymer crystallizes in a lamellar morphology. Because of the uniform arrangement of the vitamin C groups, crystal lamellae are formed with a homogeneous thickness of about 2.5 nm, corresponding to their distance in the chain. The vitamin C groups are expelled from the crystal and are located on the basal surface of the crystals. The melting temperature is 92 °C, and thus the polymer can be processed like a thermoplast with the usual process methods. Furthermore, the polymer is a suitable candidate for biomedical applications. The bioactive properties, especially the radical scavenging of the built-in vitamin C group, are transferred to the polymer. We have shown that despite the chemical modification its antioxidant function is retained and that the polymer acts as a radical scavenger. In addition, the polymer is a potential biocompatible material. The polymer is not cytotoxic and is taken up by cells in nanoparticular form via endocytotic pathways. Because of these properties, it is a promising candidate for a drug delivery system to protect sensitive drugs to bring them into the cytoplasm as a medically effective system. The next task will therefore be to investigate the biomedical properties of this vitamin C-containing polymer as a drug carrier system in more detail.

5. Nanoscale control of the surface functionality of polymeric 2D materials

Oksana Suraeva, Anke Kaltbeitzel, Katharina Landfester, Frederik R. Wurm**,** Ingo Lieberwirth

This chapter is based on unpublished results.

I performed the crystallization of homopolymers and copolymerization experiments, TEM measurements, evaluated and determined the size distribution of the obtained crystal platelets. Anke Kaltbeltzel performed confocal microscope measurements.

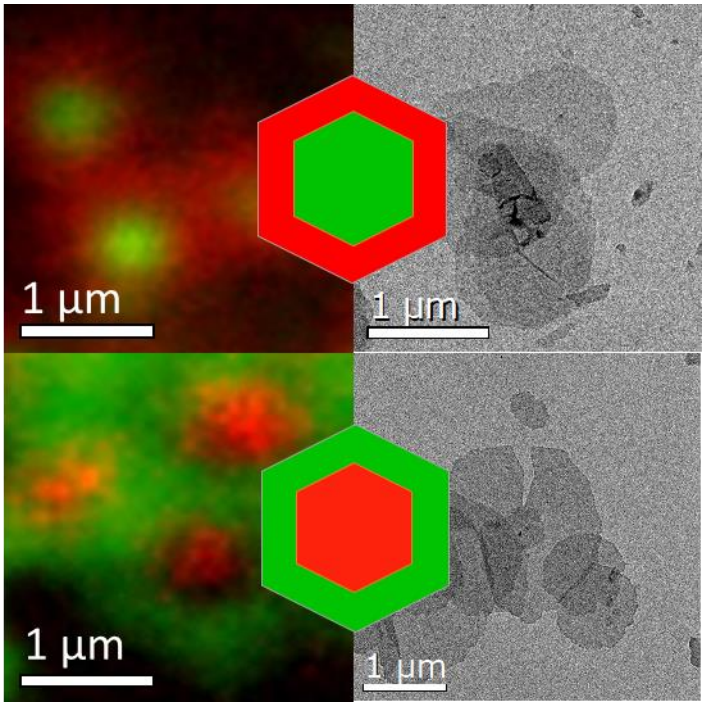

Keywords: precision polymers, defect engineering, polymer crystallization, surface functionalization, 2D organic nanoplatelets

5.1. Preface

In this chapter I will show a simple method, how to introduce a local control over functionality on the surface of polymer 2D crystals. As it was presented in all previous chapters, crystallization of polymers with precisely located functional groups results in highly anisotropic polymer crystals. In this case, the functional groups are expelled from the crystal lattice to the surface. Even though this approach is very simple and laconic, it only allows to create 2D polymers structures with a homogeneous surface.

The idea to achieve heterogeneously located groups on the surface came from the more complex systems, developed in Manners group.[92] They were utilizing a seeded growth method, called “living” crystallization-driven self-assembly (CDSA), where sequential addition of block-copolymers with different functional groups resulted in 1D and 2D structures with patchy surface. However, as this approach requires multi-step synthesis of initial source – block-copolymers, I decided to investigate the ability to reach similar result using a more simple system, such as crystallizable PE-like polymers with introduced functional groups.

Here I would want to mention once again, that this defect engineering with equidistant distribution of bulky groups along the polymer chain promotes formation of nicely shaped crystals and determines their thickness. Using ADMET polymerization, I synthesized polymers with different functional groups, but with the same length of aliphatic segment between them. Then all experiments can be divided into 3 steps.

First step is the formation of “seeds”, small polymer crystals, serving as a starting point for further growth. It turned out, that just by varying the concentration of the polymer and the ratio of solvents in the mixture I had a perfect control over the size and shape of the polymer crystals. Thus, I created an easy set up to fabricate “seeds”. In the second step I was growing polymer crystals around these seeds using only polymer with one type of functional group. This was necessary to prove the “living” nature of the process. Moreover, by sequential addition of polymer, labeled with two different fluorescent dies, I showed that even by utilizing exactly the same polymer, it is possible to have a control over the surface functionality. In the last experiment I made a step forward and presented, how polymers with the same polyethylene crystalline core and different functional groups can form single polymer 2D crystal with diverse surface functionality in the center and on the rim of the crystals. Thus, polymers with various functional defects can be utilized to create 2D crystals with defined surface chemistry using this approach.

5.2. Abstract

Usually, two-dimensional nanoplatelets have a homogeneous surface, and therefore structuring them is a major challenge. In this study, we develop a novel concept of 2D organic nanoplatelets with a heterogeneously functionalized surface. We achieve this by consecutively crystallizing two precisely synthesized polymers with different functional groups in the polymer backbone in a two-step process. First, the core platelet is formed and then the second polymer is crystallized around it. Consequently, the central area of the platelets has a different surface functionality than the periphery. Our concept offers two advantages: the resulting polymeric two-dimensional platelets are stable in dispersion, which simplifies further processing and makes both crystal surfaces accessible for subsequent functionalization. Moreover, a variety of polymers can be used, which keeps the process and the choice of surface functionalization very flexible.

5.3. Introduction

Two-dimensional (2D) organic materials are of interest for membrane applications, in biomedical settings,[3] as high surface area adsorbents, catalyst supports and sensors.[4,5] Various conceptual approaches for the production of 2D organic layer systems have already been discussed extensively in the current literature. However, almost all approaches to produce 2D materials lack the control to structure in lateral extension.

We therefore present here a new and simple concept based on the crystallization of polymers. Starting point are two precisely synthesized polymers with different functional groups integrated into the main chain. If these two different polymers are crystallized sequentially from solution, nano-platelets with different surface functionalization in the center and at the periphery are obtained.

Recent works[78,79,83,232,233] show that polymer crystallization is a promising approach to produce well-defined 2D nanoplatelets. However, all these structures are just homogeneous concerning their surface chemistry. To also gain control over the local arrangement of chemical functionalities during the self-organization of molecules or polymers, the group of Manners has developed basic concepts.[92,234] They synthesized ferrocene-based block copolymers containing a crystallizable polyferrocenyldimethylsilane (PFS) block and a non-crystallizable block, which can be easily functionalized. By covalently attaching different fluorophores to the block copolymer and subsequent crystallization-driven self-assembly (CDSA) of the polymers, they were able to form one-dimensional micelles with segmentally controlled chemical functionalization. However, labelling with the respective dyes was carried out exclusively prior to the structure-forming crystallization and the associated formation of micelles.

Herein, we go one step further and first carry out the structure formation of the nano-platelets. Only afterwards, we will exploit the different chemical identity of the surface functionalization using a selective chemical reaction. We use – in contrast to the block-co-polymers used in previous works - precisely synthesized homopolymers. This polymer consists of a polyethylene (PE) chain with equidistantly incorporated functional monomer units. If we now perform a solution crystallization with two differently functionalized polymers, we obtain a nano-platelet which has a different chemical functionalization in the center than at the periphery. In this process it is important that the two polymers crystallize one after the other. The heterogeneous functionalization on the

surface of the nano-platelets can be used for regioselective chemical reactions. In this report, we functionalized the OH-groups in the periphery of the nano-platelets locally by the reaction with trimethylchlorosilane. This is the first proof that it is possible to achieve a laterally structured chemical functionalization on the surface of polymer nanoplatelets through sequential polymer solution crystallization (SPSC).

5.4. Results and Discussion

To generate laterally structured nanoplatelets, we will exploit the solution crystallization of polyethylene (PE), a very common and well-known polymer. Already since the works of Keller[7] and Fischer[8] in 1957 it has been known that semi-crystalline polymers like PE form nanoplatelets when crystallized from a dilute solution. The polymer chain is back-folded at the basal surfaces of these platelets and the thickness of these nanoplatelets is disparagingly small compared to the lateral size. Thus, the solution-crystallized polymer crystals can be regarded as 2D organic layers or nanoplatelets. For our concept, we use precisely architectured PE. Using ADMET, we synthesized a PE with integrated vitamin C functional groups equidistantly distributed along the main chain. Because of the steric hindrance, these functional groups are expelled from the crystal to the basal surface of the crystalline nanoplatelets during the crystallization of the polymer and are thus found in a precise periodic arrangement on the surface. The thickness of the nano-platelets can be easily adjusted via the distance between the functional groups in the chain. Based on this, we can now apply sequential crystallization of the differently functionalized PE one after the other so that we obtain the desired, surface-structured nano-platelets.

First, we show the 2D organization of a polyethylene with equidistant vitamin C,[27,205] which was labeled with two different dyes before crystallization. . Using sequential polymer solution crystallization (SPSC), we can generate nanoplatelets that are marked with a different dye on the outside and inside of the sheet. To demonstrate the versatility of this SPSC-based method of precision polymers, we co-crystallize two differently functionalized precision polymers that have the same length of alkyl units between the functional groups. Here, a polyphosphoester and a vitamin C-polymer, each with 20 CH_2 units between the functional groups, were crystallized from a common solvent. Due to the different crystallization kinetics of the polymers used, locally structured nanoplatelets have formed in which the polyphosphoester is first crystallized as a seed and then the vitamin C-PE has grown in a frame around the crystal presented. To prove the locally structured chemical functionalization of the nanoplatelets thus formed, the OH groups of the vitamin C were functionalized by means of trimethylsilyl chloride (TMSCl) forming silyl ether. The principal approach of using different functionalized precision polymers to form laterally structured 2D organic nanolayers is shown in Scheme 5.1.

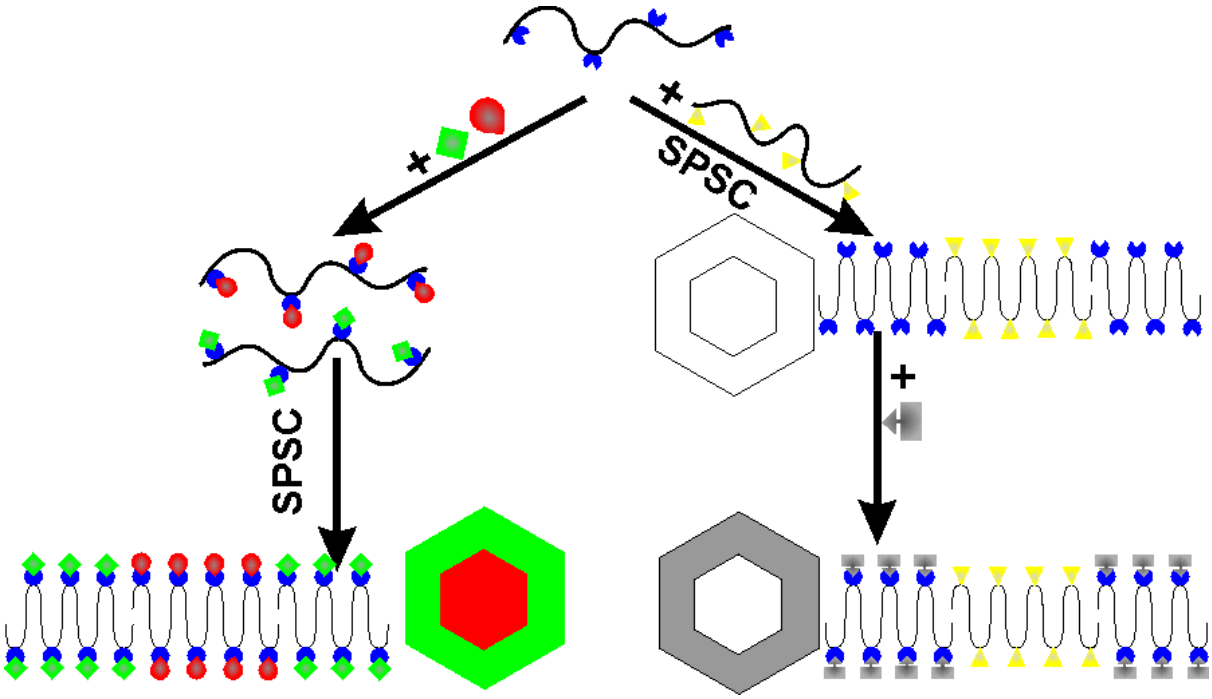

Scheme 5.1. Two ways to form polymer 2D materials with spatial control over the surface functionality at the nanoscale: the functional groups of the polymer are modified prior (left) or after (right) the structure forming sequential polymer solution crystallization. The functional groups are expelled to the surface of the nanoplatelets yielding a template of functional groups with the perfect lattice arrangement from the polymer crystal. Left: a vitamin C-PE is labeled with two different dyes and subsequently crystallized using SPSC yielding polymer nanoplatelets with e.g. a red core and a green periphery. Right: Two differently functionalized PE, vitamin C and polyphosphoester, are co-crystallized resulting in nanoplatelets with a core made of PPE and a rim made of vitamin C-PE. Subsequently, the OH groups of the vitamin C-PE were used to locally precipitate silyl ether.

Starting point for the investigation of a successive crystallization is a polyethylene, which has vitamin C groups at an exact distance of 20 CH_2 units. The vitamin C units act as defect for the crystallization. Consequently, the refolding of the polymer chain forces the vitamin C units from the crystal to the crystal surface. Finally, a lamellar crystal with a thickness of 20 CH_2 units is formed, which corresponds to about 3 nm.[27]. Moreover, since the arrangement of the vitamin C units is based on the crystallization process of the polyethylene, the vitamin C units are arranged on the crystal surface with the perfection of the crystal lattice.

We then determined, whether the covalent binding of different molecules, here the two dye molecules Cy3 and Cy5, affects the crystallization of the two batches. For polymers, it is known that even small differences in the molecular structure can lead to segregation.[235,236] This would also rule out a successive crystallization or co-crystallization of the two differently modified polymers.

Hence, we covalently attached two different dyes (Cy3 (green) and Cy5 (red)) to the vitamin C-PE (Scheme 5.2). The covalent attachment of the dyes to the polymer was proven by HPLC (Figure 5.2). To check whether the chemical modification had an influence on the co-crystallization of the two dye-labeled polymers, we performed crystallization experiments on a water surface in a LBT. We prepared a low concentrated THF

solution of each of the two differently labeled polymers. A few drops of these solutions were then dropped onto the water surface to form a thin film of the polymer solution. After evaporation of the solvent, the nanoplatelets remain in the form of lamellar polymer crystals. If the two differently labeled polymer solutions are mixed beforehand, co crystals are formed from the two labeled polymers, as can be seen from the orange crystals in Figure 5.1a). If the polymer solutions are applied one after the other, two independently fluorescent green and red crystals were detected (Figure 5.1b).

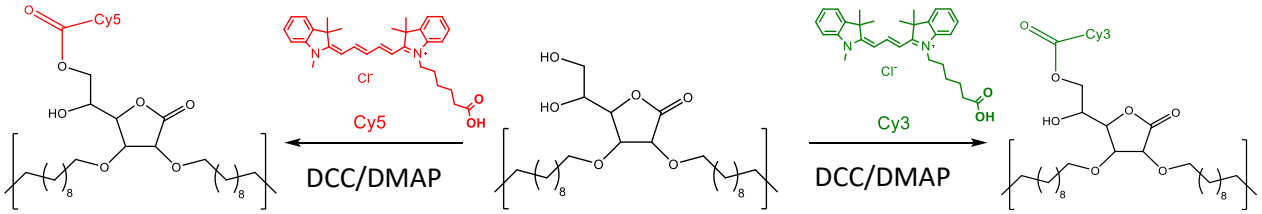

***Scheme* 5.2.** Fluorescent labeling of VC polymer with Cy3 and Cy5 dyes by Steglich Esterification reaction. Reaction was conducted according to previously published procedure[27]

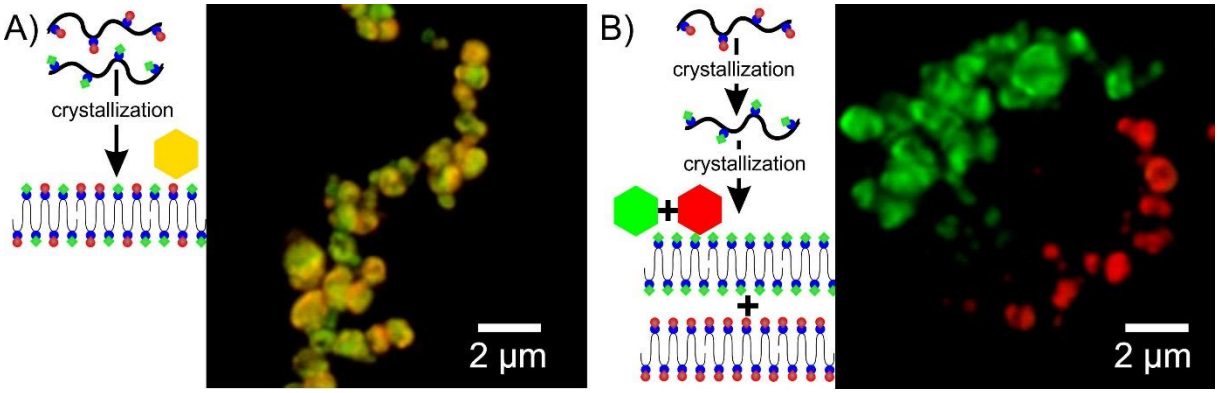

Figure 5.1. cLSM micrographs of fluorescent labeled VC polymer nanoplatelets. The diluted THF solutions have been mixed before we applied them to a water surface of a LBT (A). The two polymers co-crystallize forming a random mixture of red and green dye polymer in every polymer nanoplatelet. When we apply the two diluted solutions of red and green labeled polymer subsequently (B), the resulting polymer nanoplatelets are uniformly labeled with red or green dye, only.

The conclusion from these observations is that the two differently marked polymers can crystallize jointly (Figure 5.1A). A sequential crystallization by adding Cy5 labeled polymer to existing crystals of Cy3 labeled polymer (or *vice versa*) was not possible in this experimental configuration. We only obtained completely green and red, but no locally structured nanoplatelets. We suspect that the fast evaporation of THF is the main cause. Accordingly, the crystallization is too fast, so that a homogeneous crystallization starts immediately and thus the presented crystals do not grow further by adding the second polymer from solution. It is therefore a question of controlling the polymer crystallization to achieve sequential growth of the crystals.

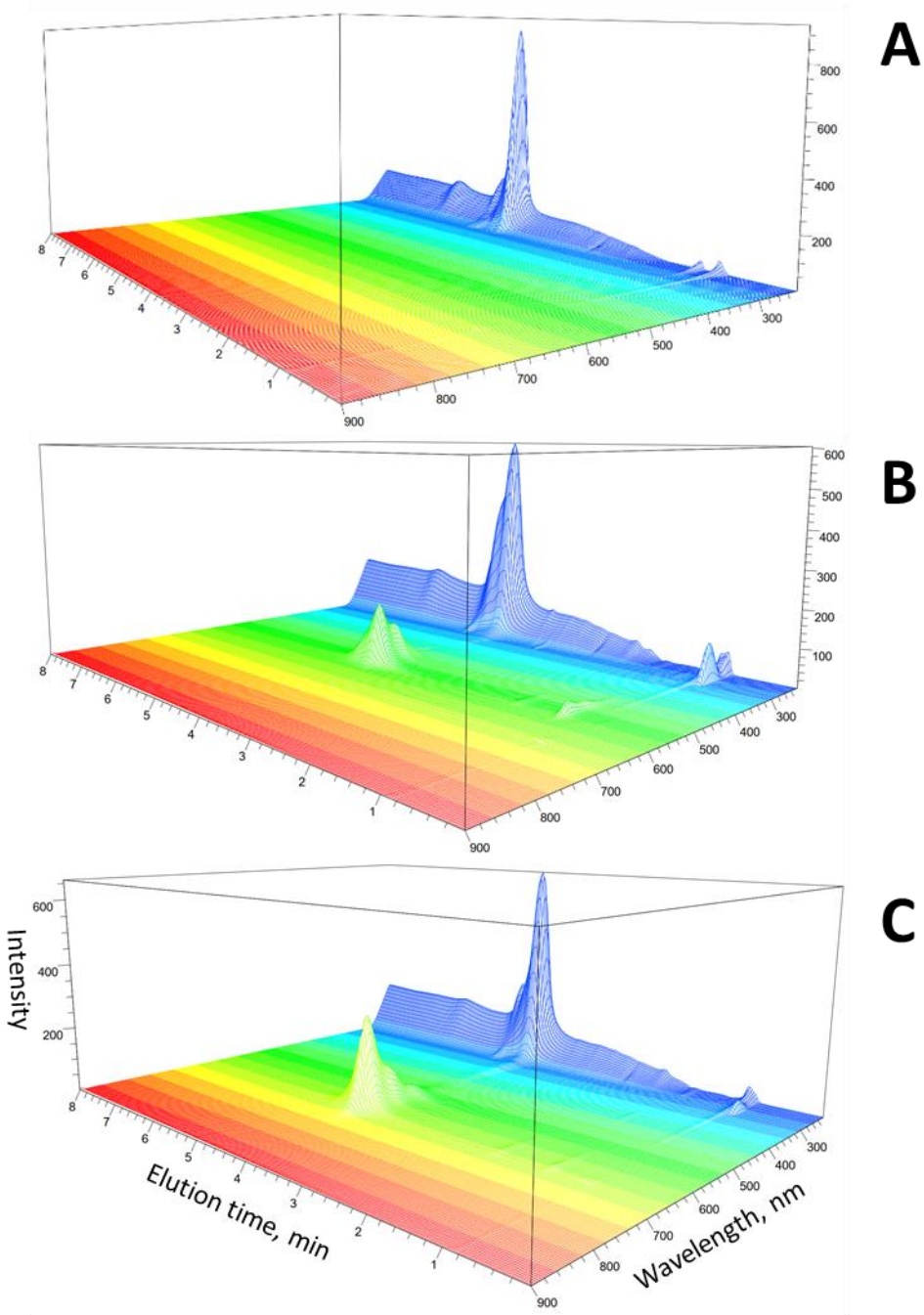

Figure 5.2. Fluorescent high-performance chromatography of pure VC polymer (A) and after attachment of fluorescent dyes Cy3 (B) and Cy5. On all three spectra the most prominent peak at 220 nm and 4.5 min corresponds to pure polymer. Samples with covalently attached dyes reveal peaks at the same elution time at 550 nm for VC-Cy3 (B) and 650 nm for VC-C5(C) respectively. Small peaks at 1.4 min and wavelength 550 and 650 nm correspond to free dye molecules.

To optimize the crystallization process and to get access to each crystal, all following experiments were not conducted on a water surface but in solution instead. As solvents, we used ethyl acetate and a THF-water mixture. Upon crystallization, the vitamin C-PE forms monolayer 2D crystals in solution. Concentration and

temperature are the crystallization controlling factors.[53] In THF-water mixtures the ratio between the two solvents plays an additional and important role.[237,238]

The crystallization process from THF-water-mixtures yields monolayer crystals as well. With the addition of water to the THF-polymer solution, the polymers' solubility decreases and thus induces the crystallization. The resulting dispersion of the 2D nanosheets was stable for several weeks due to the amphiphilic nature of the polymer. To find optimal crystallization parameters, a series of experiments with different polymer concentrations was carried out with a solvent ratio THF:water = 4:1. A concentration in the range of 0.1-0.25 mg/mL was found optimal to create monolayer crystals, which did not agglomerate according to the TEM observations (Figure 5.3).

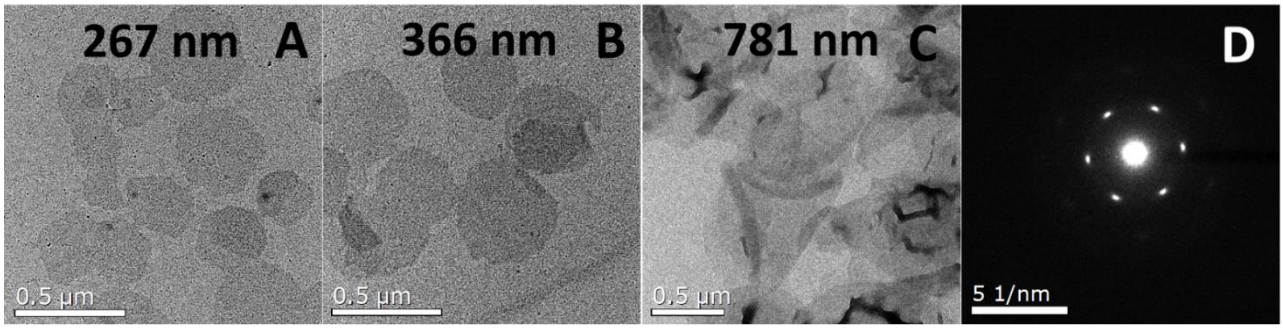

Figure 5.3. TEM bright-field micrograph of solution grown single VC polymer crystals with initial concentration of polymer 0.1 mg/mL (A), 0.25 mg/mL (d) and 0.8 mg/mL (C) from THF:water mixture 4:1 and selected area electron diffraction pattern (D). The diffraction spots reveal a nearly perfect pseudo-hexagonal crystal structure.

We could regulate the size of the crystals easily by adjusting the THF:water ratio (Figure 5.4). Since water is a poor solvent for the polymer, it induces the formation of crystal nuclei. Increasing the amount of water increases the nucleation density and thus the amount of initial crystallization seeds. As a result, more polymer crystals are generated. Accordingly, the crystals are smaller. In contrast, conducting the experiment with a lower amount of water in the mixture helps to increase the lateral size of the crystals (Figure 5.7A). Hence, we can easily control the lateral size of the 2D nanoplatelets by the water content of the THF-water solution.

In the next step, we want to continue the crystal growth process by adding additional polymer solution to the already formed dispersion of polymer crystals in the THF:water mixture (Figure 5.5). As expected, the lateral size of the crystals increased from 173 nm for the initial dispersion to 217 and 263 nm after addition of 0.05 and 0.15 mg of the vitamin C-PE, respectively. However, besides the larger crystals a substantial amount of small crystals formed during this process as well. As this two-step crystallization was conducted at room temperature, it is very likely that the small crystals formed rather immediately due to the bad solubility in the THF-water system. However, the already existing crystals have grown by the addition of the second polymer portion.

By adjusting the temperature, the separate nucleation after addition of the second fraction of the polymer was suppressed and forced it to crystallize on the existing seeds instead. To optimize this process and to find the optimal temperature, DSC measurements of the polymer crystals in dispersion were conducted (Figure 5.7B).

In contrast to the melting and crystallization in bulk,[27] for the dispersion of monolayer crystals these processes occured at much lower temperatures. The vitamin C-PE crystals melt (or dissolve) at 39 °C and crystallize at 30 °C. This defines the temperature window in which existing crystals are just stable and dissolved polymer just does not crystallize.

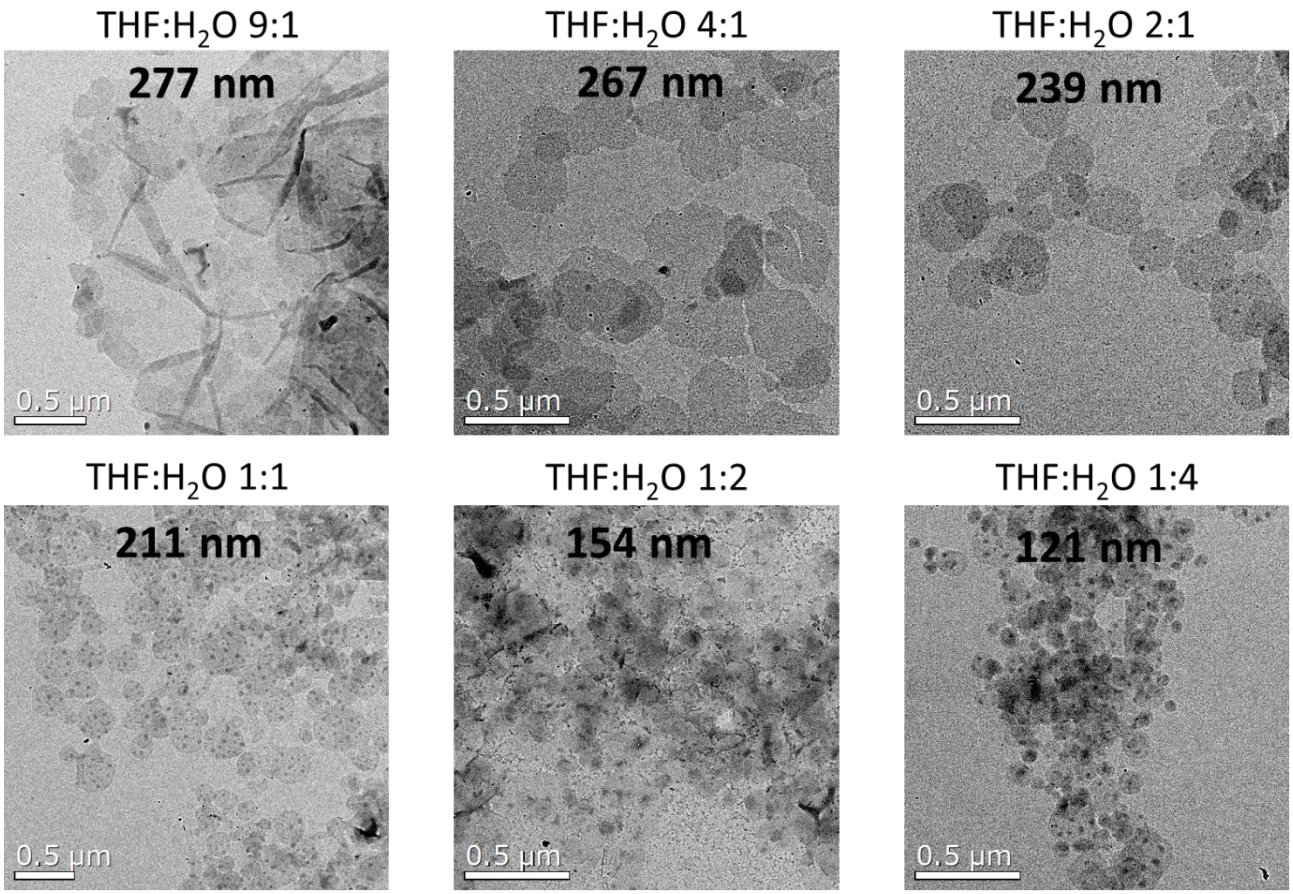

Figure 5.4. TEM bright-field micrograph of solution grown single VC polymer crystals with initial concentration of polymer 0.1 mg/mL from THF:water mixture with different ratio between THF and water from 9:1 to 1:9. In the whole range of THF-water ratios average diameter is decreasing with raising of the amount of water, but only for the ratios THF:water from 4:1 to 1:1 nice shaped 2D platelets with narrow size distributios was observed, so these conditions are optimal for further experiments.

Thus, carrying out the crystal growth experiment at 38 °C revealed a completely different picture (Figure 5.7D, Figure 5.6). Initial crystals, prepared at room temperature, have an average size of 208 nm (Figure 5.7C). Next, this dispersion was heated to 38 °C, taking care not to exceed this temperature. Subsequent addition of 0.1 mg of vitamin C-PE at 38 °C followed by a very slow cooling to room temperature yields crystals with av. size of 367 nm. No small crystals were observed this time. Accordingly, the size distribution of the lateral crystal size shifts to larger values (Figure 5.7E). Moreover, we would like to emphasize that even the variance (or polydispersity) of the size distribution is not significantly altered after the secondary growth process – the size distribution stays relatively narrow. This indicates, that the added portion of polymer solely crystallizes on the exterior of the provided initial crystals. However, in the TEM micrographs (Figure 5.7D) this core-rim structure is invisible, because we used the same polymer for initial and secondary crystallization.

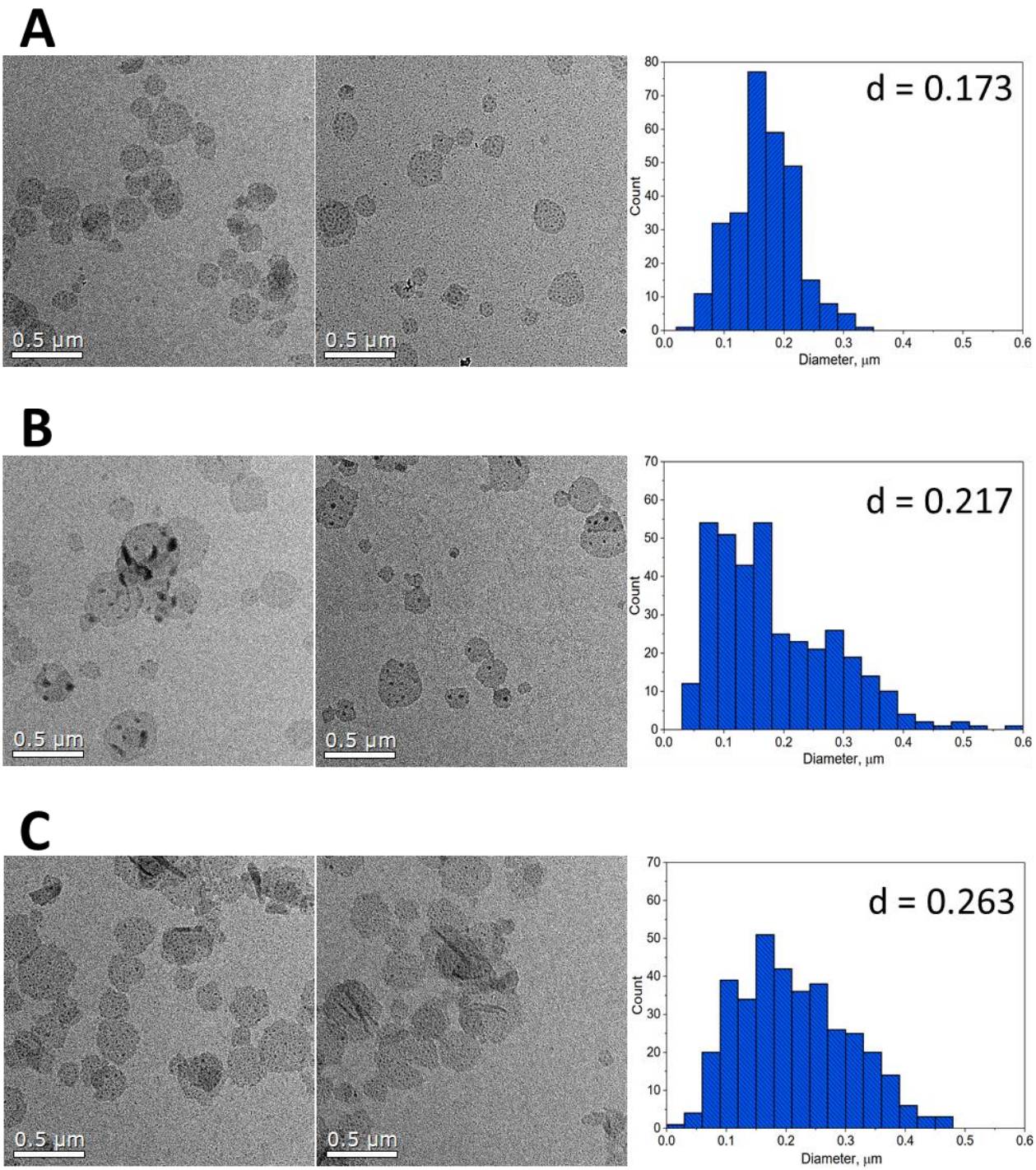

Figure 5.5. TEM bright-field micrograph of solution grown single VC polymer crystals with initial concentration of polymer 0.1 mg/mL (A) from THF:water mixture and after addition of 0.05 mg (B) and 0.15 mg (C) of polymer and corresponding crystal size distributions (right).

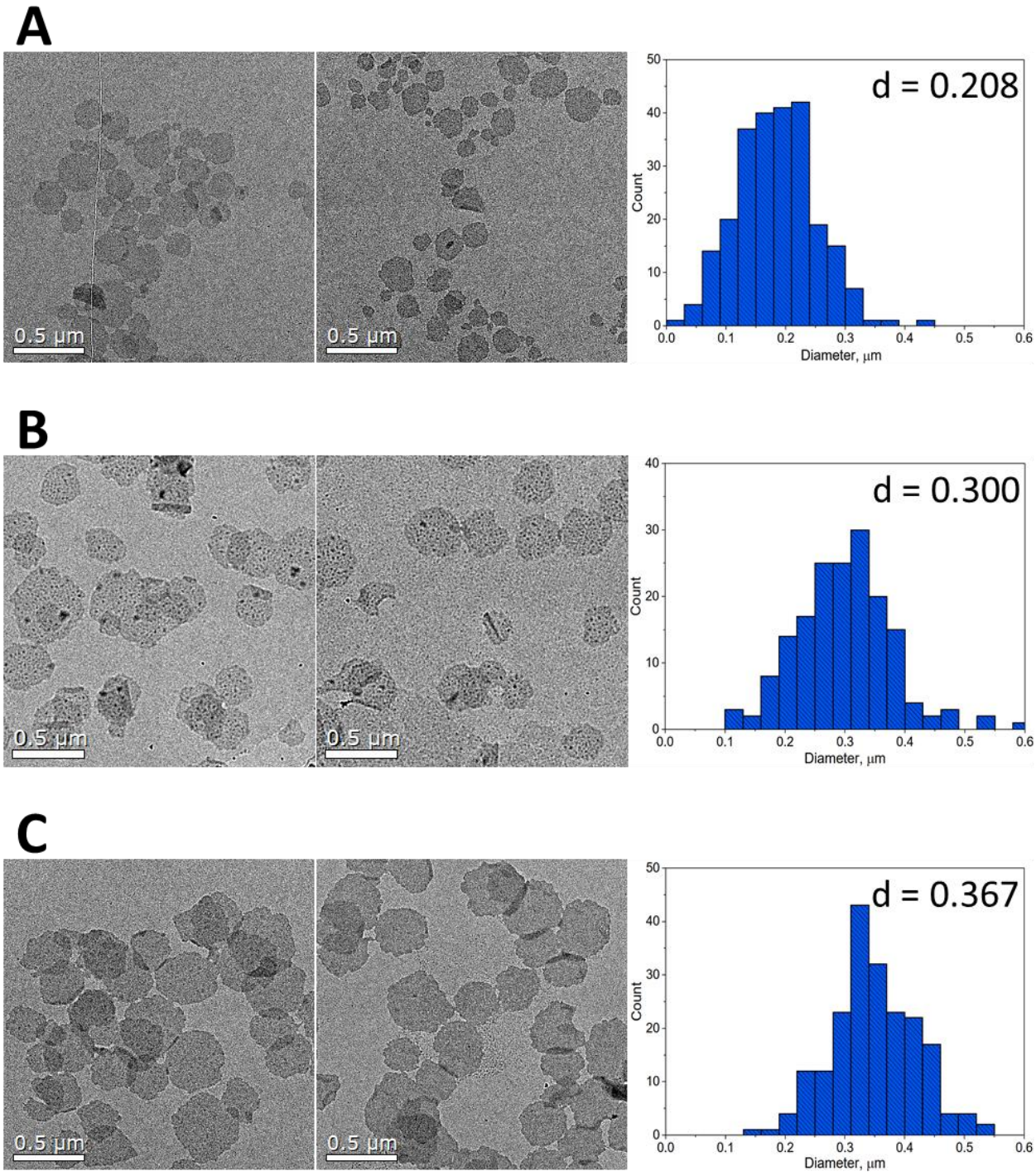

Figure 5.6. TEM bright-field micrograph of solution grown single VC polymer crystals with initial concentration of polymer 0.08 mg/mL (A) from THF:water mixture and after addition of 0.1 mg of polymer at 35°C (B) and 38°C (C) and corresponding crystal size distributions (right).

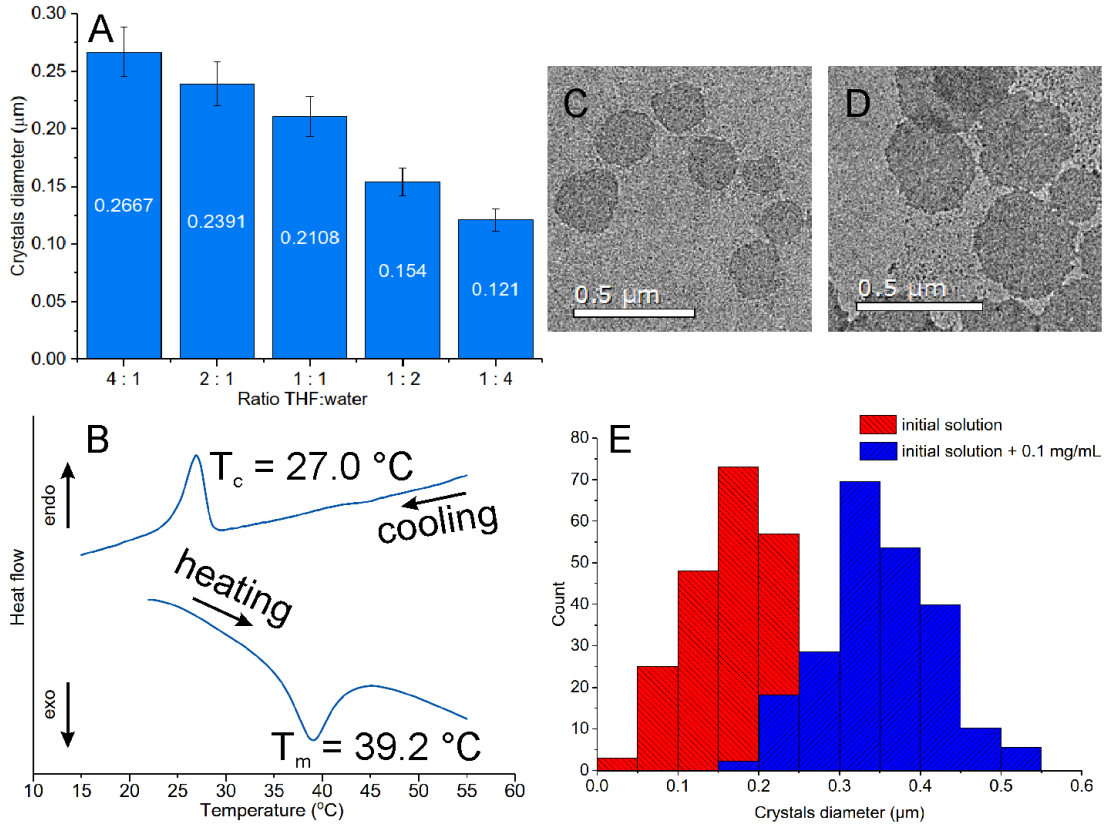

Figure 5.7. Dependence of polymer crystal size on the THF:water ratio (A), DSC thermogram of polymer crystals in dispersion in a 3:2 THF:water mixture (B), TEM bright-field micrograph of solution grown single crystal of Initial solution 0,08 mg/mL (C) and Initial solution + 0,1 mg/mL 38°C (D) from a THF:water mixture and the corresponding crystal size distribution (E).

With this optimized process at hand we now come back to the fluorescent labeled vitamin C polymers to demonstrate the potential of the sequential CDSA process: crystals with a red core and a green shell (or vice versa). The nanostructured lamellar single crystals shown in Figure 5.8 have been prepared using the above process starting with e.g. the red-labeled polymer as initial crystals, to which the green polymer was added in the second step and which formed the outer rim of the nanoplatelets. From the TEM micrographs, there is again no difference visible between the core and the shell polymer of the nanostructured 2D nanosheet crystals. However, confocal scanning laser microscopy clearly demonstrates the successful SPSC process. Since the polymers used for the core and for the shell are identical except for the fluorescent labelling, the order can be reverted at will to start with either a red or a green core, as demonstrated in Figure 5.8. . Hence, our concept of SPSC indeed yields locally structured 2D organic nanoplatelets. The key is to run the process in the temperature window between crystallization and melting.

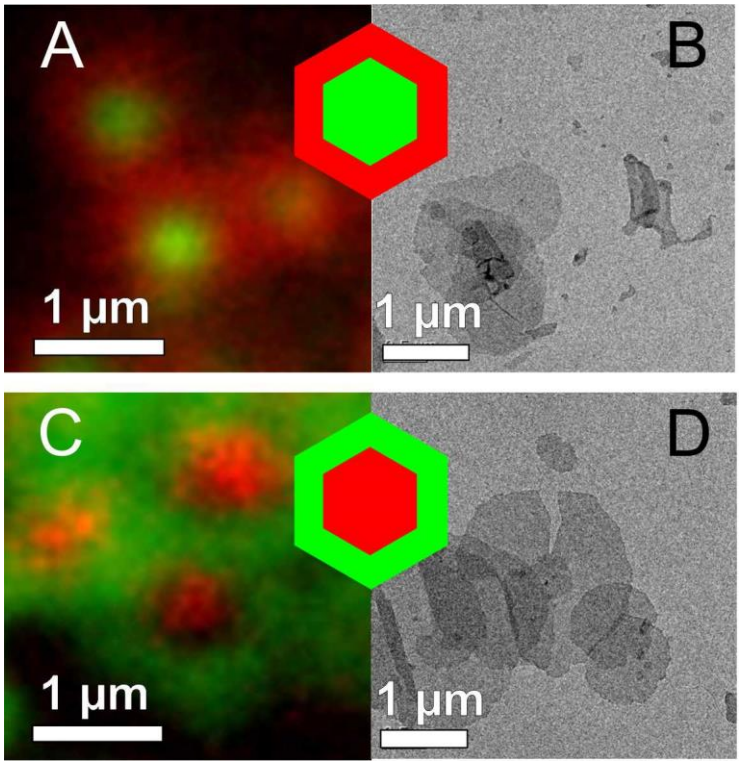

Figure 5.8. Schematic illustration of the crystals with core-shell structure, TEM bright-field micrograph solution grown crystals and confocal microscope imager, revealing desired structure. Red color – VC polymer, labeled with Cy5 dye, green color - VC polymer, labeled with Cy3 dye.

Our concept of SPSC is not limited to a special solvent or solvent mixture and we can transfer it to other suitable solvents. The prerequisite is that one can control the crystallization and melting of the polymer in solution by temperature. Here, we used ethyl acetate as solvent for the red- and green-labelled vitamin C polymers. First, we need to know the temperature window, where to perform the secondary crystallization process. Since the solubility of the vitamin C polymer in ethyl acetate is very low, there was not enough signal in DSC measurements to determine this window. Instead, we have moved to temperature-dependent DLS measurements (Figure 5.9A). Upon heating, the crystals melt at 55 °C. Therefore, we prepared the initial crystals with the red fluorescence label by slowly cooling the solution from approx. 70 °C to room temperature, yielding a dispersion of the initial crystals. Subsequently, this dispersion was carefully heated to 53 °C, just below the melting temperature. Now, a solution of the green-labeled vitamin C-PE was added followed by a slow cooling to room temperature. SEM and TEM micrographs reveal the formation monolayer single 2D crystals (Figure 5.9B, Figure 5.11). Again, electron microscopy cannot display the core-rim structure of the nanoplatelets due to missing contrast. However, since the SPSC was done with two differently labelled polymers, the cLSM clearly detects the local structure of the core-shell crystalline nanoplatelets (Figure 5.9C). The overlay of the SEM and the cLSM micrographs in Figure 5.9D finally shows that we obtained locally structured single 2D organic nanoplatelets. However, in the micrographs in Figure 5.9 there is one platelet (arrow in Figure 5.9D), that shows no local structure. It is only composed of the second, green labeled polymer.

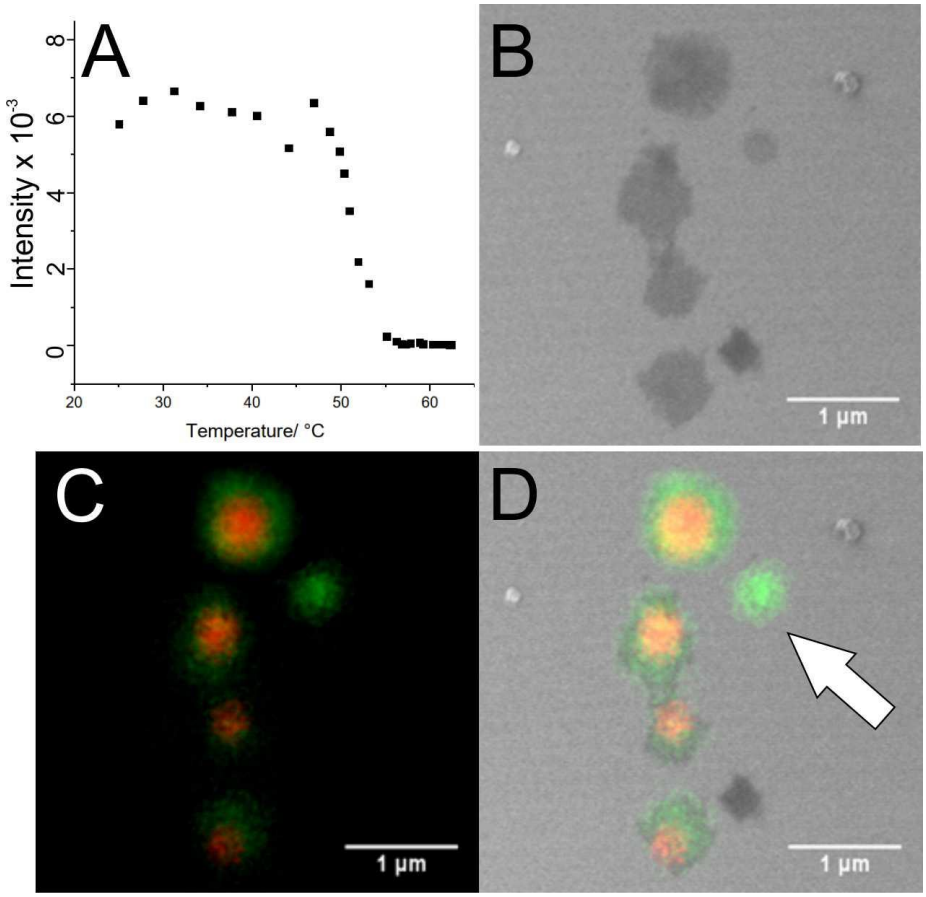

Figure 5.9. Temperature dependend light scattering of a VC polymer nanoplatelet dispersion in ethyl acetate (A), SEM (B) and cLSM (C) micrographs of SPSC grown single crystal nanoplatelets from ethyl acetate. The overlay of SEM and cLSM shows the core-rim structure of the laterally structured nanoplatelets (D).

We assume that this platelet was formed due to homogeneous nucleation. However, our SPSC process actually works and allows the formation of nanostructured 2D platelets. Only small adjustments to the process parameters may be necessary to suppress homogeneous nucleation completely.

So far, we have only used a single polymer (vitamin C-PE) for our SPSC process. To further increase the chemical functionality and to achieve a local control on the surface, two chemically different PE-like polymers with different functional groups are used: beside the vitamin C-containing polymer a polyphosphoester carrying phenyl- and phosphoric acid-groups was chosen (Scheme 5.3). Both polymers have the same PE sequence length of 20 CH_2 units between the functional groups.

Both polymers, vitamin C and polyphosphoester, were dissolved in ethyl acetate at 70 °C. Subsequently, the polymer solution was cooled down to 20 °C over a period of 25 h. The two polymers have slightly different crystallization temperatures in ethyl acetate. Upon cooling, the polyphosphoester crystallizes first and thus generates the initial seed platelets. Further cooling then induces the crystallization of the vitamin C-PE, which continues the growth of the seeds to form the outer rim of the platelets. As a result, a dispersion of 2D nanoplatelets with a polyphosphoester core and a vitamin C polymer rim is obtained. It is important to mention, that the surface chemistry is different for the core and the shell. Since the phosphate and the vitamin C groups

are expelled from the crystal core, these groups are arranged on the surface of the 2D nanoplatelets. Additionally, due to the chain folding in the crystal, they are arranged with the precision of the crystal lattice.

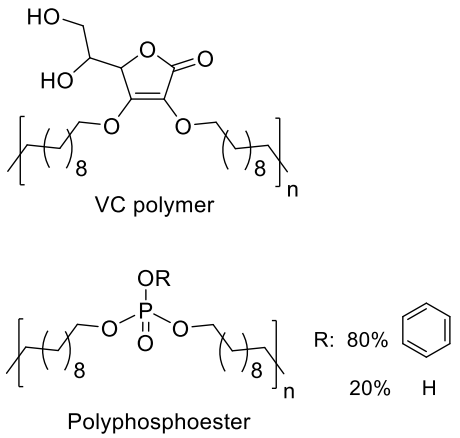

Scheme 5.3. Chemical structure of VC polymer and polyphosphoester. Polymers were synthesized according to previously published procedure[27,215]

Even though the obtained 2D nanoplatelets contain different functional groups, TEM measurement did not reveal any distinct variations in the electron density of the obtained monolayer crystals (Figure 5.12A). However, to visualize the local structure we conducted a site-selective surface functionalization at the alcohol groups of the vitamin C units. We assume to have hydroxyl groups of the vitamin C-polymer at the rim and phosphonate groups from the polyphosphoester polymer at the core. If the platelets are exposed to a trimethysilyl chloride (TMS-Cl) solution, only the vitamin C units react with the electrophilic TMS-Cl forming a silyl ether bond, while the phosphoesters, on the contrary, do not react. Hence, we dissolved TMS-Cl in chloroform or in *n*-octane and applied it to the nanostructured polymer platelets, which were already attached to a thin carbon film on a TEM grid. Excess of the TMS-Cl solution was removed using filter paper and the 2D nanoplatelets were inspected by TEM. In case of addition of TMS-Cl, dissolved in chloroform, a worm-like formation around polymer crystals is observed (Figure 5.10A). This is very likely due to the good solubility of the vitamin C-polymer in chloroform. The polymer at the rim disolves and reacts with the TMS-Cl, which explains the morphology of the system. However, the polyphosphoester core did not react with the TMS-Cl and thus no silyl ether is found in the core region of the platelets.

Using non polar *n*-octane prevents dissolution of initial crystals. In this case, a donut-like structure was observed (Figure 5.10B). Again, the inner polyphophoester core does not react with TMS-Cl, whereas the vitamin C rim is decorated. This observation clearly demonstrates that we can use the SPSC concept for regioselective chemical reactions on 2D nanosheets.

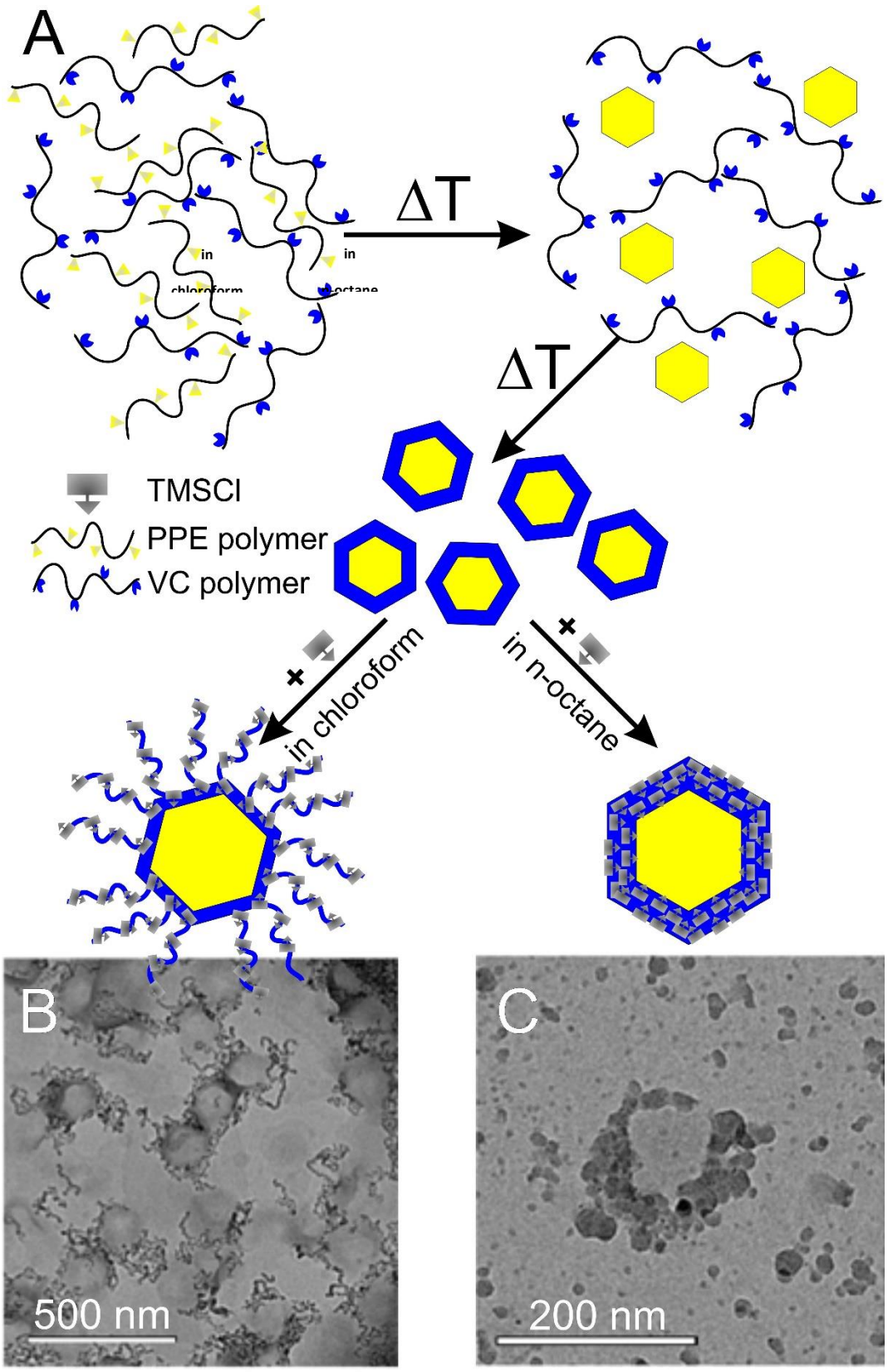

Figure 5.10. Scheme of cocrystallization between VC polymer and polyphosphoester from hot ethyl acetate and subsequent attachment of chlor(trimethyl)silan molecules to the outer part of the crystals, consisting of VC crystals with functional OH groups(A), TEM bright-field micrograph of obtained solution grown crystal in chloroform (B) and single crystals in n-octane (C)

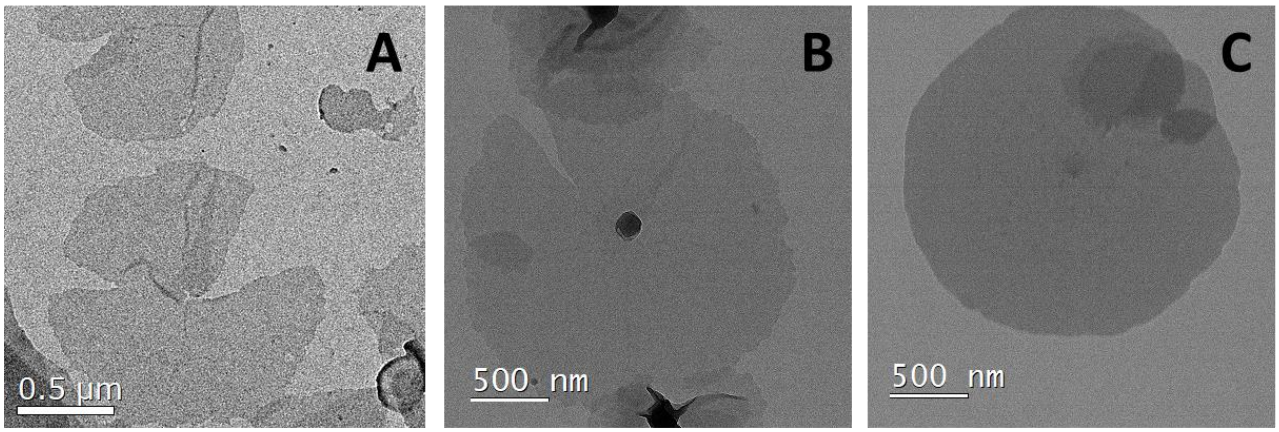

Figure 5.11. TEM bright-field micrograph of solution grown single crystals of initial VC polymer (A) and after covalent attachment of fluorescent dyes Cy3 (B) and Cy5 (C) from hot ethyl acetate.

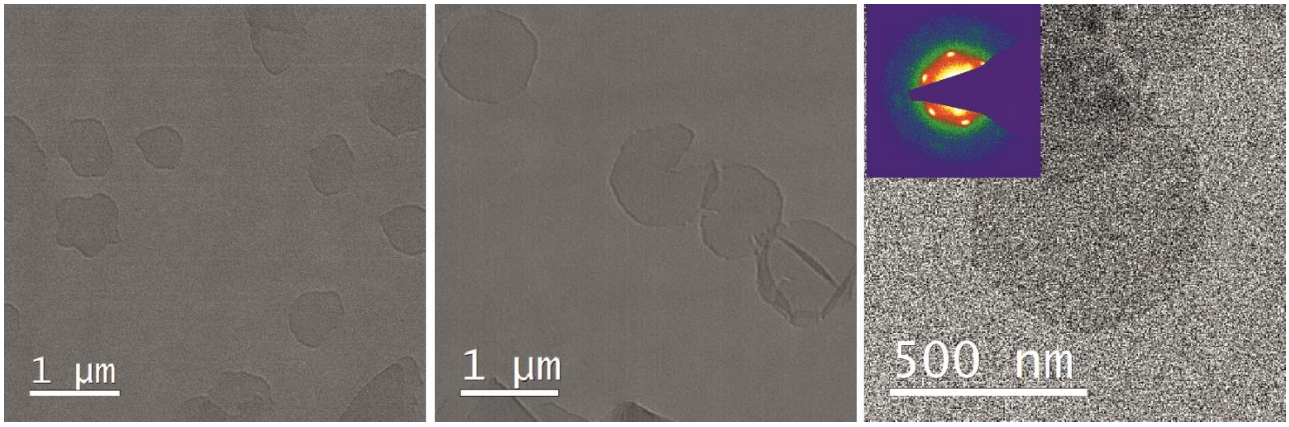

Figure 5.12. TEM bright-field micrograph of solution grown single crystals after cocrystallization of VC polymer and polyphosphoester (A) from hot ethyl acetate.

5.5. Experimental Section

Experimental

Solvents and all commercially available reagents were purchased from Acros Organics and Sigma Aldrich and used as received, unless otherwise stated. The 1st generation Grubbs catalyst was purchased from Sigma-Aldrich and stored under argon atmosphere. Deuterated solvents were purchased from Acros Organics and Sigma Aldrich. All solvents were dried using molecular sieves for at least 24 hours. Chloroform-d was stored over activated 3Å molecular sieves and anhydrous sodium carbonate, to quench residual acid.

Instrumentation

Differential Scanning Calorimetry (DSC). Thermal analysis was carried out using a Mettler-Toledo DSC 822. For nonisothermal crystallization, the samples were heated well above the melting point and kept at this temperature for 10 min. Polymer sample was then cooled at the rate of 10 K/min to 0 °C and heated again at the same rate to 120 °C. The second heating was used to determine the melting enthalpy (ΔH_m) and T_m.

Transmission Electron Microscopy (TEM). A FEI Tecnai F20 transmission electron microscope operated at an acceleration voltage of 200 kV was used to determine the crystal morphology, thickness, and crystal structure. Bright field (BF) and parallel beam nano-electron diffraction (NBED) were used for measurements. To study the crystallization behavior, polymers were dissolved in THF and crystallized by adding dropwise deionized water while gentle stirring or dissolved in hot ethyl acetate and crystallized slowly during cooling from solution.

Scanning electron microscopy (SEM). Images, providing topographic and material contrasts, were acquired using the LEO Gemini 1530 field-emission scanning electron microscope at (ultra) low (landing) voltages, respectively in the range from 100 to 200V by using the in-column ring detector Inlens-SE at working distance of around 2 mm and Line Average scan mode. Sample was applied on the ITO substrate from the ethyl acetate solution. Beam damage is considered less relevant/acceptable under the conditions being used.

Confocal Microscope. Fluorescence of the crystals was imaged on a Leica TCS SP5 confocal microscope (Leica, Wetzlar) using a HCX PL APO CS 63XNA1.40 oil immersion objective and photomultipliers as detectors. The pinhole was set to 0.5 A.U. in order to increase the resolution. Cy3 fluorophore was excited at 514nm and emission detected at 539nm - 610nm. Cy5 was excited at 633nm and detected at 652nm - 731nm. Additionally the sample was excited at 458nm and reflected light was detected at 452nm - 463nm to facilitate relocalization of the crystals in SEM.

Dynamic light scattering (DLS). Light scattering measurements were performed on an ALV spectrometer consisting of a goniometer and an ALV-5004 multiple-tau full-digital correlator (320 channels), which allows measurements over an angular range from 30° to 150. A He-Ne Laser (wavelength of 632.8 nm) is used as light source. For temperature controlled measurements the light scattering instrument is equipped with a thermostat from Julabo. The sample solution was filtered through low protein binding hydrophilic PTFE membrane filters with a pore size of 0.45 µm (LCR Millipore). Measurements were performed at 90° angle at temperatures ranging from 20°C to 62°C using a heating rate of 2.5 °C/ minute.

Fluorescent high-performance liquid chromatography (HPLC). Covalent bonds between PE-VC polymer and fluorescent dyes Cyanin 3 (Cy3) and Cyanin 5 (Cy5) was proved using an Agilent Technologies HPLC with quaternary pump Series 1100, thermostated column compartment Series 1200, diode array detector, ELSD Varian 385-LC. Experiments were conducted using two different columns Macherey-Nagel: Pyramid (RP C18) length: 125mm / diameter: 3mm / Particel size: 5µm for experiment "c" flow: 0.8ml/min / 20°C / Gradient of THF-Water+0.1%TFA starting with 40/60; in 5min 100/0 and HD8 (RP C8-"high-density") 125/4/5 for experiment "a" flow 1ml/min / 40°C / Gradient of THF/Water+0.1%TFA starting with 50/50; in 5min 100/0.

Synthesis

Synthesis of PE-VC polymer and fluorescent labeling. Synthesis of PE-like polymer with equidistantly distributed ascorbic acid (vitamin C) groups along the polymer chain and its subsequent labeling with fluorescent dyes Cy3 or Cy5 was conducted according to previously published procedure.[27] Synthesis of PE-like phosphoresther polymer, containing 20% of hydroxyl groups and 80% of phenoxy groups, was prepared according to previously published procedure.[170]

Sample preparation. Both crystallization on the water surface using Langmuir-Blodgett Trough (LBT) and in the solution methods were used for the sample preparation. Formation of single polymer crystal and polymer growth experiments were conducted in solution to obtain single separate crystals.

Single layer crystals *in ethyl acetate.* 0.1 mg of PE-VC polymer was dissolved in 1 mL of ethyl acetate. The sample was kept in a temperature-controlled oil bath at 70 °C until full dissolution, then the solution was slowly cooled down to room temperature for crystallization. Afterwards, one droplet of the dispersion was dropped onto a carbon-coated grid for further TEM measurement.

In THF-water mixture. PE-VC polymer was dissolved in certain amount of THF, after full dissolution deionized water was added dropwise to the sample while stirring. Polymer concentration, solvents ratio and average diameter are shown in Supporting Information. After addition of water, formation of single polymer crystals occurs within a minute. One droplet of obtained dispersion was applied onto a carbon-coated TEM grid for further measurement.

Crystal growth experiment *in ethyl acetate.* 0.1 mg of PE-VC polymer was dissolved in 1 mL of ethyl acetate. The sample was kept in a temperature-controlled oil bath at 70 °C until full dissolution, then the solution was slowly cooled down to room temperature for crystallization. To the obtained polymer crystals dispersion 0.05 or 0.15 mL of PE-VC with concentration 1mg/mL in THF was added dropwise while stirring. One droplet of the dispersion was applied onto a carbon-coated TEM grid for further measurement.

In THF-water mixture at room temperature. 0.1 mg of PE-VC polymer was dissolved in 600µL of THF, after full dissolution 400 µL deionized water was added dropwise to the sample while stirring. To the obtained polymer crystals dispersion 0.05 or 0.15 mL of PE-VC with concentration 1mg/mL in THF was added dropwise while stirring. One droplet of the dispersion was applied onto a carbon-coated TEM grid for further measurement.

In THF-water mixture at 38 °C: 0.08 mg of PE-VC polymer was dissolved in 600 µL of THF, after full dissolution 400 µL deionized water was added dropwise to the sample while stirring. The sample was kept in a temperature-controlled oil bath at 38 °C, 100 µL of the PE-VC polymer in THF (0.1 mg/mL) was heated up to 38 °C and added to the mixture during gentle stirring, after 5 minutes stirring and heating were switched off.

After cooling down to the room temperature, one droplet of the polymer crystals dispersion was dropped onto a carbon-coated grid for TEM measurement.

Polymer crystals assembly *on LBT*. 0.1 mol % solutions of PE-VC, labeled with fluorescent dyes Cy3 and Cy5, in THF were prepared. For the first experiment, 3-4 drops of each solutions were added subsequently on the layer of deionized water on the LBT and leave to evaporate all THF and form polymer crystals. For the second experiment, both solutions were mixed in equal volumes and obtained mixture was added dropwise on the LBT with deionized water and leave to evaporate all THF and form polymer crystals. Both samples were transferred on the glass slides and measured on the confocal microscope.

In THF-water mixture. 0.08 mg of labeled PE-VC polymer was dissolved in 600 µL of THF, after full dissolution 400 µL deionized water was added dropwise to the sample while stirring. The sample was kept in a temperature-controlled oil bath at 38 °C, 100 µL of the PE-VC polymer, labeled with the second color, in THF (0.1 mg/mL) was heated up to 38 °C and added to the mixture during gentle stirring, after 5 minutes stirring and heating were switched off. After cooling down to the room temperature, one droplet of the polymer crystals dispersion was dropped onto a carbon-coated grid for TEM measurement and on the glass slide for the measurement on the confocal microscope.

In ethyl acetate: 0.08 mg of PE-VC polymer was dissolved in 1 mL of ethyl acetate. The sample was kept in a temperature-controlled oil bath at 70 °C until full dissolution, then the solution was slowly cooled down to room temperature for crystallization. To the obtained crystals dispersion of the polymer, heated up to 53 °C, 0.1 mL of PE-VC polymer, labeled with the second color, with concentration 1 mg/mL in ethyl acetate was heated up to 60 °C and added dropwise while gentle stirring, in 5 minutes stirring and heating were switched off. After cooling down to the room temperature, one droplet of the polymer crystals dispersion was dropped onto a carbon-coated grid for TEM measurement and on the glass slide for the measurement on the confocal microscope.

Polymer co-crystallization 0.1 mg of PE-VC and 0.1 mg of polyphosphoester polymers were dissolved in 2 ml ethyl acetate. The mixture was kept in a temperature-controlled oil bath at 70 °C for 1 hour while stirring, then stirring was switched off and the sample was cooled down to the room temperature within 25 hours. One droplet of the dispersion was dropped onto a carbon-coated grid for TEM measurement.To functionalize a surface of obtained monolayer crystals, one drop of the sample was applied onto a carbon-coated TEM grid and let it dry. One droplet of trimethylsilyl chloride (TMS-Cl) was dissolved in 1 mL of chloroform ($CHCl_3$) or n-octane, added onto the grid with polymer crystals and measured on the TEM.

5.6. Conclusion

With our new concept of SPSC of polymers with a precise molecular architecture, we can generate 2D organic nanoplatelets with a patterned surface functionalization. This concept, which is based on folded polymer crystallization, is highly versatile and straightforward. The functional groups on the surface are accessible and can be used for selective local chemical reactions. Furthermore, these groups are arranged on the surface with the perfection of the crystal lattice. Another major advantage is that the platelets are stable in dispersion, which considerably simplifies their chemical modification and processing. Hence, this versatile and simple concept to laterally structure the nanoplatelets opens the way for a new class of nanostructured 2D materials.

6. Terpyridine-Induced Folding of Anisotropic Polyphosphoester Platelets

Oksana Suraeva, Tobias Haider, Ingo Lieberwirth, Frederik R. Wurm

This chapter is based on unpublished results.

I carried out the crystallization experiments to form monolayer polymer crystals. Also, I developed the complexation experiments, using TEM measurements to optimize the complexation conditions. Together with Tobias Haider we performed the interpretation of the results and developed a model to explain the ternary structure formation of the polymer crystal platelets. I wrote the part of the manuscript explaining the platelet folding and their preparation. Tobias Haider synthesized and analyzed the polymer.

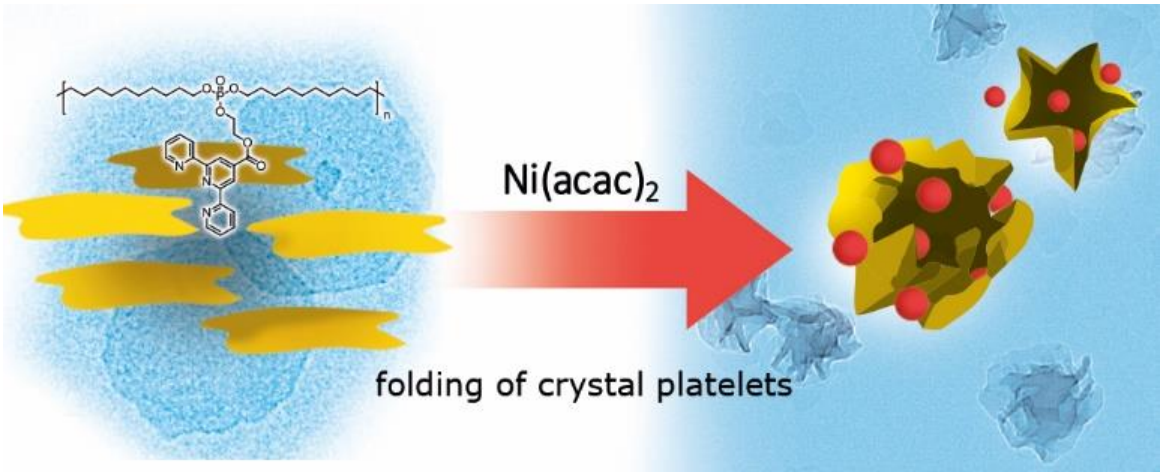

Keywords: crystal engineering, crystal assembly, polyethylene, polyphosphoester

6.1. Preface

In the last chapter I will show a completely new perspective of polymer 2D crystals – their similarity with systems existing in nature. There, depending on the complexity of the system and the interactions between its parts, one can distinguish structures of first, secondary and tertiary order. The most basic one – the primary structure – is a linear sequence of nucleotides or amino acids. Folding local segments leads to the formation of alpha helices and beta sheets, and further arrangements results in the proteins tertiary structure which is stabilized by hydrogen or ionic bonds and hydrophilic or hydrophobic interactions between the segments.

Similar logic and hierarchy can be used to describe the formation of polymer 2D crystals and further interactions between them. The polymer chains can be considered as the first order structures. Upon crystallization, they form the secondary structure – the crystal. When the incorporated defects are expelled to the crystal surface, they should be accessible to further modifications and interactions. This is a basic idea of the project, presented in this chapter.

To prove the concept that the whole polymer 2D crystals can act as a separate, independent element I used crystals with terpyridine groups as pending functional groups on the surface. These groups are capable of forming strong complexes with metal salts. The experiment was conducted in ethyl acetate, because of two reasons. On the one side, this solvent is suitable to form polymer crystals and keep them stable at room temperature. On the other side, complex-forming salts such as Nickel(II) acetylacetonate ($Ni(acac)_2$) are soluble in ethyl acetate and thus can react with every single crystal in the dispersion. In dispersion, the highly anisotropic polymer platelets are very flexible and after addition of nickel salt and gentle stirring, several terpyridine groups on different parts of the crystal can form bonds with one nickel coordination center. This finally leads to the formation of folded, ball-like structures, composed of one or several crystals. By reducing the polymer concentration the probability for the interaction of individual crystals is decreased and with that the mean number of crystals, that will form the final, ternary structure. As a result, the size of observed crumpled ball-like structures is shrinking. On the other side, by varying the amount of nickel salt, it is possible to change the amount of interactions in the system and, thus, reduce the degree of folding.

This project was a first experiment, representing perspectives of functional polymer 2D platelets as an independent element. By choosing various pairs of functional group – coordination complex, it is possible to form assemblies and to trigger the folding and unfolding.

6.2. Abstract

We report on the preparation of complex synthetic tertiary structures, consisting of folded anisotropic polymer crystal platelets. These simplified systems are intended to help to understand the folding process in more complex biomolecules. A PE-like polyphosphate was functionalized with pendant terpyridine groups by esterification, with a maximum degree of functionalization of 85%. The polymer was characterized in detail by NMR, GPC and DSC. Highly anisotropic polymer crystal platelets with terpyridine groups on the crystal surface were obtained by crystallization from ethyl acetate. Metal-ligand complexation between terpyridine and Ni^{2+} ions lead to a folding of the crystal platelets, which was investigated by TEM. Hereby, the size as well as the size distribution of the obtained assemblies could be altered by varying the concentration of metal ions present.

6.3. Introduction

Biomacromolecules such as enzymes effectively function because of their precise and dynamic three-dimensional (3D) architecture.[239] Induced by covalent and non-covalent interactions, proteins can undergo guided folding in solution to form complex architectures.[240] Van der Waals interactions, hydrogen bonding, and hydrophobic or electrostatic interactions lead to the protein's secondary structure, including helices, pleated sheets and turns.[239,241] In recent years, single chain polymer nanoparticles (SCPNs) were presented as synthetic but much simpler protein mimics.[242] SCNPs are formed by collapsed single polymer chains, which can be synthesized from highly diluted solutions by intramolecular covalent (irreversible) or non-covalent (reversible) interactions within the polymer chain.[239,242] Examining the morphology and the folding process of these simplified synthetic systems is intended to help to understand more complex biomacromolecules.[240] However, higher order assemblies of natural polymers are not limited to single polymer chains. Fibrous proteins like α-keratin or collagen are molecules whose secondary structures are their dominant structural motifs.[241] Collagen i.e. has a triple helical structure that is further organized into fibrils. To mimic such behavior with synthetic polymers, the assembly or "folding" of colloidal systems can be used. For example, anisotropic assemblies of colloids was achieved by magnetic nanoparticles[243] or MOFs[244]. However, to the best of our knowledge, the folding of anisotropic polymer crystallites had not been reported. Such "2D" polymer crystallites represent anisotropic colloids with a thickness of ca- 5-10 nm and lateral dimensions of several micrometers. They can be obtained from cystallizable polymers including both homo- and copolymers by crystallization from a dilute solution.[52,110,245] Several studies were able to create polymer platelets by crystallization-induced self-assembly of block copolymers and polymer blends.[113,117,246] Inam *et al*. showed the application of anisotropic polymer platelets made from polylactide-*block*-poly(2-dimethylaminoethyl methacrylate) block copolymers as water-in-water emulsifiers.[247] Moreover, anisotropic platelets were applied in supported catalysis[248] and as nanomotors.[249] Non-covalent interactions between polymer crystal platelets can induce assemblies of higher order: π-π interactions between poly(*p*-phenylenevinylene)-*block*-poly(2-vinyl pyridine) (PPV-*b*-P2VP) platelets lead to the formation of 2D-square micelles.[250] Non-covalent metal-ligand interactions are also commonly used to create supramolecular structures.[251] In particular chelating ligands are suitable for this purpose, with the tridentate ligand 2,2';6',2''-terpyridine as a prominent example.[252] Terpyridine forms very

stable octahedral complexes with a wide range of different metal ions including iron, ruthenium or nickel. The ligand is used both for the synthesis of metallopolymers or 2D polymer networks.[253–255]

Here, we present the synthesis of a polyethylene-like polyphosphate with precisely 20 CH_2-groups between each phosphate group and pendant terpyridine groups. Anisotropic polymer platelet dispersions were obtained after crystallization from an ethyl acetate solution. Terpyridine ligands on the platelet-surface enabled the complexation with nickel cations, which led to the folding of the polymer platelets. With this work, we contribute to a further understanding how second order assemblies can be obtained by using anisotropic polymer crystal platelets (Figure 6.1).

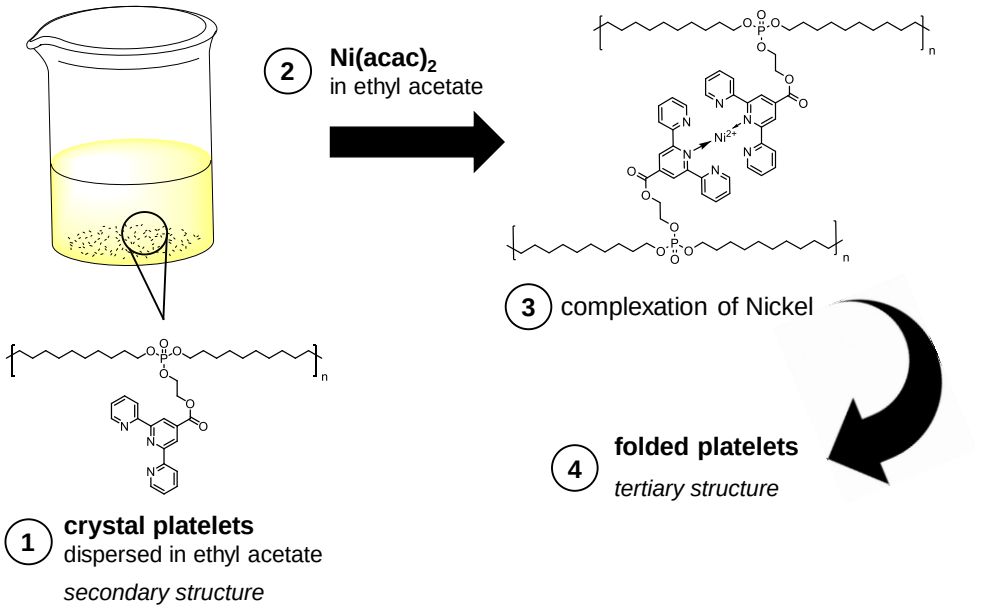

Figure 6.1. Schematic representation of experimental procedure to obtain folded polymer platelets induced by supramolecular interactions.

6.4. Results and discussion

Polymer synthesis and functionalization. To obtain anisotropic polymer crystal platelets capable of intra- and intermolecular interactions, we synthesized a polyethylene-like polyphosphate with pendant terpyridine groups. In general, polyphosphoesters, and in particular polyphosphates, are a class of highly versatile polymers: the material properties, solubility and degradation profile of the polymers thereby strongly depend on the nature of the polymer backbone and the pendant chains.[171] Furthermore, functional groups can be introduced to the polymer by a variation of the pendant chains. Hydrophobic, PE-like polyphosphates with long methylene spacers between the phosphate groups can be synthesized by acyclic diene metathesis (ADMET) polymerization, ring-opening metathesis polymerization, and transesterification.[24] ADMET polymerization is a polycondensation reaction of a *α*,*ω*-diene under the release of ethylene gas catalyzed by a transition metal catalyst (e.g. Ru-based Grubbs-catalysts).[18] Symmetric monomers, which include branches or functional groups, result in polymers with a precise spacing between each branch or functional group, respectively. Lieberwirth *et al.* investigated solution-grown polymer crystal platelets of polyethylene-like ADMET

polyphosphoesters in detail.[215] The polyethylene segments crystallized in lamellae shape with the phosphoester groups acting as crystallization defects. The length of the polyethylene segment determined the thickness of the lamellar and thus the *z*-dimension of the polymer platelets. Lieberwirth *et al.* determined the thickness of the solution-grown lamellae crystals by atomic force microscopy (AFM) and energy-filtered transmission electron microscopy (EFTEM). For the investigated polyphosphate with pendant phenyl groups and with an aliphatic spacer length of 20 CH_2 groups, a value of ca. 3.2 nm was obtained by AFM. Furthermore, they proved that for this polyphosphate, the bulky phenoxy defects were not in the lamellar crystal but urged into the amorphous phase. Thus, we assume that larger terpyridine groups in the pendant chains will also be expelled from the polymer crystal. As a result, the terpyridine functional groups are supposed to be accessible on the polymer crystal surface.

As a starting material, we used the long-chain polyphosphate **poly-1** with 20 CH_2-groups between each phosphate group and an ethoxy hydroxylside chain. Functionalization was accessible through the primary alcohol in the pendant chain, while the precise spacing between the phosphate groups ensured an even distribution of the functional groups along the surface of the later crystal platelets. The monomer synthesis, polymerization and post-polymerization hydrogenation is described in detail in chapter 3. Briefly, the monomer was obtained in a two-step reaction of $POCl_3$ with 2-(benzyloxy)ethanol and 10-undecen-1-ol. After ADMET polymerization in bulk using 1st generation Grubbs' catalyst, Pd-catalyzed hydrogenation was performed to give fully saturated **poly-1** with free hydroxyl groups in the pendant chains.

The terpyridine ligand was covalently attached to the polyphosphate side chain *via* an ester linkage. In a one-pot reaction, first an active ester of 2,2':6',2''-terpyridine-4'-carboxylic acid was formed by the reaction with carbonyldiimidazole (CDI). This active ester readily reacted with **poly-1** upon addition to give **poly-1-terpy** under the cleavage of imidazole (Figure 6.2A). The reaction was conducted at 60 °C to overcome solubility restrictions. **Poly-1-terpy** was purified by repeated precipitation into cold methanol to give a solid colorless polymer with 48% yield. **Poly-1-terpy** was analyzed by NMR spectroscopy. Figure 6.2B shows an overlay of the ^{31}P NMR spectra of **poly-1** and **poly-1-terpy**. The initial signal at 0.47 ppm, corresponding to **poly-1**, disappeared almost entirely, while an intensive new signal at -0.93 ppm indicated a successful functionalization of the polymer. Covalent attachment of the terpyridine group to the polymer was proven by ^{1}H NMR spectroscopy with signals in the range of 7.30 to 9.01 ppm being assigned to the terpyridine group (Figure 5.2C). The integration of all signals in ^{1}H and ^{31}P NMR spectra verified that a degree of functionalization of ca. 85% was achieved, despite the high steric bulk of the terypridine group. When the esterification reaction was repeated, a degree of functionalization of 60% was achieved for a second entry (Figure 6.3). The molecular weight of **poly-1-terpy** was determined by size exclusion chromatography in THF relative to a PS standard (Figure 6.4). Values of M_n = 4,100 g mol^{-1} and M_w = 17,000 g mol^{-1} were obtained. Compared to the starting material, both values dropped after functionalization (**poly-1**: M_n = 7,400 g mol^{-1}, M_w = 21,000 g mol^{-1}). Furthermore, an intensive tailing of the SEC trace of **poly-1-terpy** indicated a possible interaction between the polymer and the column material. In contrast to **poly-1**, the elugram of **poly-1-terpy** shows an intensive UV trace, which further proved the covalent linkage of the UV-active terpyridine group to the polymer backbone. The thermal properties of **poly-1-terpy** were examined by differential scanning calorimetry (Figure S5.2). A glass transition temperature (T_g) at 19 °C and a melting point (T_m) at 66 °C (Figure 6.5) with a melting enthalpy

ΔH_m of -36.2 J g^{-1} were observed. T_m decreased by 20 °C in comparison to **poly-1** (T_m = 86 °C) due to the absence of hydrogen bonding. By comparing ΔH_m of **poly-1-terpy** to 100% crystalline polyethylene (ΔH_m = 293 J g^{-1}),[178] the crystallinity of the polymer was calculated. The obtained value of 12% crystallinity was lower compared to **poly-1** (35%) and to a long-chain polyphosphate with the same aliphatic spacer length but an ethoxy pendant chain (26%). This indicates a strong effect of the bulky terpyridine groups on the crystallization behavior of the polymer.

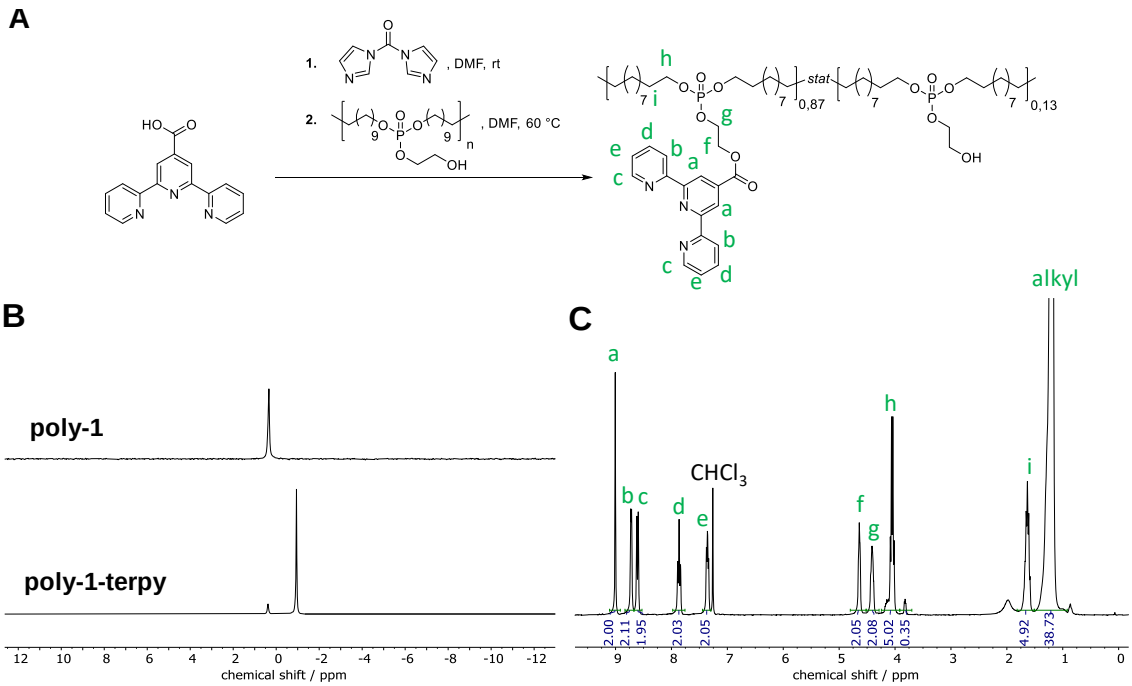

Figure 6.2. A) Synthesis of **poly-1-terpy** via carboxylic acid activation by carbonyldiimidazole (CDI). B) ^{31}P NMR (121 MHz at 298 K, in $CDCl_3$) of **poly-1** (top) and **poly-1-terpy** (bottom). C) ^{1}H NMR (300 MHz at 298 K, in $CDCl_3$) of **poly-1-terpy**.

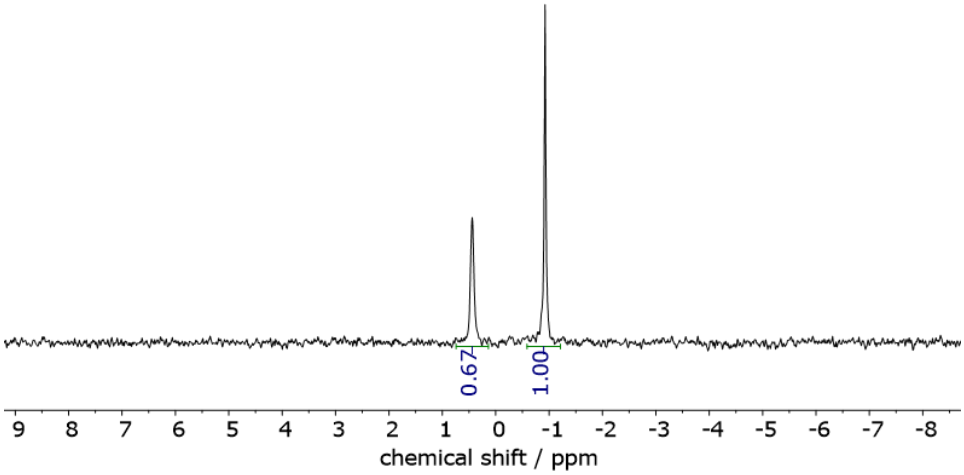

Figure 6.3. ^{31}P NMR of **poly-1-terpy** (entry 2) in $CDCl_3$ at 121 MHz at 298 K.

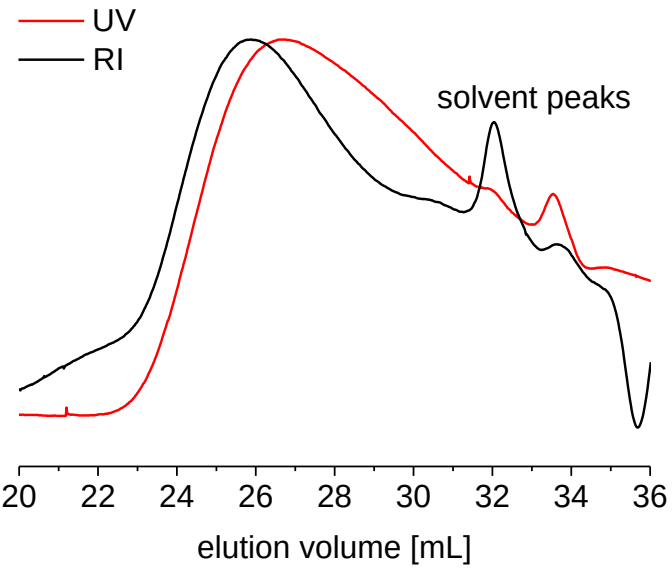

Figure 6.4. SEC elugram of **poly-1-terpy**.

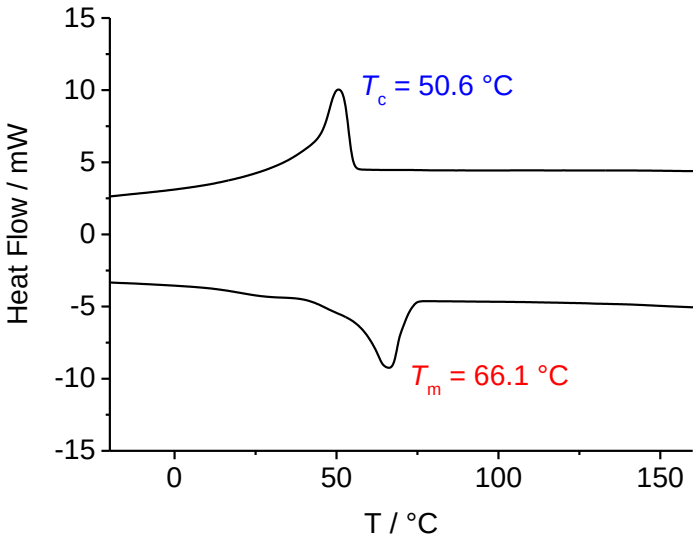

Figure 6.5. DSC thermogramm of **poly-1-terpy**.

Solution-grown polymer platelets from poly-1 and poly-1-terpy. Anisotropic polymer crystal platelets can be prepared by crystallization of PE-like polymers from dilute solutions.[215] For the crystallization of **poly-1-terpy**, entry 2 was used with a degree of terpyridine functionalization of 60%. Solutions of **poly-1-terpy** in ethyl acetate with concentrations of 1 mg mL^{-1} and 0.1 mg mL^{-1}, respectively, were slowly cooled down from 70 °C to room temperature (ca. 23 °C) overnight to give anisotropic platelet dispersions. Transition electron microscopy (TEM) was used to analyze the platelets (Figure 6.6). The size of the platelets was visually determined using ImageJ software. We calculated the number average platelet diameter D_n and diameter average platelet diameter D_w as well as the dispersity (Table 6.1).[92] Overall, the size of the platelets depended

on the concentration of the initial solutions. For an initial polymer concentration of 1 mg mL^{-1}, D_n was 590 nm and D_w was 1.16 µm, indicating a relatively broad size distribution of ca D_w/D_n=2 (Figure 6.6). Platelets obtained from solutions with a concentration of 0.1 mg mL^{-1} were significantly smaller (D_n = 360 nm and D_w = 450 nm) with a narrower size distribution (D_w/D_n=1.25). The thickness of the platelets was determined by the chemical structure of the polymer: with an aliphatic spacer length of 20 CH_2-groups between each defect, the thickness is in the range of several nanometers (cf. Chapter 2 and Lieberwirth *et al.*[215]). Comparing the platelets of **poly-1-terpy** to solution-grown crystal platelets of the initial **poly-1** (Figure 6.7), monolayer crystals with similar shape and size were observed despite the high steric bulk of the terpyridine group and the reduced crystallinity of **poly-1-terpy**. Due to their large size, the terypridine groups are expected to be expelled from the crystal, being accessible for metal-ligand supramolecular interactions.

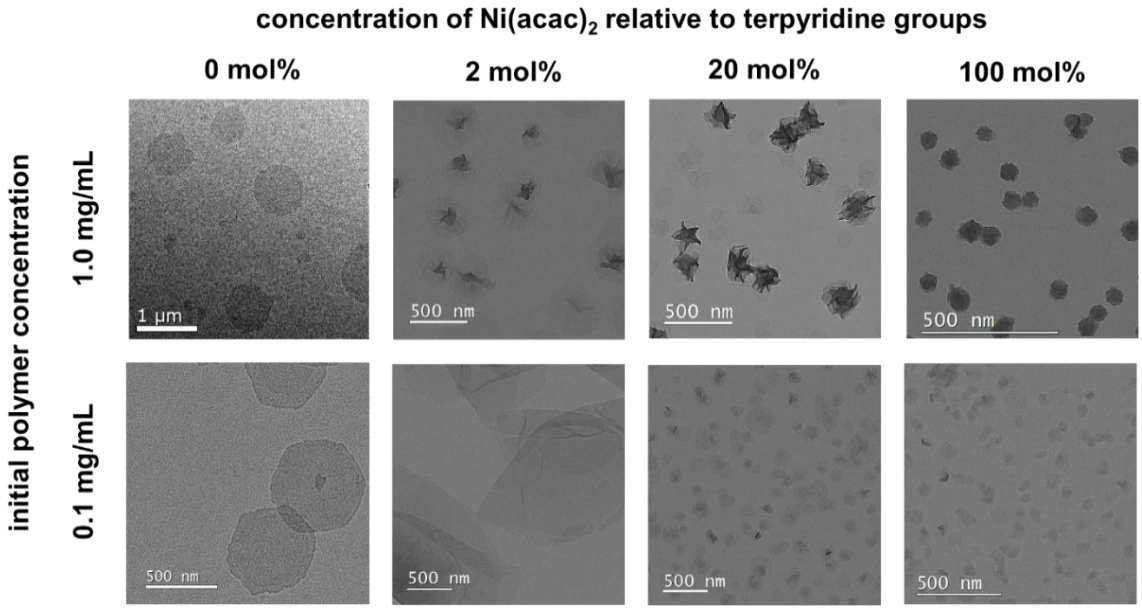

Figure 6.6. TEM bright-field images of **poly-1-terpy** crystals upon addition of different concentrations of $Ni(acac)_2$. Images on the left represent the initial polymer crystals.

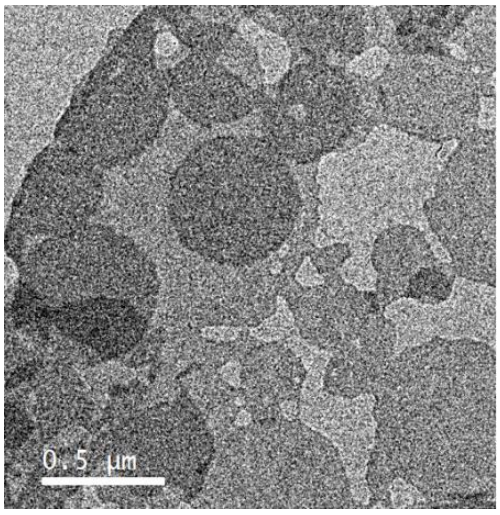

Figure 6.7. TEM bright-field images of **poly-1** crystals (D_n = 430 nm, D_w = 500 nm, D_w/D_n=1.14).

To induce a supramolecular interaction between the terpyridine groups on the surface of the polymer platelets, Nickel(II) bis(acetylacetonate) ($Ni(acac)_2$, dissolved in ethyl acetate) were added to the dispersion of **poly-1-terpy** crystal platelets in ethyl acetate. Ni^{2+}-ions form octahedral complexes with two terpyridine ligands (Figure 6.1).[252] The ratio of $Ni(acac)_2$: terpyridine units was varied from 2 to 100 mol% respective to terpyridine units in the polymer. At both concentrations, the complexation of Ni^{2+} by terpyridine-functionalized platelets resulted in a folding of the platelets (Figure 6.6), which further led to a decrease in the size of the platelets for all samples expect the sample with 2 mol% $Ni(acac)_2$ and 0.1 mg mL^{-1} initial polymer concentration.

D_n decreased with increasing concentration of Ni^{2+} ions, down to 70 nm for the sample with 100 mol% $Ni(acac)_2$ and 0.1 mg mL^{-1} initial polymer concentration. From this data it can be assumed that the addition of Ni^{2+}-ions resulted in complexation of two terpyridine units of the same polymer platelet and that by increasing the amount of metal ions, a higher number of ligand-metal complexes were formed resulting in higher degree of folding of the platelets. For samples with 2 and 20 mol% $Ni(acac)_2$ added, the amount of Ni^{2+} present was not enough to form completely spherical folded assemblies. Thus, the lateral sizes of the obtained conformations were larger in comparison to samples with 100 mol% $Ni(acac)_2$ added. Also, there is a probability of the formation of ligand-metal complexes between two different crystals (inter-crystal interactions), so the obtained assemblies may contain several different platelets. Platelets from the initial crystal dispersion with a size below 200 nm presumably took part in inter-crystal assemblies with larger platelets explaining why no very small folded crystal formation could be observed. This may also explain increased D_n and D_w for the sample with 2 mol% $Ni(acac)_2$ and 0.1 mg mL^{-1} polymer concentration compared to the initial polymer platelets, as no small assemblies below 300 nm could be detected. Compared to the initial platelets, the dispersities of the platelet size distribution decreased significantly for each experiment after addition of $Ni(acac)_2$. The narrowing of the size distributions (Figure 6.8) indicated that for each concentration the size diameter/surface area of the resulting tertiary structures converged to an optimum value for the given conditions.

Table 6.1. Size distributions of obtained polymer platelets.

	polymer concentration 1.0 mg mL^{-1}				**polymer concentration 0.1 mg mL^{-1}**			
c ($Ni(acac)_2$)	**0 mol%**	**2 mol%**	**20 mol%**	**100 mol%**	**0 mol%**	**2 mol%**	**20 mol%**	**100 mol %**
D_n / nm	590	390	170	80	360	580	150	70
D_w / nm	1,160	420	190	90	450	600	170	80
D_w/D_n	1.97	1.08	1.10	1.08	1.25	1.03	1.08	1.11

In general, the folding process induced by the supramolecular interactions proved a certain flexibility of the crystal platelets. Furthermore, the formation of the higher order assemblies proved a successful surface functionalization of the crystal platelets and the accessibility of these groups for metal-ligand interactions. The diffraction pattern of the crystal platelets confirmed that the samples were still crystalline after addition of the metal salt solutions. However, the diffraction pattern was less prominent compared to the initial diffraction pattern of **poly-1-terpy** platelets in ethyl acetate (Figure 6.9). While for the initial **poly-1-terpy** polymer the structure of monolayer crystals can be determined from the position of the diffraction spots, the multilayered

nature of the obtained folded structures and chaotic arrangement of the theses layers lead to the less prominent and broad diffraction pattern.

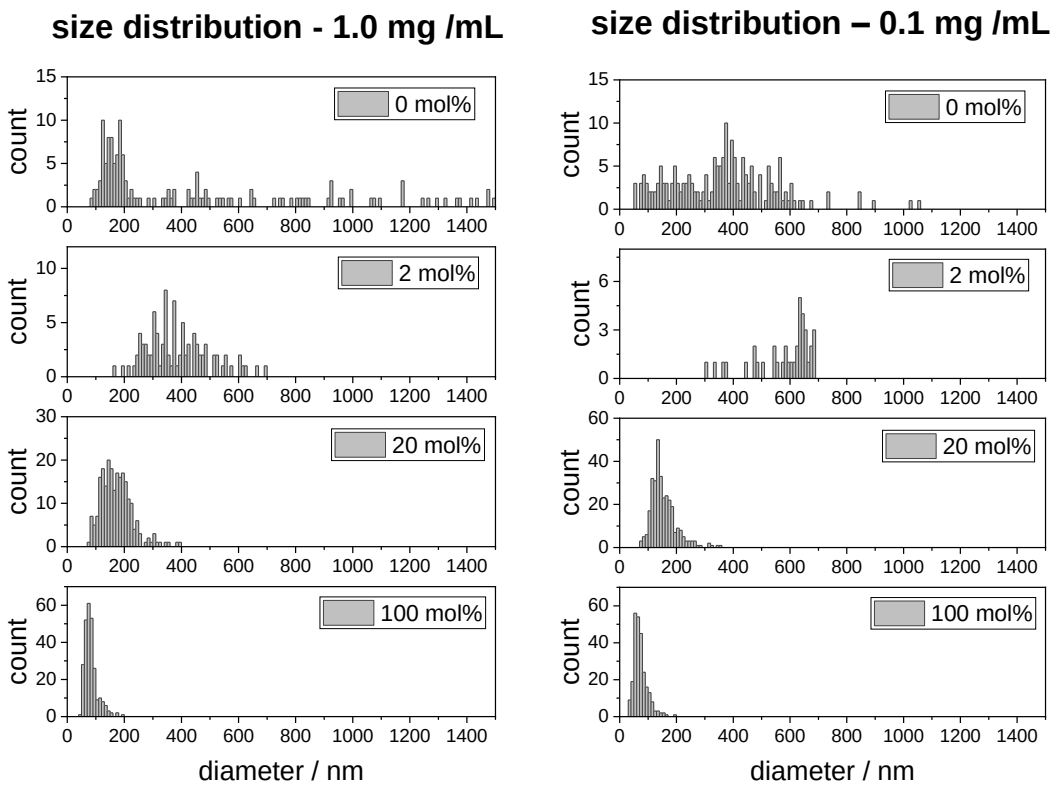

Figure 6.8. Platelet size distributions for dispersions prepared from 1.0 mg mL^{-1} (left) and 0.1 mg mL^{-1} (right) polymer solutions in ethyl acetate.

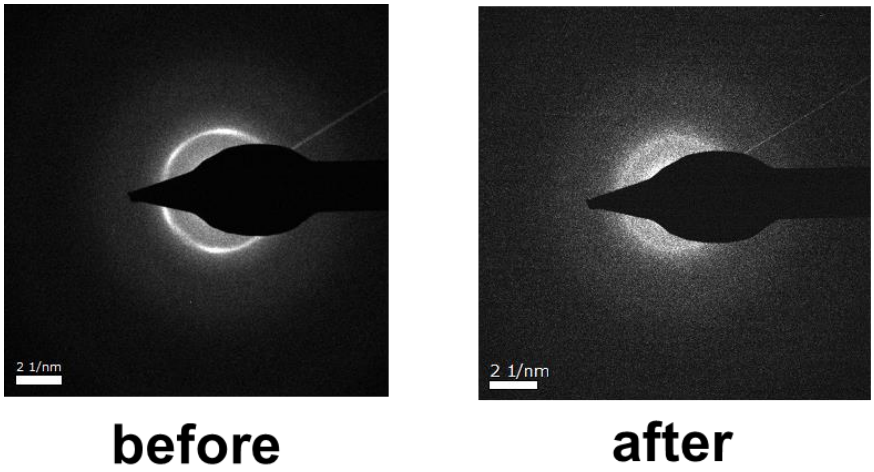

Figure 6.9. TEM diffraction pattern of **poly-1-terpy** crystals before (left) and after (right) formation of tertiary order assemblies upon addition of $Ni(acac)_2$.

6.5. Experimental section

Experimental section

Materials. All commercially available reagents were purchased from Sigma Aldrich, Carl Roth and Alfa Aesar and were used without further purification. $CDCl_3$ was purchased from Sigma Aldrich.

Instrumentation and Characterization Techniques. For nuclear magnetic resonance (NMR) analysis ^{1}H, ^{13}C and ^{31}P NMR spectra of the monomers were recorded on a Bruker AVANCE III 300, 400, 500 or 700 MHz spectrometer. All spectra were measured in $CDCl_3$ at 298 K. The spectra were calibrated against the solvent signal and analyzed using MestReNova 12 from Mestrelab Research S.L. Size exclusion chromatography (SEC) measurements were performed in THF on an Agilent Technologies 1260 instrument consisting of an autosampler, pump and column oven. The column set consists of 3 columns: SDV 10^6 Å, SDV 10^4 Å and SDV 500Å (PSS Standards Service GmbH, Mainz, Germany), all of 300 x 8 mm and 10µm average particle size were used at a flow rate of 1.0 mL/min and a column temperature of 30 °C. The injection volume was 100 µL. Detection was accomplished with an RI detector (Agilent Technologies) and UV detector. The data acquisition and evaluation were performed using PSS WINGPC UniChrom (PSS Polymer Standards Service GmbH, Mainz, Germany). Calibration was carried out by using polystyrene provided by PSS Polymer Standards Service GmbH (Mainz, Germany). The thermal properties of the synthesized polymers have been measured by differential scanning calorimetry (DSC) on a Mettler Toledo DSC 823 calorimeter. Three scanning cycles of heating/cooling were performed in a nitrogen atmosphere (30 mL/min) with a heating and cooling rate of 10 °C/min. The crystal morphology was determined using FEI Tecnai F20 transmission electron microscope operated at an acceleration voltage of 200 kV. Bright field (BF) technique was used for measurements. The size of the crystal platelets was visually determined using ImageJ software. Histograms of the diameter distribution were constructed using Origin Pro 9. From these data, values of D_n and D_w were calculated as shown below (D, diameter of platelet; N, number).

$$D_n = \frac{\sum_{i=1}^{n} N_i D_i}{\sum_{i=1}^{n} N_i} \qquad D_w = \frac{\sum_{i=1}^{n} N_i {D_i}^2}{\sum_{i=1}^{n} N_i D_i}$$

Synthetic Procedures. To prevent any contamination with Fe irons during the reaction, no syringes with metal needles were used during the reaction. Instead, all reagents were added in solution via plastic or glass pipettes.

Synthesis of poly1-terpy: Carbonyldiimidazole (61 mg, 0.22 mmol) was placed in a 25 mL Schlenk tube and dissolved in 0.5 mL DMF. A solution of 2,2':6',2''-terpyridine-4'-carboxylic acid (35 mg, 0.22 mmol) in 1.0 mL DMF was added dropwise to the CDI solution under vigorous stirring. Evolving gas bubbles indicated the start of the reaction. The solution was kept stirring at room temperature for 30 minutes before heating up to 60 °C. Then, a solution of poly(2-hydroxyethyl eicosyl phosphate) (89 mg, 0.21 mmol) in 1.0 mL DMF was added and the Schlenk tube was closed with a Teflon stop-cock. The color of the solution turned slightly purple over time. After stirring at 60 °C for 72 h, the hot solution was dropped into ice cold methanol (-18 °C). **Poly1-terpy** precipitated as a white solid. The precipitation step in methanol was repeated one more time. After centrifugation, the polymer was isolated and dried under reduced pressure. Yield: 48%. ^{1}H NMR (300 MHz, $CDCl_3$) δ = 9.01 (s, 2H), 8.72 (d, J = 4.8 Hz, 2H), 8.61 (d, J = 8.0 Hz, 2H), 7.86 (t, J = 7.8 Hz, 2H), 7.40 – 7.30

(m, 2H), 4.64 (t, *J* = 4.7 Hz, 2H), 4.41 (q, *J* = 5.2, 4.2 Hz, 2H), 4.05 (q, *J* = 6.8 Hz, 4H), 1.64 (h, *J* = 6.9, 6.4 Hz, 4H), 1.31 – 1.15 (m, 32H). ^{13}C NMR (75 MHz, $CDCl_3$) δ = 165.12, 156.64, 155.34, 149.32, 139.30, 136.89, 124.19, 121.25, 120.39, 68.12 (d, *J* = 6.2 Hz), 64.95, 64.19, 30.25 (d, *J* = 6.7 Hz), 29.63 (dd, *J* = 11.9, 5.4 Hz), 29.15, 25.41. ^{31}P NMR (121 MHz, $CDCl_3$) δ = 0.47, -0.93.

Polymer crystal assembly. *Solution grown crystals of poly-1-terpy:* A 1 mg mL^{-1} and a 0.1 mg mL^{-1} solution of **poly-1-terpy** in ethyl acetate was prepared. The solution was heated to 70 °C in a temperature-controlled oil bath for 1 hour and slowly cooled down to room temperature within 24 h. One drop of the resulting dispersion was drop-cast onto a carbon coated TEM grid, the excess liquid was blotted off with a filter paper and the specimen was allowed to dry under ambient conditions before TEM measurements were performed.

Supramolecular folding of polymer platelets: Solution of $Ni(acac)_2$ in ethyl acetate were prepared with a relative ratio of 2, 20 and 100 mol% relative to terpyridine units in **poly-1-terpy**. The solutions were added dropwise to initial polymer crystal suspension. The final mixture was stirred for several seconds before sample preparation for TEM measurements were performed analog to the initial **poly-1-terpy** crystals.

6.6. Conclusion and outlook

In this work, we have demonstrated that synthetic tertiary structures can be obtained by inter- and intra-molecular metal-ligand interactions of anisotropic polymer crystal platelets, which represent secondary structures themselves. Therefore, a PE-like polyphosphate with precise 20 CH_2 groups between the phosphate units was functionalized with pendant terpyridine groups by esterification. A maximum degree of functionalization of 85% was achieved. Solution-grown anisotropic platelets with mean average diameters of 380 and 590 nm were obtained from two polymer solutions with different initial polymer concentration. The platelet size was dependent on polymer concentration. No significant difference between crystal platelets of polyphosphate with and without pendant terpyridine groups was observed. In contrast, the terpyridine groups were accessible on the crystal surface for supramolecular interactions, enabling the formation of higher-order assemblies upon addition of $Ni(acac)_2$. Complex formation induced folding of the platelets resulting in assemblies with significantly smaller diameters and narrower size distribution compared to the initial platelets. Variation of the metal ion concentration allowed control over the size of the obtained structures. The crystallinity of the platelet assemblies was confirmed by diffraction pattern from TEM.

Future work lies on the preparation of single chain nanoparticles (SCNPs) of the synthesized polymer to investigate the probability to form secondary structures similar to protein conformations in nature. These experiments will try to demonstrate that a formation of secondary and tertiary order assemblies from the same initial polymer is possible and solely depends on the experimental conditions.

References

1. Geim, A. K. & Novoselov, K. S. The rise of graphene. *Nat. Mater.* **6**, 183–191 (2007).

2. K. S. Novoselov, A. K. Geim, S. V. Morozov, D. Jiang, Y. Zhang, S. V. Dubonos, I. V. G. and A. A. F. Electric Field Effect in Atomically Thin Carbon Films. **306**, 666–669 (2016).

3. Fujie, T. Development of free-standing polymer nanosheets for advanced medical and health-care applications. *Polym. J.* **48**, 773–780 (2016).

4. Kim, J. H., Bohra, M., Singh, V., Cassidy, C. & Sowwan, M. Smart composite nanosheets with adaptive optical properties. *ACS Appl. Mater. Interfaces* **6**, 13339–13343 (2014).

5. Fujie, T. *et al.* Hydrodynamic transformation of a freestanding polymer nanosheet induced by a thermoresponsive surface. *ACS Appl. Mater. Interfaces* **1**, 1404–1413 (2009).

6. Feng, X., Kawabata, K., Whang, D. M. & Osuji, C. O. Polymer Nanosheets from Supramolecular Assemblies of Conjugated Linoleic Acid-High Surface Area Adsorbents from Renewable Materials. *Langmuir* **33**, 10690–10697 (2017).

7. Keller, A. A note on single crystals in polymers: Evidence for a folded chain configuration. *Philos. Mag.* **2**, 1171–1175 (1957).

8. Fischer, E. W. Stufen- und spiralförmiges Kristallwachstum bei Hochpolymeren. *Zeitschrift Fur Naturforsch. Part a-Astrophysik Phys. Und Phys. Chemie* **12**, 753–754 (1957).

9. Lieberwirth, I. G. Orientation-induced evolution of crystal morphologies in semi-crystalline polymers. (Technische Universiteit Eindhoven, 2001). doi:10.6100/IR658251

10. Nasilowski, M., Mahler, B., Lhuillier, E., Ithurria, S. & Dubertret, B. Two-Dimensional Colloidal Nanocrystals. *Chem. Rev.* **116**, 10934–10982 (2016).

11. Mer, V. K. La. Nucleation in Phase Transitions. *Ind. Eng. Chem.* **44**, 1270–1277 (1952).

12. Becker, R. & Döring, W. Kinetische Behandlung der Keimbildung in übersättigten Dämpfen. *Ann. Phys.* **416**, 719–752 (1935).

13. Polte, J. Fundamental growth principles of colloidal metal nanoparticles - a new perspective. *CrystEngComm* **17**, 6809–6830 (2015).

14. Gibbs, J. W. Equilibrium of Heterogenous Substances. *Am. J. Sci.* **16**, 441–458 (1878).

15. Wulff, G. Zur Frage der Geschwindigkeit des Wachsthums und der Auflösung der Krystallflächen. *Zeitschrift Für Krist. - Cryst. Mater.* **34**, 449–530 (1901).

16. Schulz, M. D., Sauty, N. F. & Wagener, K. B. Morphology control in precision polyolefins. *Appl. Petrochemical Res.* **5**, 3–8 (2015).

17. Rojas, G., Inci, B., Wei, Y., Wagener, K. B. & Gaines, V. Precision Polyethylene : Changes in Morphology as a Function of Alkyl Branch Size. *J. Am. Chem. Soc.* **131**, 17376–17386 (2009).

18. Wagener, K. B., Boncella, J. M. & Nel, J. G. Acyclic Diene Metathesis (ADMET) Polymerization. *Macromolecules* **24**, 2649–2657 (1991).

19. Haider, T. *et al.* Controlling the crystal structure of precisely spaced polyethylene-like polyphosphoesters. *Polym. Chem.* **11**, 3404–3415 (2020).

20. Song, S. F. *et al.* Synthesis and Crystallization Behavior of Equisequential ADMET Polyethylene Containing Arylene Ether Defects: Remarkable Effects of Substitution Position and Arylene Size. *Macromolecules* **49**, 6001–6011 (2016).

21. Wu, X. *et al.* Nucleating Agents for High-Density Polyethylene—A Review. *Polym. Eng. Sci.* 1–10 (2011). doi:10.1002/pen

22. Seymour, R. B., Carraher, C. E., Seymour, R. B. & Carraher, C. E. Physical Structure of Polymers. in *Structure—Property Relationships in Polymers* 19–30 (1984). doi:10.1007/978-1-4684-4748-4_2

23. Song, L. *et al.* Ultra-strong long-chain polyamide elastomers with programmable supramolecular interactions and oriented crystalline microstructures. *Nat. Commun.* **10**, 1–8 (2019).

24. Bauer, K. N., Tee, H. T., Velencoso, M. M. & Wurm, F. R. Main-chain poly(phosphoester)s: History, syntheses, degradation, bio-and flame-retardant applications. *Prog. Polym. Sci.* **73**, 61–122 (2017).

25. Haider, T. *et al.* Long-Chain Polyorthoesters as Degradable Polyethylene Mimics. *Macromolecules* **52**, 2411–2420 (2019).

26. Trigg, E. B. *et al.* Self-assembled highly ordered acid layers in precisely sulfonated polyethylene produce efficient proton transport. *Nat. Mater.* **17**, 725–731 (2018).

27. Suraeva, O. *et al.* Vitamin C Loaded Polyethylene: Synthesis and Properties of Precise Polyethylene with Vitamin C Defects via Acyclic Diene Metathesis Polycondensation. *Macromolecules* (2020). doi:10.1021/acs.macromol.0c00086

28. Leonard, J. K., Turek, D., Sloan, K. B. & Wagener, K. B. Polyethylene prodrugs using precisely placed pharmaceutical agents. *Macromol. Chem. Phys.* **211**, 154–165 (2010).

29. Llevot, A., Grau, E., Carlotti, S., Grelier, S. & Cramail, H. From Lignin-derived Aromatic Compounds to Novel Biobased Polymers. *Macromol. Rapid Commun.* **37**, 9–28 (2016).

30. Nomura, K., Chaijaroen, P. & Abdellatif, M. M. Synthesis of Biobased Long-Chain Polyesters by Acyclic Diene Metathesis Polymerization and Tandem Hydrogenation and Depolymerization with Ethylene. *ACS Omega* **5**, 18301–18312 (2020).

31. Holmberg, A. L., Reno, K. H., Wool, R. P. & Epps, T. H. Biobased building blocks for the rational design of renewable block polymers. *Soft Matter* **10**, 7405–7424 (2014).

32. Mutlu, H. Sustainable, efficient approaches to renewable platform chemicals and polymers. (2012).

33. Jiang, Y. & Loos, K. Enzymatic synthesis of biobased polyesters and polyamides. *Polymers (Basel).* **8**, (2016).

34. Lebarbé, T. *et al.* Bio-based aliphatic polyurethanes through ADMET polymerization in bulk and green solvent. *Macromol. Rapid Commun.* **35**, 479–483 (2014).

35. Hibert, G., Grau, E., Pintori, D., Lecommandoux, S. & Cramail, H. ADMET polymerization of α,ω-unsaturated glycolipids: synthesis and physico-chemical properties of the resulting polymers. *Polym. Chem.* **8**, 3731–3739 (2017).

36. Fache, M., Boutevin, B. & Caillol, S. Vanillin, a key-intermediate of biobased polymers. *Eur. Polym. J.* **68**, 488–502 (2015).

37. Wenbing, H. *Polymer Physics. A Molecular Approach*. (2013). doi:https://doi.org/10.1007/978-3-7091-0670-9

38. Storks, K. H. An Electron Diffraction Examination of Some Linear High Polymers. *J. Am. Chem. Soc.* **60**, 1753–1761 (1938).

39. Keller, A. Polymer single crystals. *Polymer (Guildf).* **3**, 393–421 (1962).

40. Holdsworth, P. J. & Keller, A. The crystallization of ethyl and methyl branched copolymers of polyethylene from dilute solution. *J. Polym. Sci. Part B Polym. Lett.* **5**, 605–612 (1967).

41. Flory, P. J. On the Morphology of the Crystalline State in Polymers. *J. Am. Chem. Soc.* **84**, 2857–2867 (1962).

42. Zachmann, H. G. Der Einfluß der Konfigurationsentropie auf das Kristallisations- und Schmelzverhalten von hochpolymeren Stoffen. *Kolloid-Zeitschrift Zeitschrift für Polym.* **216**, 180–191 (1967).

43. Zachmann, H. G. Statistische Thermodynamik des Kristallisierens und Schmelzens von hochpolymeren Stoffen. *Kolloid-Zeitschrift Zeitschrift für Polym.* **231**, 504–534 (1969).

44. Zhang, M. C., Guo, B. H. & Xu, J. *A review on polymer crystallization theories*. *Crystals* **7**, (2017).

45. Bu, H. *et al.* Single-Molecule Single Crystals. *J. Polym. Sci. Part B Polym. Phys.* **29**, 139–152 (1991).

46. Fischer, E. W. & Schmidt, G. F. Long Periods in Drawn Polyethylene. *Angew. Chemie* **I**, 488–499 (1962).

47. Hoffman, J. D., Guttman, C. M. & DiMarzio, E. A. On the problem of crystallization of polymers from the melt with chain folding. *Faraday Discuss. Chem. Soc.* **68**, 177–197 (1979).

48. Mandelkern, L. *Crystallization of Polymers*. *Polymer International* (McGraw-Hill, New York, 1964). doi:10.1002/pi.1882

49. Hu, W., Frenkel, D. & Mathot, V. B. F. Intramolecular Nucleation Model for Polymer Crystallization. *Macromolecules* **36**, 8178–8183 (2003).

50. Grozev, N., Botiz, I. & Reiter, G. Morphological instabilities of polymer crystals. *Eur. Phys. J. E* **27**, 63–71 (2008).

51. Blundell, D. J., Keller, A. & Kovacs, A. J. A new self-nucleation phenomenon and its application to the growing of polymer crystals from solution. *J. Polym. Sci. Part B Polym. Lett.* **4**, 481–486 (1966).

52. Boott, C. E., Nazemi, A. & Manners, I. Synthetic Covalent and Non-Covalent 2D Materials. *Angew. Chemie - Int. Ed.* **54**, 13876–13894 (2015).

53. Blundell, D. J. & Keller, A. Nature of Self-Seeding Polyethylene Crystal Nuclei. *J. Macromol. Sci. Part B* **2**, 301–336 (1968).

54. Xu, J., Ma, Y., Hu, W., Rehahn, M. & Reiter, G. Cloning polymer single crystals through self-seeding. *Nat. Mater.* **8**, 348–353 (2009).

55. Hashimoto, M., O'Ishi, J., Moriya, S. & Fujiwara, S. Melt memory of a spherulite nucleus formed through a seeding process in the crystal growth of isotactic polystyrene. *Polym. J.* **47**, 481–486 (2015).

56. Bassett, D. C. *Principles of Polymers Morphology*. (Cambridge Univ. Press, 1981).

57. Geil, P. H. *Polymer single crystals*. *Polymer* (Wiley, 1963). doi:10.1016/0032-3861(62)90094-0

58. Nakamura, J. & Kawaguchi, A. In situ observations of annealing behavior of polyethylene single crystals on various substrates by AFM. *Macromolecules* **37**, 3725–3734 (2004).

59. Weber, C. H. M. *et al.* Single lamella nanoparticles of polyethylene. *Nano Lett.* **7**, 2024–2029 (2007).

60. Grau, E. *et al.* Aqueous Dispersions of Nonspherical Polyethylene Nanoparticles from Free-Radical Polymerization under Mild Conditions. *Angew. Chemie* **122**, 6962–6964 (2010).

61. Godin, A., Göttker-Schnetmann, I. & Mecking, S. Nanocrystal Formation in Aqueous Insertion Polymerization. *Macromolecules* **49**, 8825–8837 (2016).

62. Huang, Y. *et al.* Reliable Exfoliation of Large-Area High-Quality Flakes of Graphene and Other Two-Dimensional Materials. *ACS Nano* **9**, 10612–10620 (2015).

63. Zhang, Y., Zhang, L. & Zhou, C. Review of chemical vapor deposition of graphene and related applications. *Acc. Chem. Res.* **46**, 2329–2339 (2013).

64. Sahabudeen, H. *et al.* Wafer-sized multifunctional polyimine-based two-dimensional conjugated polymers with high mechanical stiffness. *Nat. Commun.* **7**, 1–8 (2016).

65. Takada, K. *et al.* Electrochromic Bis(terpyridine)metal Complex Nanosheets. *J. Am. Chem. Soc.* **137**, 4681–4689 (2015).

66. Chen, Y. *et al.* Room temperature synthesis of a covalent monolayer sheet at air/water interface using a shape-persistent photoreactive amphiphilic monomer. *ACS Macro Lett.* **3**, 153–158 (2014).

67. Bauer, T. *et al.* Synthesis of free-standing, monolayered organometallic sheets at the air/water interface. *Angew. Chemie - Int. Ed.* **50**, 7879–7884 (2011).

68. Xu, S. Q. *et al.* The construction of a two-dimensional supramolecular organic framework with parallelogram pores and stepwise fluorescence enhancement. *Chem. Commun.* **51**, 16417–16420 (2015).

69. Baek, K. *et al.* Free-standing, single-monomer-thick two-dimensional polymers through covalent self-assembly in solution. *J. Am. Chem. Soc.* **135**, 6523–6528 (2013).

70. Beyer, H., Kory, M. J., Hofer, G., Stemmer, A. & Schlüter, A. D. Exfoliation of two-dimensional polymer single crystals into thin sheets and investigations of their surface structure by high-resolution atomic force microscopy. *Nanoscale* **9**, 9481–9490 (2017).

71. Kryuchkov, V. A., Daigle, J. C., Skupov, K. M., Claverie, J. P. & Winnik, F. M. Amphiphilic polyethylenes leading to surfactant-free thermoresponsive nanoparticles. *J. Am. Chem. Soc.* **132**, 15573–15579 (2010).

72. Li, H., Rojas, G. & Wagener, K. B. Precision Long-Chain Branched Polyethylene via Acyclic Diene Metathesis Polymerization. *ACS Macro Lett.* **4**, 1225–1228 (2015).

73. Sauty, N. F., Caire Da Silva, L., Gallagher, C., Graf, R. & Wagener, K. B. Unveiling the hyperbolic thermal behaviour of poly(p-phenylene alkylene)s. *Polym. Chem.* **6**, 6073–6082 (2015).

74. Hosoda, S. *et al.* Effect of the sequence length distribution on the lamellar crystal thickness and thickness distribution of polyethylene: Perfectly equisequential ADMET polyethylene vs ethylene/α-Olefin Copolymer. *Macromolecules* **44**, 313–319 (2011).

75. Rojas, G., Inci, B., Wei, Y. & Wagener, K. B. Precision polyethylene: Changes in morphology as a function of alkyl branch size. *J. Am. Chem. Soc.* **131**, 17376–17386 (2009).

76. De Ten Hove, C. L. F., Penelle, J., Ivanov, D. A. & Jonas, A. M. Encoding crystal microstructure and chain folding in the chemical structure of synthetic polymers. *Nat. Mater.* **3**, 33–37 (2004).

77. Machatschek, R., Ortmann, P., Reiter, R., Mecking, S. & Reiter, G. Assembling semiconducting molecules by covalent attachment to a lamellar crystalline polymer substrate. *Beilstein J. Nanotechnol.* **7**, 784–798 (2016).

78. Hasan, N. *et al.* Crystallization of a polyphosphoester at the air-water interface. *Eur. Polym. J.* **101**, 350–357 (2018).

79. Ortmann, P., Trzaskowski, J., Krumova, M. & Mecking, S. Precise microstructure self-stabilized polymer nanocrystals. *ACS Macro Lett.* **2**, 125–127 (2013).

80. Rank, C., Yan, L., Mecking, S. & Winey, K. I. Periodic Polyethylene Sulfonates from

Polyesterification: Bulk and Nanoparticle Morphologies and Ionic Conductivities. *Macromolecules* **52**, 8466–8475 (2019).

81. Rank, C. *et al.* Anisotropic Extended-Chain Polymer Nanocrystals. *Macromolecules* **52**, 6142–6148 (2019).

82. Osichow, A. *et al.* Ideal polyethylene nanocrystals. *J. Am. Chem. Soc.* **135**, 11645–11650 (2013).

83. Li, Y. *et al.* Two-dimensional polymers with versatile functionalities via gemini monomers. *Sci. Adv.* **5**, 1–14 (2019).

84. Whitesides, G. M. & Grzybowski, B. Self-assembly at all scales. *Science (80-.).* **295**, 2418–2421 (2002).

85. Swiegers, G. F., Balakrishnan, S. & Huang, J. *Assemblies and Self-Assembly*. *Reference Module in Chemistry, Molecular Sciences and Chemical Engineering* (Elsevier Inc., 2016). doi:10.1016/b978-0-12-409547-2.11710-x

86. Sacanna, S., Pine, D. J. & Yi, G. R. Engineering shape: The novel geometries of colloidal self-assembly. *Soft Matter* **9**, 8096–8106 (2013).

87. Timp, G. L. *Nanotechnology*. (AIP Press, 1999).

88. van Dommelen, R., Fanzio, P. & Sasso, L. Surface self-assembly of colloidal crystals for micro- and nano-patterning. *Adv. Colloid Interface Sci.* **251**, 97–114 (2018).

89. Ganda, S. & Stenzel, M. H. Concepts, fabrication methods and applications of living crystallization-driven self-assembly of block copolymers. *Prog. Polym. Sci.* **101**, 101195 (2020).

90. Mai, Y. & Eisenberg, A. Self-assembly of block copolymers. *Chem. Soc. Rev.* **41**, 5969–5985 (2012).

91. Vilgis, T. & Halperin, A. Aggregation of Coil-Crystalline Block Copolymers: Equilibrium Crystallization. *Macromolecules* **24**, 2090–2095 (1991).

92. Hudson, Z. M. *et al.* Tailored hierarchical micelle architectures using living crystallization-driven self-assembly in two dimensions. *Nat. Chem.* **6**, 893–898 (2014).

93. Yu, B., Jiang, X. & Yin, J. Size-tunable nanosheets by the crystallization-driven 2D self-assembly of hyperbranched poly(ether amine) (hPEA). *Macromolecules* **47**, 4761–4768 (2014).

94. Gilroy, J. B. *et al.* Monodisperse cylindrical micelles by crystallization-driven living self-assembly. *Nat. Chem.* **2**, 566–570 (2010).

95. Wang, X., Manners, I. & Winnik, M. a. Cylindrical Block Copolymer Micelles and Co-Micelles of Controlled Length and Architecture. *Science (80-.).* **644**, 644–648 (2007).

96. Gädt, T., Ieong, N. S., Cambridge, G., Winnik, M. A. & Manners, I. Complex and hierarchical micelle architectures from diblock copolymers using living, crystallization-driven polymerizations. *Nat. Mater.* **8**, 144–150 (2009).

97. Sinturel, C., Vayer, M., Erre, R. & Amenitsch, H. Thermal induced mobility of self-assembled platelets of polyethylene-block-poly(ethylene oxide) in liquid precursors of unsaturated polyester thermoset. *Eur. Polym. J.* **45**, 2505–2512 (2009).

98. Gournis, D. & Floudas, G. 'Hairy' Plates: Poly(ethylene oxide)-b-polyisoprene Copolymers in the Presence of Laponite Clay. *Chem. Mater.* **16**, 1686–1692 (2004).

99. Bonderer, L. J., Studart, A. R. & Gauckler, L. J. Bioinspired Design and Assembly of Platelet Reinforced Polymer Films. *Science (80-.).* **205411**, 1069–1073 (2007).

100. Li, B., Wang, B., Ferrier, R. C. M. & Li, C. Y. Programmable nanoparticle assembly via polymer single crystals. *Macromolecules* **42**, 9394–9399 (2009).

101. Wang, J., Zhu, W., Peng, B. & Chen, Y. A facile way to prepare crystalline platelets of block copolymers by crystallization-driven self-assembly. *Polymer (Guildf).* **54**, 6760–6767 (2013).

102. Yu, B., Jiang, X. & Yin, J. Responsive hybrid nanosheets of hyperbranched poly(ether amine) as a 2D-platform for metal nanoparticles. *Chem. Commun.* **49**, 603–605 (2013).

103. Shen, L. *et al.* A micellar sphere-to-cylinder transition of poly(ferrocenyldimethylsilane- b-2-vinylpyridine) in a selective solvent driven by crystallization. *Macromolecules* **41**, 4380–4389 (2008).

104. Rizis, G., Van De Ven, T. G. M. & Eisenberg, A. Crystallinity-driven morphological ripening processes for poly(ethylene oxide)-block-polycaprolactone micelles in water. *Soft Matter* **10**, 2825–2835 (2014).

105. Palacios, J. K., Zhao, J., Hadjichristidis, N. & Müller, A. J. How the Complex Interplay between Different Blocks Determines the Isothermal Crystallization Kinetics of Triple-Crystalline PEO-b-PCL-b-PLLA Triblock Terpolymers. *Macromolecules* **50**, 9683–9695 (2017).

106. Cao, L., Manners, I. & Winnik, M. A. Influence of the interplay of crystallization and chain stretching on micellar morphologies: Solution self-assembly of coil-crystalline poly(isoprene-block-ferrocenylsilane). *Macromolecules* **35**, 8258–8260 (2002).

107. Rizis, G., Van De Ven, T. G. M. & Eisenberg, A. 'Raft' Formation By Two-Dimensional Self-Assembly of Block Copolymer Rod Micelles in Aqueous Solution. *Angew. Chemie - Int. Ed.* **53**, 9000–9003 (2014).

108. Rizis, G., Van De Ven, T. G. M. & Eisenberg, A. Homopolymers as structure-driving agents in semicrystalline block copolymer micelles. *ACS Nano* **9**, 3627–3640 (2015).

109. Su, M., Huang, H., Ma, X., Wang, Q. & Su, Z. Poly(2-vinylpyridine)-block -Poly(ε-caprolactone) Single Crystals in Micellar Solution. *Macromol. Rapid Commun.* **34**, 1067–1071 (2013).

110. Pearce, S. *et al.* Uniform, High-Aspect-Ratio, and Patchy 2D Platelets by Living Crystallization-Driven Self-Assembly of Crystallizable Poly(ferrocenyldimethylsilane)-Based Homopolymers with Hydrophilic Charged Termini. *Macromolecules* **52**, 6068–6079 (2019).

111. Cha, Y. *et al.* Crystallization-Driven Self-Assembly of Metallo-Polyelectrolyte Block Copolymers with a

Polycaprolactone Core-Forming Segment. *ACS Macro Lett.* **8**, 835–840 (2019).

112. Hsiao, M. S., Yusoff, S. F. M., Winnik, M. A. & Manners, I. Crystallization-driven self-assembly of block copolymers with a short crystallizable core-forming segment: Controlling micelle morphology through the influence of molar mass and solvent selectivity. *Macromolecules* **47**, 2361–2372 (2014).

113. Yusoff, S. F. M., Hsiao, M. S., Schacher, F. H., Winnik, M. A. & Manners, I. Formation of lenticular platelet micelles via the interplay of crystallization and chain stretching: Solution self-assembly of poly(ferrocenyldimethylsilane)- Block -poly(2-vinylpyridine) with a crystallizable core-forming metalloblock. *Macromolecules* **45**, 3883–3891 (2012).

114. Chen, W. Y. *et al.* 'Chemically shielded' poly(ethylene oxide) single crystal growth and construction of channel-wire arrays with chemical and geometric recognitions on a submicrometer scale. *Macromolecules* **37**, 5292–5299 (2004).

115. Zhu, J. *et al.* Disk-cylinder and disk-sphere nanoparticles via a block copolymer blend solution construction. *Nat. Commun.* **4**, 1–7 (2013).

116. He, X. *et al.* Complex and Hierarchical 2D Assemblies via Crystallization-Driven Self-Assembly of Poly(l -lactide) Homopolymers with Charged Termini. *J. Am. Chem. Soc.* **139**, 9221–9228 (2017).

117. Nazemi, A. *et al.* Uniform 'patchy' Platelets by Seeded Heteroepitaxial Growth of Crystallizable Polymer Blends in Two Dimensions. *J. Am. Chem. Soc.* **139**, 4409–4417 (2017).

118. He, X. *et al.* Two-dimensional assemblies from crystallizable homopolymers with charged termini. *Nat. Mater.* **16**, 481–488 (2017).

119. Saaem, I. & Labean, T. H. Overview of DNA origami for molecular self-assembly. *Wiley Interdiscip. Rev. Nanomedicine Nanobiotechnology* **5**, 150–162 (2013).

120. Grabow, W. W. & Jaeger, L. RNA self-assembly and RNA nanotechnology. *Acc. Chem. Res.* **47**, 1871–1880 (2014).

121. Suzuki, Y. *et al.* Self-assembly of coherently dynamic, auxetic, two-dimensional protein crystals. *Nature* **533**, 369–373 (2016).

122. Wei, G. *et al.* Self-assembling peptide and protein amyloids: From structure to tailored function in nanotechnology. *Chem. Soc. Rev.* **46**, 4661–4708 (2017).

123. Nam, K. T. *et al.* Free-floating ultrathin two-dimensional crystals from sequence-specific peptoid polymers. *Nat. Mater.* **9**, 454–460 (2010).

124. Lu, Y., Yin, Y. & Xia, Y. A Self-Assembly Approach to the Fabrication of Patterned, Two-Dimensional Arrays of Microlenses of Organic Polymers. **13**, 34–37 (2001).

125. Zhang, X. *et al.* The design and biomedical applications of self-assembled two-dimensional organic biomaterials. *Chem. Soc. Rev.* **48**, 5564–5595 (2019).

126. Wang, L., Gong, C., Yuan, X. & Wei, G. Controlling the self-assembly of biomolecules into functional nanomaterials through internal interactions and external stimulations: A review. *Nanomaterials* **9**, (2019).

127. Gong, C. *et al.* Hierarchical nanomaterials: Via biomolecular self-assembly and bioinspiration for energy and environmental applications. *Nanoscale* **11**, 4147–4182 (2019).

128. Bai, Y., Luo, Q. & Liu, J. Protein self-assembly: Via supramolecular strategies. *Chem. Soc. Rev.* **45**, 2756–2767 (2016).

129. Dai, B. *et al.* Tunable assembly of amyloid-forming peptides into nanosheets as a retrovirus carrier. *Proc. Natl. Acad. Sci. U. S. A.* **112**, 2996–3001 (2015).

130. Battigelli, A. *et al.* Glycosylated Peptoid Nanosheets as a Multivalent Scaffold for Protein Recognition. *ACS Nano* **12**, 2455–2465 (2018).

131. Walter, H. K. *et al.* DNA Origami Traffic Lights with a Split Aptamer Sensor for a Bicolor Fluorescence Readout. *Nano Lett.* **17**, 2467–2472 (2017).

132. Jang, H. S. *et al.* Tyrosine-mediated two-dimensional peptide assembly and its role as a bio-inspired catalytic scaffold. *Nat. Commun.* **5**, 1–11 (2014).

133. Li, C., Adamcik, J. & Mezzenga, R. Biodegradable nanocomposites of amyloid fibrils and graphene with shape-memory and enzyme-sensing properties. *Nat. Nanotechnol.* **7**, 421–427 (2012).

134. Hemmig, E. A. *et al.* Programming Light-Harvesting Efficiency Using DNA Origami. *Nano Lett.* **16**, 2369–2374 (2016).

135. Bolisetty, S. & Mezzenga, R. Amyloid-carbon hybrid membranes for universal water purification. *Nat. Nanotechnol.* **11**, 365–371 (2016).

136. Brodin, J. D. *et al.* Metal-directed, chemically tunable assembly of one-, two- and three-dimensional crystalline protein arrays. *Nat. Chem.* **4**, 375–382 (2012).

137. Hsieh, M. C., Liang, C., Mehta, A. K., Lynn, D. G. & Grover, M. A. Multistep Conformation Selection in Amyloid Assembly. *J. Am. Chem. Soc.* **139**, 17007–17010 (2017).

138. Zhao, Y. *et al.* Tuning the self-assembly of short peptides via sequence variations. *Langmuir* **29**, 13457–13464 (2013).

139. Clerici, F., Erba, E., Gelmi, M. L. & Pellegrino, S. Non-standard amino acids and peptides: From self-assembly to nanomaterials. *Tetrahedron Lett.* **57**, 5540–5550 (2016).

140. Brodin, J. D., Carr, J. R., Sontz, P. A. & Tezcan, F. A. Exceptionally stable, redox-active supramolecular protein assemblies with emergent properties. *Proc. Natl. Acad. Sci. U. S. A.* **111**, 2897–2902 (2014).

141. Sanii, B. *et al.* Structure-determining step in the hierarchical assembly of peptoid nanosheets. *ACS*

Nano **8**, 11674–11684 (2014).

142. Flood, D. *et al.* Improved chemical and mechanical stability of peptoid nanosheets by photo-crosslinking the hydrophobic core. *Chem. Commun.* **52**, 4753–4756 (2016).

143. Olivier, G. K. *et al.* Antibody-mimetic peptoid nanosheets for molecular recognition. *ACS Nano* **7**, 9276–9286 (2013).

144. Castelletto, V. *et al.* Crystallization and lamellar nanosheet formation of an aromatic dipeptoid. *Chem. Commun.* **55**, 5867–5869 (2019).

145. Gao, J., Wang, M., Wang, F. & Du, J. Synthesis and Mechanism Insight of a Peptide-Grafted Hyperbranched Polymer Nanosheet with Weak Positive Charges but Excellent Intrinsically Antibacterial Efficacy. *Biomacromolecules* **17**, 2080–2086 (2016).

146. Vyborna, Y., Vybornyi, M. & Häner, R. From Ribbons to Networks: Hierarchical Organization of DNA-Grafted Supramolecular Polymers. *J. Am. Chem. Soc.* **137**, 14051–14054 (2015).

147. Yu, H., Alexander, D. T. L., Aschauer, U. & Häner, R. Synthesis of Responsive Two-Dimensional Polymers via Self-Assembled DNA Networks. *Angew. Chemie - Int. Ed.* **56**, 5040–5044 (2017).

148. Huang, Y. *et al.* Temperature-Dependent Multidimensional Self-Assembly of Polyphenylene-Based 'Rod-Coil' Graft Polymers. *J. Am. Chem. Soc.* **137**, 11602–11605 (2015).

149. Li, B. *et al.* Biomimetic Bone-like Hydroxyapatite by Mineralization on Supramolecular Porous Fiber Networks. *Langmuir* **33**, 8493–8502 (2017).

150. Lin, Y. *et al.* Self-assembled 2D free-standing janus nanosheets with single-layer thickness. *J. Am. Chem. Soc.* **139**, 13592–13595 (2017).

151. PlasticsEurope. Plastics – the Facts 2018. *Plast. – Facts 2018*

152. Vasile, C. *Handbook of Polyolefins*. **60**, (CRC Press, Boca Raton, 2000).

153. Lechner, M. D., Gehrke, K. & Nordmeier, E. H. *Makromolekulare Chemie*. *Nachrichten aus der Chemie* **62**, (Springer Spektrum, Berlin, Heidelberg, 2014).

154. Alamo, R. G. & Mandelkern, L. Thermodynamic and Structural Properties of Ethylene Copolymers. *Macromolecules* **22**, 1273–1277 (1989).

155. Clas, S. -D. *et al.* Crystallinities of copolymers of ethylene and 1-alkenes. *J. Polym. Sci. Part B Polym. Phys.* **26**, 1271–1286 (1988).

156. Inci, B. *et al.* Decreasing the alkyl branch frequency in precision polyethylene: Effect of alkyl branch size on nanoscale morphology. *Macromolecules* **45**, 3367–3376 (2012).

157. Matsui, K. *et al.* Influence of branch incorporation into the lamella crystal on the crystallization behavior of polyethylene with precisely spaced branches. *Macromolecules* **46**, 4438–4446 (2013).

158. Sworen, J. C., Smith, J. A., Berg, J. M. & Wagener, K. B. Modeling branched polyethylene: Copolymers possessing precisely placed ethyl branches. *J. Am. Chem. Soc.* **126**, 11238–11246 (2004).

159. Rojas, G., Berda, E. B. & Wagener, K. B. Precision polyolefin structure: Modeling polyethylene containing alkyl branches. *Polymer (Guildf).* **49**, 2985–2995 (2008).

160. Yan, L., Rank, C., Mecking, S. & Winey, K. I. Gyroid and Other Ordered Morphologies in Single-Ion Conducting Polymers and Their Impact on Ion Conductivity. *J. Am. Chem. Soc.* **142**, 857–866 (2020).

161. Yan, L., Hauler, M., Bauer, J., Mecking, S. & Winey, K. I. Monodisperse and telechelic polyethylenes form extended chain crystals with ionic layers. *Macromolecules* **52**, 4949–4956 (2019).

162. Zhang, X., Zuo, X., Ortmann, P., Mecking, S. & Alamo, R. G. Crystallization of Long-Spaced Precision Polyacetals I: Melting and Recrystallization of Rapidly Formed Crystallites. *Macromolecules* **52**, 4934–4948 (2019).

163. Chikkali, S., Stempfle, F. & Mecking, S. Long-chain polyacetals from plant oils. *Macromol. Rapid Commun.* **33**, 1126–1129 (2012).

164. Haider, T. *et al.* Long-Chain Polyorthoesters as Degradable Polyethylene Mimics. *Macromolecules* **52**, 2411–2420 (2019).

165. Menges, M. G., Penelle, J., Le Fevere De Ten Hove, C., Jonas, A. M. & Schmidt-Rohr, K. Characterization of long-chain aliphatic polyesters: Crystalline and supramolecular structure of PE22,4 elucidated by X-ray scattering and nuclear magnetic resonance. *Macromolecules* **40**, 8714–8725 (2007).

166. Pepels, M. P. F., Hansen, M. R., Goossens, H. & Duchateau, R. From polyethylene to polyester: Influence of ester groups on the physical properties. *Macromolecules* **46**, 7668–7677 (2013).

167. Ortmann, P. & Mecking, S. Long-spaced aliphatic polyesters. *Macromolecules* **46**, 7213–7218 (2013).

168. Song, S. *et al.* Synthesis and Crystallization Behavior of Equisequential ADMET Polyethylene Containing Arylene Ether Defects : Remarkable Effects of Substitution Position and Arylene Size. *Macromolecules* **49**, 6001−6011 (2016).

169. Friebel, J. *et al.* Synthesis of precision poly(1,3-adamantylene alkylene)s via acyclic diene metathesis polycondensation. *Macromolecules* **52**, 4483–4491 (2019).

170. Zheng, Y. R. *et al.* Morphology and Thermal Properties of Precision Polymers: The Crystallization of Butyl Branched Polyethylene and Polyphosphoesters. *Macromolecules* **49**, 1321–1330 (2016).

171. Steinbach, T. & Wurm, F. R. Poly(phosphoester)s: A New Platform for Degradable Polymers. *Angew. Chemie - Int. Ed.* **54**, 6098–6108 (2015).

172. Majumder, S., Busch, H., Poudel, P., Mecking, S. & Reiter, G. Growth Kinetics of Stacks of Lamellar Polymer Crystals. *Macromolecules* **51**, 8738–8745 (2018).

173. Bauer, K. N., Tee, H. T., Lieberwirth, I. & Wurm, F. R. In-Chain Poly(phosphonate)s via Acyclic Diene Metathesis Polycondensation. *Macromolecules* **49**, 3761−3768 (2016).

174. Lehman, S. E., Schwendeman, J. E., O'Donnell, P. M. & Wagener, K. B. Olefin isomerization promoted by olefin metathesis catalysts. *Inorganica Chim. Acta* **345**, 190–198 (2003).

175. Fokou, P. A. & Meier, M. A. R. Use of a renewable and degradable monomer to study the temperature- dependent olefin isomerization during ADMET polymerizations. *J. Am. Chem. Soc.* **131**, 1664–1665 (2009).

176. Li, H., Caire da Silva, L., Schulz, M. D., Rojas, G. & Wagener, K. B. A review of how to do an acyclic diene metathesis reaction. *Polym. Int.* **66**, 7–12 (2017).

177. Ortmann, P., Wimmer, F. P. & Mecking, S. Long-Spaced Polyketones from ADMET Copolymerizations as Ideal Models for Ethylene/CO Copolymers. *ACS Macro Lett.* **4**, 704–707 (2015).

178. Busch, H., Schiebel, E., Sickinger, A. & Mecking, S. Ultralong-Chain-Spaced Crystalline Poly(H-phosphonate)s and Poly(phenylphosphonate)s. *Macromolecules* **50**, 7901–7910 (2017).

179. Cankaya, A., Steinmann, M., Bülbül, Y., Lieberwirth, I. & Wurm, F. R. Side-chain poly(phosphoramidate)s: Via acyclic diene metathesis polycondensation. *Polym. Chem.* **7**, 5004–5010 (2016).

180. Bunn, C. W. The crystal structure of long-chain normal paraffin hydrocarbons. The "shape" of the <CH2 group. *Trans. Faraday Soc.* **35**, 482–491 (1939).

181. Hong, Y. L., Koga, T. & Miyoshi, T. Chain trajectory and crystallization mechanism of a semicrystalline polymer in melt- and solution-grown crystals as studied using 13C-13C double-quantum NMR. *Macromolecules* **48**, 3282–3293 (2015).

182. Flory, P. J. Polymer Crystallization – Literature Review. in *Structural Orders in Polymers* (eds. Ciardelli, F. & Giusti, P.) (Pergamon Press, 1981). doi:10.1016/0022-0248(80)90268-7

183. Trigg, E. B., Stevens, M. J. & Winey, K. I. Chain Folding Produces a Multilayered Morphology in a Precise Polymer: Simulations and Experiments. *J. Am. Chem. Soc.* **139**, 3747–3755 (2017).

184. Hoffman, J. D. & Lauritzen, J. I. Crystallization of bulk polymers with chain folding: theory of growth of lamellar spherulites. *J. Res. Natl. Bur. Stand. Sect. A Phys. Chem.* **65A**, 297 (1961).

185. Hong, Y. L., Chen, W., Yuan, S., Kang, J. & Miyoshi, T. Chain Trajectory of Semicrystalline Polymers As Revealed by Solid-State NMR Spectroscopy. *ACS Macro Lett.* **5**, 355–358 (2016).

186. Wang, S. *et al.* Structural Unit of Polymer Crystallization in Dilute Solution As Studied by Solid-State NMR and 13C Isotope Labeling. *Macromolecules* **51**, 8729–8737 (2018).

187. Wang, S. *et al.* Intramolecular and intermolecular packing in polymer crystallization. *Macromolecules* **52**, 4739–4748 (2019).

188. Ma, Z. *et al.* Quantifying the Chain Folding in Polymer Single Crystals by Single-Molecule Force Spectroscopy. *ACS Macro Lett.* **8**, 1194–1199 (2019).

189. Weiss, H. *et al.* Mesoscopic correlation functions in heterogeneous ionic liquids. *J. Phys. Chem. B* **121**, 620–629 (2017).

190. Maynard, H. D. & Grubbs, R. H. Purification technique for the removal of ruthenium from olefin metathesis reaction products. *Tetrahedron Lett.* **40**, 4137–4140 (1999).

191. Yoshino, K. *et al.* Electrical and optical properties of conducting polymer-fullerene and conducting polymer-carbon nanotube composites. *Fuller. Sci. Technol.* **7**, 695–711 (1999).

192. Bajpai, M., Srivastava, R., Dhar, R. & Tiwari, R. S. Review on Optical and Electrical Properties of Conducting Polymers. *Indian J. Mater. Sci.* **2016**, 1–8 (2016).

193. Kimura, M. Conductive Polymer Fibers for Sensor Devices. in *Handbook of Smart Textiles* 63–78 (2015). doi:10.1007/978-981-4451-45-1

194. McCullough, R. D. The chemistry of conducting polythiophenes. *Adv. Mater.* **10**, 93–116 (1998).

195. Barnes, G., Yau, C. P. & Heeney, M. Poly(thiophene)s. in *Encyclopedia of Polymeric Nanomaterials* 1–15 (2014). doi:https://doi.org/10.1007/978-3-642-36199-9_120-1

196. Chanunpanich, N. *et al.* Grafting polythiophene on polyethylene surfaces. *Polym. Int.* **52**, 172–178 (2003).

197. Mamo, M. D., Shin, E. S. & Noh, Y. Y. Self-aligned patterning of conductive films on plastic substrates for electrodes of flexible electronics. *J. Mater. Chem. C* **5**, 10900–10906 (2017).

198. Sauty, N. F., da Silva, L. C., Schulz, M. D., Few, C. S. & Wagener, K. B. Acyclic diene metathesis polymerization and precision polymers. *Appl. Petrochemical Res.* **4**, 225–233 (2014).

199. Schulz, M. D. & Wagener, K. B. Precision Polymers through ADMET Polymerization. *Macromol. Chem. Phys.* **215**, 1936–1945 (2014).

200. Hamzah, M., Saion, E., Kassim, A., Yahya, N. & Mahmud, E. Conjugated Conducting Polymers : A Brief Overview. *Springer Ser. Solid-State Sci.* **2**, 63–68 (1992).

201. Katritzky, A. R. *et al. Comprehensive Heterocyclic Chemistry III: A Review of the Literature 1995-2007*. (Elsevier Science, 2008). doi:10.1016/C2009-1-28335-3

202. Shen, J., Masaoka, H., Tsuchiya, K. & Ogino, K. Synthesis and properties of a novel brush-type copolymers bearing thiophene backbone and 3-(N-carbazolyl)propyl acrylate side chains for light-emitting applications. *Polym. J.* **40**, 421–427 (2008).

203. Niemi, V. M., Knuuttila, P., Österholm, J. E. & Korvola, J. Polymerization of 3-alkylthiophenes with FeCl3. *Polymer (Guildf).* **33**, 1559–1562 (1992).

204. R.D.Gould. Structure and electrical conduction properties of phthalocyanine thin films. *Coord. Chem.*

Rev. **156**, 237–274 (1996).

205. Luleburgaz, S., Abuaf, M., Tunca, U., Hizal, G. & Durmaz, H. Synthesis of Poly(vitamin C) through ADMET. *Macromol. Rapid Commun.* **38**, 1–6 (2017).

206. Ritter, H. Functionalized polymers: Synthesis and properties. *Beilstein J. Org. Chem.* **6**, 1–2 (2010).

207. Schulz, D. N. & Patil, A. O. Functional Polymers: An Overview. *ACS Symp. Ser.* **704**, 1–14 (1998).

208. Crompton, T. R. Functional Groups in Polymers. in *Practical Polymer Analysis* 241–255 (Springer US, 1993). doi:10.1007/978-1-4615-2874-6_6

209. Mutlu, H., Espinosa, M. De & Meier, M. A. R. Acyclic diene metathesis: a versatile tool for the construction of defined polymer architectures. *Chem. Soc. Rev* **40**, 1404–1445 (2011).

210. Aitken, B. S. *et al.* Precision ionomers: Synthesis and thermal/mechanical characterization. *Macromolecules* **45**, 681–687 (2012).

211. Mandal, J., Prasad, S. K., Rao, D. S. S. & Ramakrishnan, S. Periodically Clickable Polyesters: Study of Intrachain Self- Segregation Induced Folding, Crystallization, and Mesophase Formation. *J. Am. Chem. Soc.* **136**, 2538−2545 (2014).

212. Bendich, A., Machlin, L. J., Scandurra, O., Burton, G. W. & Wayner, D. D. M. The antioxidant role of vitamin C. *Adv. Free Radic. Biol. Med.* **2**, 419–444 (1986).

213. Van Der Reest, J. & Gottlieb, E. Anti-cancer effects of Vitamin C revisited. *Cell Res.* **26**, 269–270 (2016).

214. Capuzzi, G., Nostro, P. Lo, Kulkarni, K. & Fernandez, J. E. Mixtures of Stearoyl-6-O-ascorbic Acid and α-Tocopherol: A Monolayer Study at the Gas / Water Interface. *Langmuir* **12**, 3957–3963 (1996).

215. Zheng, Y. *et al.* Morphology and Thermal Properties of Precision Polymers: The Crystallization of Butyl Branched Polyethylene and Polyphosphoesters. *Macromolecules* **49**, 1321−1330 (2016).

216. Friebel, J. *et al.* Synthesis of precision poly(1,3-adamantylene alkylene)s via acyclic diene metathesis polycondensation. *Macromolecules* **52**, 4483–4491 (2019).

217. Ballesteros, O. R. De, Auriemma, F., Guerra, G. & Corradini, P. Molecular Organization in the Pseudo-hexagonal Crystalline Phase of Ethylene - Propylene Copolymers. *Macromolecules* **29**, 7141–7148 (1996).

218. Baita Calleja, F. J. Gonzalez Ortega, J. C. and Martinez de Salazar, J. Distribution of chain defects and microstructure of melt crystallized polyethylene. *Polymer (Guildf).* **19**, 1094–1099 (1978).

219. Hoffman, J. D. & Weeks, J. Melting Process and the Equilibrium Melting Temperature of Polychlorotrifluoroethylene. **66A**, (1962).

220. Valenti, D. J. & Wagener, K. B. Direct synthesis of well-defined alcohol-functionalized polymers via acyclic diene metathesis (ADMET) polymerization. *Macromolecules* **31**, 2764–2773 (1998).

221. Boz, E., Wagener, K. B., Ghosal, A., Fu, R. & Alamo, R. G. Synthesis and crystallization of precision ADMET polyolefins containing halogens. *Macromolecules* **39**, 4437–4447 (2006).

222. Tasaki, M. *et al.* Microscopically-viewed relationship between the chain conformation and ultimate Young's modulus of a series of arylate polyesters with long methylene segments. *Polymer (Guildf).* **55**, 1799–1808 (2014).

223. Santonja-Blasco, L., Zhang, X. & G. Alamo, R. *Crystallization of Precision Ethylene Copolymers*. *Adv Polym Sci* **276**, (2017).

224. Peterson, J. D., Vyazovkin, S. & Wight, C. A. Kinetics of the thermal and thermo-oxidative degradation of polystyrene, polyethylene and poly(propylene). *Macromol. Chem. Phys.* **202**, 775–784 (2001).

225. Ortmann, P., Heckler, I. & Mecking, S. Physical properties and hydrolytic degradability of polyethylene-like polyacetals and polycarbonates. *Green Chem.* **16**, 1816–1827 (2014).

226. Wang, H. P. *et al.* Characterization of some new olefinic block copolymers. *Macromolecules* **40**, 2852–2862 (2007).

227. Data analysis software for for Small Angle Scattering Analysis www.sasview.org.

228. Egerton, R. *Electron Energy-loss Spectroscopy in the Electron Microscope*. *Egerton, R. Electron Energy-Loss Spectroscopy in the Electron Microscope; Springer Science & Business Media* (2011). doi:10.1080/09500348714550571

229. W. Brand-Williams, M. E. C. and C. B. Use of a Free Radical Method to Evaluate Antioxidant Activity. *Leb. u.-Technol.* **28**, 25–30 (1995).

230. Promega. CellTiter 96® Aqueous One Solution Cell Proliferation Assay Protocol, Instruction for use of products G3580, G3581 and G3582. [Online document]. 12.2012 [zuletzt aufgerufen am 05.09.2017]. Verfügbar unter: https://www.promega.de/-/media/files/resources/pr. 608–277

231. Jung, M. E. & Shaw, T. J. Total Synthesis of (R)-Glycerol Acetonide and the Antiepileptic and Hypotensive Drug (-)-γ-Amino-β-hydroxybutyric Acid (GABOB): Use of Vitamin C as a Chiral Starting Material. *J. Am. Chem. Soc.* **102**, 6304–6311 (1980).

232. Sakurai, T. *et al.* Electron-transporting foldable alternating copolymers of perylenediimide and flexible macromolecular chains. *Mater. Chem. Front.* **2**, 718–729 (2018).

233. Agbolaghi, S., Alizadeh-Osgouei, M., Zenoozi, S., Abbaspoor, S. & Abbasi, F. Fine fibrillar and rectangular/hexagonal ordered grains of poly(3-hexyl thiophene) and poly(ethylene glycol) developed by seeding technique. *J. Nanostructure Chem.* **7**, 15–27 (2017).

234. Hudson, Z. M., Lunn, D. J., Winnik, M. A. & Manners, I. Colour-tunable fluorescent multiblock micelles. *Nat. Commun.* **5**, 1–8 (2014).

235. Zhao, L. & Choi, P. A review of the miscibility of polyethylene blends. *Mater. Manuf. Process.* **21**,

135–142 (2006).

236. Crist, B. & Hill, M. J. Recent developments in phase separation of polyolefin melt blends. *J. Polym. Sci. Part B Polym. Phys.* **35**, 2329–2353 (1997).

237. Lambermont-Thijs, H. M. L., van Kuringen, H. P. C., van der Put, J. P. W., Schubert, U. S. & Hoogenboom, R. Temperature induced solubility transitions of various poly(2-oxazoline)s in ethanol-water solvent mixtures. *Polymers (Basel).* **2**, 188–199 (2010).

238. Xu, L., Zhang, H., Lu, Y., An, L. & Shi, T. The effects of solvent polarity on the crystallization behavior of thin π-conjugated polymer film in solvent mixtures investigated by grazing incident X-ray diffraction. *Polymer (Guildf).* **190**, 122259 (2020).

239. Altintas, O., Fischer, T. S. & Barner-Kowollik, C. Synthetic Methods Toward Single-Chain Polymer Nanoparticles. in *Single-Chain Polymer Nanoparticles* 1–45 (Wiley-VCH Verlag GmbH & Co. KGaA, 2017). doi:10.1002/9783527806386.ch1

240. Hanlon, A. M., Lyon, C. K. & Berda, E. B. What Is Next in Single-Chain Nanoparticles? *Macromolecules* **49**, 2–14 (2016).

241. Voet, D. & Voet, J. G. *Biochemistry*. (John Wiley & Sons, 2004).

242. Artar, M., Huerta, E., Meijer, E. W. & Palmans, A. R. A. Dynamic single chain polymeric nanoparticles : from structure to function. in *Sequence-Controlled Polymers: Synthesis, Self-Assembly, and Properties* **1170**, 313–325 (American Chemical Society, 2014).

243. Hu, M. *et al.* Shaping the Assembly of Superparamagnetic Nanoparticles. *ACS Nano* **13**, 3015–3022 (2019).

244. Sindoro, M., Yanai, N., Jee, A. Y. & Granick, S. Colloidal-sized metal-organic frameworks: Synthesis and applications. *Acc. Chem. Res.* **47**, 459–469 (2014).

245. Hudson, Z. M. *et al.* Tailored hierarchical micelle architectures using living crystallization-driven self-assembly in two dimensions. *Nat. Chem.* **6**, 893–898 (2014).

246. Qiu, H. *et al.* Uniform patchy and hollow rectangular platelet micelles from crystallizable polymer blends. *Science* **352**, 697–702 (2016).

247. Inam, M. *et al.* Controlling the size of two-dimensional polymer platelets for water-in-water emulsifiers. *ACS Cent. Sci.* **4**, 63–70 (2018).

248. Dong, B., Miller, D. L. & Li, C. Y. Polymer single crystal as magnetically recoverable support for nanocatalysts. *J. Phys. Chem. Lett.* **3**, 1346–1350 (2012).

249. Dong, B., Zhou, T., Zhang, H. & Li, C. Y. Directed self-assembly of nanoparticles for nanomotors. *ACS Nano* **7**, 5192–5198 (2013).

250. Han, L. *et al.* Uniform two-dimensional square assemblies from conjugated block copolymers driven

by π-π Interactions with controllable sizes. *Nat. Commun.* **9**, 1–12 (2018).

251. Shunmugam, R., Gabriel, G. J., Aamer, K. A. & Tew, G. N. Metal-ligand-containing polymers: Terpyridine as the supramolecular unit. *Macromol. Rapid Commun.* **31**, 784–793 (2010).

252. Hofmeier, H. & Schubert, U. S. Recent developments in the supramolecular chemistry of terpyridine-metal complexes. *Chem. Soc. Rev.* **33**, 373–399 (2004).

253. Whittell, G. R., Hager, M. D., Schubert, U. S. & Manners, I. Functional soft materials from metallopolymers and metallosupramolecular polymers. *Nat. Mater.* **10**, 176–188 (2011).

254. Winter, A. & Schubert, U. S. Synthesis and characterization of metallo-supramolecular polymers. *Chem. Soc. Rev.* **45**, 5311–5357 (2016).

255. Gallina, M. E. *et al.* Luminescent multi-terpyridine ligands: Towards 2D polymer formation in solution. *Photochem. Photobiol. Sci.* **13**, 997–1004 (2014).